LBNL-41223

A Chaotic-Dynamical Conceptual Model to Describe Fluid Flow and Contaminant Transport in a Fractured Vadose Zone

Boris Faybishenko, Christine Doughty, Jil Geller, Sharon Borglin, Lea Cox,
John Peterson, Jr., Michael Steiger, and Kenneth Williams
Earth Sciences Division
Ernest Orlando Lawrence Berkeley National Laboratory
University of California
Berkeley, California 94720

Thomas Wood and Robert Podgorney
Parsons Infrastructure and Technology, Inc.
Idaho Falls, Idaho 83401

Thomas Stoops
Idaho National Engineering and Environmental Laboratory
Idaho Falls, Idaho 83401

Stephen Wheatcraft, Maria Dragila, and Jane Long
University of Nevada
Reno, Nevada 89557

July 1998

1997 Progress Report and Presentations at the Annual Meeting held at
Ernest Orlando Lawrence Berkeley National Laboratory on
December 3–4, 1997

This work was supported by the Environmental Management Science Program managed by the Office of Environmental Management and the Office of Energy Research, of the U.S. Department of Energy under Contract No. DE-AC03-76SF00098.

DISCLAIMER

Lawrence Berkeley National Laboratory
EMSP Annual Progress Report - December 1997

Table of Contents

I.

FY 97 Summary Report:

A Chaotic-Dynamical Conceptual Model to Describe Fluid Flow and Contaminant Transport in a Fractured Vadose Zone

ABSTRACT

Understanding subsurface flow and transport processes is critical for effective assessment, decision-making, and remediation activities for contaminated sites. However, for fluid flow and contaminant transport through fractured vadose zones, traditional hydrogeological approaches are often found to be inadequate. In this project, we examine flow and transport through a fractured vadose zone as a deterministic chaotic dynamical process, and develop a model of it in these terms. Initially, we examine separately the geometric model of fractured rock and the flow dynamics model needed to describe chaotic behavior. Ultimately we will put the geometry and flow dynamics together to develop a chaotic-dynamical model of flow and transport in a fractured vadose zone.

We investigate water flow and contaminant transport on several scales, ranging from small-scale laboratory experiments in fracture replicas and fractured cores, to field experiments conducted in a single exposed fracture at a basalt outcrop, and finally to a ponded infiltration test using a pond of 7 by 8 m. In the field experiments, we measure the time-variation of water flux, moisture content, and hydraulic head at various locations, as well as the total inflow rate to the subsurface. Such variations reflect the changes in the geometry and physics of water flow that display chaotic behavior, which we try to reconstruct using the data obtained.

In the analysis of experimental data, a chaotic model can be used to predict the long-term bounds on fluid flow and transport behavior, known as the attractor of the system, and to examine the limits of short-term predictability within these bounds. This approach is especially well suited to the need for short-term predictions to support remediation decisions and long-term bounding studies.

I.1 OBJECTIVES AND STRUCTURE OF THE PROJECT

Our primary objective is to determine when and if deterministic chaos theory is applicable to infiltration of fluid and contaminants through the vadose zone in fractured rock. To the extent that

this theory is applicable we will develop algorithms for predicting flow and transport based on this theory.

In classical analysis, the system components are commonly taken to be cubes of equivalent porous media that tessellate the volume of interest. The rules used to describe multi-phase fluid flow are commonly given by Richard's Equation, a version of Darcy's Law, which describes how much fluid will be transferred as a function of the hydraulic head gradient and relative permeability.

For the case of infiltration in fractured rock, we will describe the geometry of the fracture network and determine the rules describing how fluid is transmitted as dynamical processes. The result of evaluating these processes will be an entirely new approach to the description of flow and transport behavior. The objectives of this project will be achieved through the development of:

- A hierarchical description of fracture geometry that controls fluid flow and transport,
- A dynamical description of infiltration and transport of contaminants in single fractures,
- An algorithm for flow and transport that combines the hierarchical geometry and the description of dynamical flow and transport,
- Appropriate techniques needed to detect chaotic behavior of flow in the field,
- Evaluation of deterministic chaos in laboratory and field experiments,
- Field investigations were conducted at the Box Canyon site in Idaho near the INEEL.

I.2 Background Information on Chaotic Dynamics and Fractal Structures

One of the central problems in the prediction of water, heat, and mass transfer in soils and fractured rocks is how to use past observations in order to predict the future. Field measurements can only employ a limited number of probes that cannot collect all needed information. Consequently, the quality of prediction using classical deterministic and stochastic differential equations with a set of initial and boundary conditions and volume-averaged parameters may be poor. One of the alternative approaches views a time series of data as a result of chaotic dynamics, which can appear even in a simple deterministic system. Random-looking data may in fact represent chaotic rather than stochastic processes. For predictive purposes, it is critical to recognize which is which, because for chaotic systems often only short-term predictions can be made. For example, it was shown that the weather predictability will approach zero for predictions of more than two weeks (Lorenz, 1982).

The differences between regular (non-chaotic deterministic), random, and chaotic systems are illustrated in Figure 2.1, which shows trajectories typical for each type of motion. Note that the flow trajectories for chaotic systems are different from both regular and stochastic systems. In general, the term chaotic process is used to describe a dynamical process with the following features: random processes are not a dominant part of the system, the trajectories describing the future states of the system are strongly dependent on initial conditions, adjacent trajectories diverge exponentially with time, the information on initial conditions cannot be recovered from later states of the system, and behavior is often characterized by an attractor that has a fractal geometry.

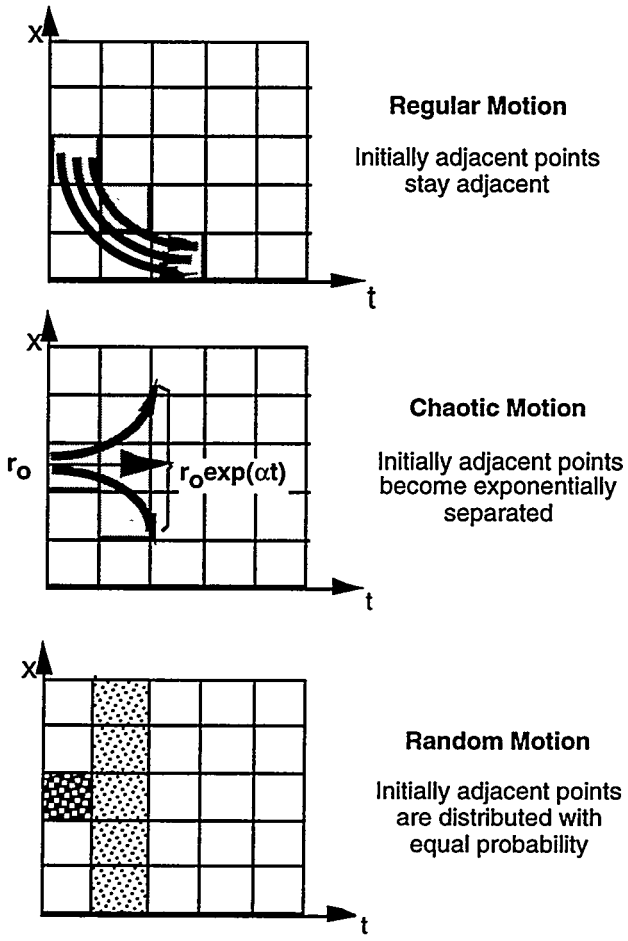

Figure 2.1 Comparison of regular (i.e., non-chaotic deterministic), chaotic, and random behavior (modified from Schuster, 1993).

Chaotic flow behavior in heterogeneous fractured media may result from hydrodynamic instabilities and a sensitive dependence of flow on (1) boundary conditions (precipitation, ambient temperature and pressure, groundwater fluctuations, etc.), (2) initial conditions (distribution of water content, pressure, and temperature), and (3) the current state of the system (water content, pressure, and temperature). Flow depends upon coupled effects of several non-linear factors such as the geometrical connectivity of the fracture system, air entrapment and its removal, clogging of the conductive fractures, biofilms, kinetics of the matrix-fracture water exchange, variability of effective hydraulic porosity and hydraulic permeability, and others.

The coupled effect of several non-linear processes in an unsaturated heterogeneous and fractured material causes non-linear behavior, governed by non-linear ordinary and partial differential equations, which may have bounded, nonperiodic solutions. These equations may be either: (1) purely deterministic where no random quantities appear in the equations (Moon, 1987; Tsonic, 1992), (2) chaotic-stochastic, or (3) have a noisy component (Kapitaniak, 1988). Therefore, one of the main problems in data analysis is to properly identify the type of the equation describing the flow system.

There are numerous examples of dynamical systems that display non-linear chaotic behavior for some system parameters. Some examples relevant to our study are: avalanche fluctuations

resulting from the perturbation of sandpiles of various sizes (Rosendahl et al., 1993), falling off of water droplets (Cheng et al., 1989), atmospheric temperature, river discharge, and precipitation (Pasternack, 1996; Pelletier, 1996), and oxygen isotope concentrations (Nicolis and Prigogine, 1989). One of the simplest examples is a dripping faucet (Shaw, 1984). Figure 2.2 shows a conceptual model of flow in fractured rocks based on a model of irregularly dripping water through a fracture, which produces non-periodic and non-repetitive behavior in both time and space.

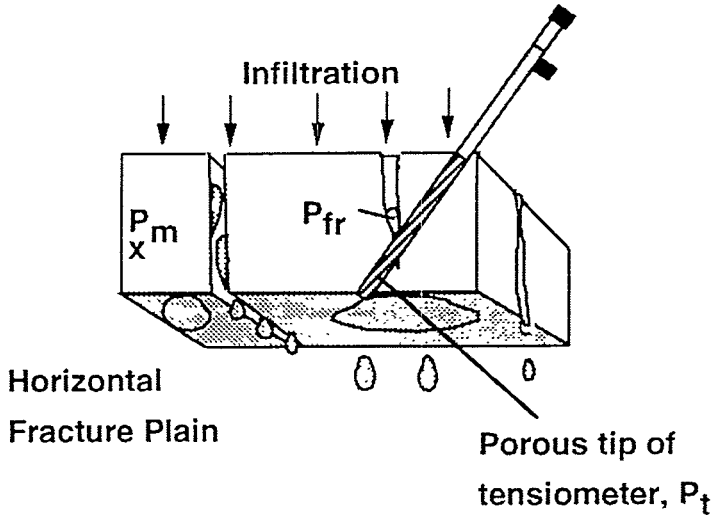

Figure 2.2 Conceptual model of flow and measurement in partially saturated fractured rocks. $P_x m$ = matrix water pressure; P_{fr} = fracture water pressure; P_t = tensiometer water pressure

It has been recognized that fractal structure is a possible indication of chaotic behavior of a system (Mandelbrot, 1977). Fractal analysis has been applied to many earth sciences problems, such as topography, fault traces, fracture networks, fracture surfaces, porous aggregate geometry, permeability distribution, flow and transport through heterogeneous media, erosion and chemical dissolution, etc. La Pointe (1988) used fractal geometry to characterize fracture density and connectivity. There are several papers in which the fractal properties of fractured tuff at Yucca Mountain were investigated (e.g., Carr, 1989). Fractal analysis was also used to predict bypass flow in rocks (Nolte et al., 1989; Cox and Wang, 1993) and clay soils with vertically continuous macropores (Hatano and Booltink, 1992).

I.3 Laboratory Tests (LBNL)

I.3.1 Introduction and Motivation

Observations of water seepage in fractures in the laboratory have shown the pervasiveness of highly localized and extremely non-uniform flow paths in the plane of the fracture (Geller et al., 1996). These channels exhibit intermittent flow behavior as portions undergo cycles of draining and filling, and small connecting threads snap and reform. This unsteady behavior occurs even in the presence of constant pressure boundary conditions. These observations motivated us to study dripping water between parallel plates as an idealized model of some of the flow behavior characteristic of water seepage through fractured rock. This study extends the classic chaos

experiment of the "dripping faucet" to drips in the presence of capillary forces as they are affected by the surface properties and the small aperture of the parallel plates.

The objective of these experiments is to collect data records that can be analyzed to determine whether or not, and under what conditions, the dripping of water in parallel plates is chaotic, random, or periodic. This work was further motivated by preliminary experiments that showed the sensitivity of pressure measurements to the formation and release of water drops through a needle in open air and inserted between parallel plates. Much of this year's work was invested in developing the experimental system to reliably obtain usable data records.

I.3.2 Experimental Results

Experiments were performed at a variety of flow rates to evaluate the system for chaotic behavior. Four basic types of experiments were conducted. Type A are pressure fluctuations caused by the 28 gauge needle dripping water into open air. Type B measure the baseline pressure fluctuations of the 28 gauge needle delivering water with a constant pressure condition at the needle outlet. (A constant pressure at the needle outlet was maintained by submerging the needle tip under water.) Type C use the 28 gauge needle to deliver water between smooth glass plates with a 0.35 mm gap at an angle of 60 degrees from the horizontal. Type D are identical to type C except for the use of rough glass plates. In each experiment, a constant flow rate of water was delivered as the magnitude of the pressure at the syringe needle was measured.

The smooth glass plates (type C) experiments were run at flow rates of 0.25, 0.5, 1.0, 1.5, 2.0, and 3.0 ml/hr. Typical pressure data for these flow rates are shown in Figure 3.1. In Figure 3.2 the frequency of drips and height of the average pressure fluctuation are plotted against the flow rates of the experiments in Figure 3.1. The experiments plotted in Figure 3.2 show a trend toward more frequent drip events and decreased height of pressure fluctuation as the flow rate increased. Visual observation of the drip events confirmed an increase in length of the thread of water as flow rate increased. However, duplicate experiments at each flow rate demonstrated that both the height of pressure fluctuations and the frequency of the drips vary between type C experiments with the same flow rate. The formation of the threads appear to depend qualitatively upon the initial condition of the plates. Some of the factors suspected to influence the drip frequency and length of thread formation are the amount of moisture on the plates, whether the drip was following a pre-existing flow path determined by a previous flow rate, and the cleanliness of the plates.

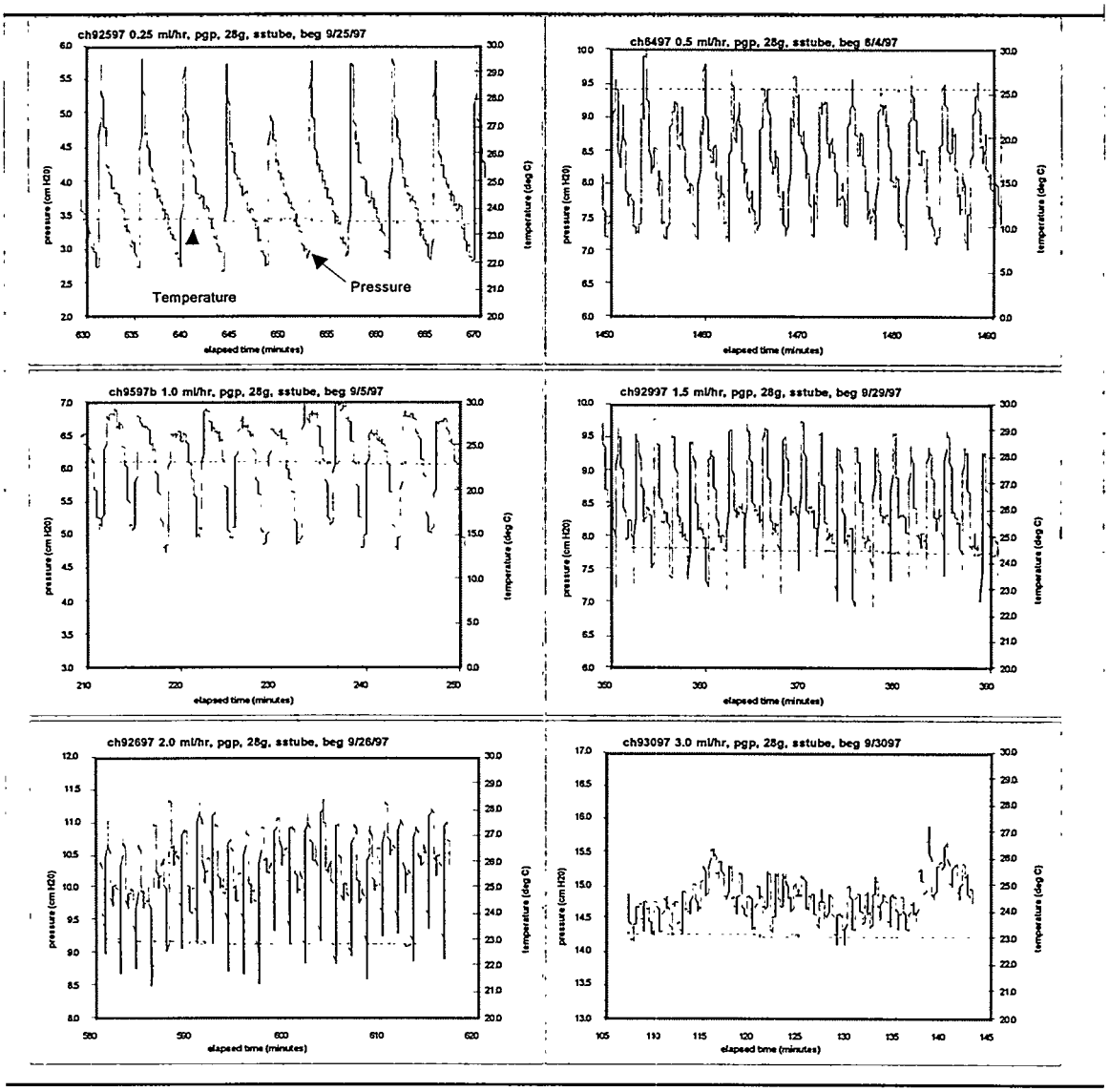

Figure 3.1: Smooth parallel glass plates. Pressure fluctuations caused by dripping water between smooth parallel glass plates at flow rates of 0.25, 0.5, 1.0, 1.5, 2.0, 3.0 ml/hr.

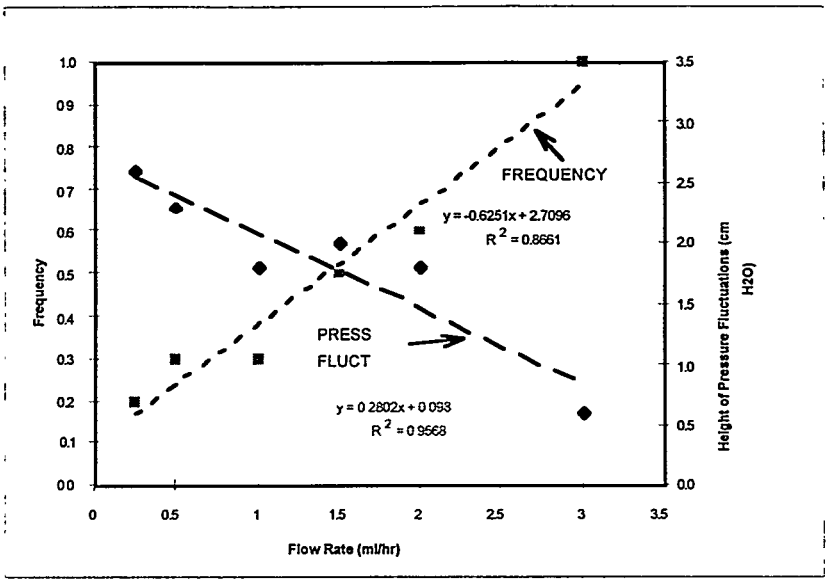

Figure 3.2: Observed trends in frequency and magnitude.

Experiments in roughened glass plates were conducted to test the effect of surface variability on drip behavior. Two types of plates were utilized: sand-blasted and shower-door glass (type D) plates. Both plates were separated by 0.35 mm shims. The sandblasted plates had an overall consistency of fine sandpaper with an even coating of fine (approximately 0.1 mm) irregularities on the surface. When the water was introduced into the sandblasted plates, a halo developed on the plate as the water advanced and film flow occurred, but drops did not form. The pressure signature observed from the sandblasted plates was similar to that observed for the baseline monitoring (see below).

The shower-door glass plates had larger, smooth irregularities or nubs on the surface (average scale of 2-3 mm). When the drips were introduced into the shower glass plates, the larger spaces between the nubs allowed drips to form at the end of the needle. The drops grew to different sizes before they snapped off and moved down the plate. Occasionally, short threads formed before the drop snapped off completely. After snapping off, the drop either moved quickly down the plate and was removed from the system or it remained close to the end of the needle, held back by a narrow throat formed by adjacent nubs. When the next drop formed, it tended to combine with the previous drop and the new larger drop would travel down between the plates.

The pressure fluctuation from the drips of water from the 28 gauge needle into open air (type A experiments) were recorded as a basis for comparison to the glass plate experiments. It was determined that the presence of capillary forces induced by the glass plates causes a decrease in drip frequency and a decrease in the height of the pressure fluctuation.

The experiments demonstrate the variation of observed pressure fluctuations and the importance of both identifying and controlling initial conditions to achieve consistent results. Although quantitative analysis of the results is not yet complete, these features suggest that chaotic dynamics play an important role.

I.4 Fractured Rock Outcrop Experiments (INEEL)

The outcrop scale experiments were designed and conceptualized to fill a gap of knowledge between the laboratory and field (Box Canyon, Idaho) scales of investigation. A research site was

selected at Hell's Half Acre Lava Field in Idaho where a single fracture could be studied. The site consisted of a basalt outcrop approximately 1 m thick that extended approximately 1.5 m outward from the rock wall. An infiltration gallery (0.5 x 1 m) was constructed above the fracture to perform constant head infiltration tests. On the underside of the overhang, drip sensors were installed to count and timestamp drops of water falling from the fracture. More traditional monitoring parameters, such as tension, temperature, and barometric pressure were also collected. Figure 4.1 shows the general site and instrument layout.

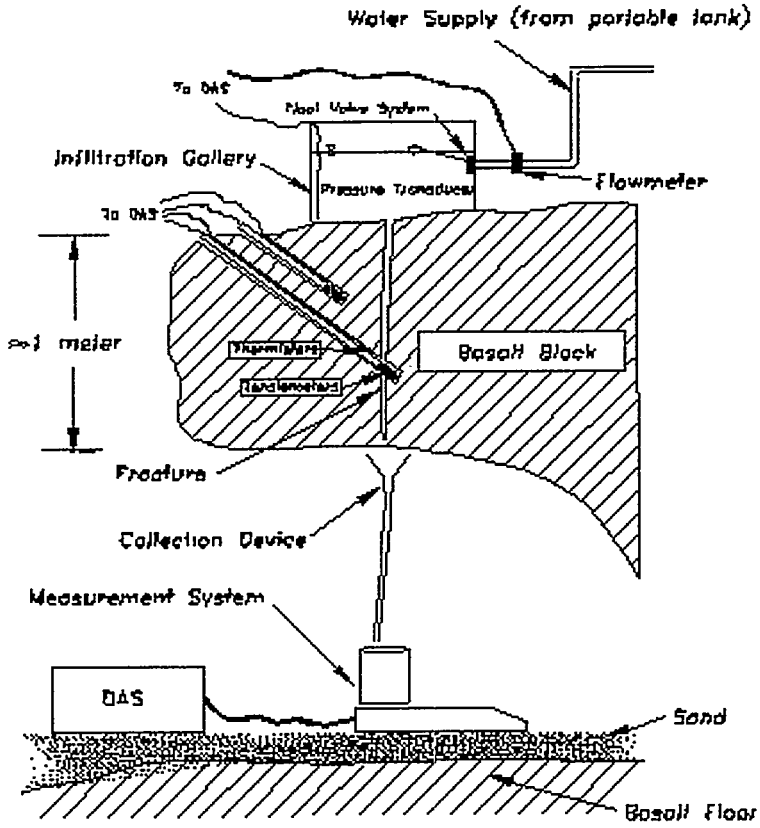

Figure 4.1. Field site characteristics and instrument layout. Note figure not to scale.

The field site was instrumented to collect data that would be amenable to a chaotic-dynamical analysis, which typically requires long time-series of data. Data collected included time stamping individual drip events for 20 distinct drip locations (to perform an analysis similar to that in Shaw, 1984); measurements of the inflow and outflow rates into the system (to compare temporal and spatial variability as well as do mass balance calculations); and moisture tension, temperature, and barometric pressure (to examine and compare with flow and drip data).

I.4.1 Field Test Setup and Instrumentation

Field work at the site began in June 1997 and continued until October 1997. Seven ponded infiltration tests were conducted, each with 4 to 48 hour duration and a varying amount of dry-out time (hours to weeks) between tests. Individual drips were monitored as they landed, using an array of specially designed piezo-electric sensors that sent a signal to the data acquisition system in response to the pressure increase accompanying a landing drip.

I.4.2 Field Observations and Preliminary Data Analysis

Preliminary reductions indicate that between 0 and 20,000 drips were collected for each location during each test. During the later tests (4-7) over 5,000 drip events were recorded at approximately 50% of the drip locations. The parameters of moisture tension, temperature, barometric pressure, and flow rates/water levels were collected at 1 minute intervals for the duration of the tests.

As the data analysis has yet to be conducted, a detailed discussion of the results cannot be presented at this time, however the following were observed during the testing:

- Flow rates were observed to vary between and during tests, ranging from near negligible inflow rates to as high as 0.8 l/min;
- The ambient moisture conditions in the basalt may exhibit some control on the flow through the fracture;
- Temporal and spatial variability was observed in the location of the first appearance of drips.

I.5 Box Canyon Pulsed Ponded Infiltration Experiment (LBNL)

The Box Canyon, Idaho experiment consists of a series of pulses of ponded infiltration, in which a fixed volume of water containing a known concentration of tracer (potassium bromide) is added to the pond all at once, allowed to infiltrate for two days, then pumped out of the pond, allowing air to enter the subsurface. This sequence of water and air boundary conditions is believed to be conducive to the development of chaotic flow and chemical transport behavior in the fractured basalt. In addition to monitoring water infiltration and evaporation rates from the pond, two types of measurements were conducted in the subsurface below the infiltration pond in order to study the flow and transport behavior in fractured basalt. First, time series of measurements at point locations were collected, to study the local dynamics of flow and transport and examine it for chaotic behavior. Second, snapshots of the spatial distribution of moisture and tracer movement were collected with geophysical techniques, to study the geometrical pattern of flow and transport and examine it for evidence of fractal geometry.

I.5.1 Infiltration Tests and Pond Data Collected

Three pulse infiltration tests of approximately 48 hours each were conducted in September-October 1997. Table 5.1 shows specifics for each test.

Table 5.1. Pulsed ponded infiltration tests conducted at Box Canyon in 1997.

Beginning of ponding		Test number	Volume added (m^3)	Duration of ponding (days)	Volume infiltrated and evaporated (m^3)
9/11/97	12:15	1	11.23	2.02	5.55
9/18/97	14:56	2	11.03	2.08	5.37
10/2/97	15:40	3	11.00	2.01	4.63

Potassium bromide slurry was added to the tanks before each test resulting in a concentration of approximately 3 mg/L. Water samples were taken from the tanks and the pond once infiltration began to check for uniformity of concentration. Analysis of these water samples is ongoing.

Water levels in the pond were measured and cumulative infiltration rates accounting for evaporation were calculated for each test. Evaporation was monitored using a pool within the berm walls. As can be seen from the final column of Table 5.1, the cumulative flow rate into the pond decreased from pulse to pulse.

I.5.2 Point Measurements

Time domain reflectometry (TDR) measurements were taken during the three infiltration tests and during dormant periods. During infiltration, measurements were taken every 15 minutes, and during dormant periods, every 1 or 2 hours, depending on the length of time between the tests.

Electrical resistivity (ER) measurements using miniature ER probes were taken at 15 minute intervals during and between tests. Forty-five existing probes installed at multiple depths in 5 wells were used as well as newly installed single probes placed in the bottom of 3 wells. Thirteen probes were placed within the pond, and 1 probe was placed in the water tank.

Tensiometry measurements of water pressure were done using 26 tensiometers installed within and outside the pond.

Water sampling was conducted using suction lysimeters installed in boreholes. Sampling was carried out a total of 17 times. The purpose of the sampling was to detect the movement of the bromide tracer, and construct breakthrough curves as the water infiltrated downward through the fractured basalt. Analysis of the water samples is ongoing.

I.5.3 Geophysical Measurements

Neutron well logging provides a one-dimensional picture of moisture distribution. It was carried out in 7 wells 10-12 times before, during, and after each ponding period. Preliminary results indicate increases in water content during infiltration in wells located within and close to the pond.

Cross-borehole ground penetrating radar (GPR) provides a two-dimensional tomogram of moisture distribution by using variations in the velocity of electromagnetic waves with dielectric constant. GPR surveys were conducted between six different well pairs. Preliminary analysis confirms that ambient conditions are wetter this year than last year, but radar tomograms still identify the central fracture zone and the rubble zone as low velocity zones.

Electrical resistivity tomography (ERT) provides a three-dimensional picture of the subsurface electrical conductivity distribution, which may be related to moisture distribution. ERT measurements were provided by Steam Tech, Inc. These measurements involved the development of special ER probes installed in three deep (20 m) boreholes outside the pond, three shallow (2 m) boreholes within the pond, and 15 surface ER probes. The data analysis is ongoing.

I.6 Non-Linear Dynamical Processes in Unsaturated Fracture Flow (UNR)

Systems exhibiting chaotic behavior are characterized by the ability to make short-term predictions. Long-term predictions are impossible because of an exponential loss rate of information on the system state. We identify and develop the conditions under which chaotic behavior in unsaturated flow can be expected so that realistic limits can be placed on predictions about the future state of the system. We cast the problem in terms of thin film flow in fractures with aperiodic saturation events using Navier-Stokes governing equations. Initial conditions consist of constant inflow rates at the top of the fracture. If the rates are small enough and surface tension dominates, the thin film will reach a steady flow rate. Above a certain threshold flow rate, as gravity begins to dominate, periodic solitons develop. Above still another threshold, aperiodic solitons take over, and the flow characteristics are chaotic.

I.7 Estimating Total Mass of Contaminant Plumes from Sparse Well Data (LBNL)

A major problem we encounter in trying to develop models (chaotic or otherwise) for flow and transport in fractured basalts is that it is extremely difficult to develop a picture of the overall spatial structure of these processes from isolated point measurements, due to the extreme heterogeneity of the system.

We consider the estimation of the total mass of a contaminant plume as a model problem to investigate means of using sparse data effectively. Generally, the estimation of the volume or mass and shape of the plume is based on sampling and analyzing water and soil. We have generated several complex hypothetical contaminant plumes. We then test the ability of different prediction methods and different sample spacing to estimate the mass of the contaminant plume. Comparisons among the methods should tell us something about the performance of different estimation methods for different types of complex distributions. They should also indicate what resolution of sampling is required to make an acceptable mass estimation.

I.7.1 Methods

We approach the problem of sample minimization by using several simulated heterogeneous distributions obtained from fractal generating algorithms, and a real distribution obtained from a fracture infiltration experiment. We initially select 15 well locations, based on a quasi-random scheme, along a two-dimensional cross-section. The extension of this approach to three dimensions would involve taking several two-dimensional cross-sections. The wells are sampled at equally spaced vertical intervals. Sequential predictions of the total mass of contaminant are computed as each successive well is sampled. Figure 7.1 shows the fractal plume and the wells used to sample the field. The numbers indicate the sequence in which the wells are sampled.

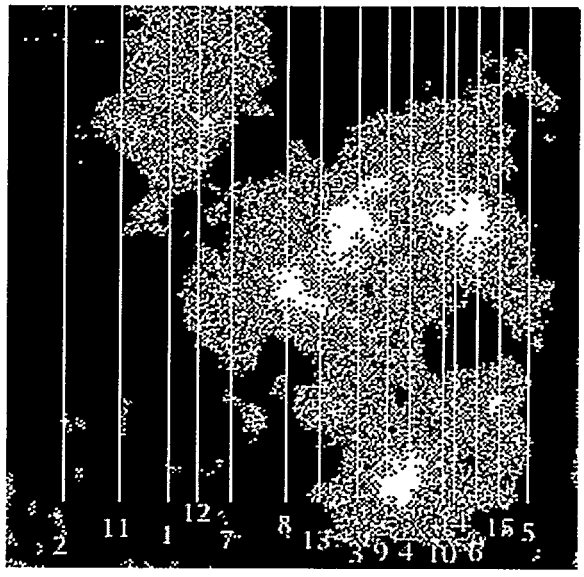

Figure 7.1. Synthetic contaminant plume with fractal geometry and locations of sampling wells.

We use several estimation techniques such as simple averaging, spatial integration, fractal and neural network models, to predict the total mass of the plume from the sample data. Parameters of the concentration distribution for the plume determined from the sparse well data were compared to those for the computer-generated plume. The convergence of the estimated plume mass to the

actual known mass, as well as the number of wells required for convergence, were used as criteria to compare the different methods.

I.7.2 Preliminary Results

Analyzing the concentration distribution, we found little or no spatial correlation between samples collected from adjacent wells, indicating that the wells are far enough apart to provide independent information. In general, for the examples we studied simple averaging, spatial integration, and neural network predictions performed comparably well and estimates of total mass did not significantly improve after five wells had been sampled. In contrast, the fractal-based methods proved less successful, in part because they depend strongly on the value of the fractal dimension of the plume, which is very difficult to determine from sparse well data. A comparison of some of the estimation methods is plotted in Figure 7.2 for a synthetic fractal plume with a fractal dimension prescribed to be 1.5. This plot shows how the estimation changes as each additional well is sampled. The bar indicates a perfect estimation. Interestingly, the least successful method is a fractal-based method that assumes a fractal dimension of 1.5, supposedly the actual fractal dimension of the plume. The much better performance of a fractal method that uses a fractal dimension of 1.3 suggests that perhaps the algorithm used to create the plume does not actually produce the desired fractal dimension. This topic is currently under investigation.

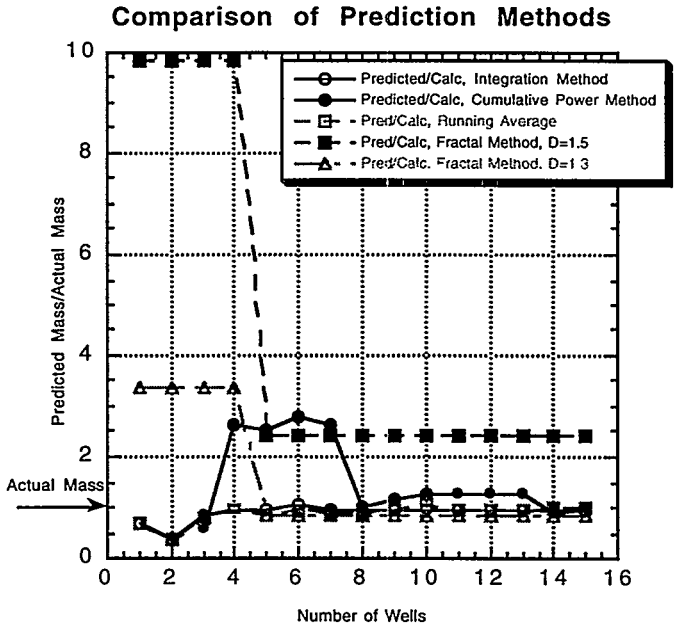

Figure 7.2. Summary of predictions for a fractal plume with a fractal dimension prescribed to be 1.5. The curves labeled cumulative power method, fractal 1.5, and fractal 1.3 all use various forms of fractal-based approaches.

I.8 Topics of On-Going Research

I.8.1 Theoretical

- Study the physics of water flow and chemical transport in fractured rocks using dynamical models of chaos theory, fuzzy logic, and a combined fuzzy-chaotic approach (a tool for managing and optimizing remediation activities under conditions for which chaotic processes are important).
- Use fractal and neural network approaches to determine three-dimensional spatial distributions of properties or processes in soils and fractured rocks from point-type measurements in boreholes.
- Apply the theory of linguistic variables to lithological analysis of data from boreholes.
- Re-examine water flow and tracer transport in fractured basalt from the Large-Scale Infiltration Test in light of chaotic dynamic models.
- Compare laboratory and field methods for the determination of quasi-saturated hydraulic conductivity of soils, and use a deterministic-chaotic model to describe a variable hydraulic conductivity within the zone of fluctuation of water table.
- Examine the relationship between the spatial structure of geologic heterogeneity (using methods of fractal geometry) and chaotic dynamics, as related to infiltration through a fractured basalt vadose zone.
- Construct and investigate fractal structures created with iterated function systems (IFS), which can simulate realistic characteristics of natural fracture patterns in basalt.

I.8.2 Experimental

- Evaluate the performance of tensiometers in fractured rocks, using laboratory cores and modeling, taking into account the interaction between the matrix and fractures.
- Use ground penetrating radar to investigate flow in soils and fractured rocks.
- Use 2-D and 3-D ERT to evaluate zones of preferential flow in fractured rocks.
- Conduct a series of pulsed infiltration tests at Box Canyon and Hell's Half Acre field sites in Idaho.

I.9 Acknowledgment

This work was sponsored by the Environmental Management Science Program managed by the Office of Environmental Management and the Office of Energy Research, of the U.S. Department of Energy under Contract No. DE-AC03-76SF00098. The report was reviewed by Ardyth Simmons and Janet Jacobsen.

I.10 References

Carr, J.R., 1989. Fractal characterization of and joint surface roughness in welded tuff at Yucca Mountain, Nevada, in Proceedings of the Thirtieth U.S. Symposium Rock Mechanics, Morgantown, West Virginia, A.W. Khair, ed. (Balema, Rotterdam), pp. 193-200.

Cheng, Z., S. Redner, P. Meakin, and F. Family, 1989. Avalanche dynamics in a deposition model with "sliding," Physical Review A, vol. 40, no. 10, pp. 5922-5935.

Cox, B.L. and J.S.Y. Wang, 1993. Fractal analysis of anisotropic fracture surfaces, Fractals, vol. 1, no. 13, pp. 547-559.

Geller, J. T., G. Su and K. Pruess, 1996. Preliminary Studies of Water Seepage through Rough-Walled Fractures, LBNL Report 38810, July.

Hatano, R. and H.W.G. Booltink, 1992. Using fractal dimensions of stained flow patterns in a clay soil to predict bypass flow, Journal of Hydrology, vol. 135, pp. 121-131.

Kapitaniak, T., 1988. Chaos in Systems with Noise, World Scientific, Teanick, N.J.

La Pointe, P.R., 1988. A method to characterize fracture density and connectivity through fractal geometry, International Journal Rock Mech. Min. Sci. and Geotech. Abstract, vol. 25, no. 6, pp. 421-429.

Lorenz, E.N., 1982. Atmospheric predictability experiments with a large numerical model, Tellus, vol. 34, pp. 505-513.

Mandelbrot, B.B., 1977. The Fractal Geometry of Nature, W.H. Freeman and Company, New York.

Moon, F.C., 1987. Chaotic Vibrations, an Introduction for Applied Scientists and Engineers, John Wiley, New York.

Nicolis, G. and I. Prigogine, 1989. Exploring Complexity: An Introduction, W.H. Freeman and Company, New York, NY.

Nolte, D.D., L.J. Pyrak-Nolte, and N.W.G. Cook, 1989. The fractal geometry of flow paths in natural fractures in rock and the approach to percolation, Pure and Applied Geophysics, vol. 131, nos. 1/2, pp. 111-138.

Pasternak, G.B., 1996. Assessing claims for chaos in hydrologic records, Hydrology Days, pp. 395-406.

Pelletier, J.D., 1996. Power spectral analyses of climatological and hydrological time series: Identification of the Hurst phenomenon and application to drought hazard assessment, Hydrology Days, pp. 407-422.

Rosendahl, J., M. Vekic, and J. Kelley, 1993. Persistent self-organization of sandpiles, Physical Review E, vol. 47, no. 2, pp. 1401-1447.

Schuster, H.G., Deterministic Chaos: An Introduction, Weinheim, VCH, 1989.

Shaw, R., 1984. The Dripping Faucet as a Model Chaotic System, Aerial Press, Santa Cruz, CA.

Tsonic, A.A., 1992. Chaos: From Theory to Applications, Plenum Press.

Wood, T.R., and G.T.Norrell, Integrated Large-Scale Aquifer Pumping and Infiltration Tests. Groundwater Pathways OU 7-06. Summary Report, INEEL-96/0256, Lockheed Martin Idaho Technologies Company, Idaho, 1996.

II.

APPENDIX

PRESENTATIONS AT THE ANNUAL MEETING.

DECEMBER 3-4, 1997

II.1

BOX Canyon Infiltration Test Summary of 1996-97 Results

Boris Faybishenko and Michael Steiger

Goal: Develop a conceptual model of geometry and physics of liquid flow and chemical transport for an intermediate scale of investigations in unsaturated-saturated fractured basalt

Environmental Management Sites with Fracture Rocks

- **INEEL, Idaho, Basalt**
- **Oak Ridge, Tennessee,** Shale & karst
- **Hanford, Washington** Basalt
- **NTS, Nevada, Tuff**
- **LANL, New Mexico** Tuff and basalt
- **SLAC, California** Sedimentary rock
- **PPL, New Jersey** Sandstone & shale aquifer

Outline

- Box Canyon site in a hierarchy of investigations in fractured basalt
- Geology
- Well layout, types of measurements and tests
- Flow rate
- Water pressure
- Breakthrough curves
- Water level in boreholes
- Moisture content
- Borehole single ER probes
- Conclusions

INEEL Needs

- VOCs and radionucludes (Cs, Sr, U, Tc) in groundwater and perched water zones in ***fractured rock*** at 200 to 600 ft depths

Hierarchy of Tests

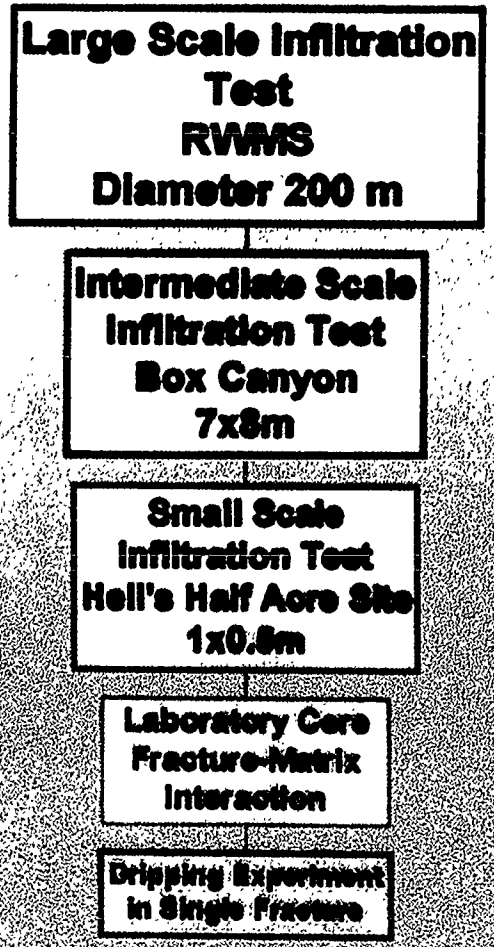

Hierarchy of Scales in Basalt

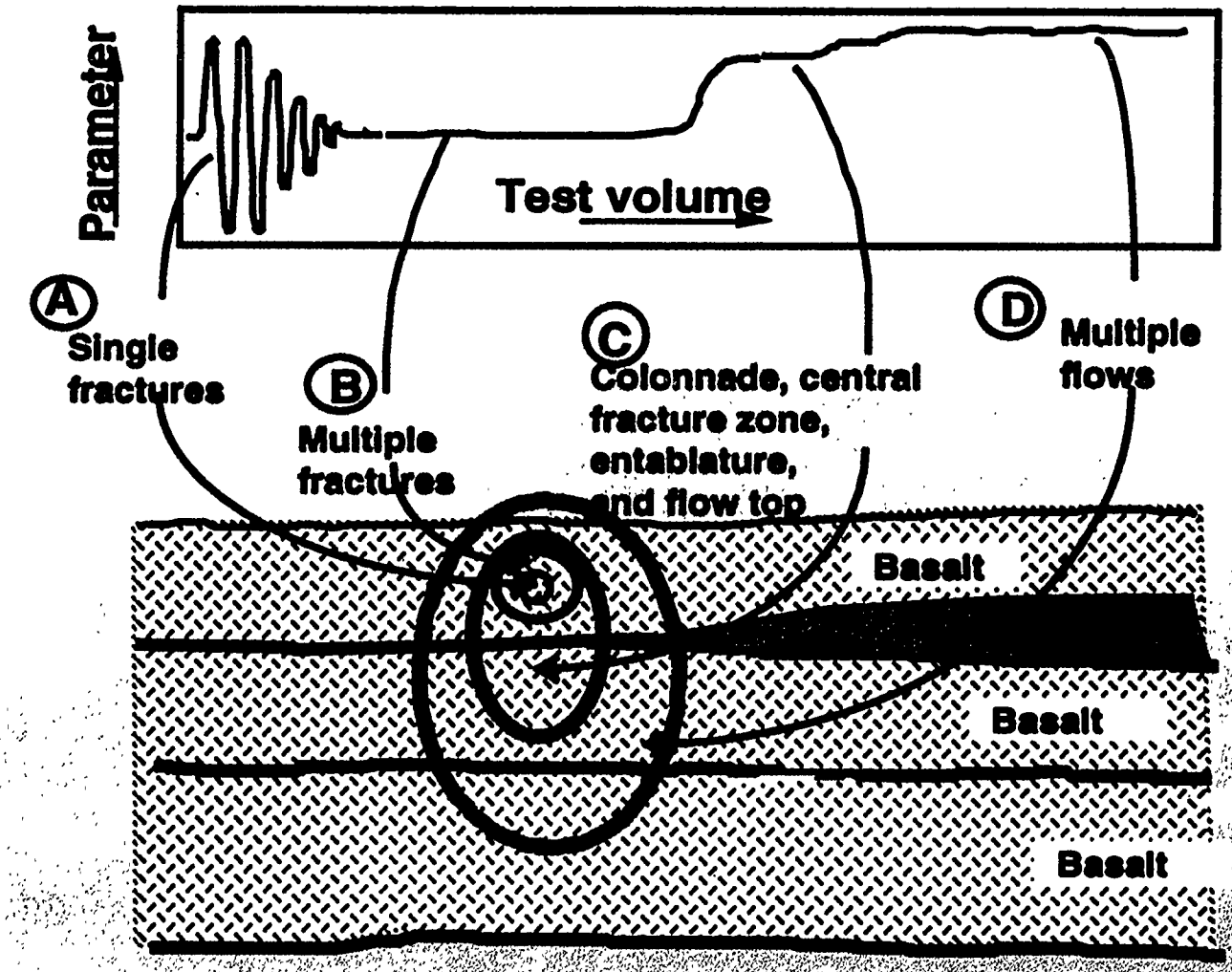

Modified from DOE, 1986

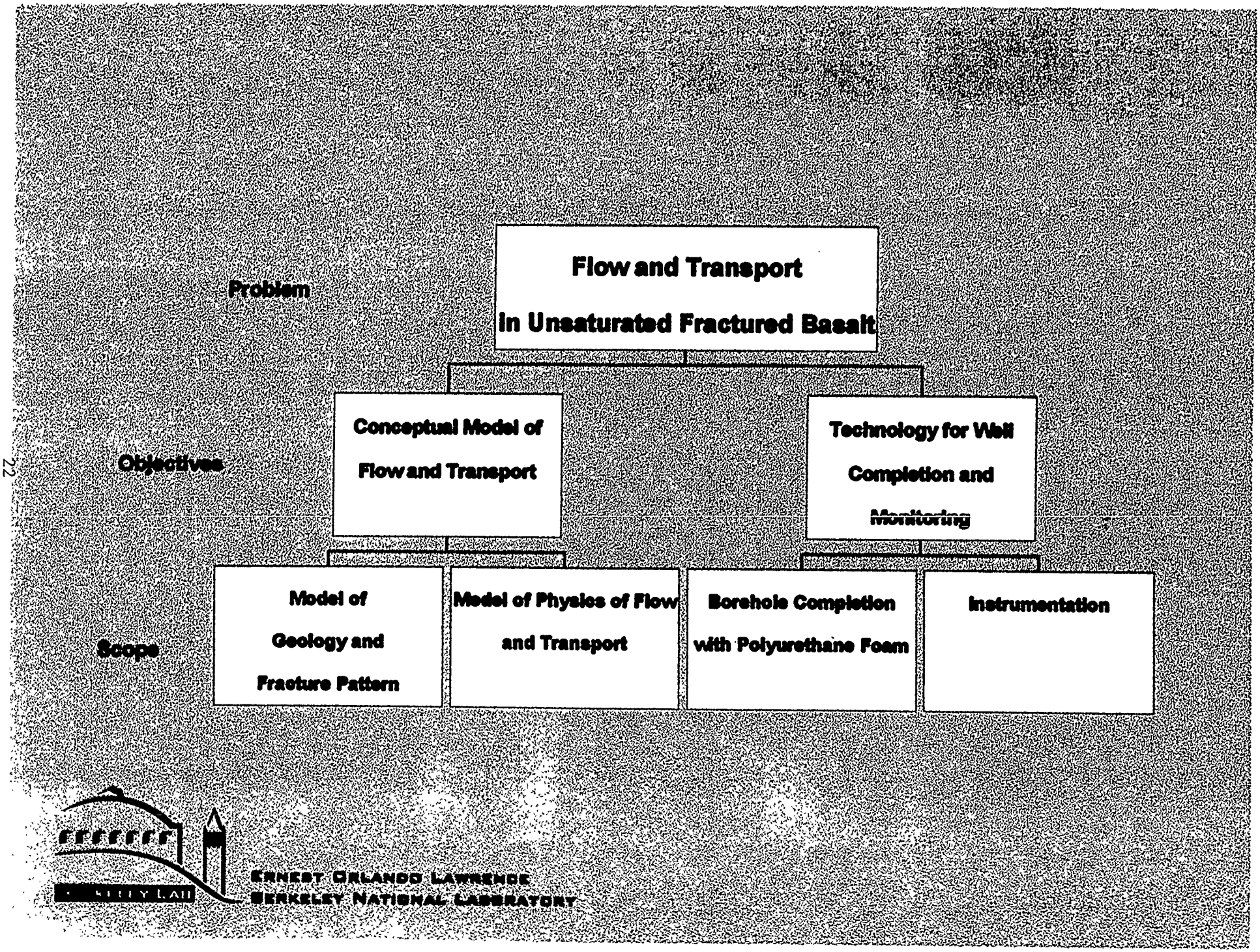
Problem
Flow and Transport
In Unsaturated Fractured Basalt
Objectives
Conceptual Model of
Flow and Transport
Technology for Well
Completion and
Monitoring
Scope
Model of
Geology and
Fracture Pattern
Model of Physics of Flow
and Transport
Borehole Completion
with Polyurethane Foam
Instrumentation
ERNEST ORLANDO LAWRENCE
BERKELEY NATIONAL LABORATORY

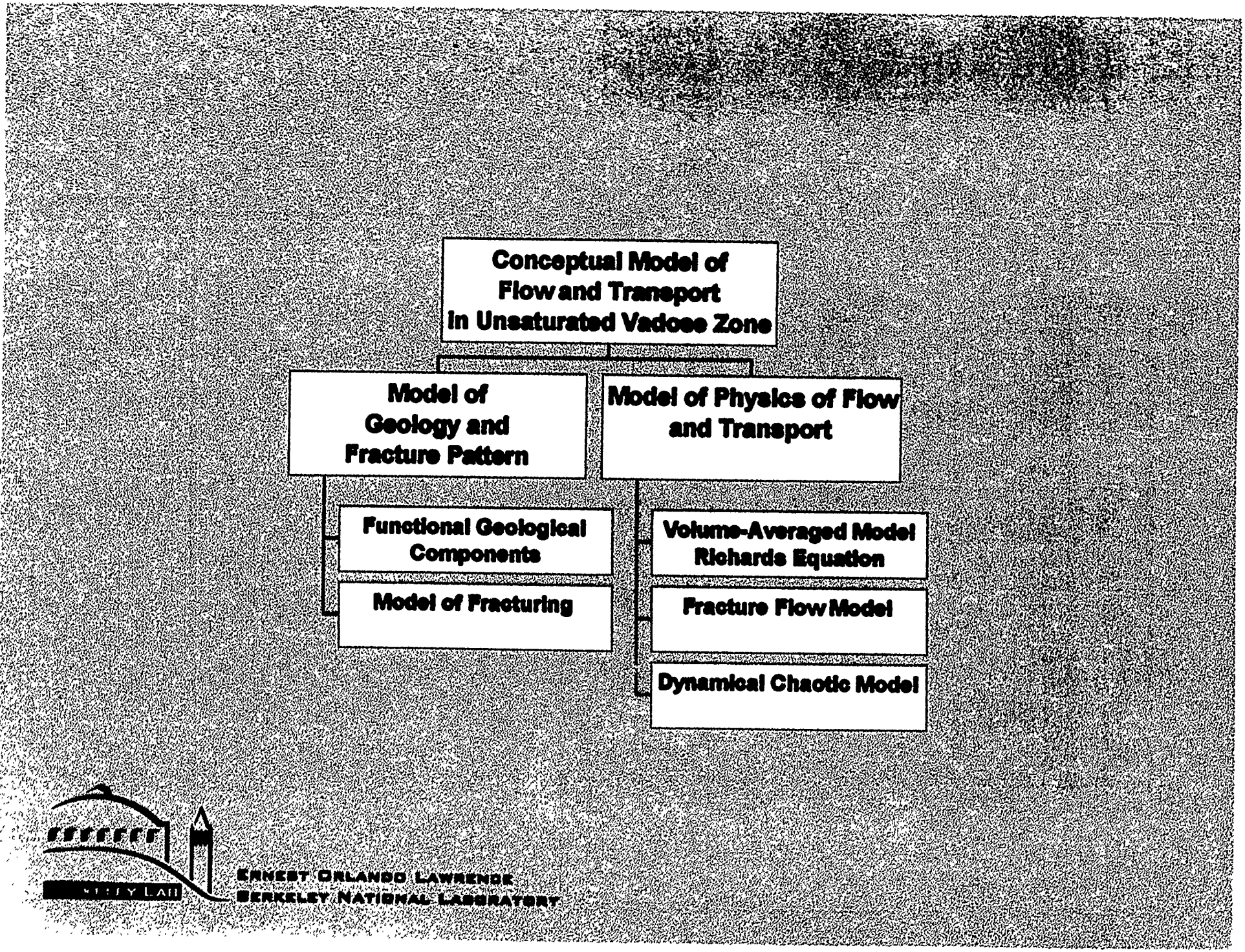
Conceptual Model of Flow and Transport in Unsaturated Vadose Zone
Model of Geology and Fracture Pattern
Model of Physics of Flow and Transport
Functional Geological Components
Model of Fracturing
Volume-Averaged Model Richards Equation
Fracture Flow Model
Dynamical Chaotic Model

Binary connectivity map of the fractures exposed below the investigation site at Box Canyon

Red shading --> Interpreted flow pathways from surface given simple percolation
Blue shading --> field evidence of past fluid flow egress from canyon wall

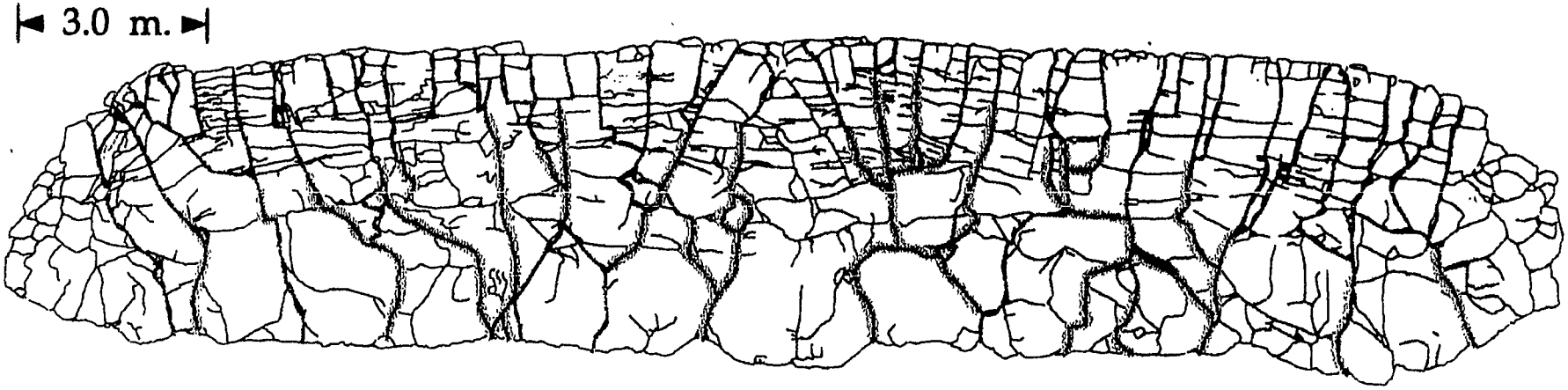

Perspective View of Well Locations – Box Canyon, Idaho

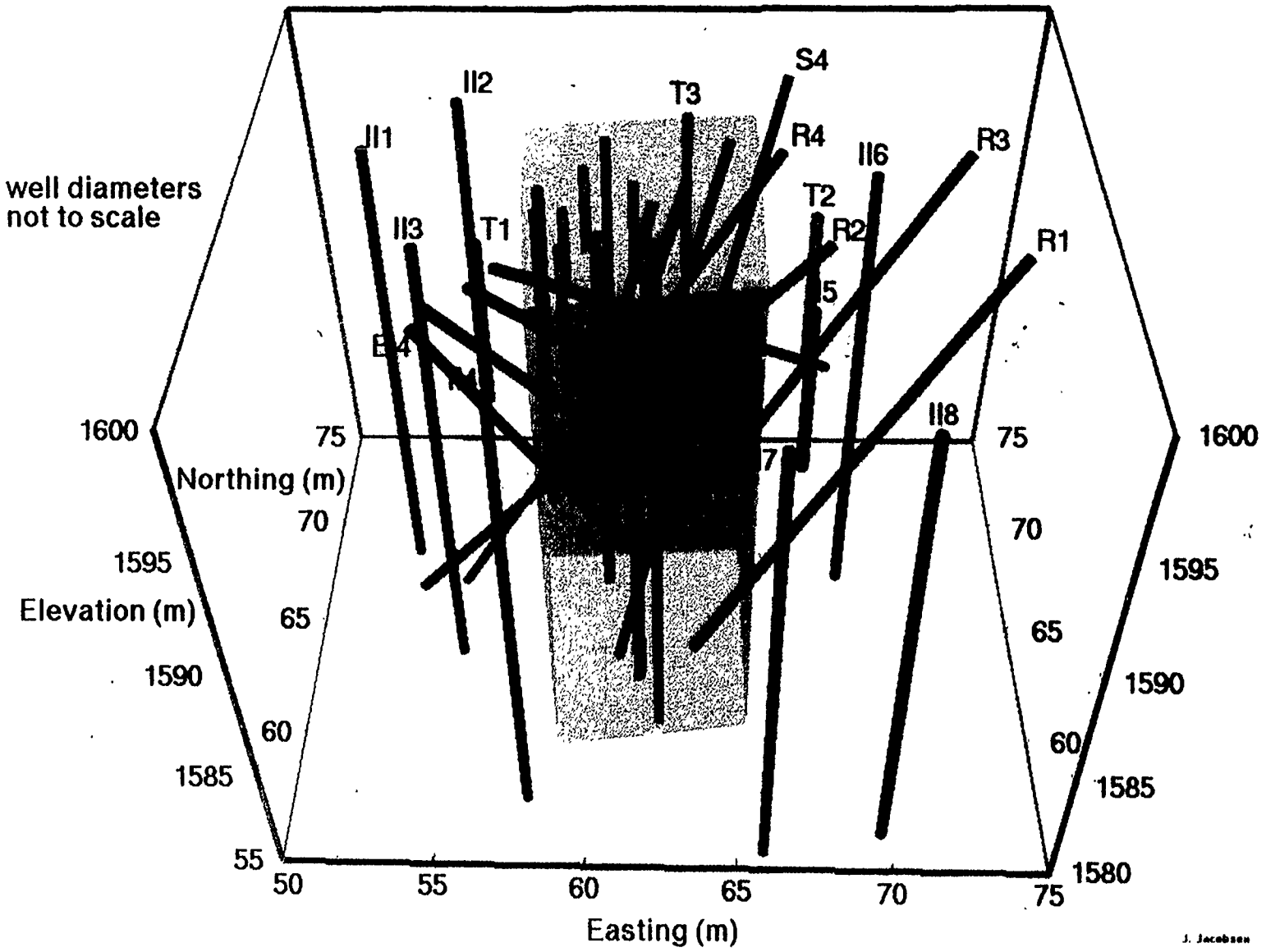

Single- and Cross-Borehole Monitoring Technology for Fractured Rocks

- **Slanted wells (to intersect vertical fractures)**

- **Borehole completion using polyurethane foam**

"Single-type" probes - tensiometers, suction lysimeters, time domain reflectometry, TDR, thermistors, miniature electrical resistivity, and ER, and

- **Cross-hole measurements - GPR, and ERT**

Installation Technology

Conventional

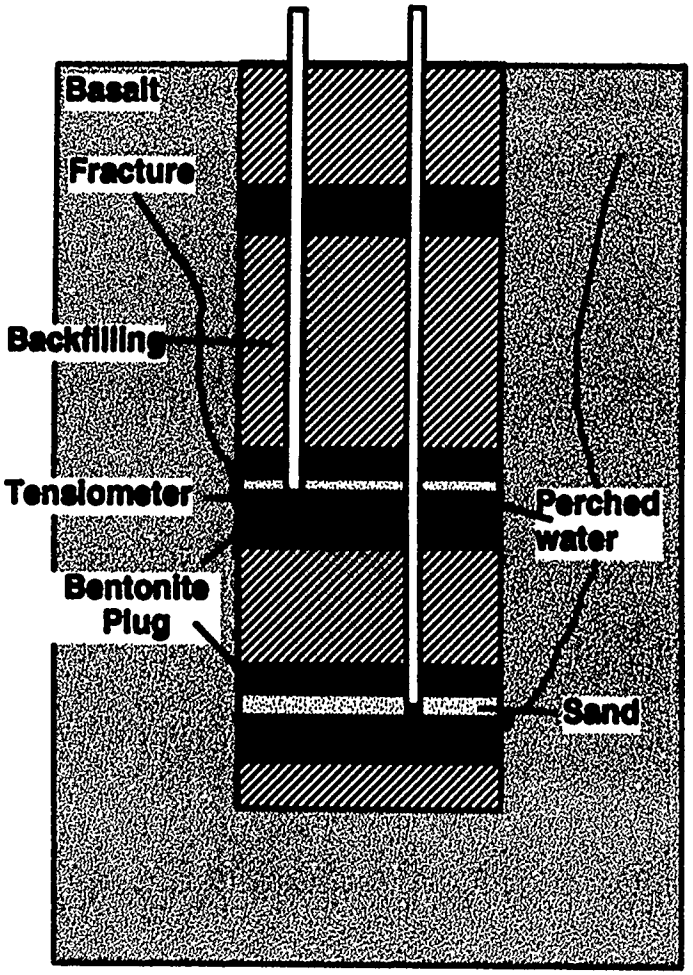

New

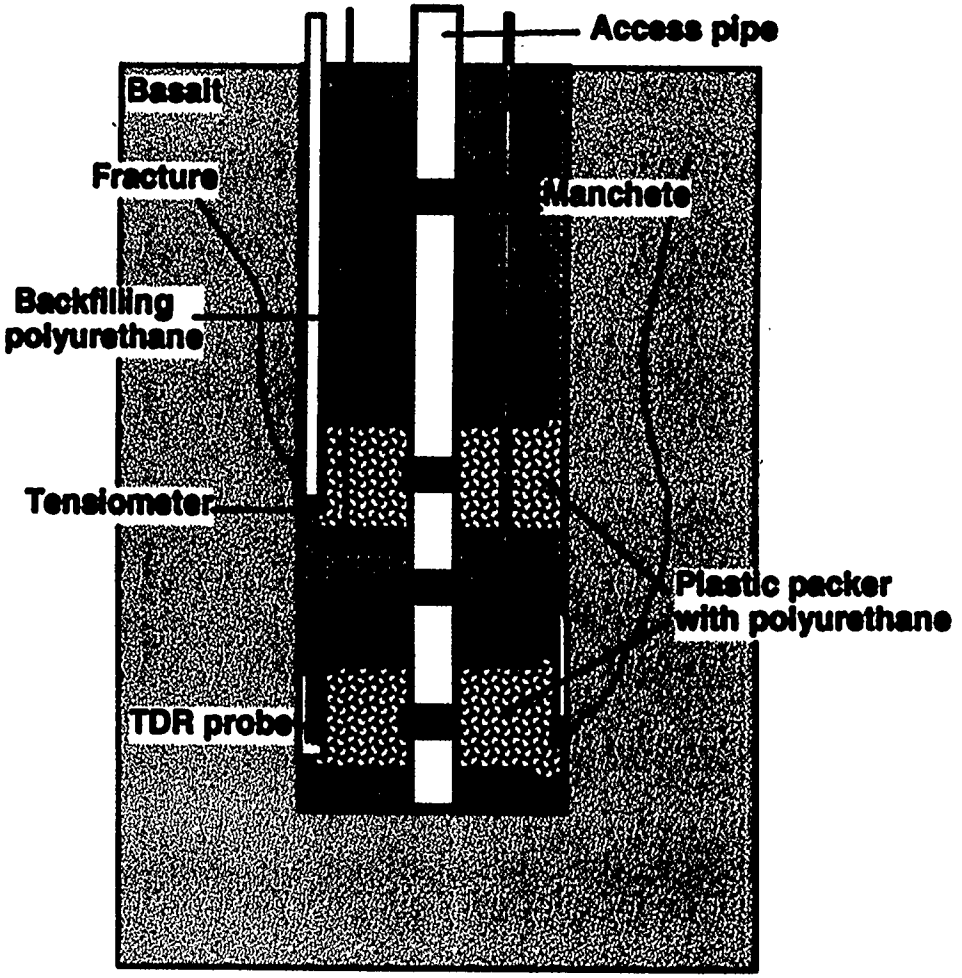

Conceptual Model of Tensiometry Measurements

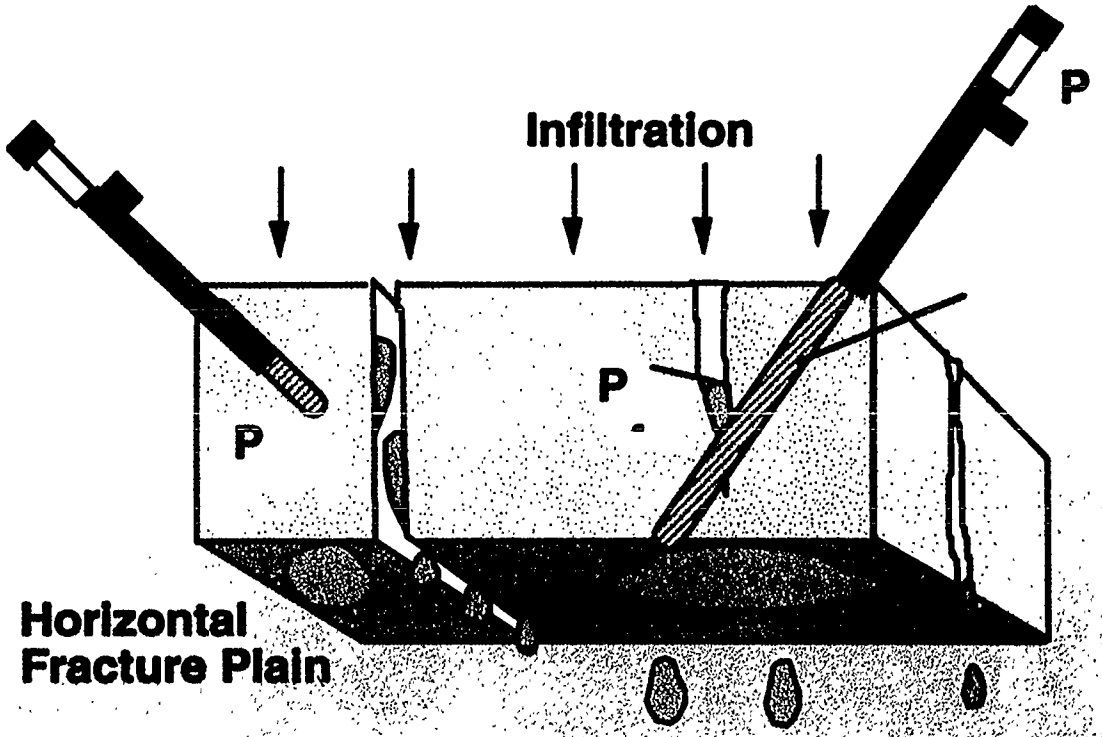

$$P = \alpha(t)P_{mx} + \beta(t)P_{fr} \quad \gamma(t)P_a$$

Scheme of Zones of Influence of Sensors in in Fractured Rocks

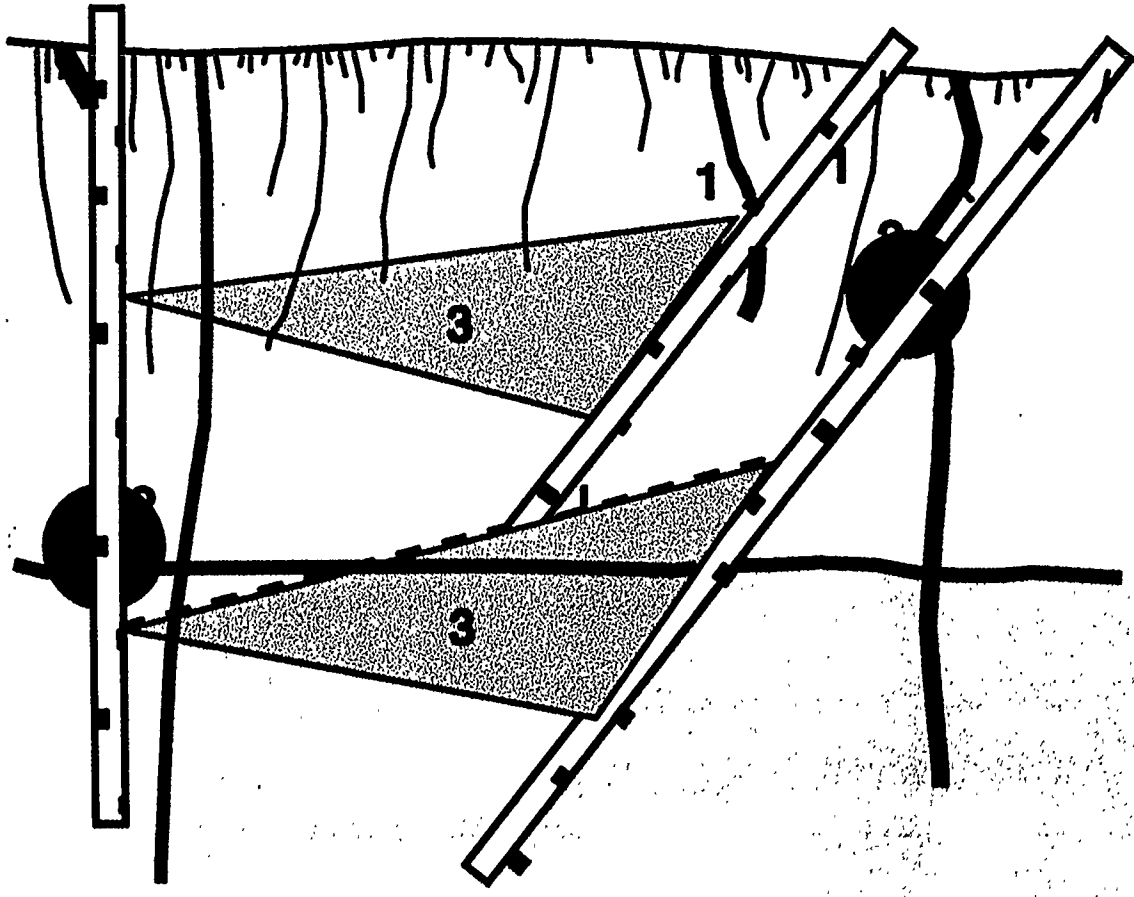

1. Passive measurements (ER probes, TDR, tensiometers)

2. Near borehole measurements (suction lysimeter, neutron logger)

3. Cross-hole measurements (ERT, GPR)

Cumulative Infiltration
Box Canyon Pulsed Infiltration Tests

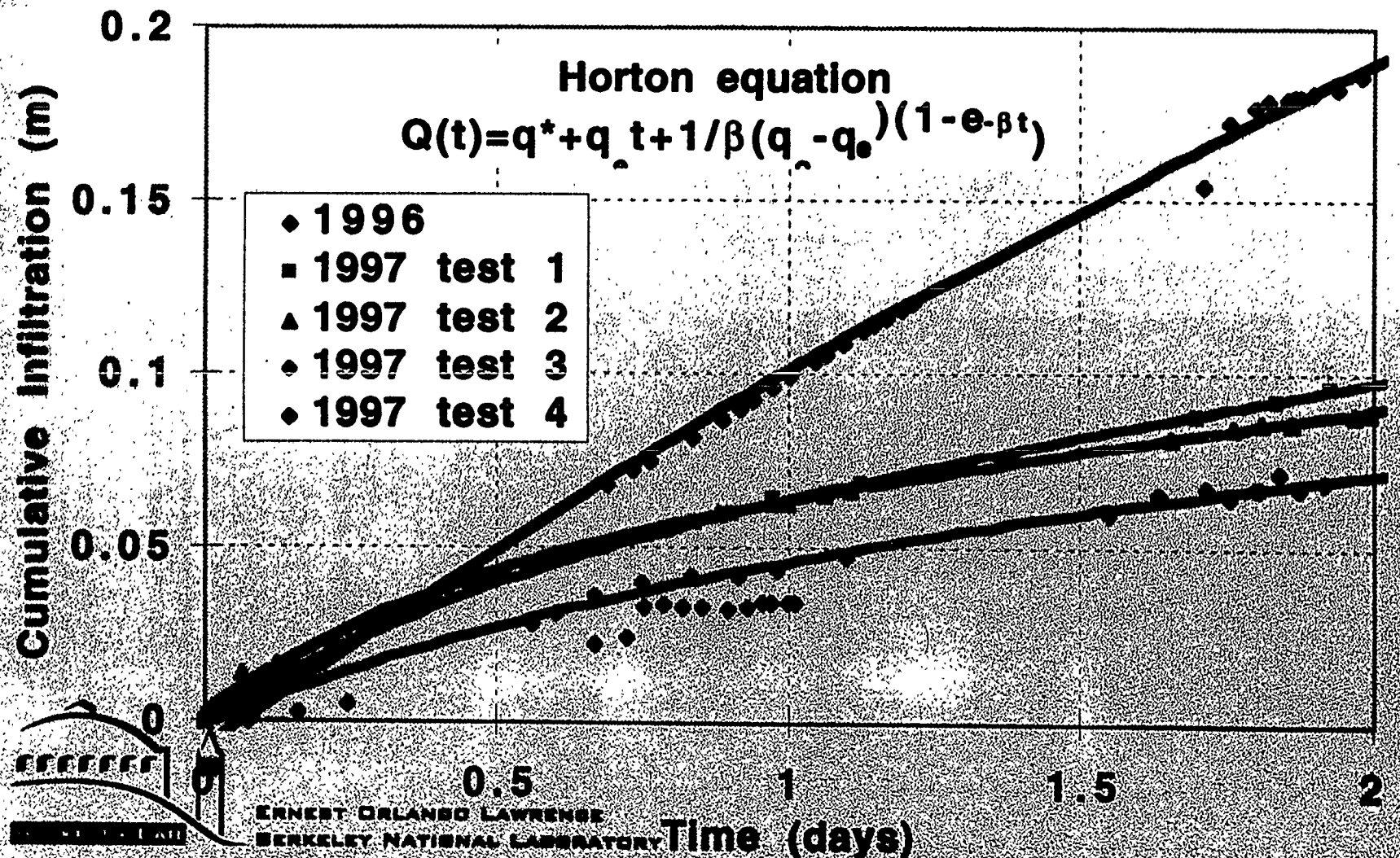

Relative neutron counts in well R1 before, during, and after each pulsed infiltration test

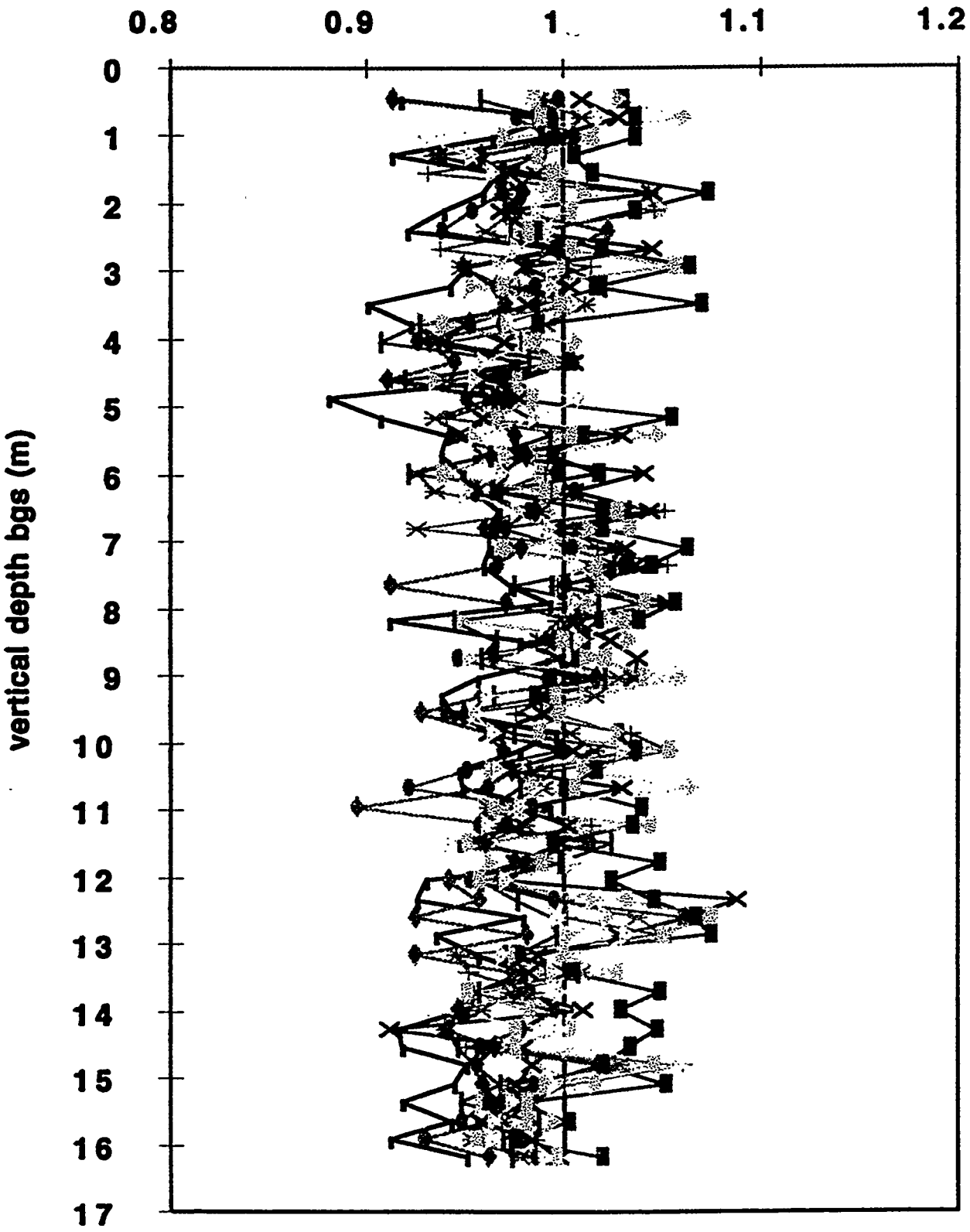

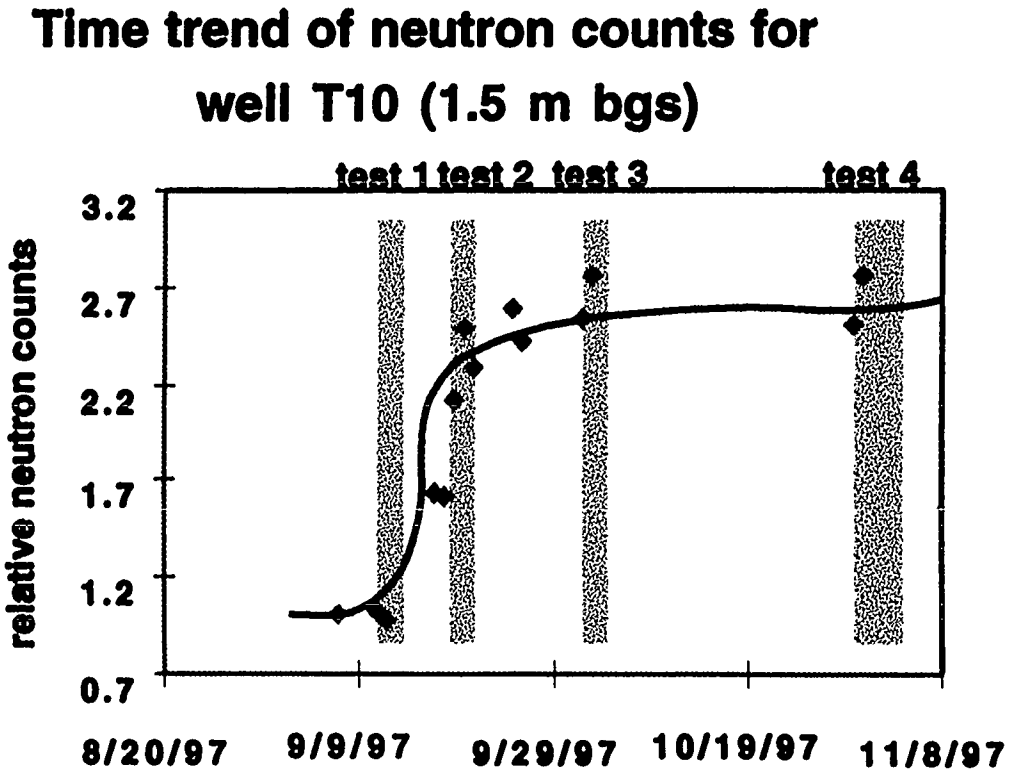
Time trend of neutron counts for well T10 (1.5 m bgs)
test 1
test 2
test 3
test 4
relative neutron counts
3.2
2.7
2.2
1.7
1.2
0.7
8/20/97
9/9/97
9/29/97
10/19/97
11/8/97

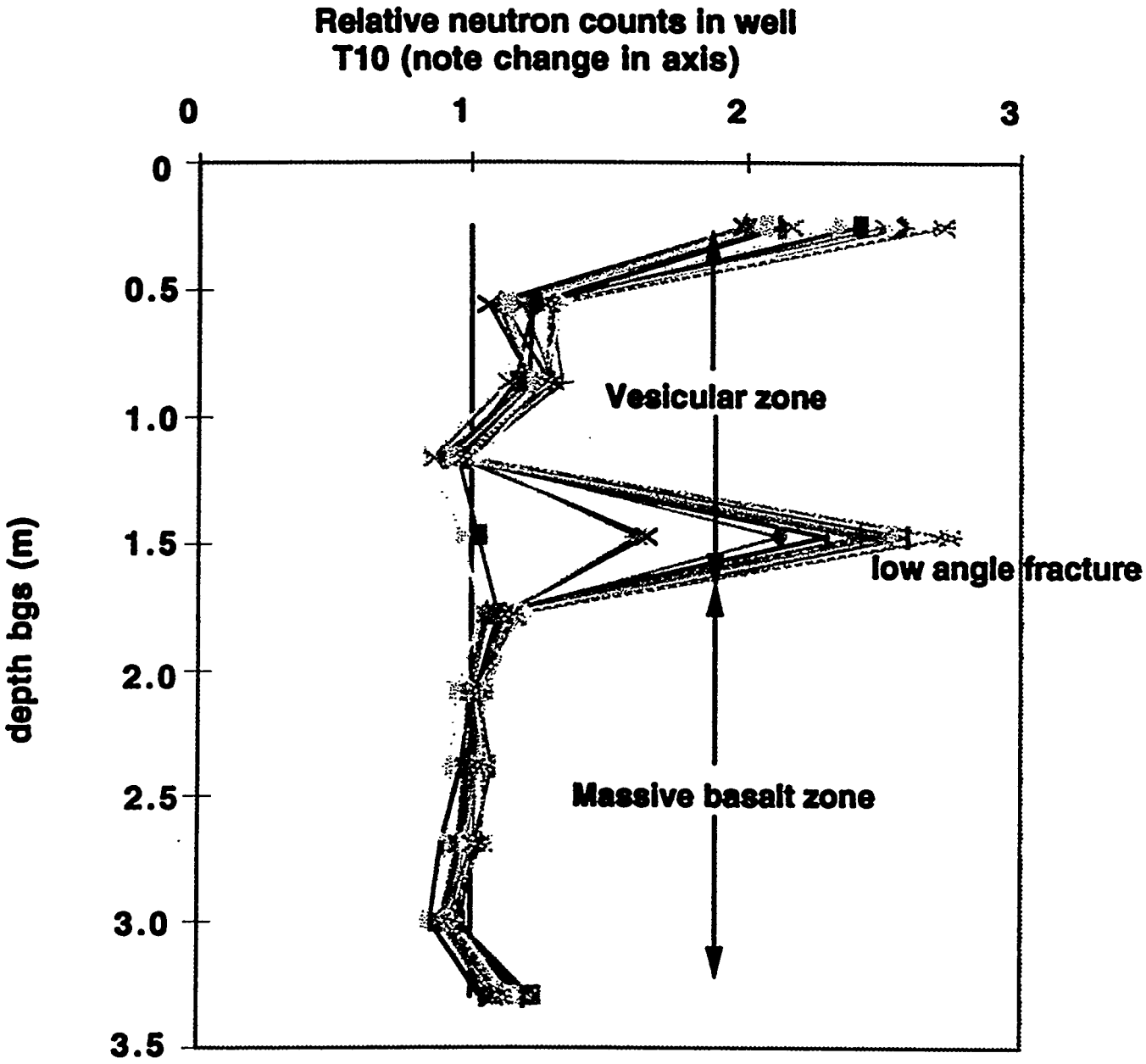
Relative neutron counts in well
T10 (note change in axis)
0
1
2
3
0
0.5
1.0
1.5
2.0
2.5
3.0
3.5
depth bgs (m)
Vesicular zone
low angle fracture
Massive basalt zone

Moisture content (based on neutron logging)

- The same lithological units were affected in 1996 and 1997
- The rocks are much more saturated in 1997 than in 1996
- NO changes in the slanted holes during the 1997 tests
- Changes from the surface to 1.5 m within the pond in 1997

Results of Measurements of Water Pressure

- Fast response
- Preferential and bypass flow
- Fracture-matrix interaction

Changes of Water Pressure during the 1996 Infiltration Test

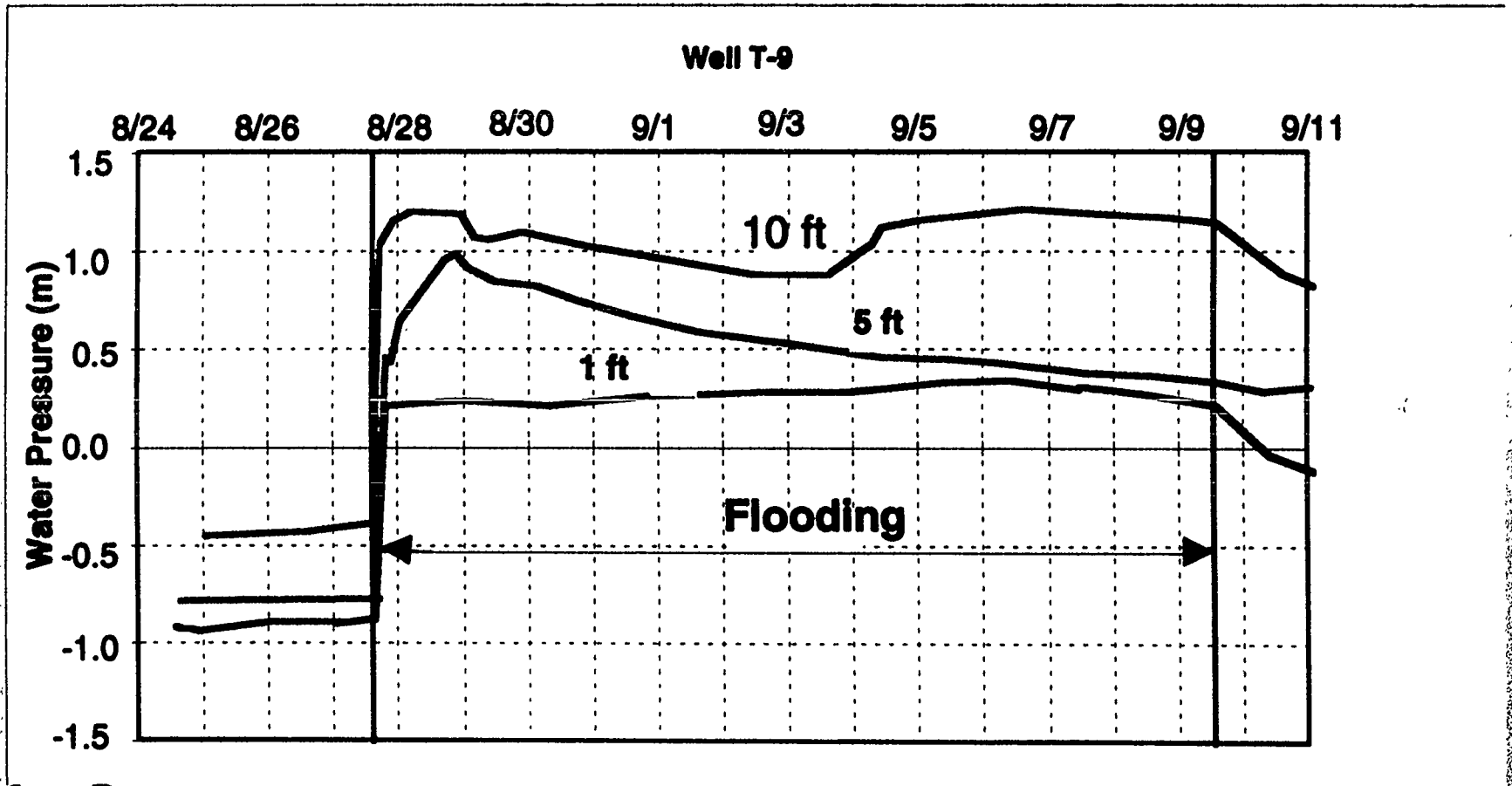

What Does a Tensiometer Measure in Fractured Rocks?

- The gauge pressure is primarily affected by the conducting component that transmits water into or out of the ceramic cup of the tensiometer:
  - During drying - by matrix pressure, and
  - During wetting - by the fracture pressure.

Initial flow rate vs. Final flow rate for pulsed infiltration tests (1997) and continuous infiltration test (1996)

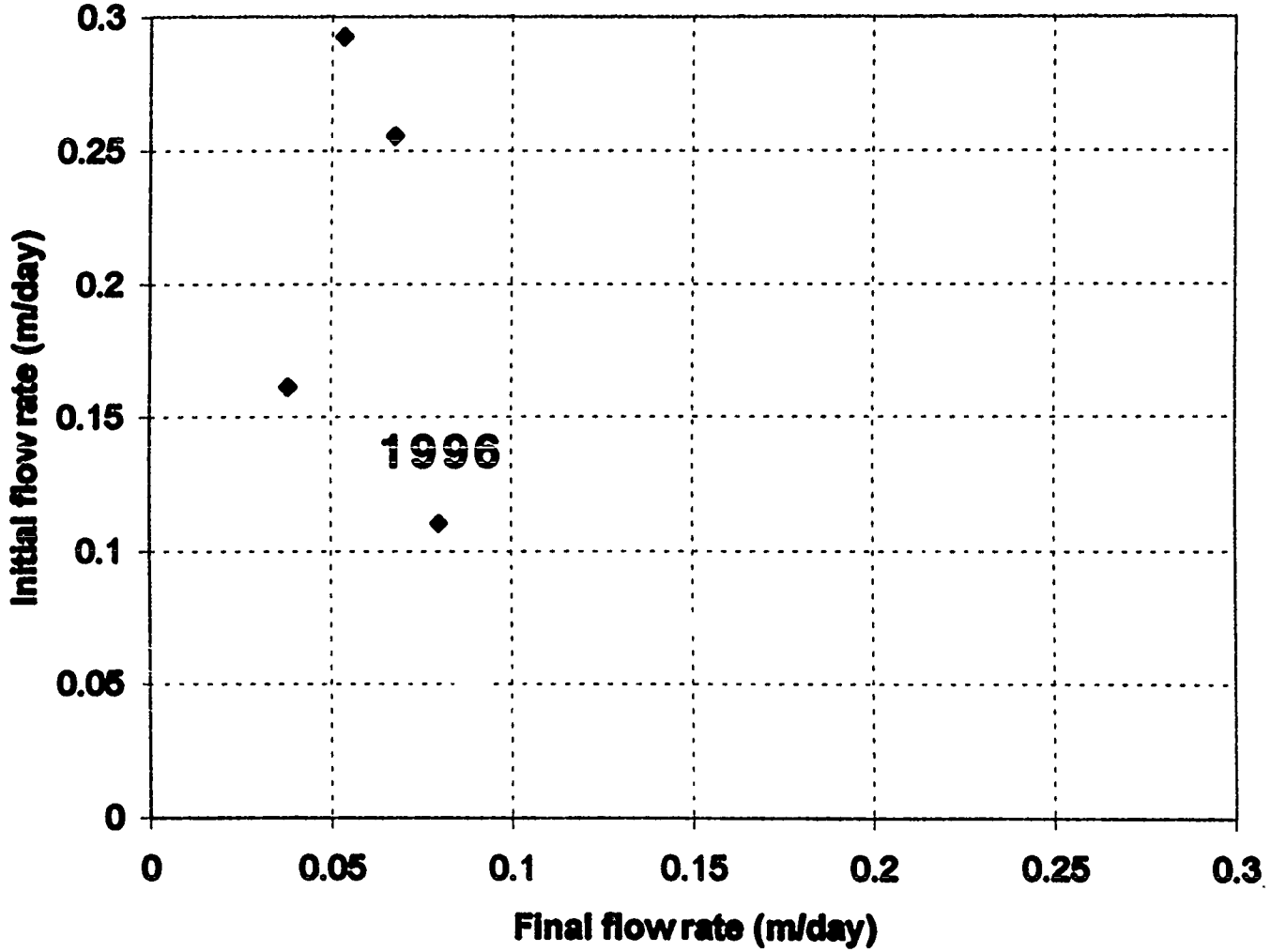

Types of Tests

- 1996 - 2-week continuous ponding including a 2-day pulse of 3 g/l KBr
-
- 1997 - Four 2-day pulses of ponding with 3 g/l of KBr

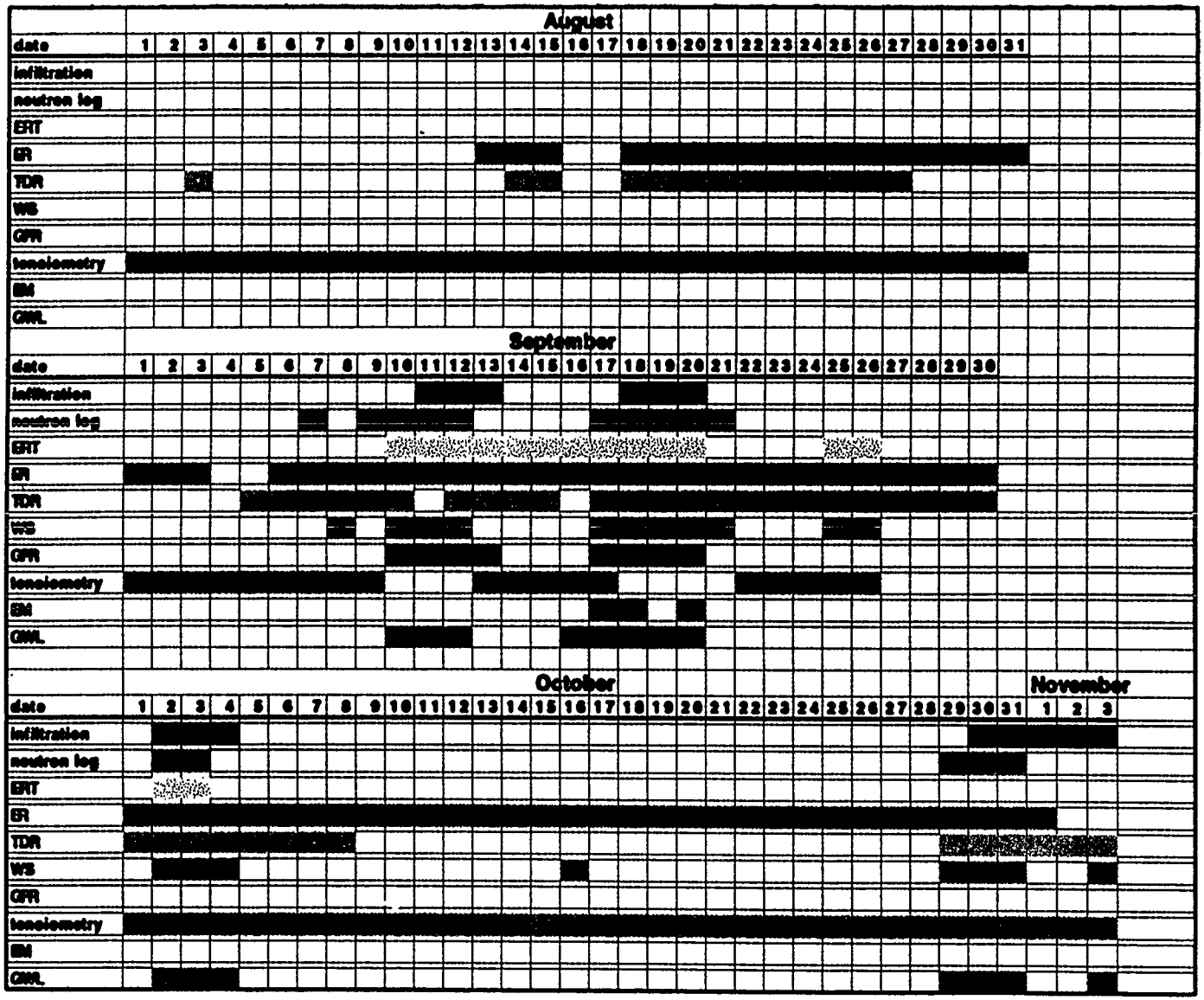
August
date
1 2 3 4 5 6 7 8 9 10 11 12 13 14 15 16 17 18 19 20 21 22 23 24 25 26 27 28 29 30 31
infiltration
neutron log
ERT
ER
TDR
WS
GPR
tensiometry
EM
GWL
September
date
1 2 3 4 5 6 7 8 9 10 11 12 13 14 15 16 17 18 19 20 21 22 23 24 25 26 27 28 29 30
infiltration
neutron log
ERT
ER
TDR
WS
GPR
tensiometry
EM
GWL
October
November
date
1 2 3 4 5 6 7 8 9 10 11 12 13 14 15 16 17 18 19 20 21 22 23 24 25 26 27 28 29 30 31 1 2 3
infiltration
neutron log
ERT
ER
TDR
WS
GPR
tensiometry
EM
GWL

test	start of ponding	end of ponding	volume of H_2O infiltrated (m^3)	mass of salt infiltrated (kg)
test 4	10/30/97 13:51	11/3/97 15:00	6.79	20.37
test 3	10/15/97 16:40	10/4/97 16:00	3.91	11.73
test 2	9/18/97 14:56	9/20/97 16:46	5.01	15.03
test 1	9/11/97 12:15	9/13/97 12:45	5.42	16.26
1997 totals	—	—	21.13	63.39
1998	8/27/98 12:57	9/9/98 11:00	25.00	38.64

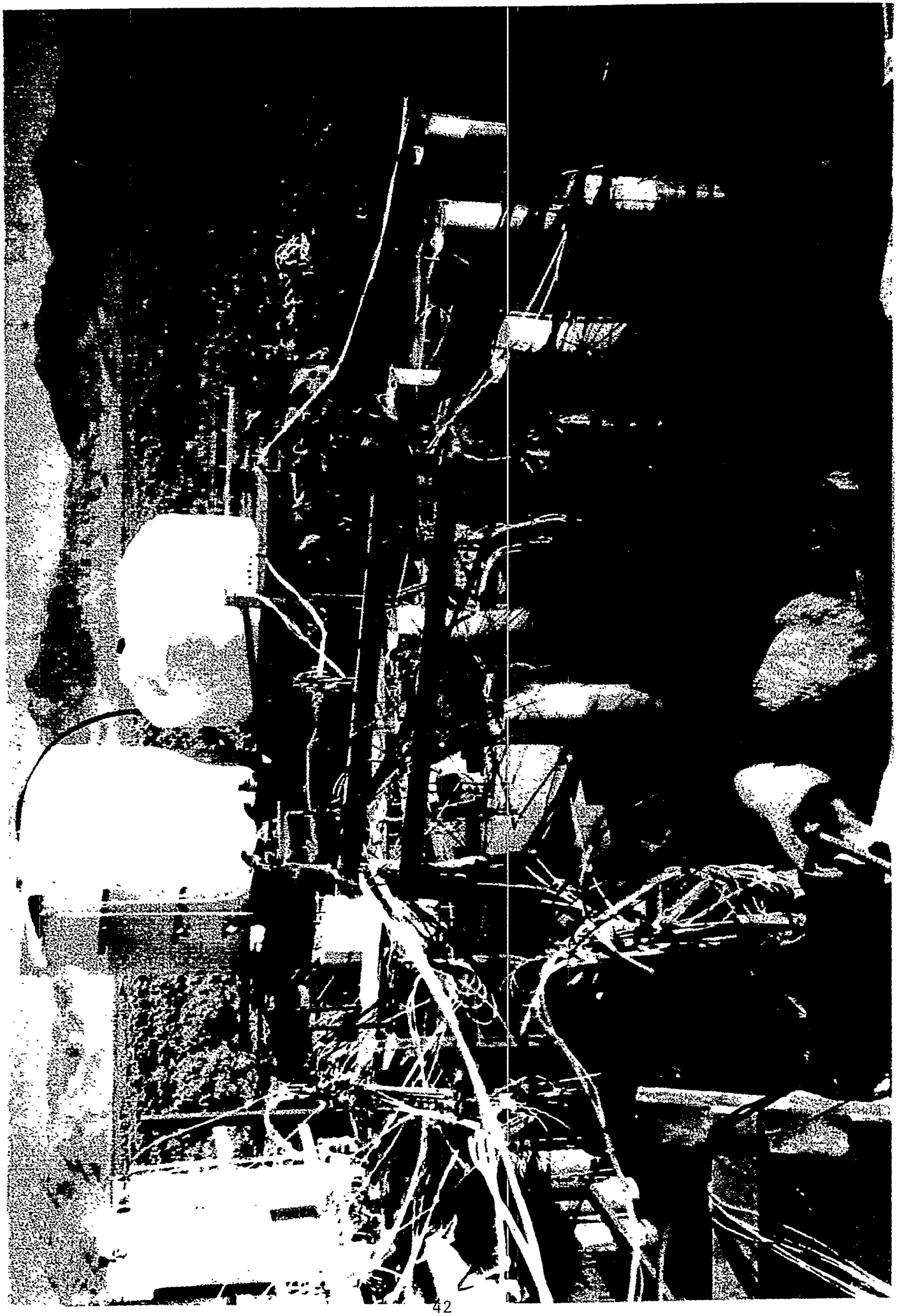

Cumulative Infiltration
Box Canyon Pulsed Infiltration Tests

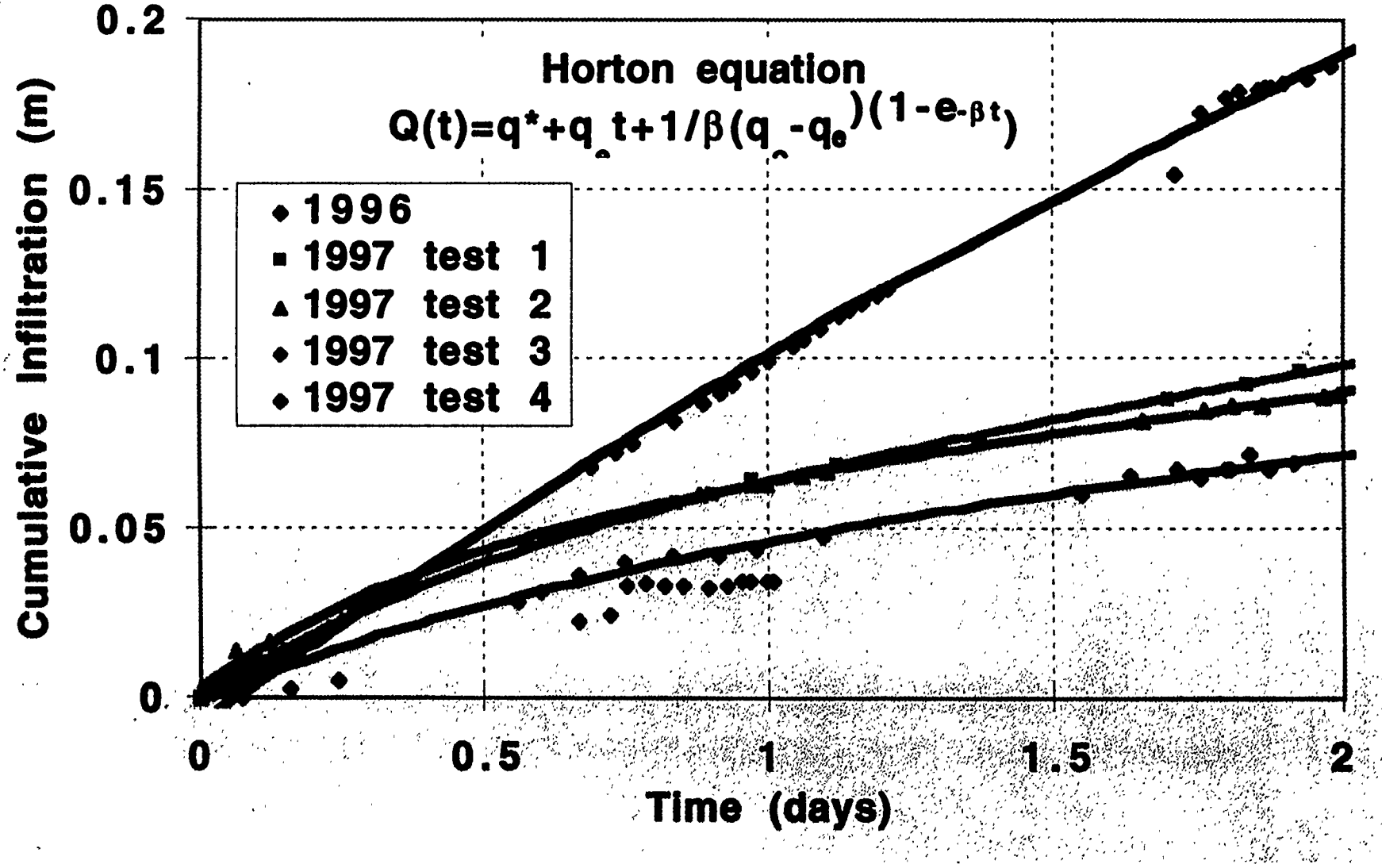

Instantaneous flux for pulsed infiltration tests calculated from parameters using Horton's equation

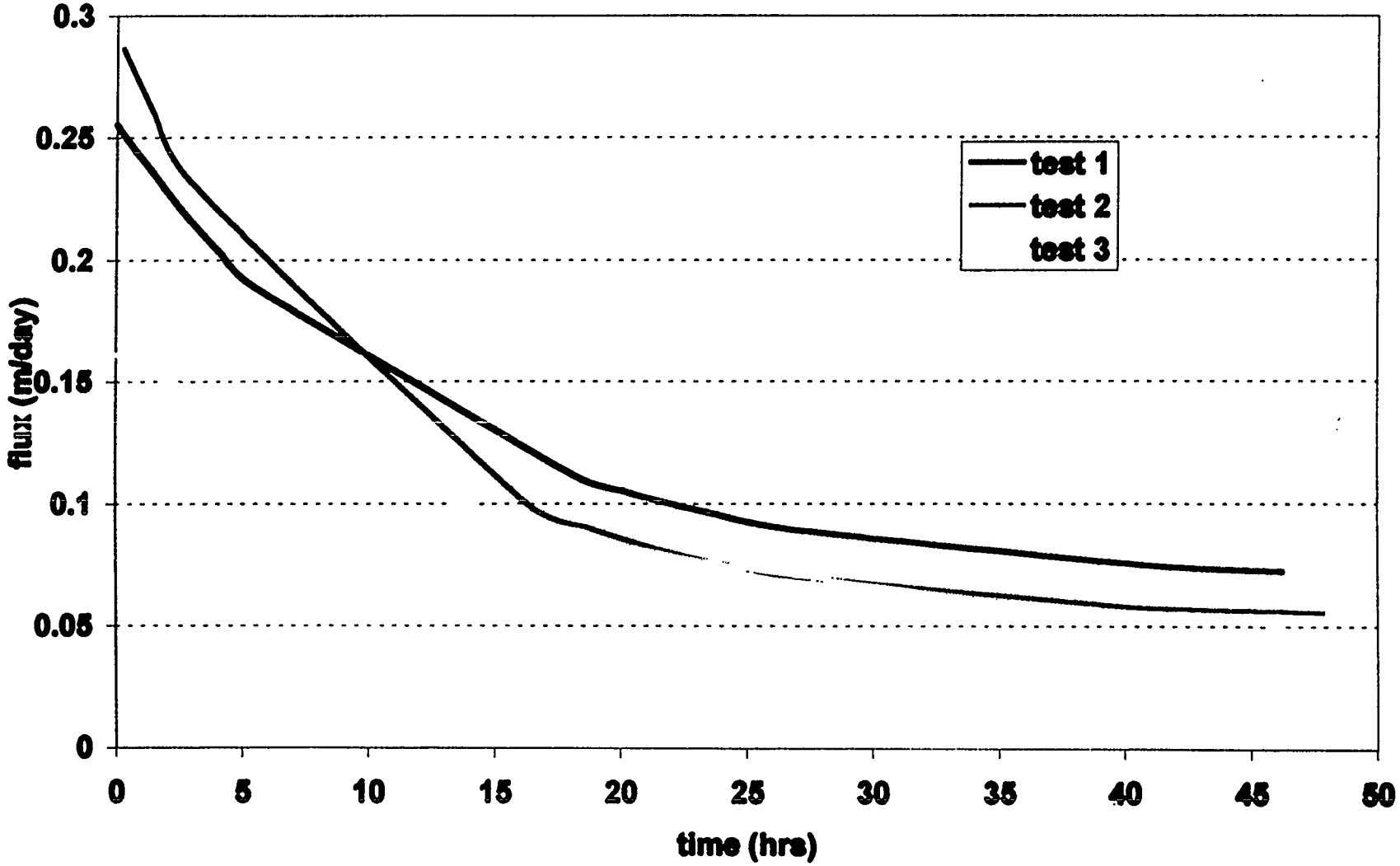

Flow rate

- Exponential temporal decrease in the flow rate in all tests

- Significant variation of the flow rate at the beginning of infiltration, and then convergence to a narrow range

Miniature ER probes

- Background Conditions:
  - Lower resistivity in fracture zones and rubble zones
    Higher resistivity in dense basalt zones
- Infiltration Tests:
  - Decrease in resistivity as affected by the tracer movement in hydraulically conductive zones:
    - Central fractured zone
    - Rubble zone
    - Some single fractures
  - No changes in dense basalt

Breakthrough Curves

- Multi-modal curves associated with transport through different sets of fractures

- Advective transport is a main process of chemical transport

Bromide tracer breakthrough, Depth 0.3 m. 1996 Infiltration Test at Box Canyon, Idaho. All three wells are located within the infiltration pond.

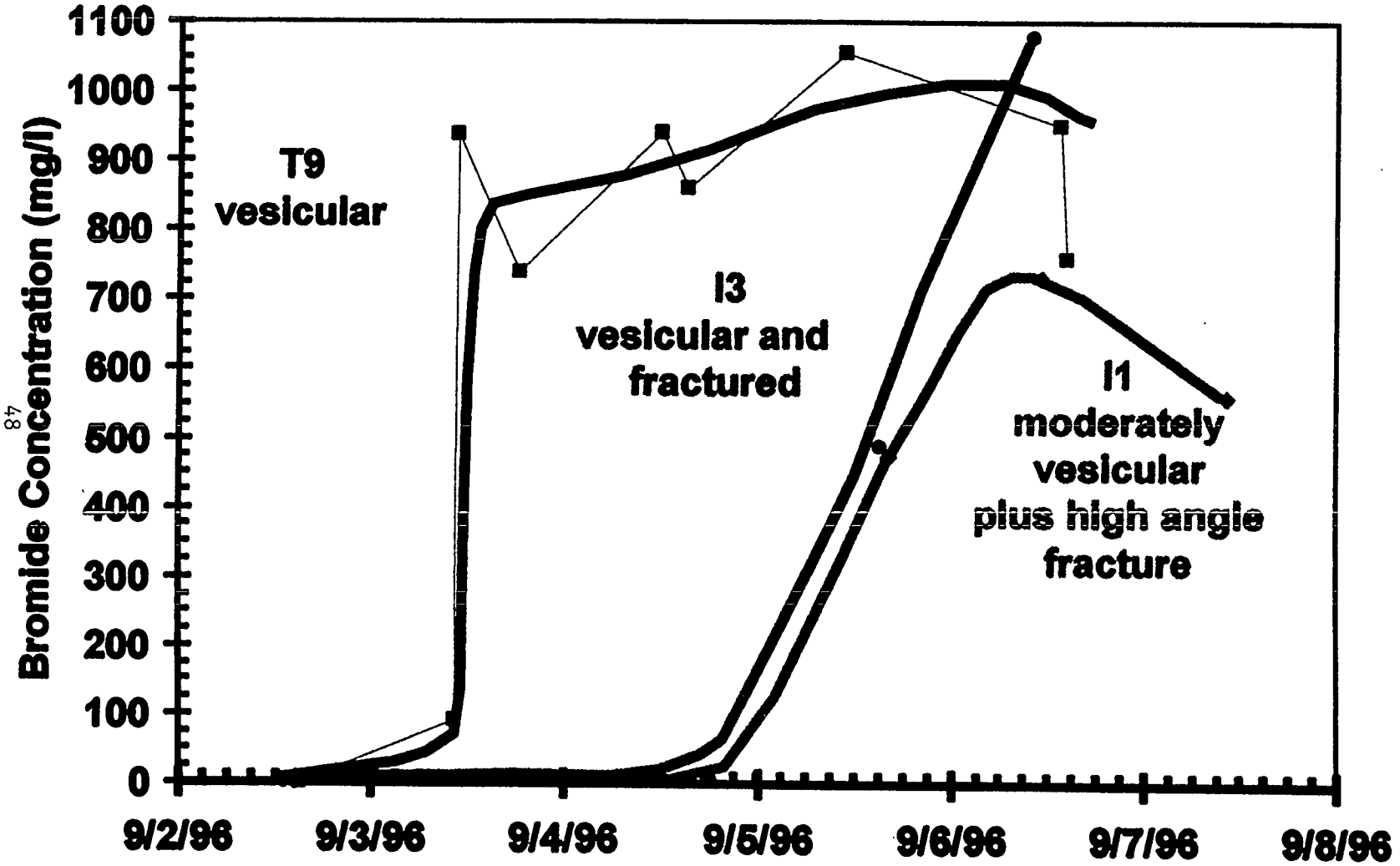

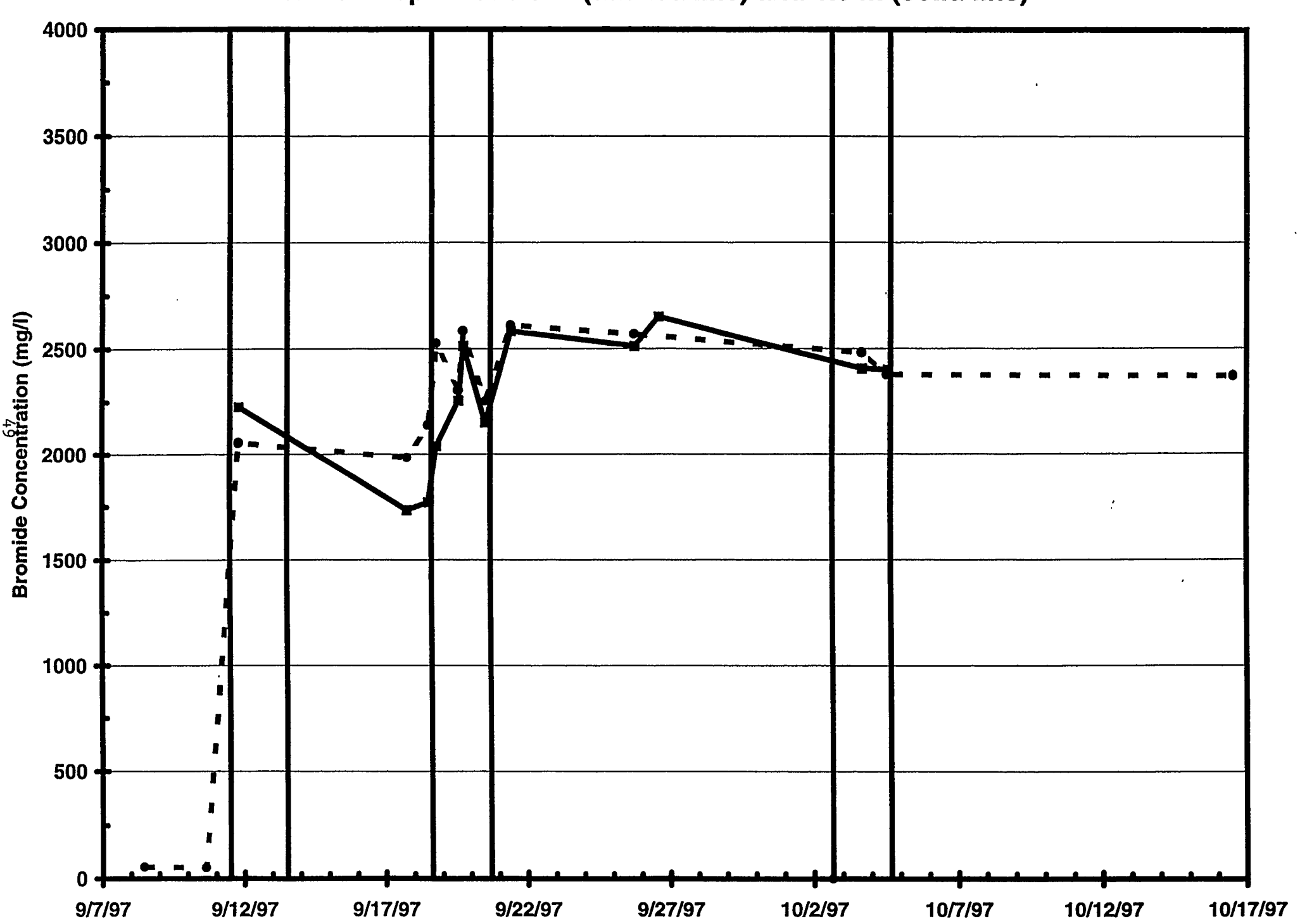
Well T9 - Depths of 0.3 m (dashed line) and 1.5 m (solid line)
Bromide Concentration (mg/l)
4000
3500
3000
2500
2000
1500
1000
500
0
9/7/97
9/12/97
9/17/97
9/22/97
9/27/97
10/2/97
10/7/97
10/12/97
10/17/97

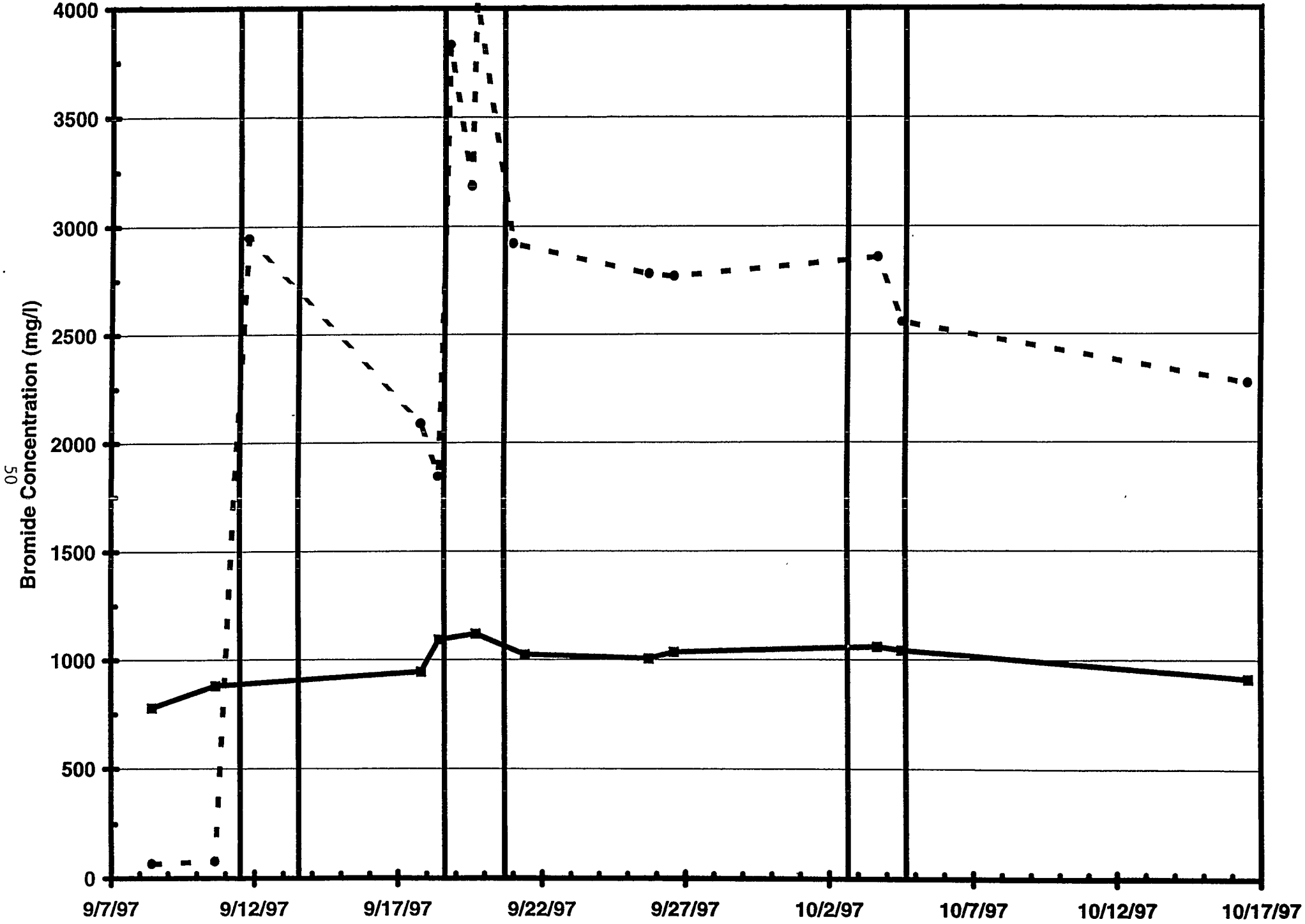
Well T7 - Depths of 0.6 m (2 ft) (dashed line) and 1.8 m (6 ft) (solid line)
Bromide Concentration (mg/l)
4000
3500
3000
2500
2000
1500
1000
500
0
9/7/97
9/12/97
9/17/97
9/22/97
9/27/97
10/2/97
10/7/97
10/12/97
10/17/97

Well 14 - Depths of 3.8 m (dotted line), 4.3 m (dashed line), and 5.8 m (solid line). Note change in vertical scale.

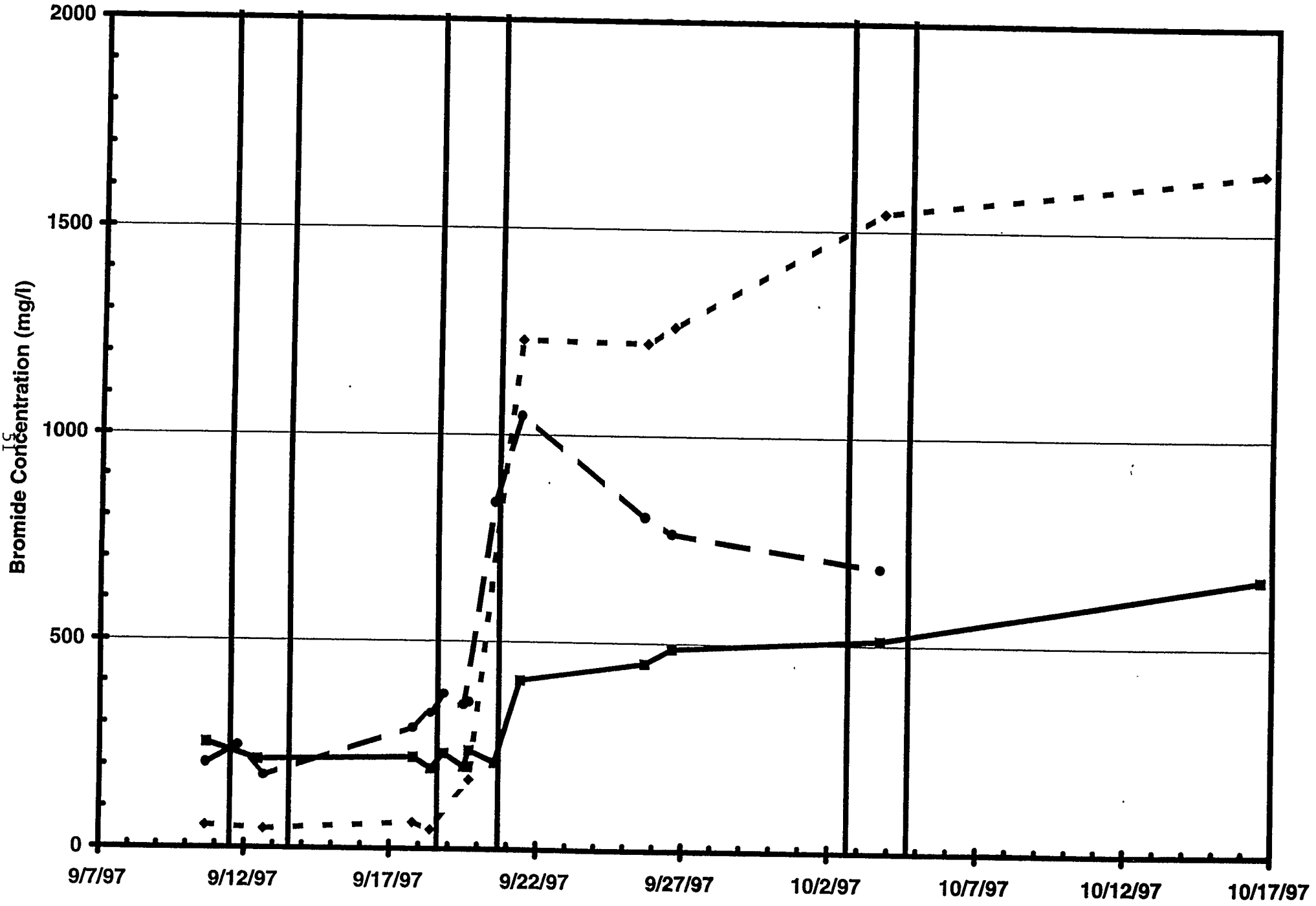

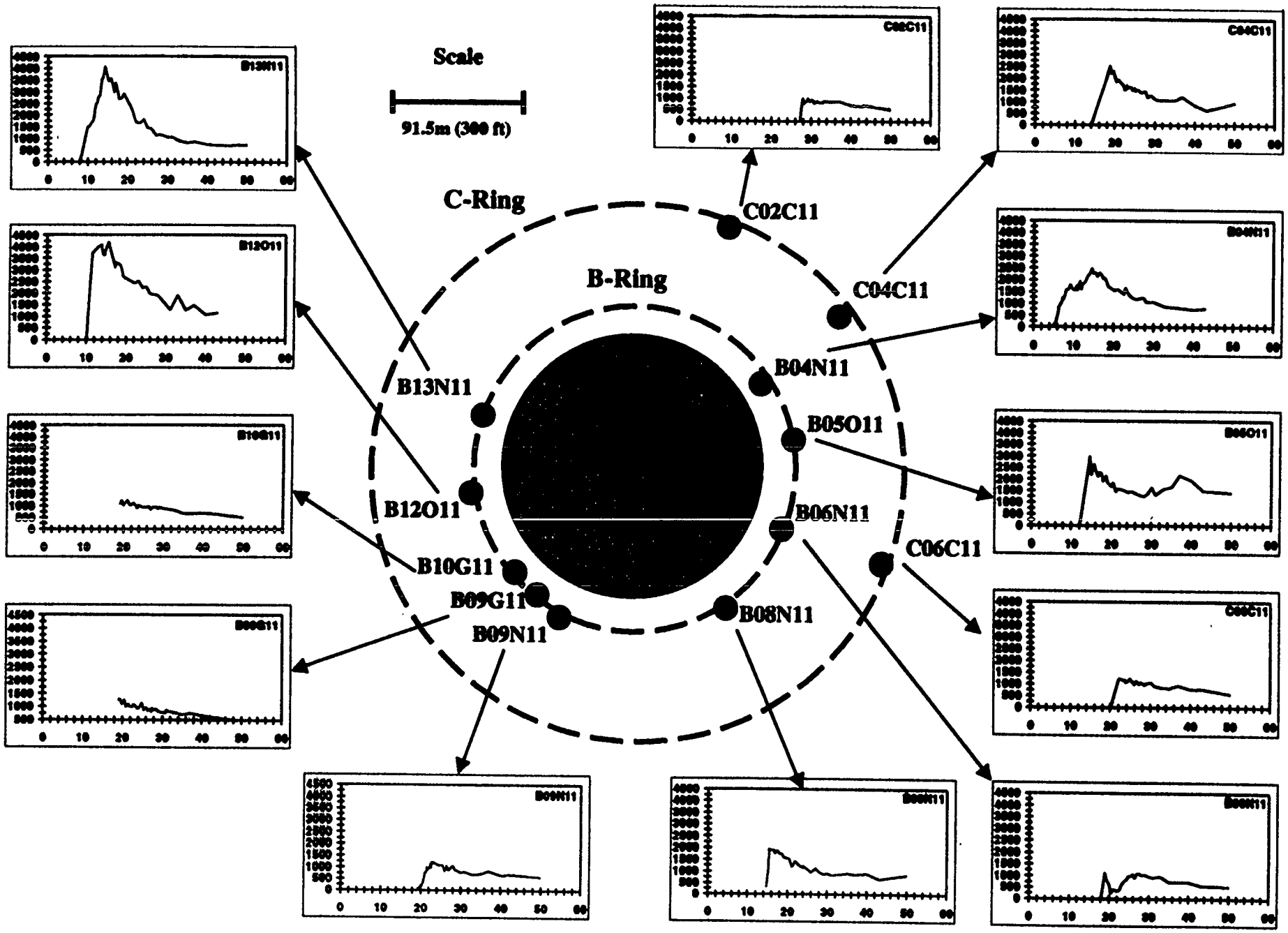
Scale
91.5m (300 ft)
C-Ring
B-Ring
C02C11
C04C11
B04N11
B05O11
B06N11
C06C11
B08N11
B09N11
B09G11
B10G11
B12O11
B13N11

Water level in well I-5 during pulsed infiltration tests

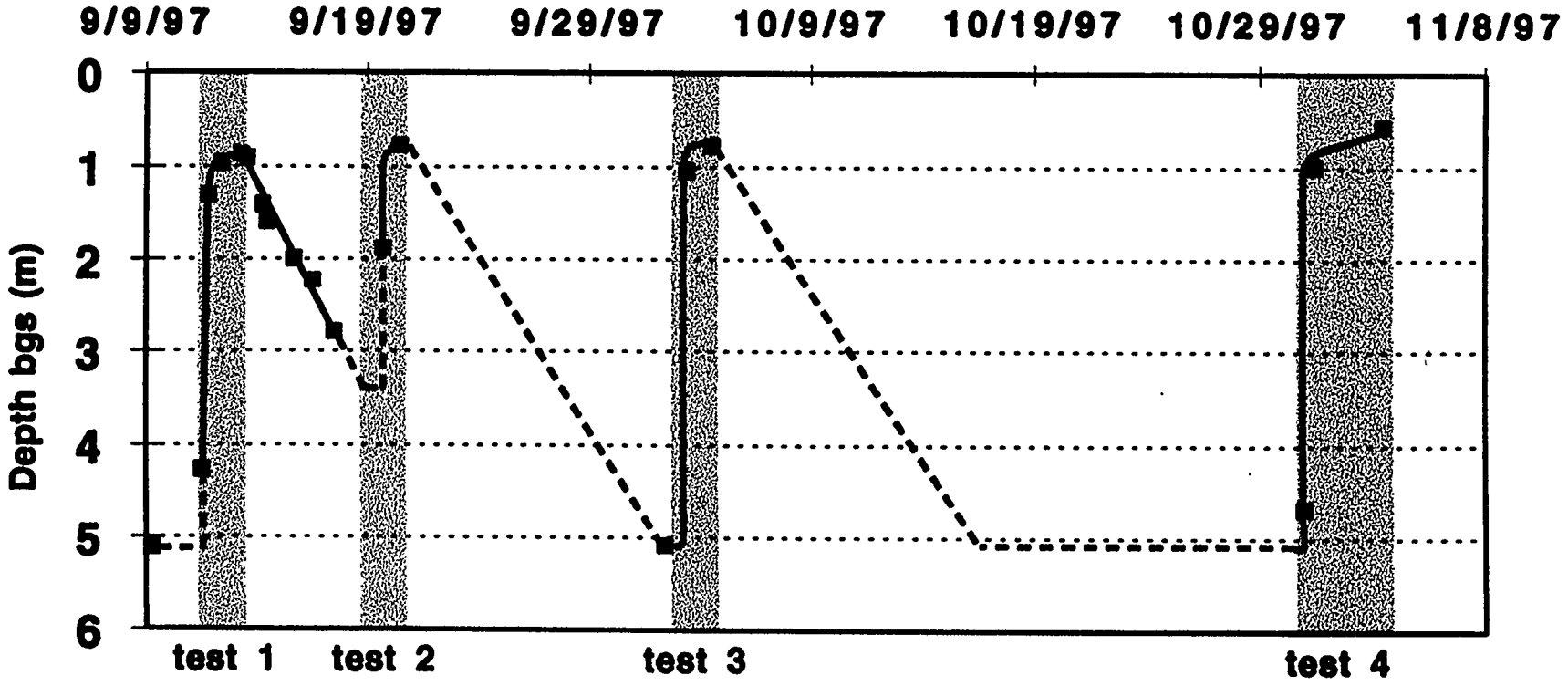

Geological Components of Fractured Basalt

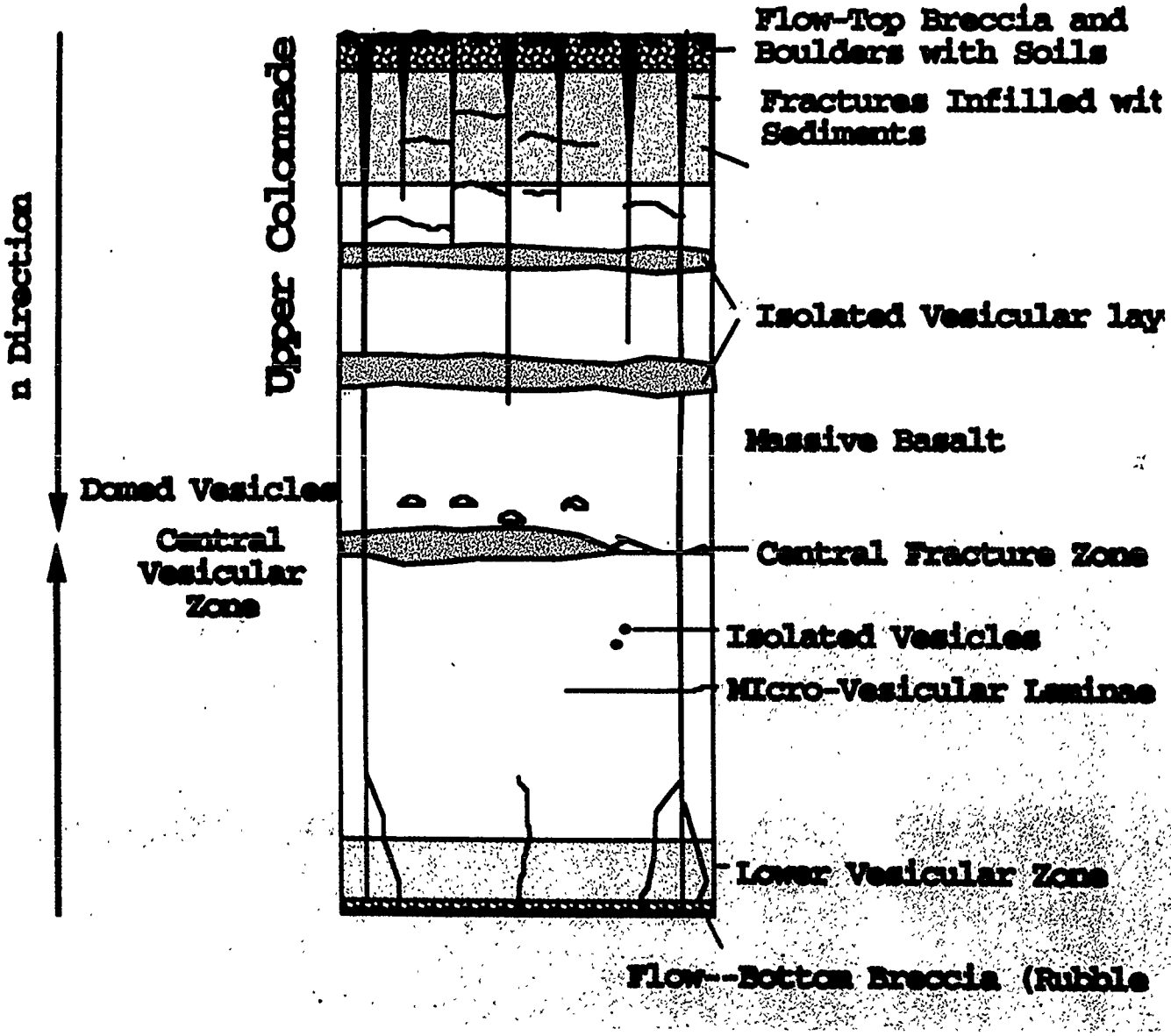

Fractured Basalt:

– is highly heterogeneous with localized and fast flow paths.

- has non-conductive fractures and matrix where contaminants are accumulated.

Numerical Models

- **TOUGH2**
- **PathFinder**
- **Chaotic Model**

IMPROVED CONCEPTUAL MODEL OF WATER FLOW IN FRACTURED BASALT

- Transient unsaturated-saturated conditions
- Variable temporal and spatial permeability of soils and rocks
- Preferential flow:

  -- vertical flow along column bounding fractures

  -- lateral flow in the central fractured zone and rubble zone
- Rapid redistribution of water in fractures
- Sorption of water by matrix
- Entrapped air
- Small changes in initial and boundary conditions may lead to significant changes in water pressure, saturation, permeability

II.2

Radar Results at Box Canyon

John Peterson

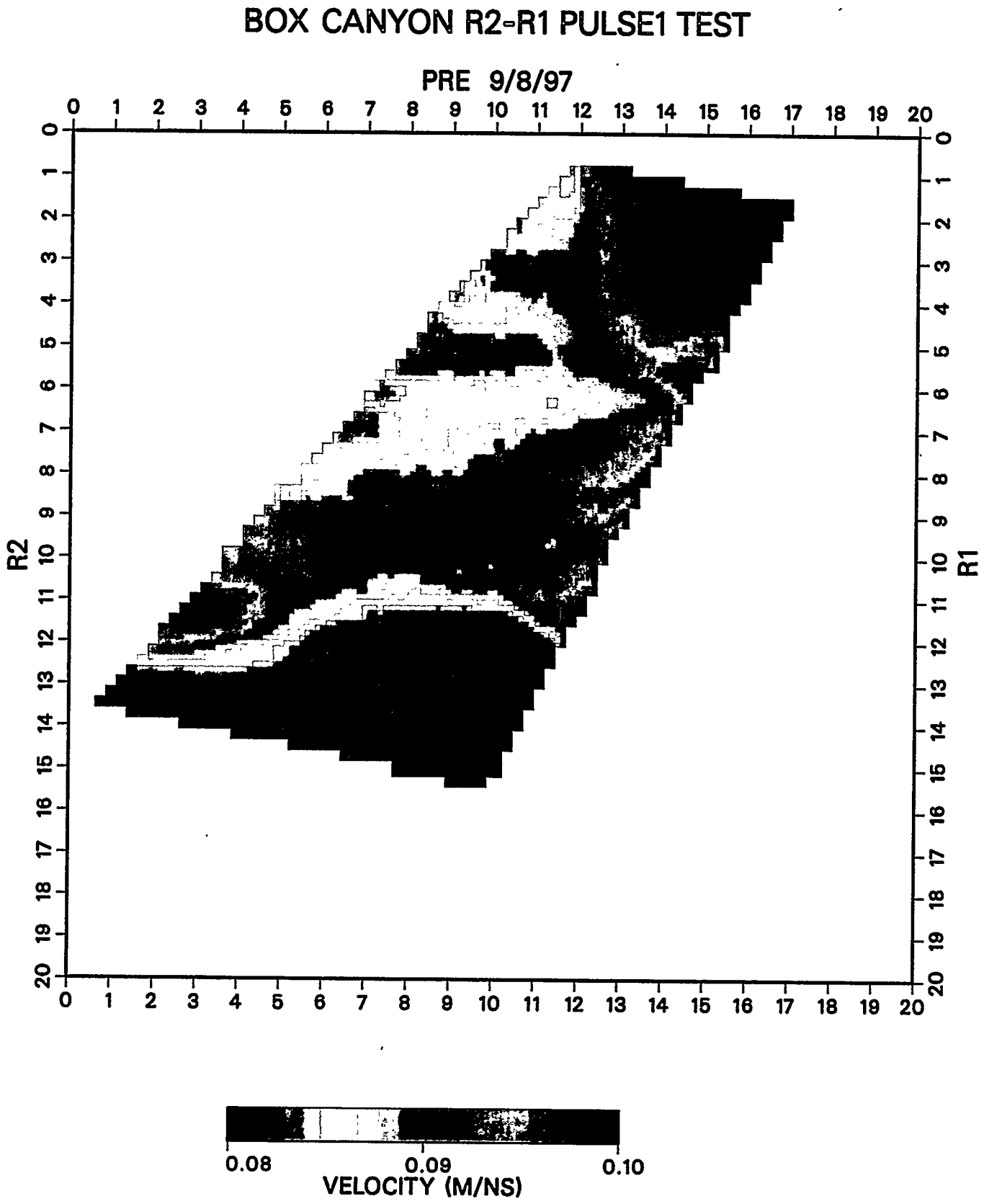
BOX CANYON R2-R1 PULSE1 TEST
PRE 9/8/97
R2
R1
0 1 2 3 4 5 6 7 8 9 10 11 12 13 14 15 16 17 18 19 20
0.08
0.09
0.10
VELOCITY (M/NS)

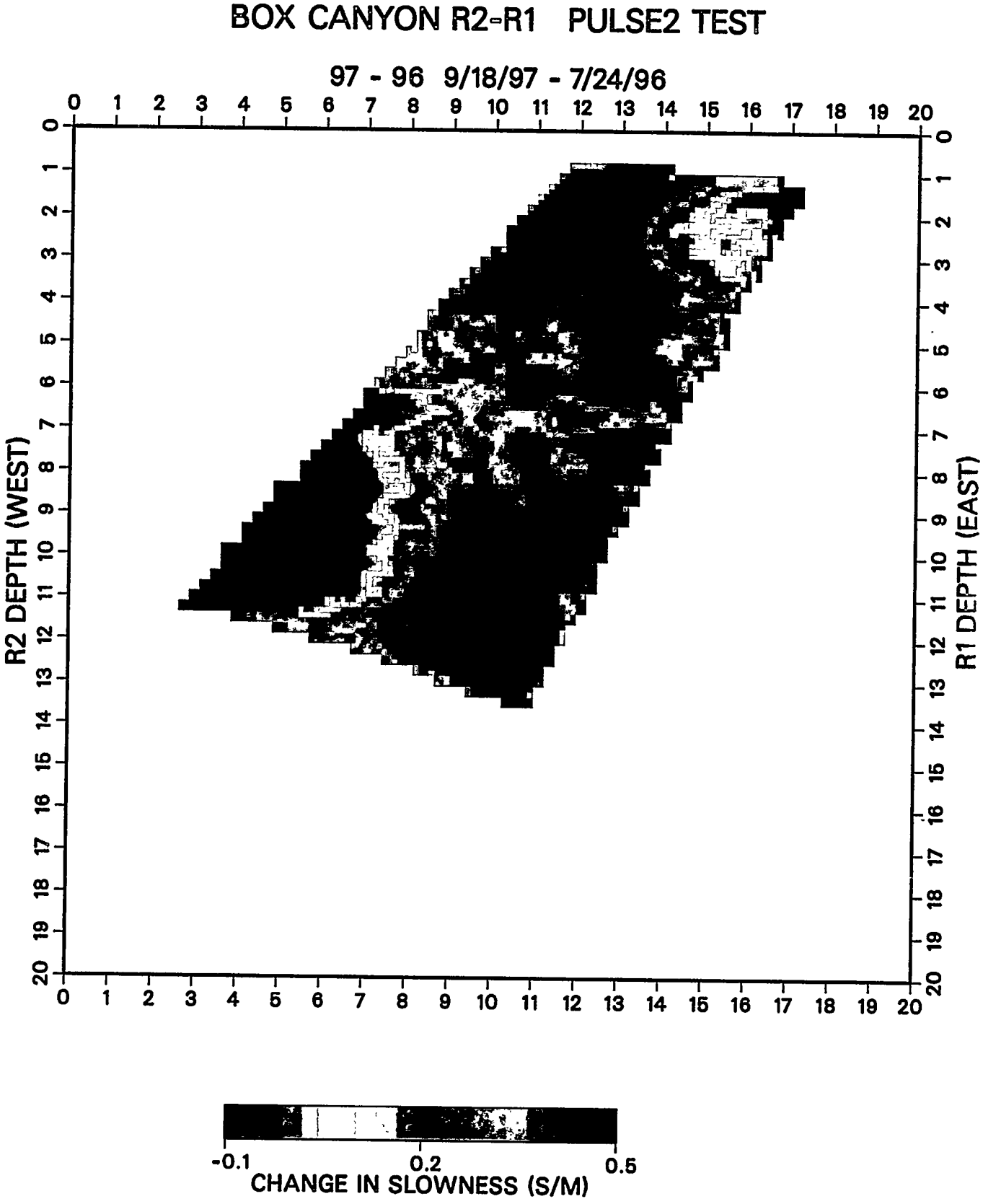
BOX CANYON R2-R1 PULSE2 TEST
97 - 96 9/18/97 - 7/24/96
R2 DEPTH (WEST)
R1 DEPTH (EAST)
0 1 2 3 4 5 6 7 8 9 10 11 12 13 14 15 16 17 18 19 20
-0.1
0.2
0.5
CHANGE IN SLOWNESS (S/M)

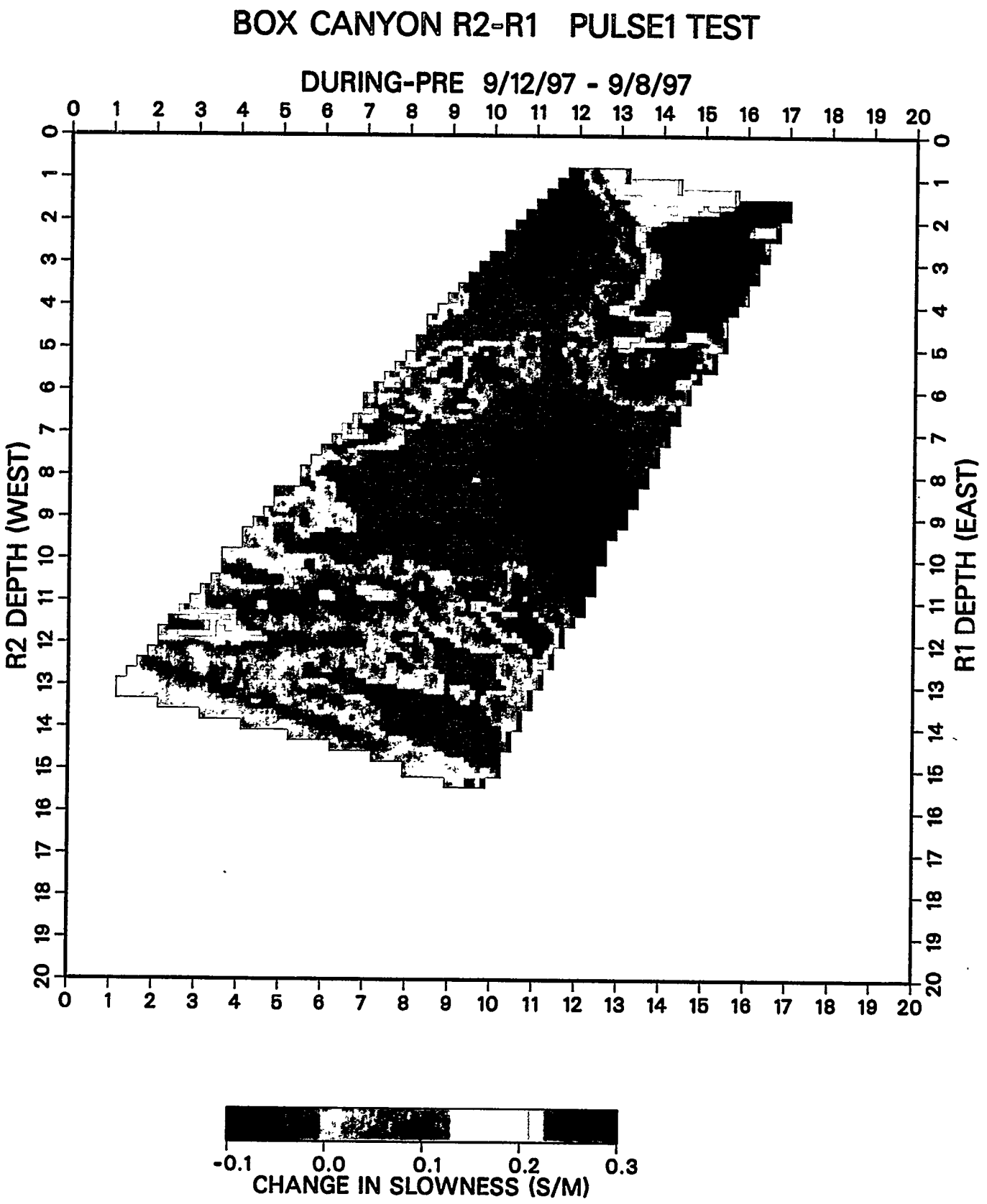
BOX CANYON R2-R1 PULSE1 TEST
DURING-PRE 9/12/97 - 9/8/97
R2 DEPTH (WEST)
R1 DEPTH (EAST)
0 1 2 3 4 5 6 7 8 9 10 11 12 13 14 15 16 17 18 19 20
-0.1 0.0 0.1 0.2 0.3
CHANGE IN SLOWNESS (S/M)

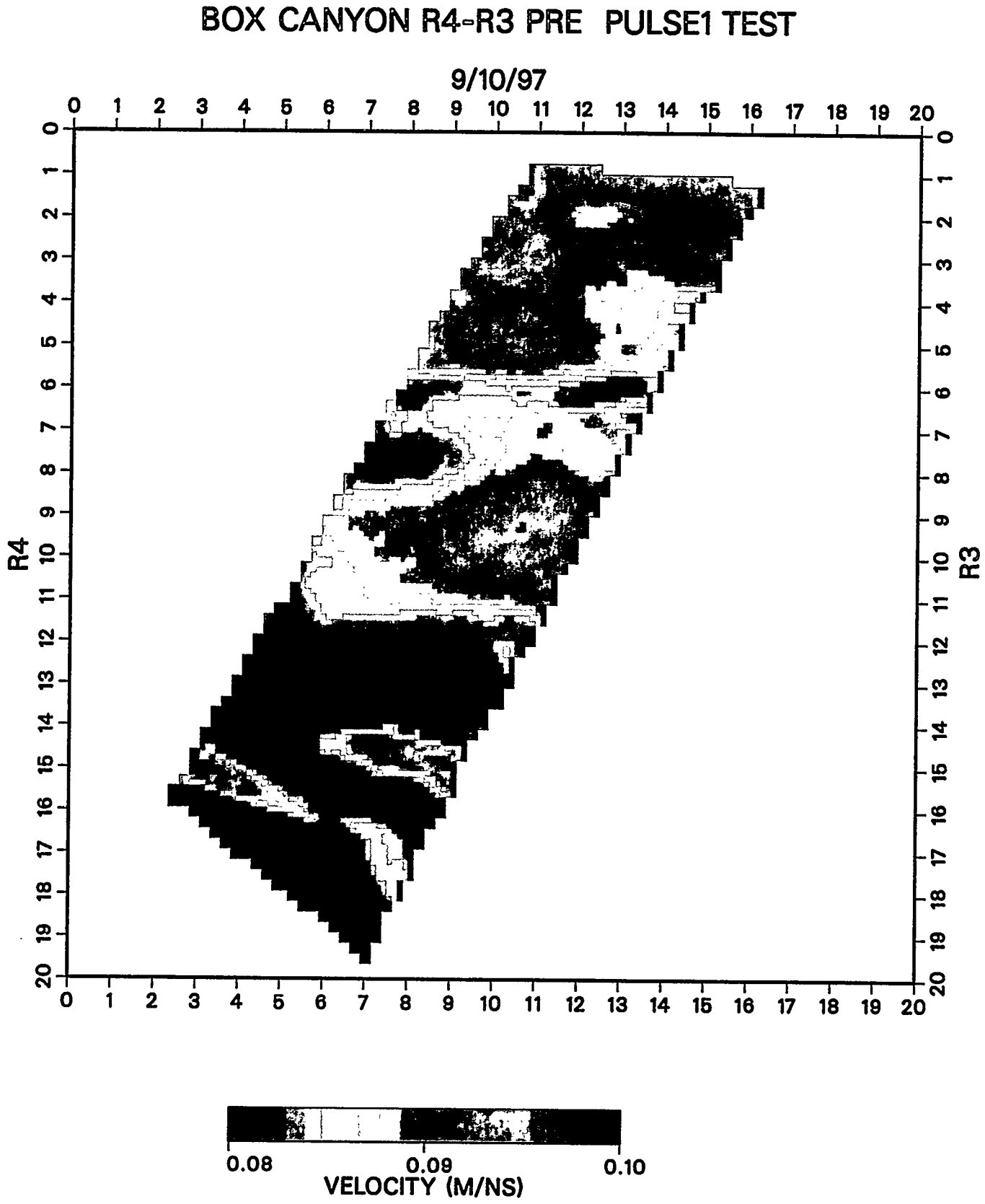
BOX CANYON R4-R3 PRE PULSE1 TEST
9/10/97
R4
R3
0 1 2 3 4 5 6 7 8 9 10 11 12 13 14 15 16 17 18 19 20
0.08
0.09
0.10
VELOCITY (M/NS)

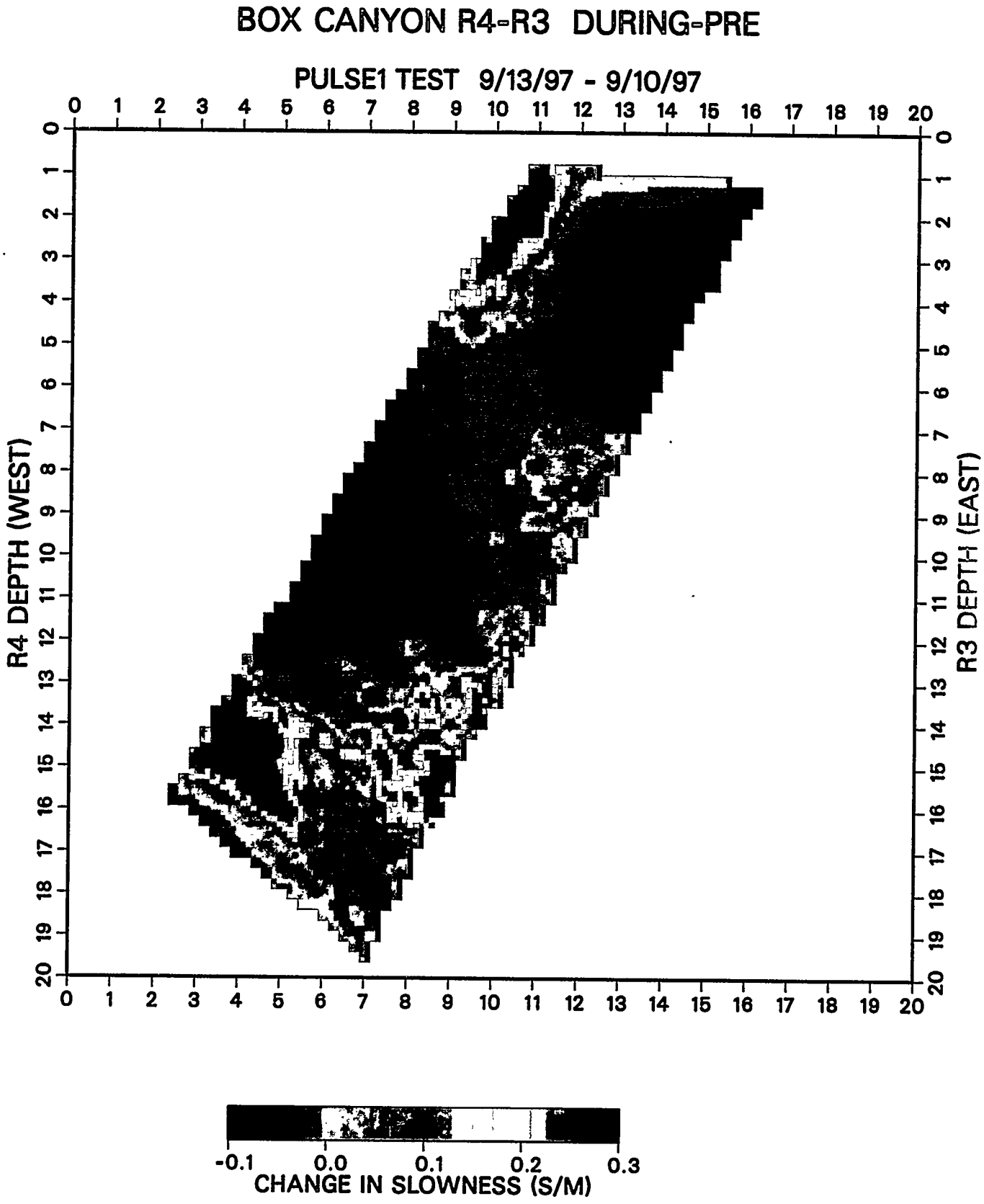
BOX CANYON R4-R3 DURING-PRE
PULSE1 TEST 9/13/97 - 9/10/97
R4 DEPTH (WEST)
R3 DEPTH (EAST)
0 1 2 3 4 5 6 7 8 9 10 11 12 13 14 15 16 17 18 19 20
-0.1 0.0 0.1 0.2 0.3
CHANGE IN SLOWNESS (S/M)

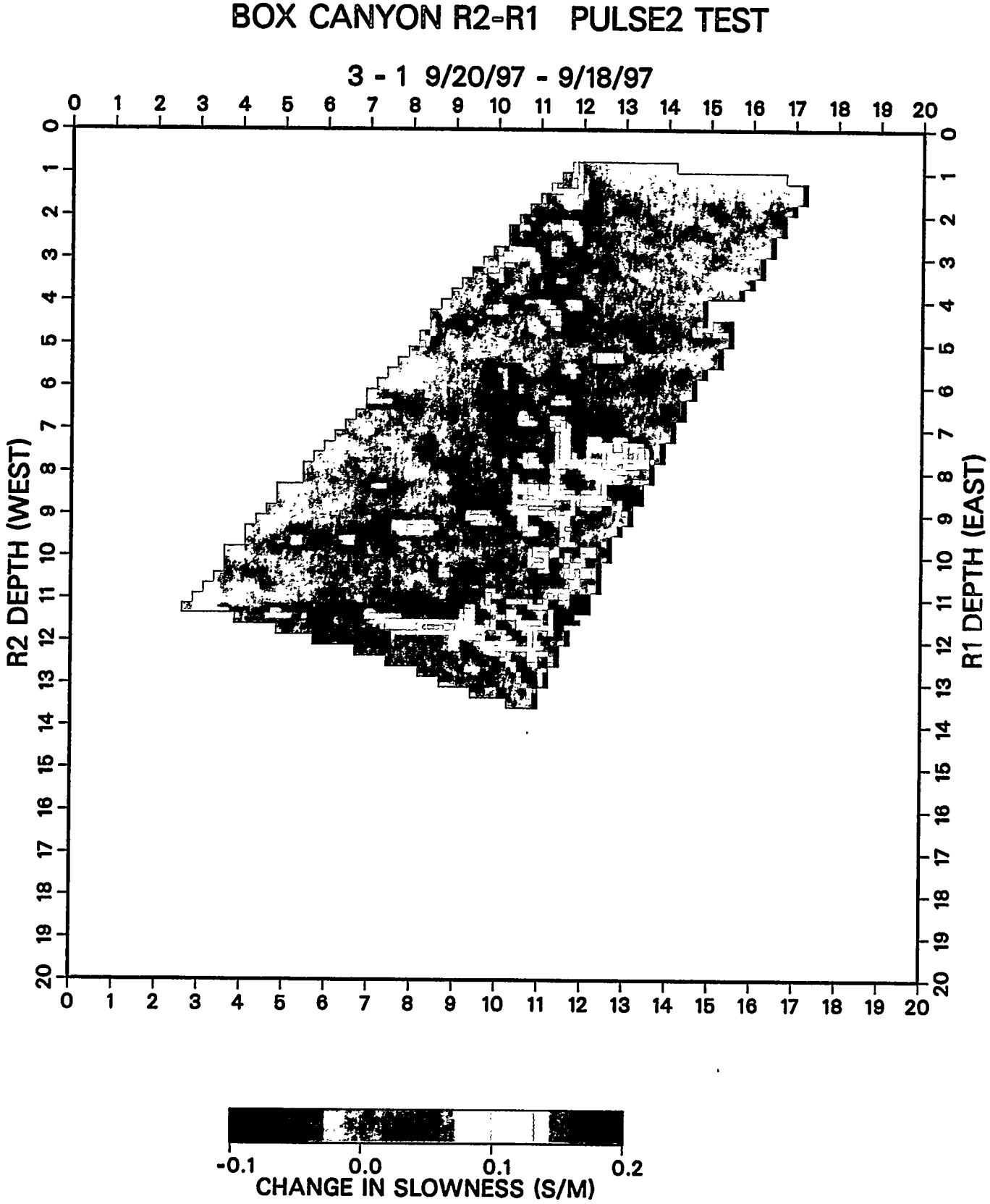
BOX CANYON R2-R1 PULSE2 TEST
3 - 1 9/20/97 - 9/18/97
R2 DEPTH (WEST)
R1 DEPTH (EAST)
0 1 2 3 4 5 6 7 8 9 10 11 12 13 14 15 16 17 18 19 20
-0.1 0.0 0.1 0.2
CHANGE IN SLOWNESS (S/M)

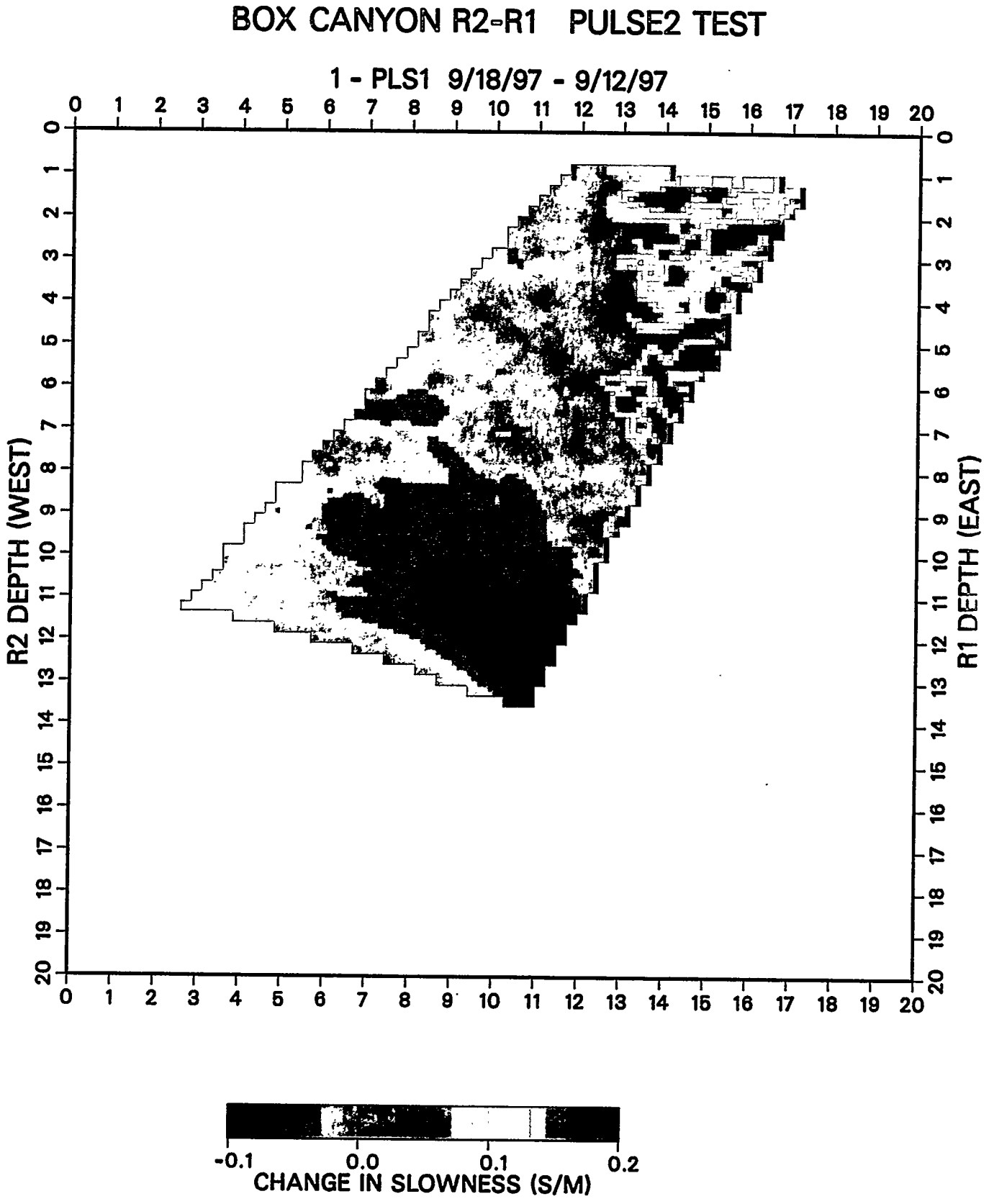
BOX CANYON R2-R1 PULSE2 TEST
1 - PLS1 9/18/97 - 9/12/97
R2 DEPTH (WEST)
R1 DEPTH (EAST)
0 1 2 3 4 5 6 7 8 9 10 11 12 13 14 15 16 17 18 19 20
-0.1 0.0 0.1 0.2
CHANGE IN SLOWNESS (S/M)

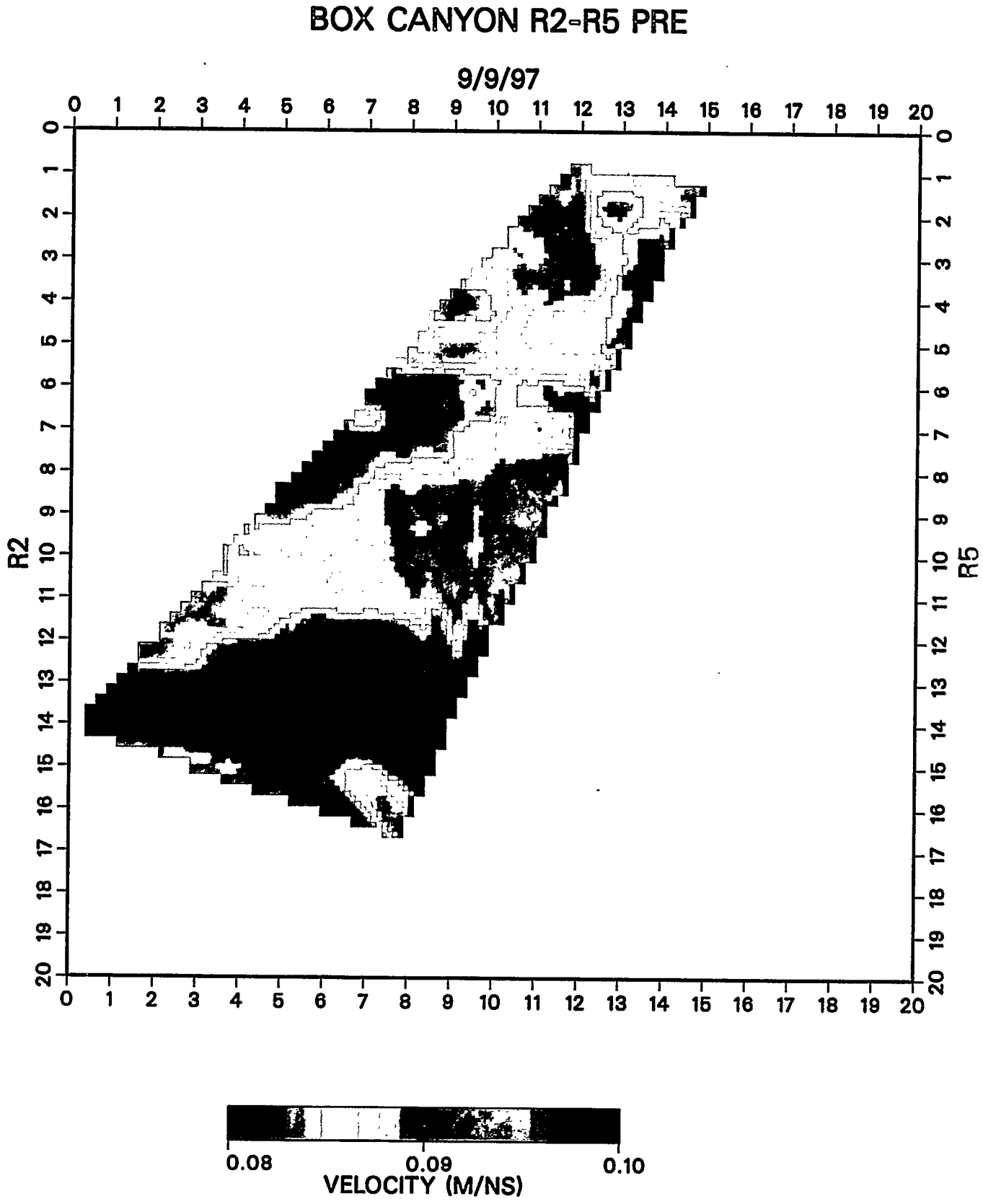
BOX CANYON R2-R5 PRE
9/9/97
R2
R5
0 1 2 3 4 5 6 7 8 9 10 11 12 13 14 15 16 17 18 19 20
0.08
0.09
0.10
VELOCITY (M/NS)

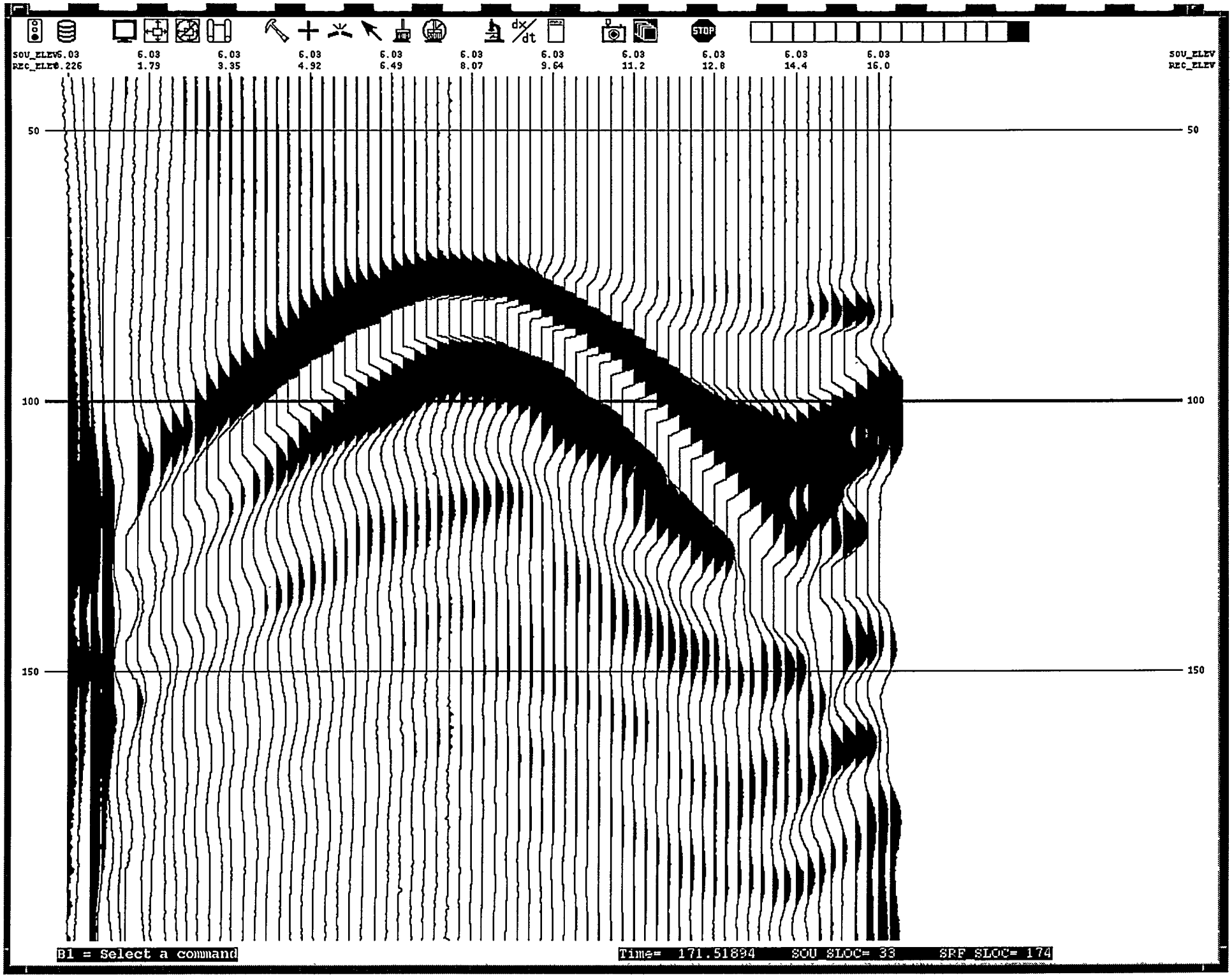
SOU_ELEV 6.03 6.03 6.03 6.03 6.03 6.03 6.03 6.03 6.03 6.03 6.03 SOU_ELEV
REC_ELEV 0.226 1.79 3.35 4.92 6.49 8.07 9.64 11.2 12.8 14.4 16.0 REC_ELEV
50
100
150
B1 = Select a command
Time= 171.51894 SOU SLOC= 33 SRF SLOC= 174

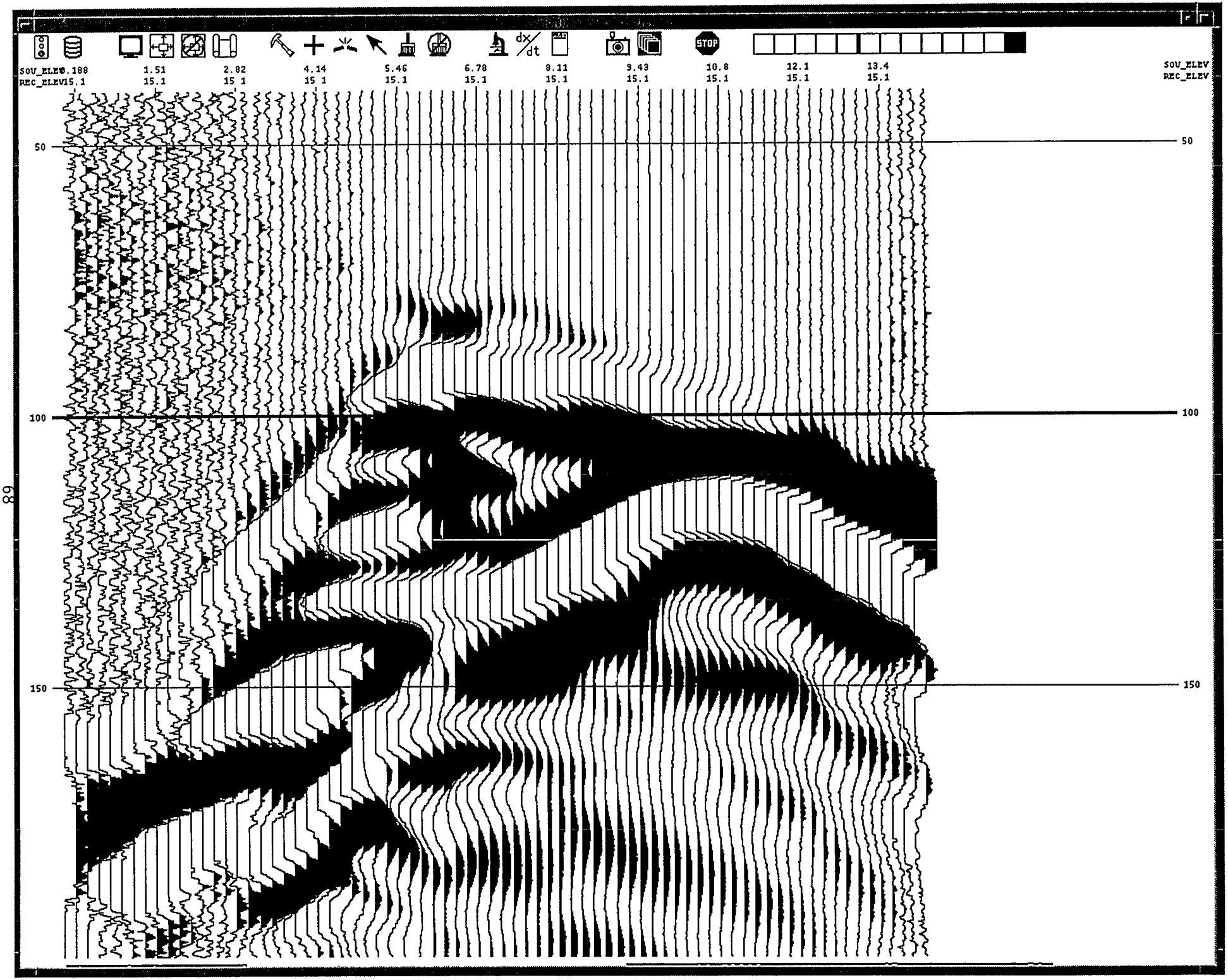
SOU_ELEV0.188
REC_ELEV15.1
1.51
15.1
2.82
15 1
4.14
15 1
5.46
15.1
6.78
15.1
8.11
15.1
9.43
15.1
10.8
15.1
12.1
15.1
13.4
15.1
SOU_ELEV
REC_ELEV
STOP
dx/dt
50
100
150

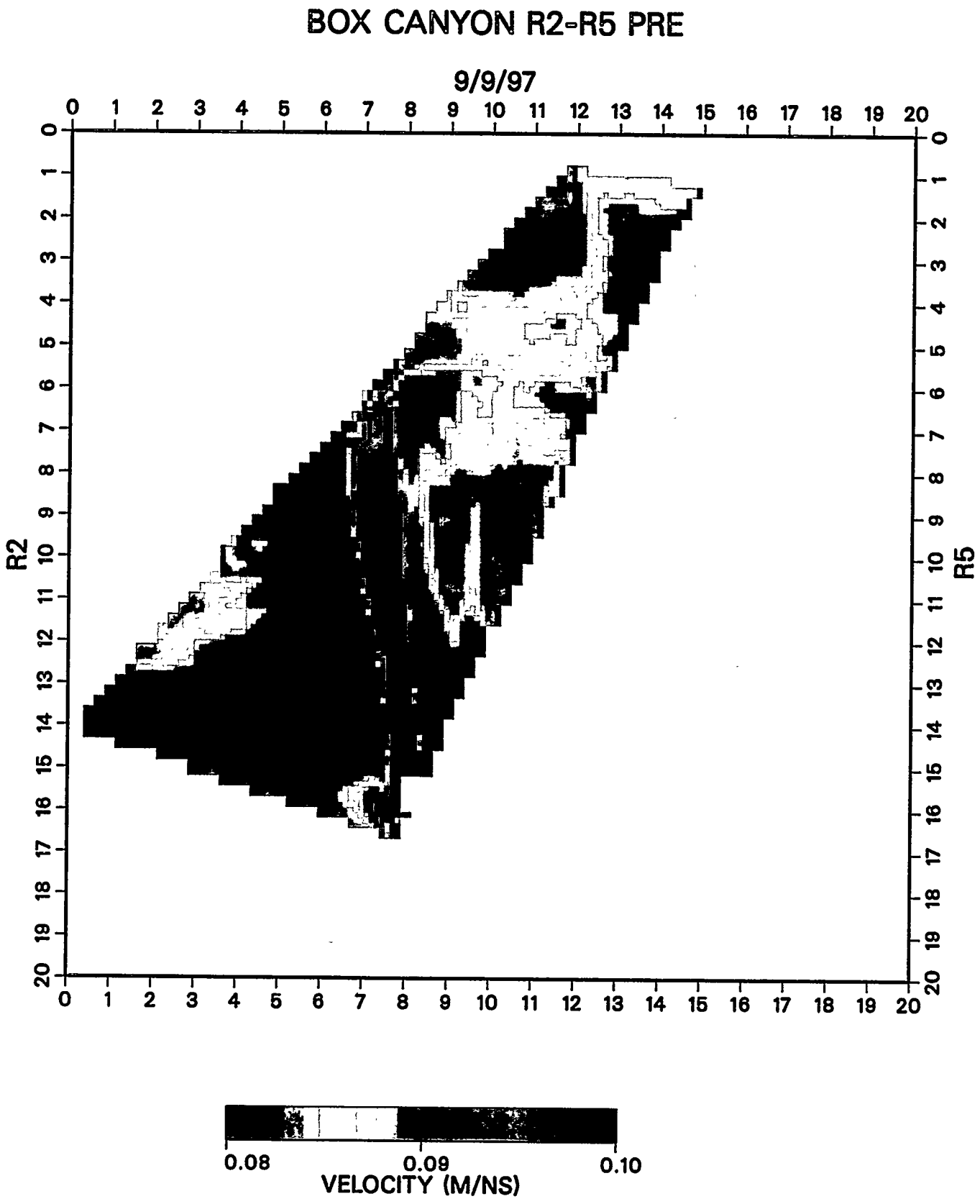
BOX CANYON R2-R5 PRE
9/9/97
R2
R5
0 1 2 3 4 5 6 7 8 9 10 11 12 13 14 15 16 17 18 19 20
0.08
0.09
0.10
VELOCITY (M/NS)

R1-R2 PLANE

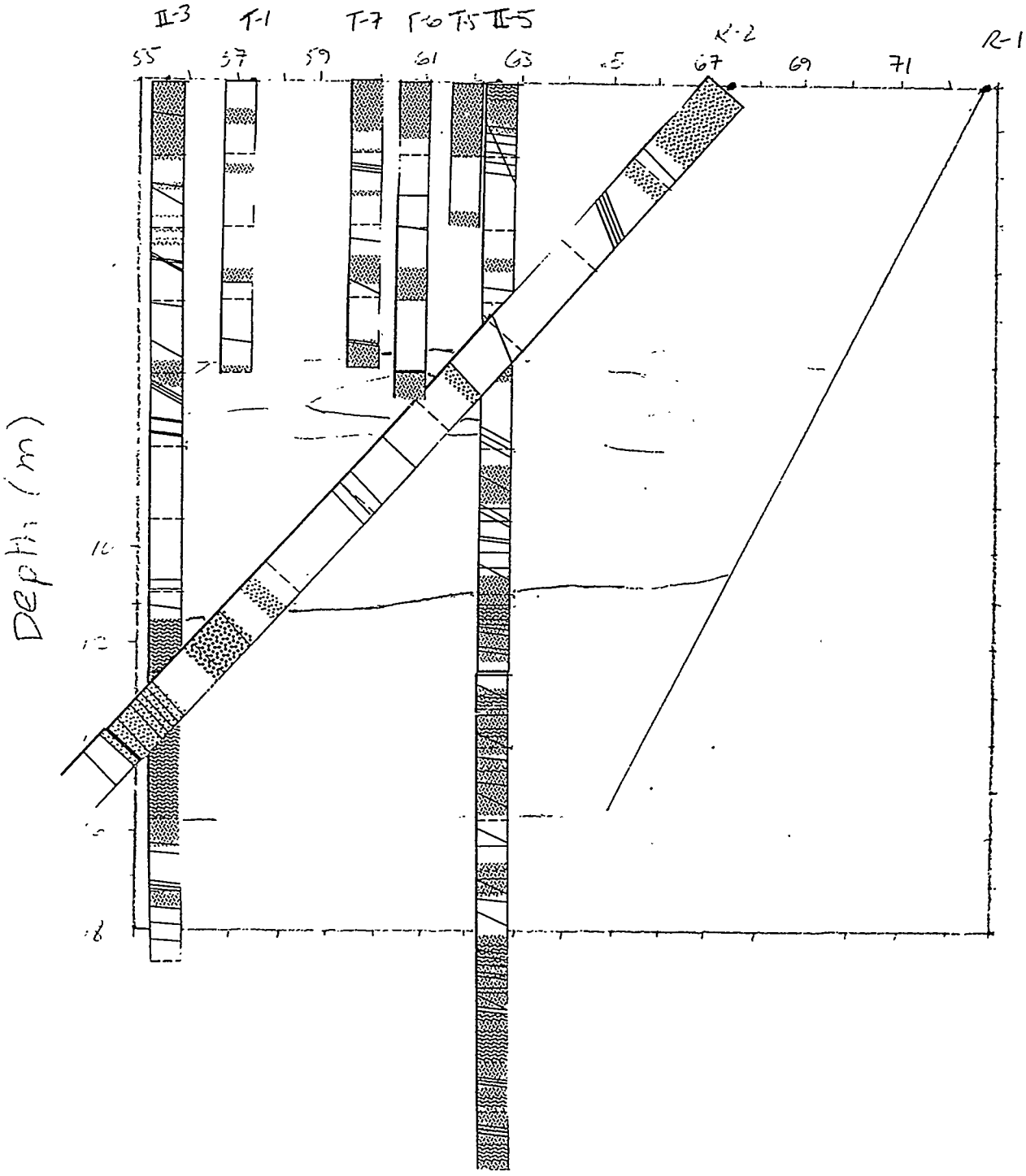

II.3

ERT Results from the Box Canyon Infiltration Experiment

Douglas LaBrecque
and
Gail Heath
SteamTech Environmental Services

Outline

- The ERT Method
- BXC Setup
  - Large Scale Survey Configuration
  - Small Scale Survey Configuration
- Results
  - Small Scale Survey
  - Large Scale Survey
- Conclusions

3D Electrical Resistivity Tomography

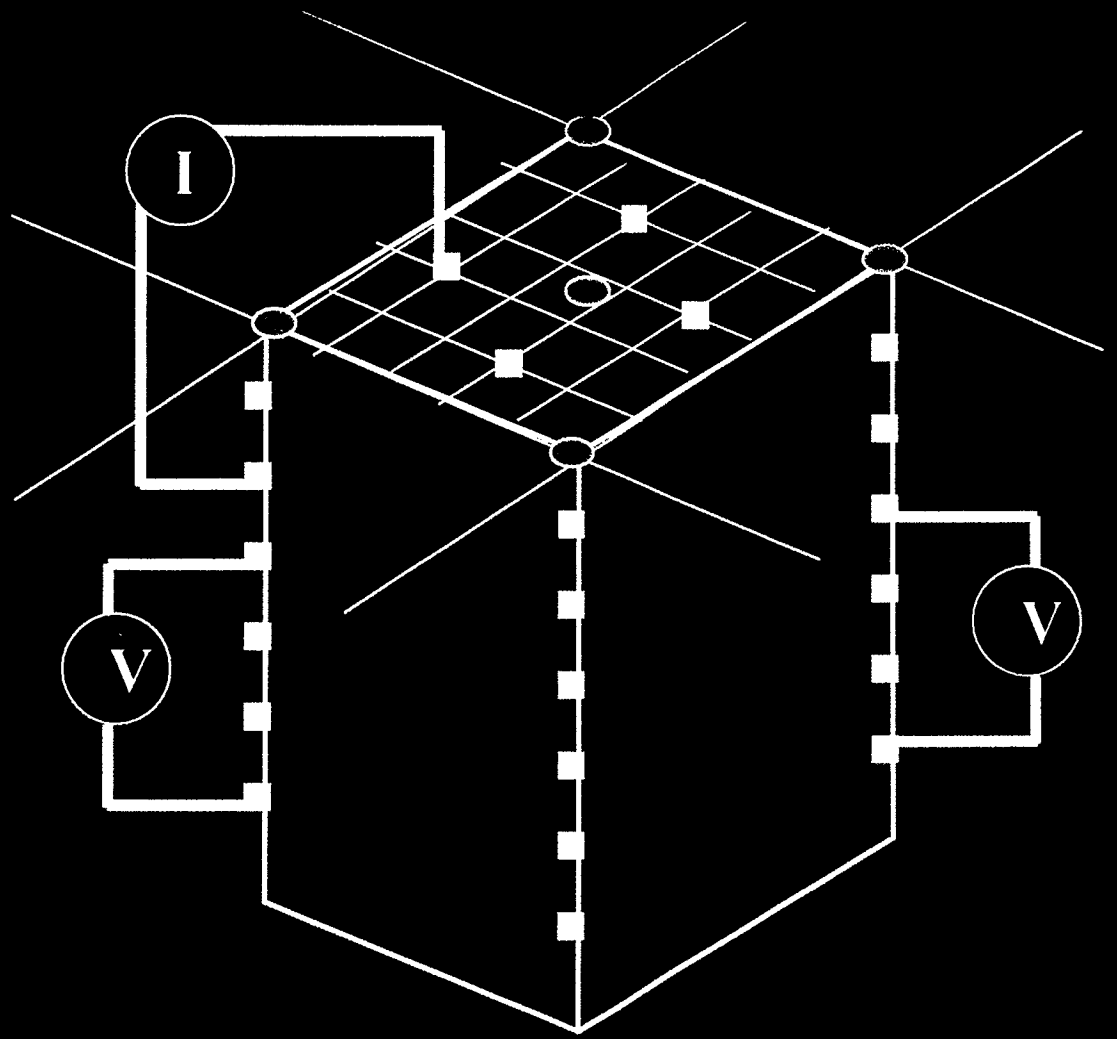

The 3D interpretation algorithm

3D Finite Differences forward modeling

Inverse problem solved with a Preconditioned Conjugate Gradients technique

Effects of conductive boreholes and anomalous objects can be modeled

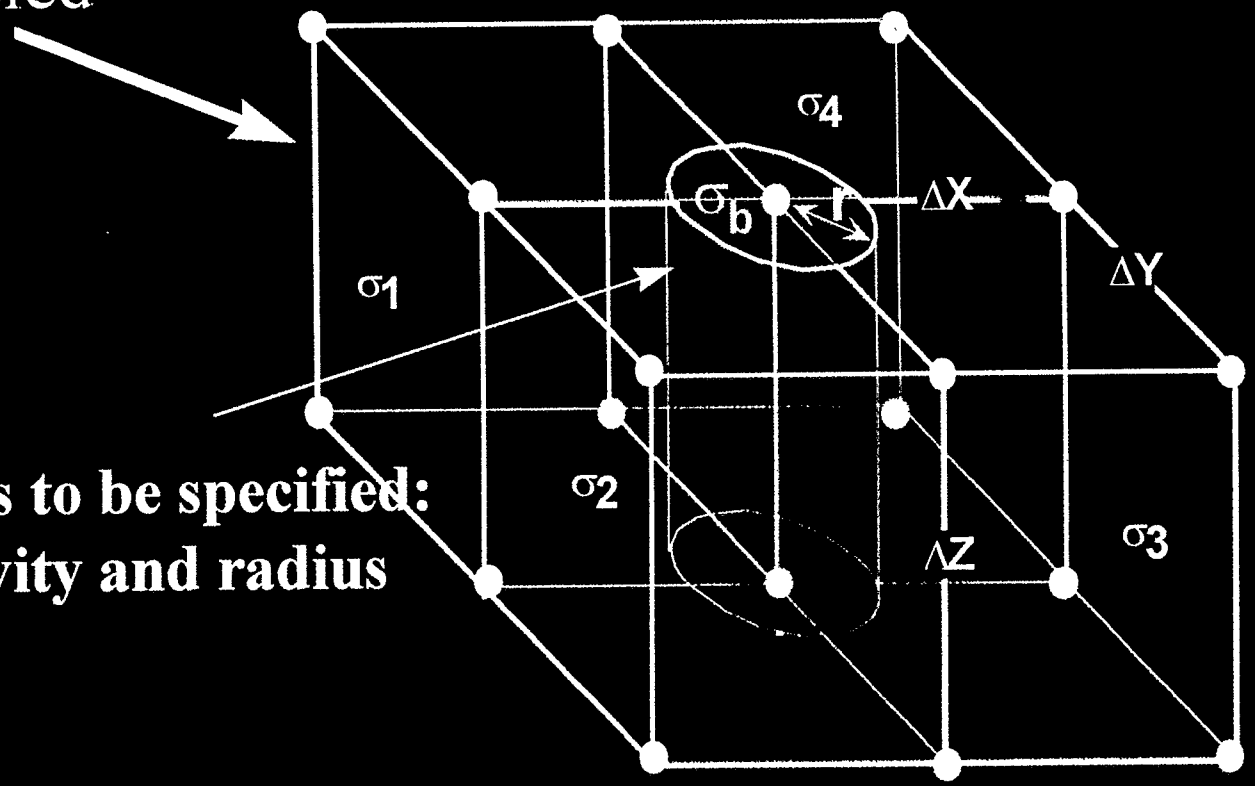

parameters to be specified: conductivity and radius

Nonlinear Inversion

Iteratively update the vector of parameters

$$\underline{P}_{k+1} = \underline{P}_k + \underline{\Delta P}_k$$

by approximately solving the linear system

$$\underline{\Delta P}_k = -\left(\underline{\mathbf{A}}_k^T \underline{\mathbf{W}} \underline{\mathbf{A}}_k + \underline{\mathbf{R}} \right)^{-1} \left(\underline{\mathbf{W}} \left(\underline{D} - F(\underline{P}_k) \right) - \underline{\mathbf{R}} \underline{P}_k \right)$$

with the Conjugate-Gradient Method

cal survey

Wells With Packers

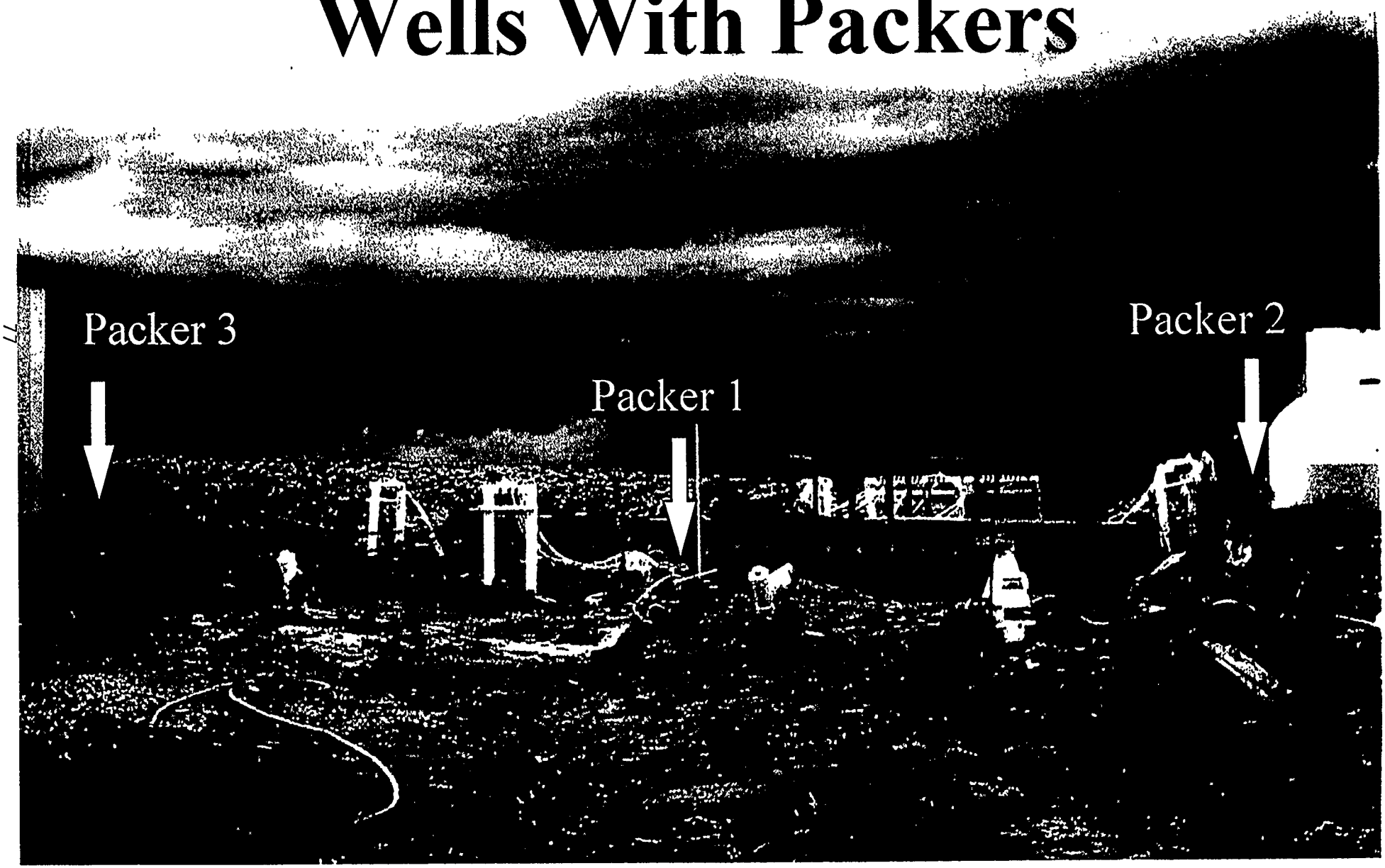

Packer Design

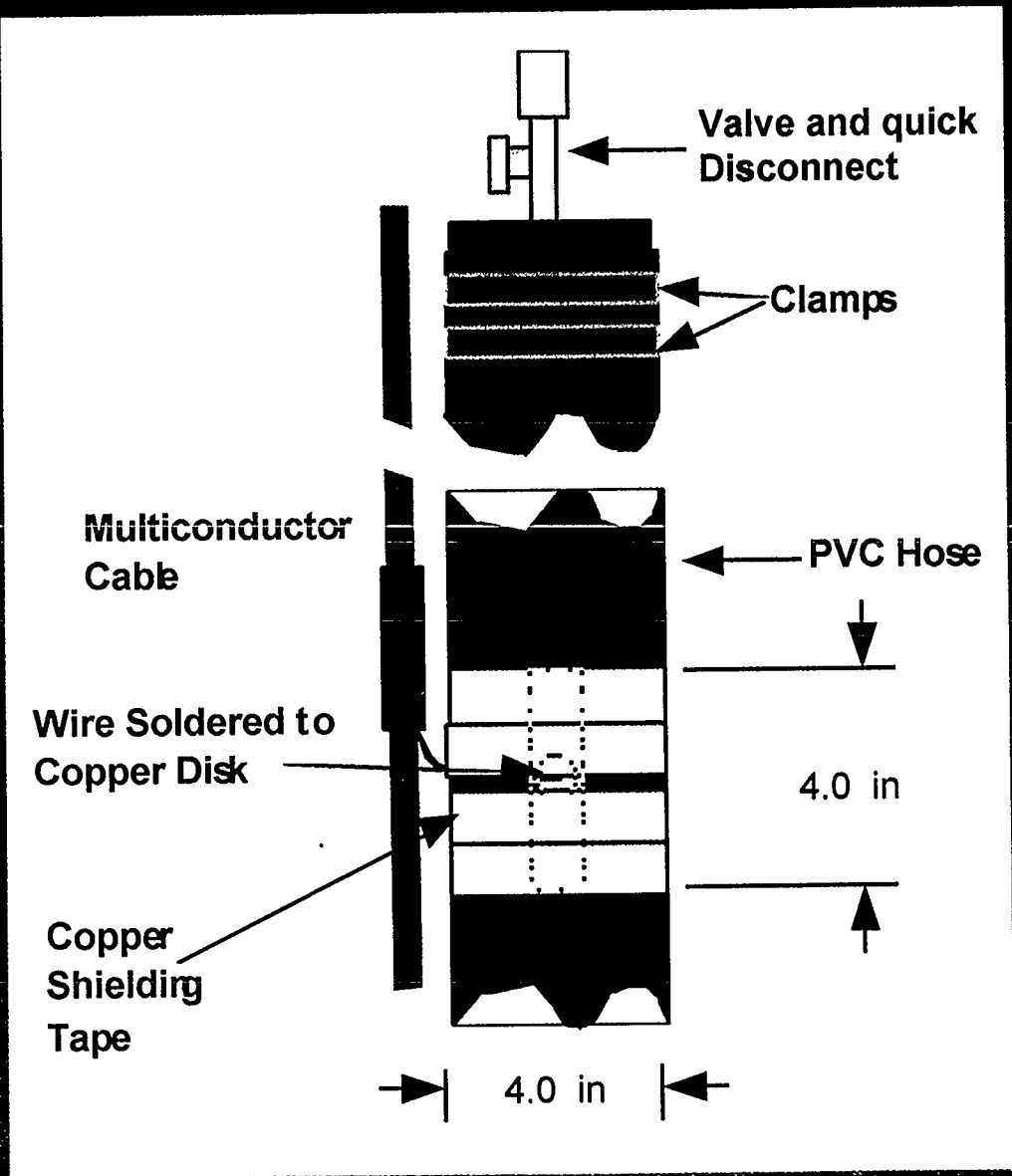

Large Scale Survey Well and Electrode Configuration

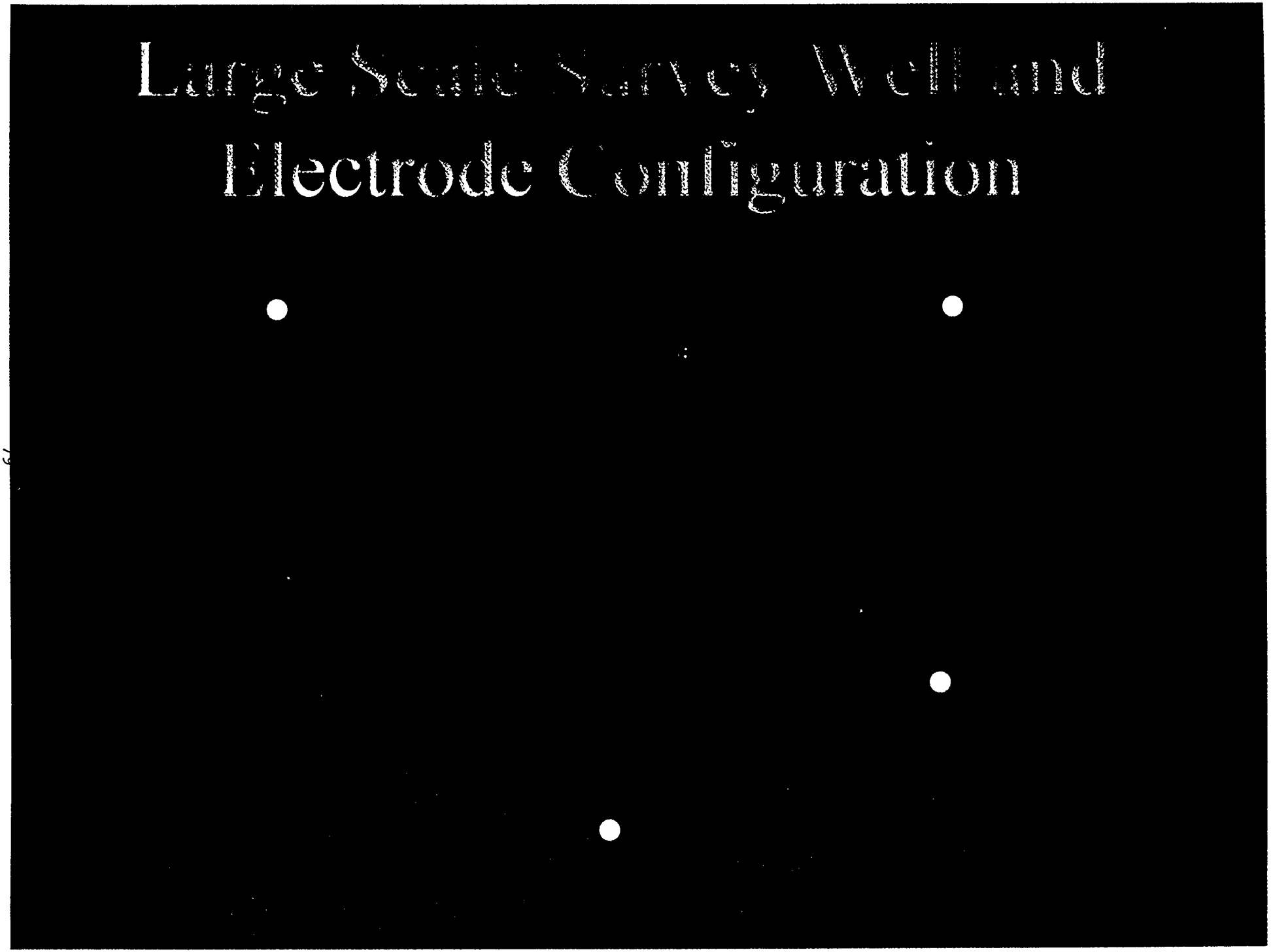

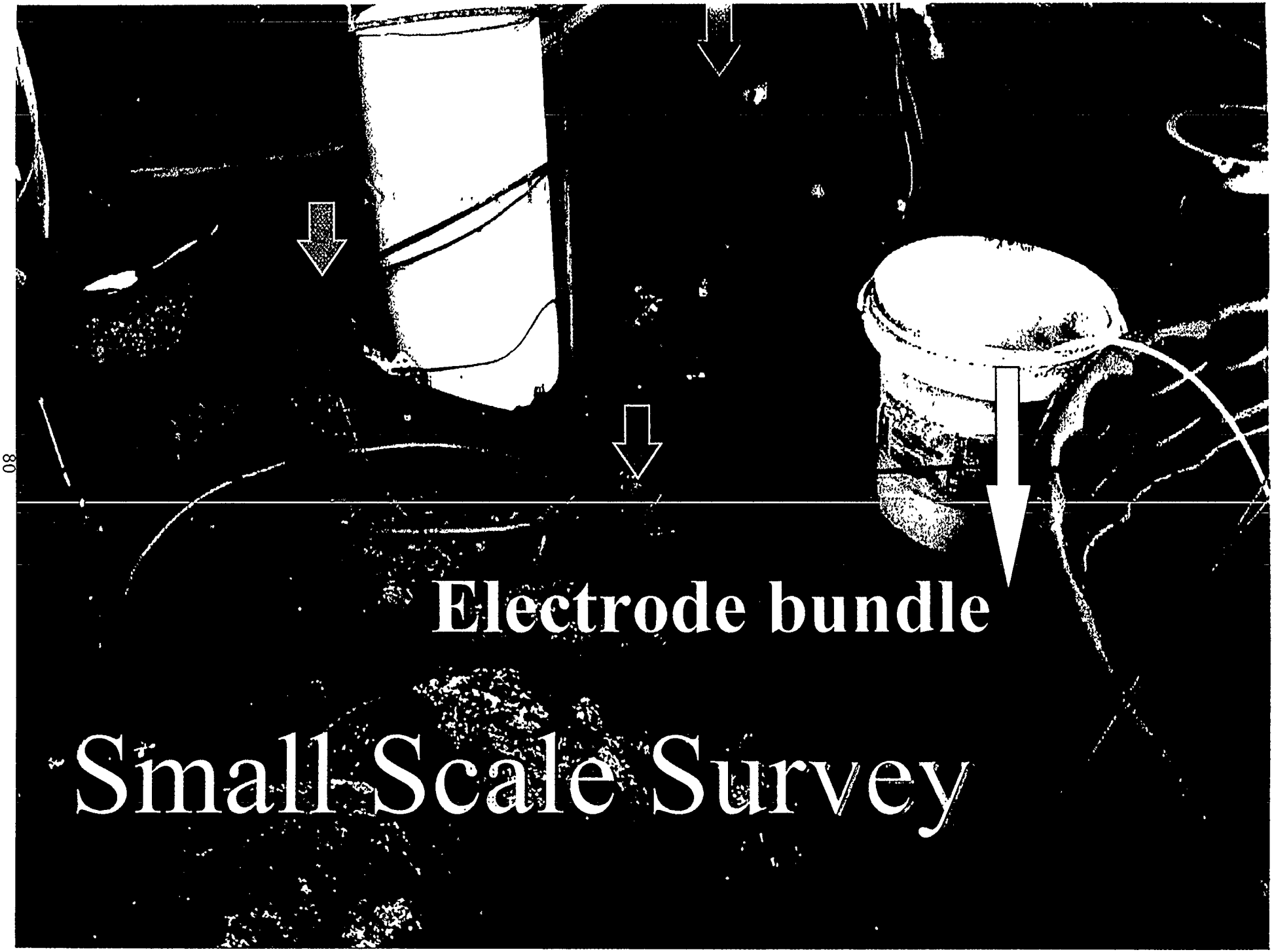
Electrode bundle
Small Scale Survey

Layout of Sinkhole Seismic Survey

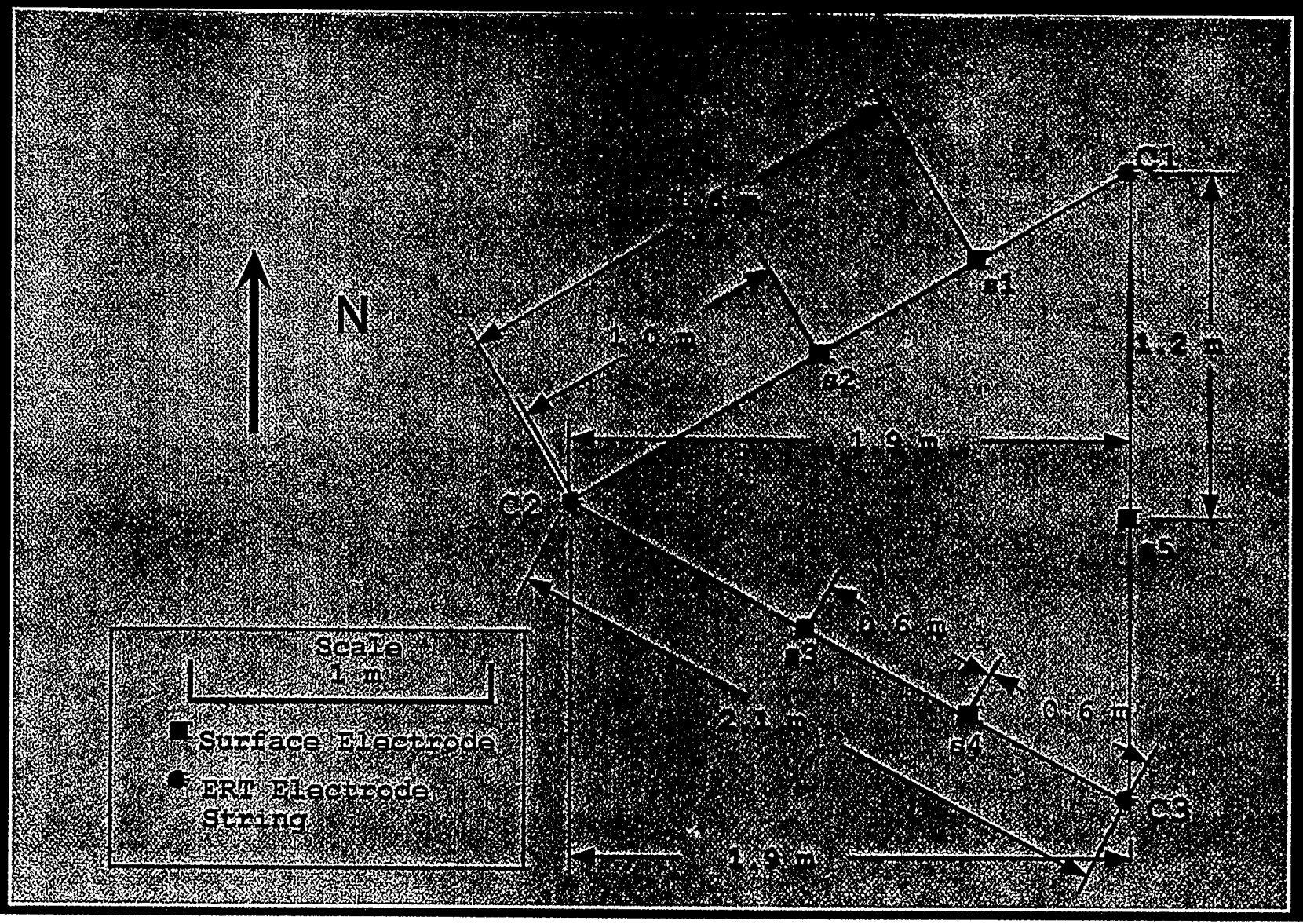

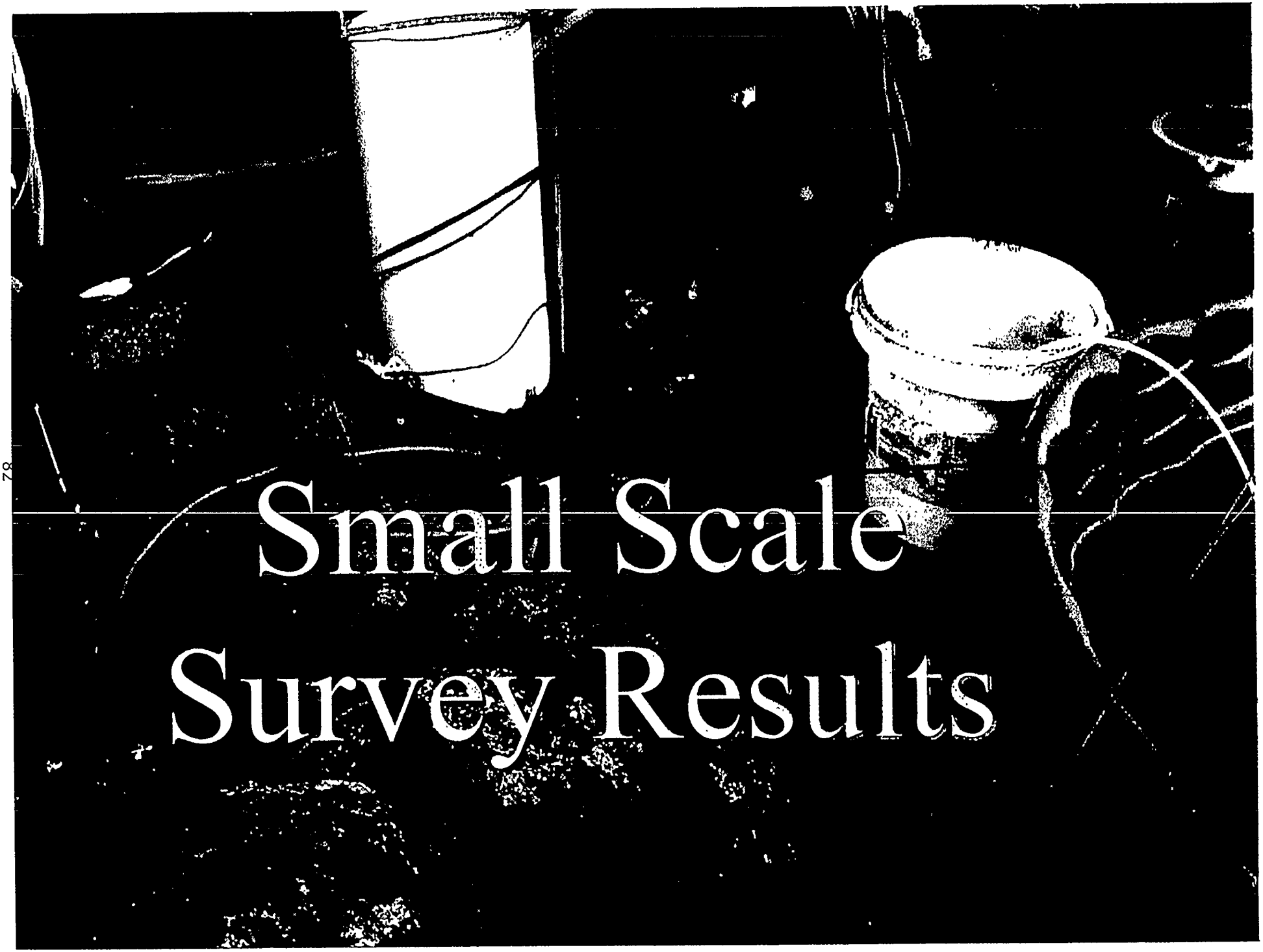

Small Scale Survey Results

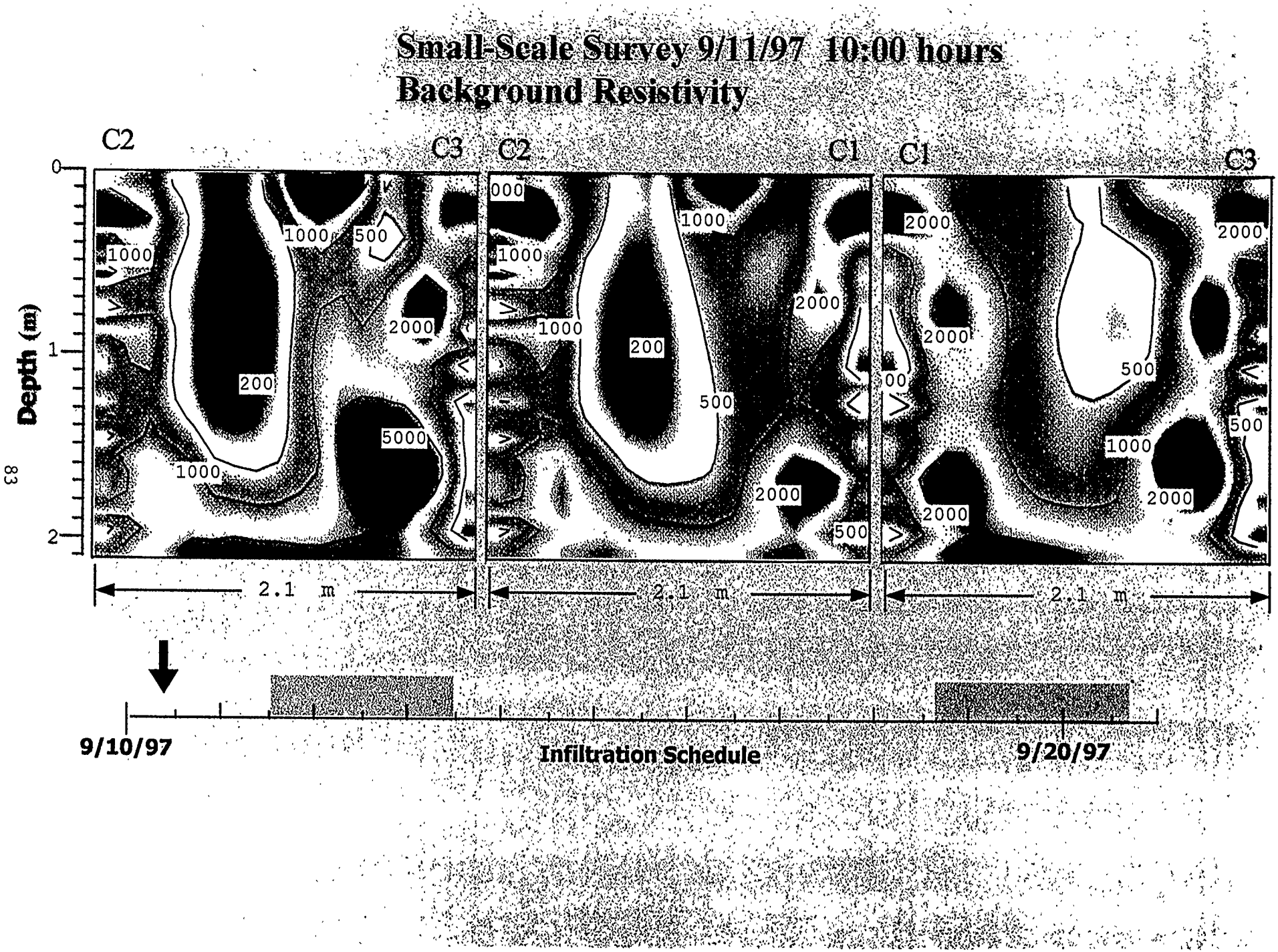
Small-Scale Survey 9/11/97 10:00 hours
Background Resistivity
C2
C3
C2
C1
C1
C3
Depth (m)
0
1
2
1000
500
2000
200
5000
1000
1000
200
500
2000
2000
500
2000
2000
500
1000
2000
2000
2.1 m
2.1 m
2.1 m
9/10/97
Infiltration Schedule
9/20/97

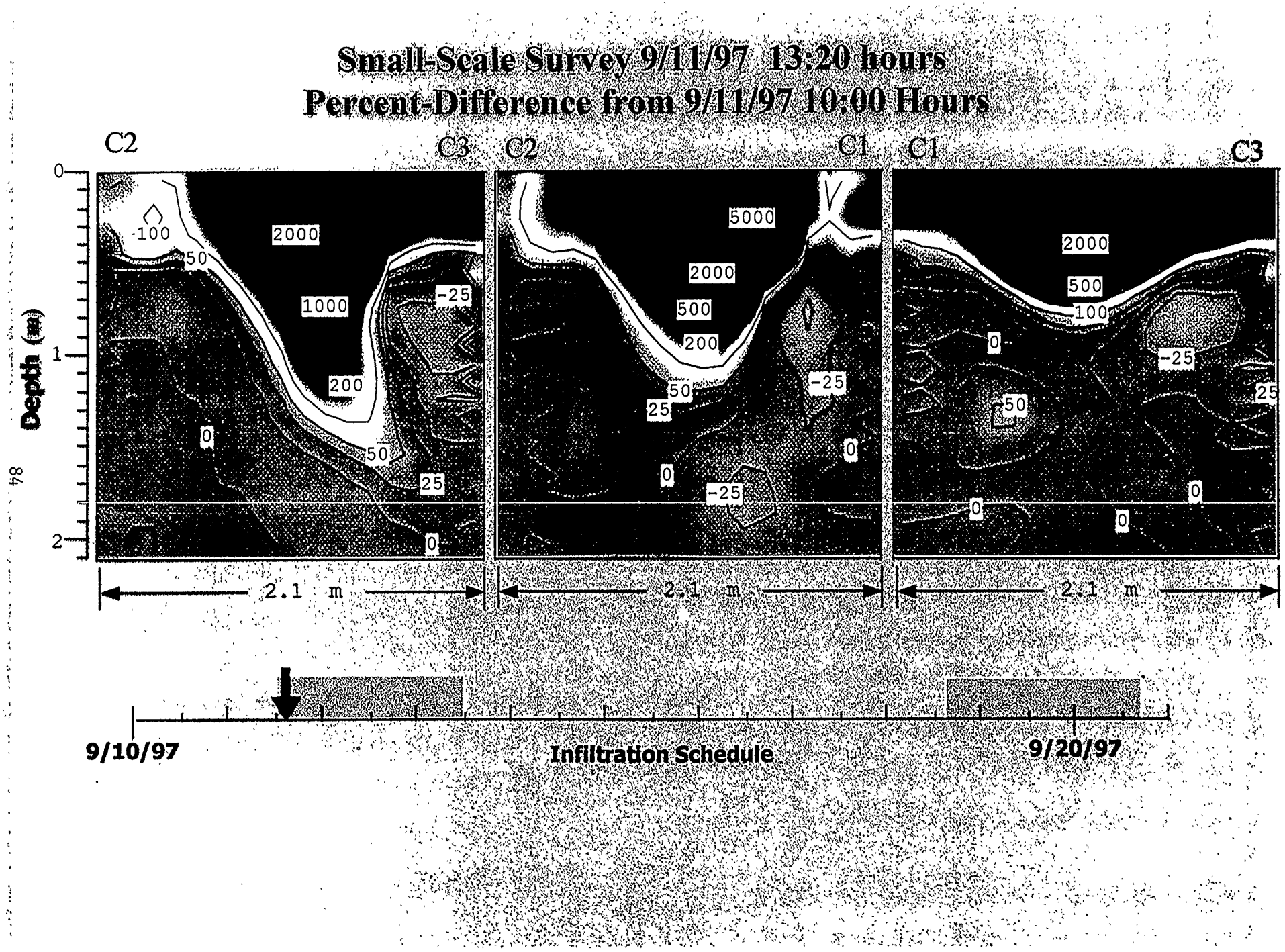
Small-Scale Survey 9/11/97 13:20 hours
Percent-Difference from 9/11/97 10:00 Hours
C2
C3
C2
C1
C1
C3
Depth (m)
0
1
2
-100
50
2000
1000
200
0
50
25
-25
0
5000
2000
500
200
50
25
-25
0
0
-25
2000
500
100
0
50
-25
25
0
0
0
2.1 m
2.1 m
2.1 m
9/10/97
Infiltration Schedule
9/20/97

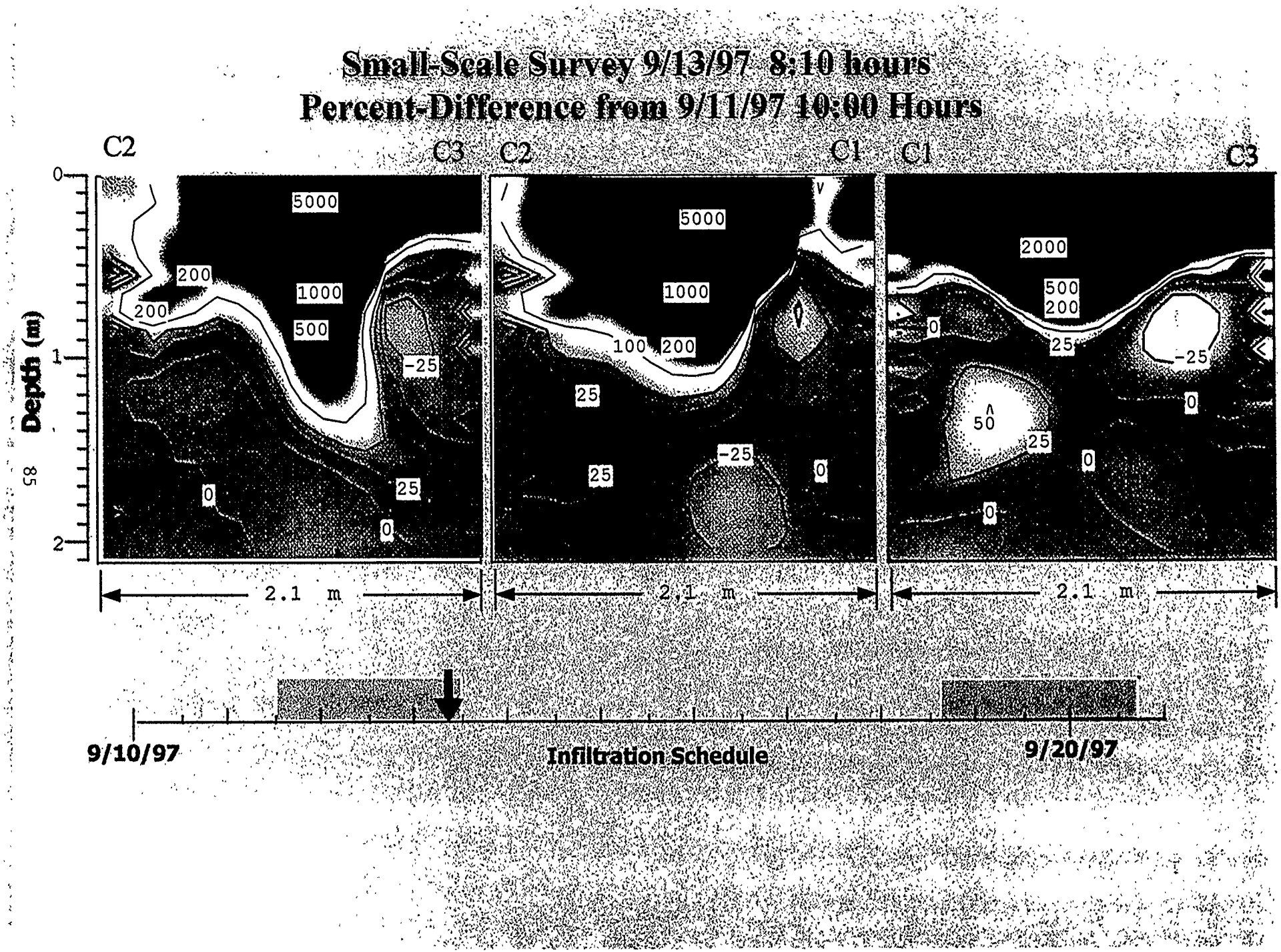
Small-Scale Survey 9/13/97 8:10 hours
Percent-Difference from 9/11/97 10:00 Hours
C2
C3
C2
C1
C1
C3
Depth (m)
0
1
2
5000
200
200
1000
500
-25
0
25
0
5000
1000
100
200
25
25
-25
0
2000
500
200
0
25
-25
50
25
0
0
2.1 m
2.1 m
2.1 m
9/10/97
Infiltration Schedule
9/20/97

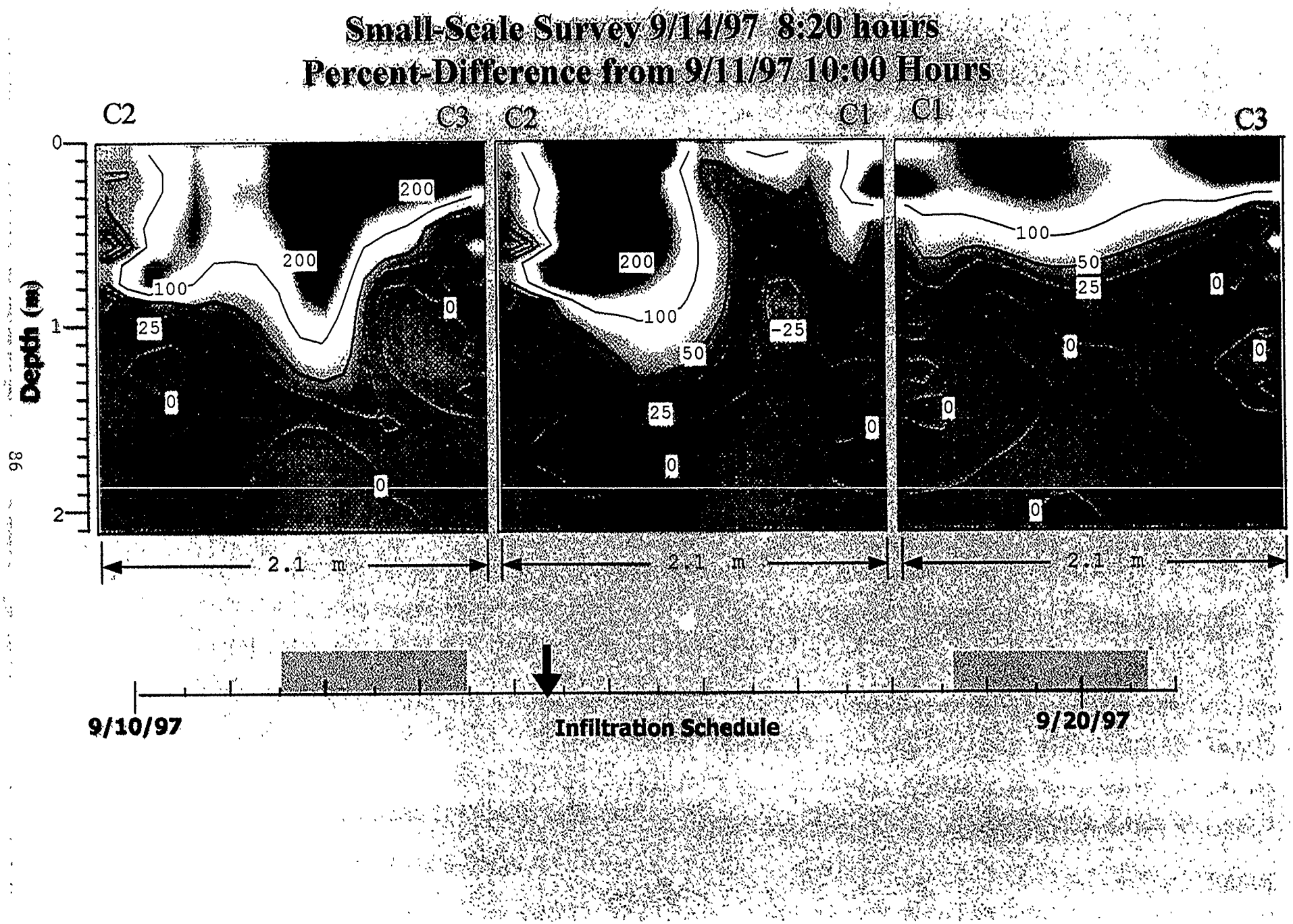
Small-Scale Survey 9/14/97 8:20 hours
Percent-Difference from 9/11/97 10:00 Hours
C2
C3
C2
C1
C1
C3
Depth (m)
0
1
2
200
100
25
0
-25
50
2.1 m
2.1 m
2.1 m
9/10/97
Infiltration Schedule
9/20/97

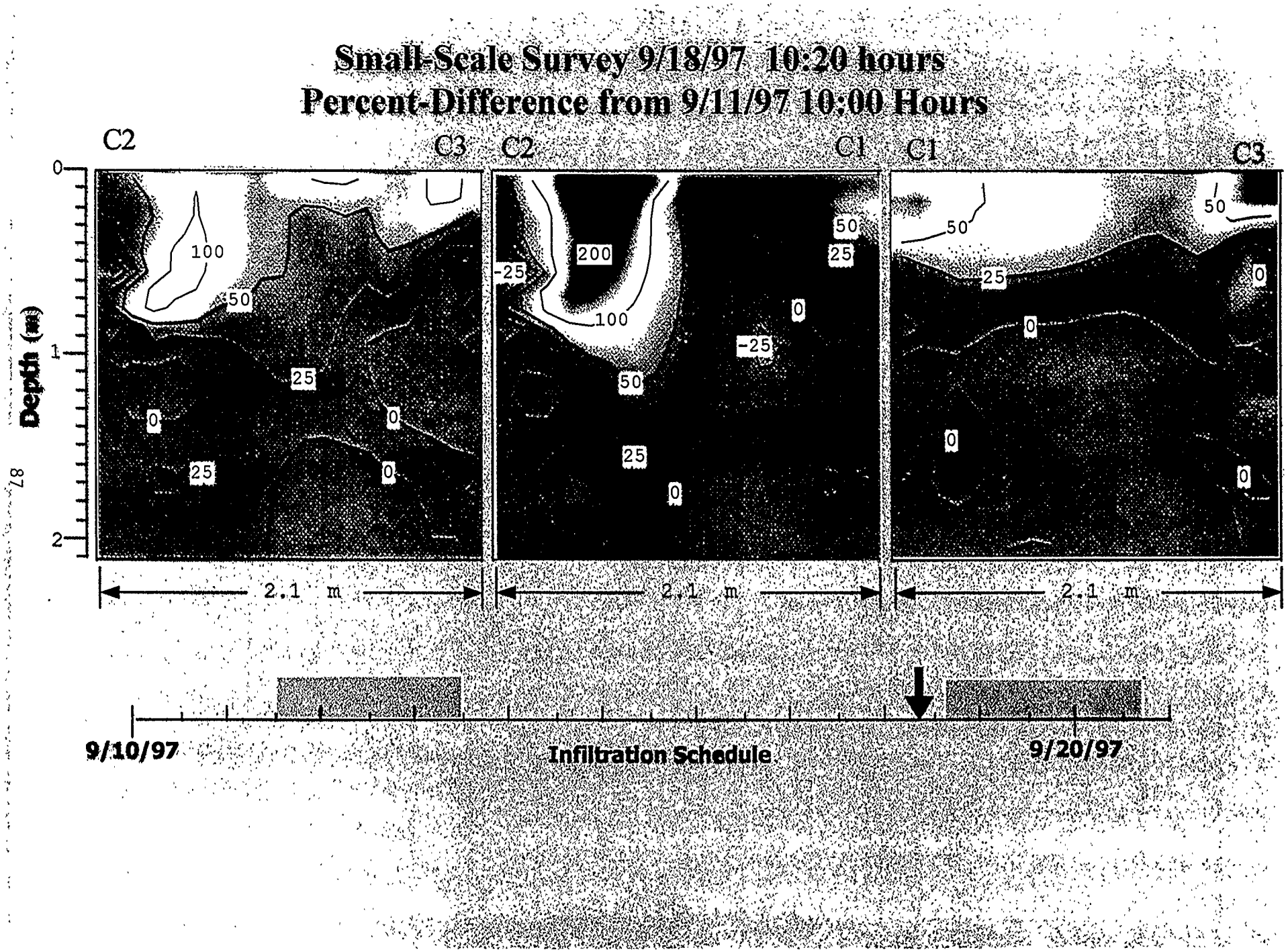
Small-Scale Survey 9/18/97 10:20 hours
Percent-Difference from 9/11/97 10:00 Hours
C2
C3
C2
C1
C1
C3
Depth (m)
0
1
2
100
50
25
0
0
25
0
200
-25
50
25
0
-25
100
50
25
0
50
50
25
0
0
0
2.1 m
2.1 m
2.1 m
9/10/97
Infiltration Schedule
9/20/97

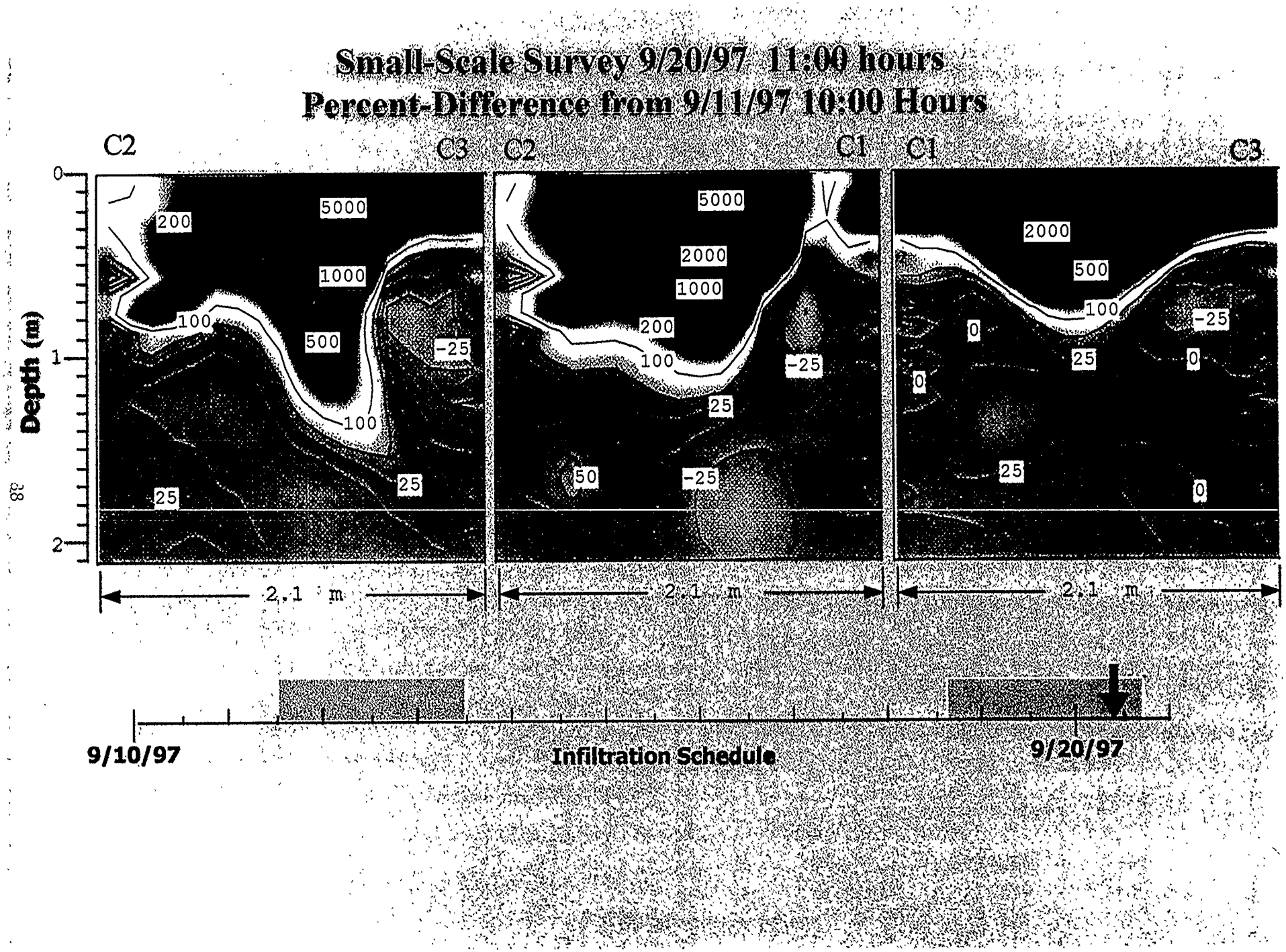
Small-Scale Survey 9/20/97 11:00 hours
Percent-Difference from 9/11/97 10:00 Hours
C2
C3
C2
C1
C1
C3
Depth (m)
0
1
2
5000
200
1000
100
500
-25
25
5000
2000
1000
200
100
-25
25
50
-25
2000
500
100
-25
0
25
0
25
0
2.1 m
2.1 m
2.1 m
9/10/97
Infiltration Schedule
9/20/97

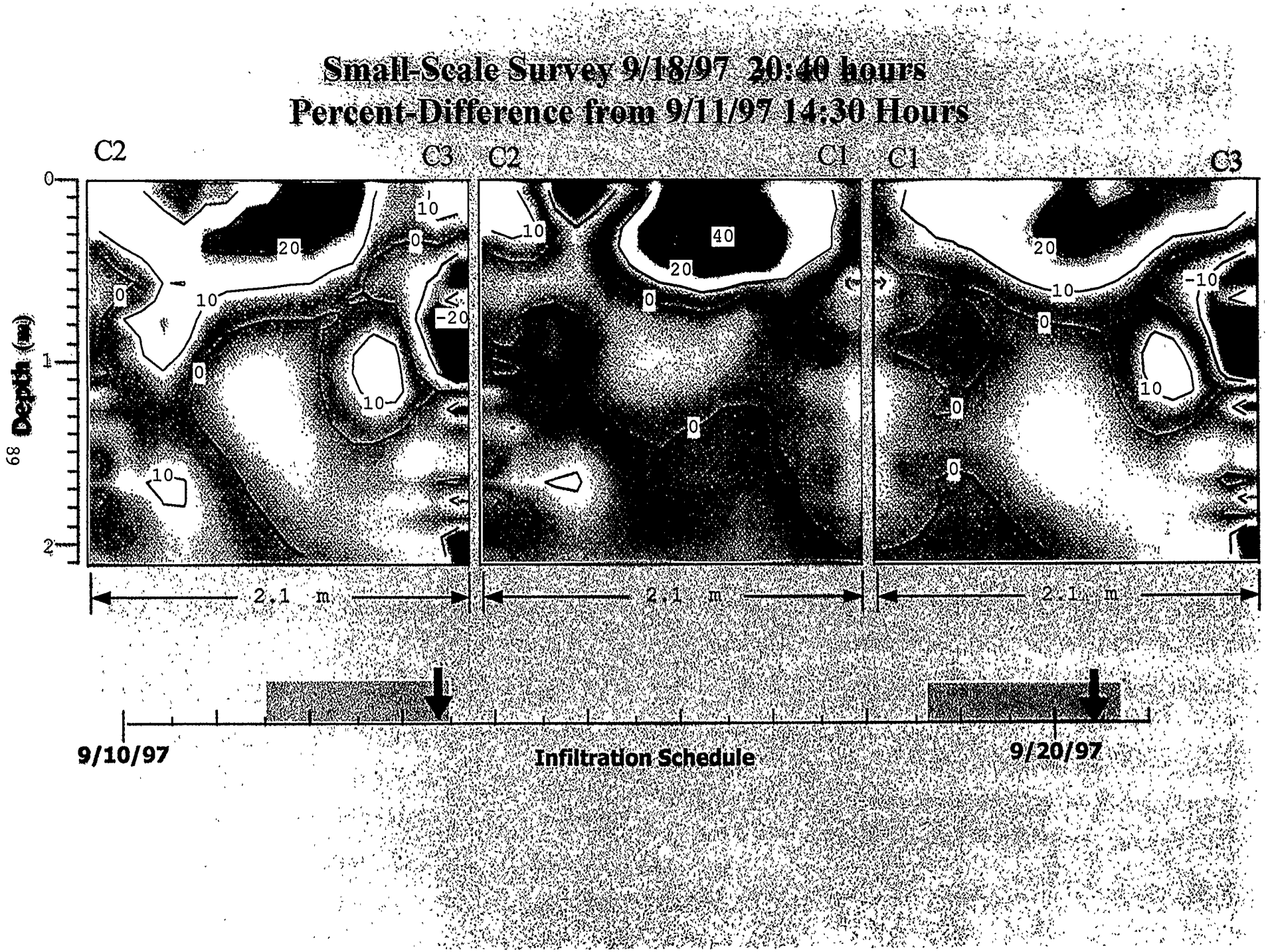
Small-Scale Survey 9/18/97 20:40 hours
Percent-Difference from 9/11/97 14:30 Hours
C2
C3
C2
C1
C1
C3
Depth (m)
0
1
2
2.1 m
2.1 m
2.1 m
9/10/97
Infiltration Schedule
9/20/97

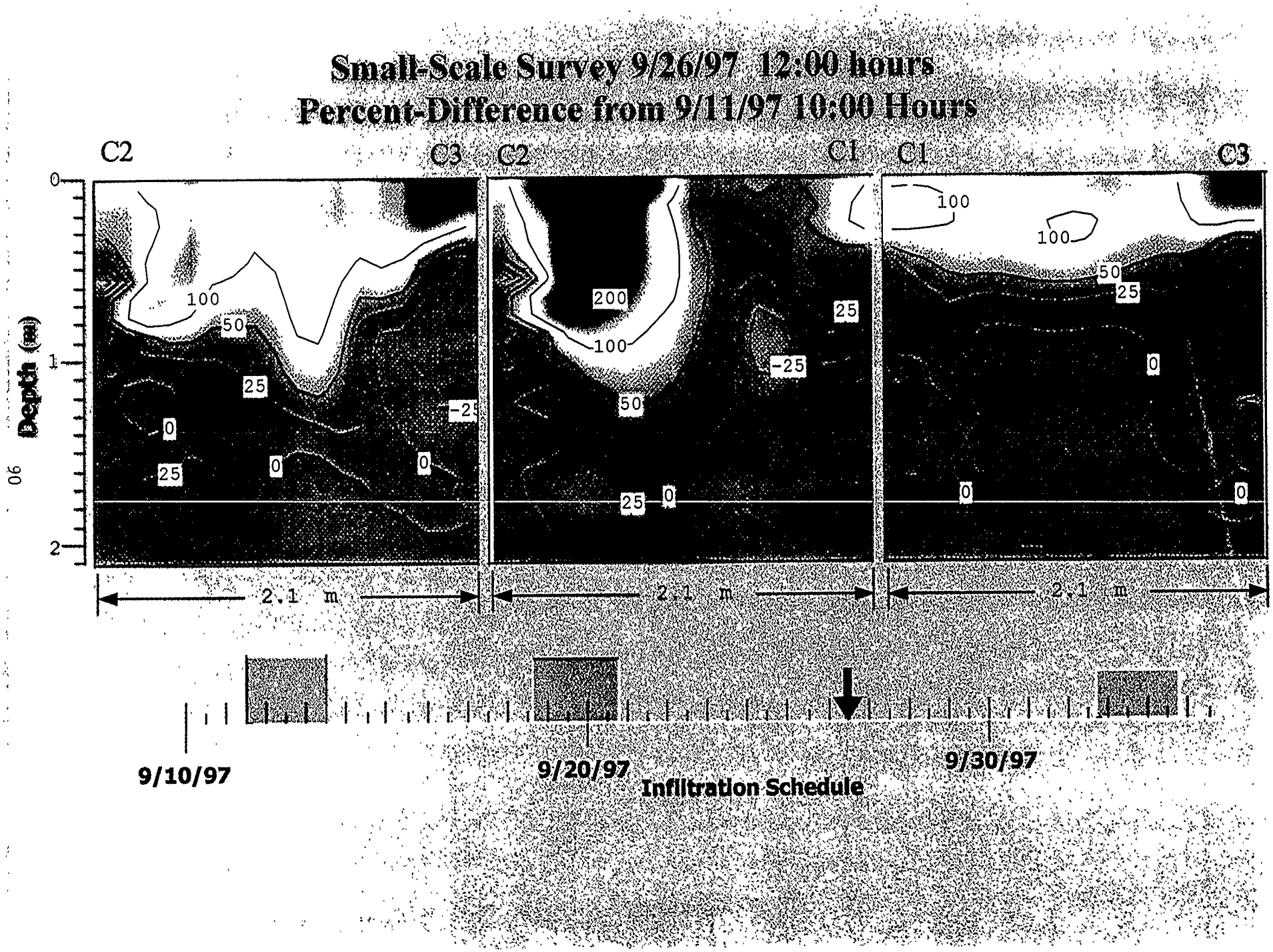
Small-Scale Survey 9/26/97 12:00 hours
Percent-Difference from 9/11/97 10:00 Hours
C2
C3
C2
C1
C1
C3
Depth (m)
0
1
2
100
50
25
0
-25
200
2.1 m
2.1 m
2.1 m
9/10/97
9/20/97
9/30/97
Infiltration Schedule

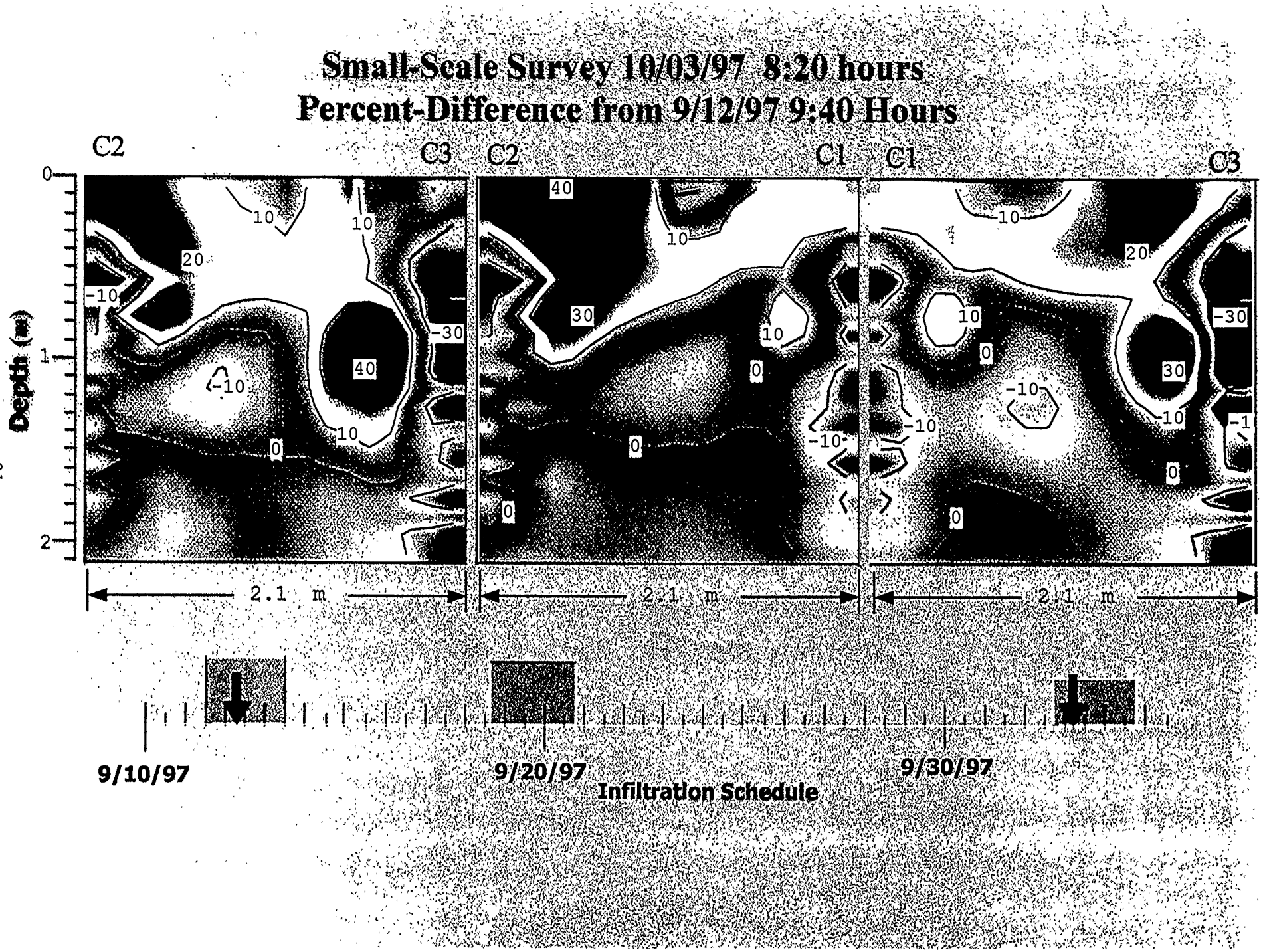
Small-Scale Survey 10/03/97 8:20 hours
Percent-Difference from 9/12/97 9:40 Hours
C2
C3
C2
C1
C1
C3
Depth (m)
0
1
2
2.1 m
2.1 m
2.1 m
9/10/97
9/20/97
9/30/97
Infiltration Schedule

Small-Scale Survey Percent-Difference Contours from 10/18 Overlaid on Background Resistivity Images

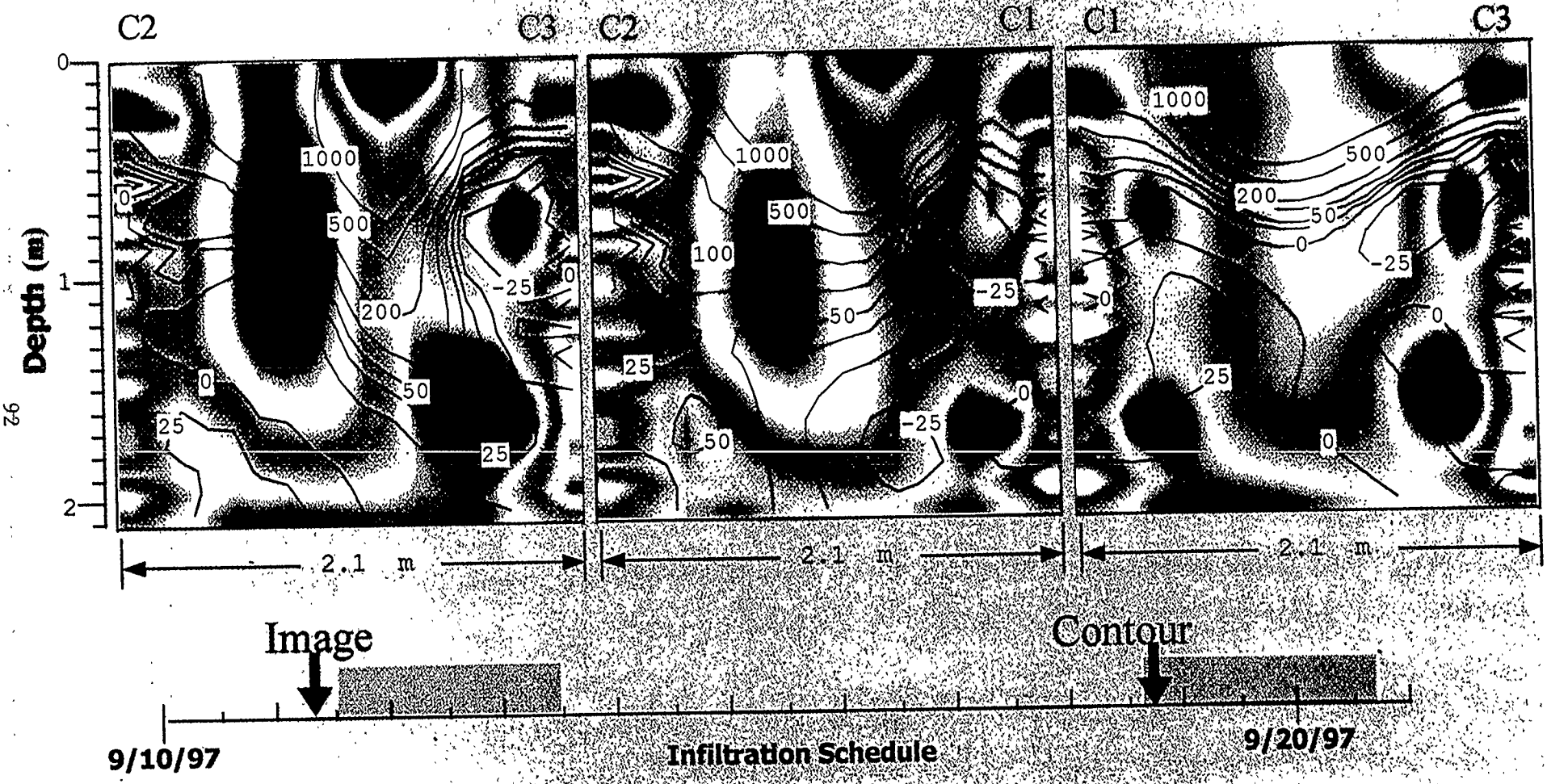

Conclusions

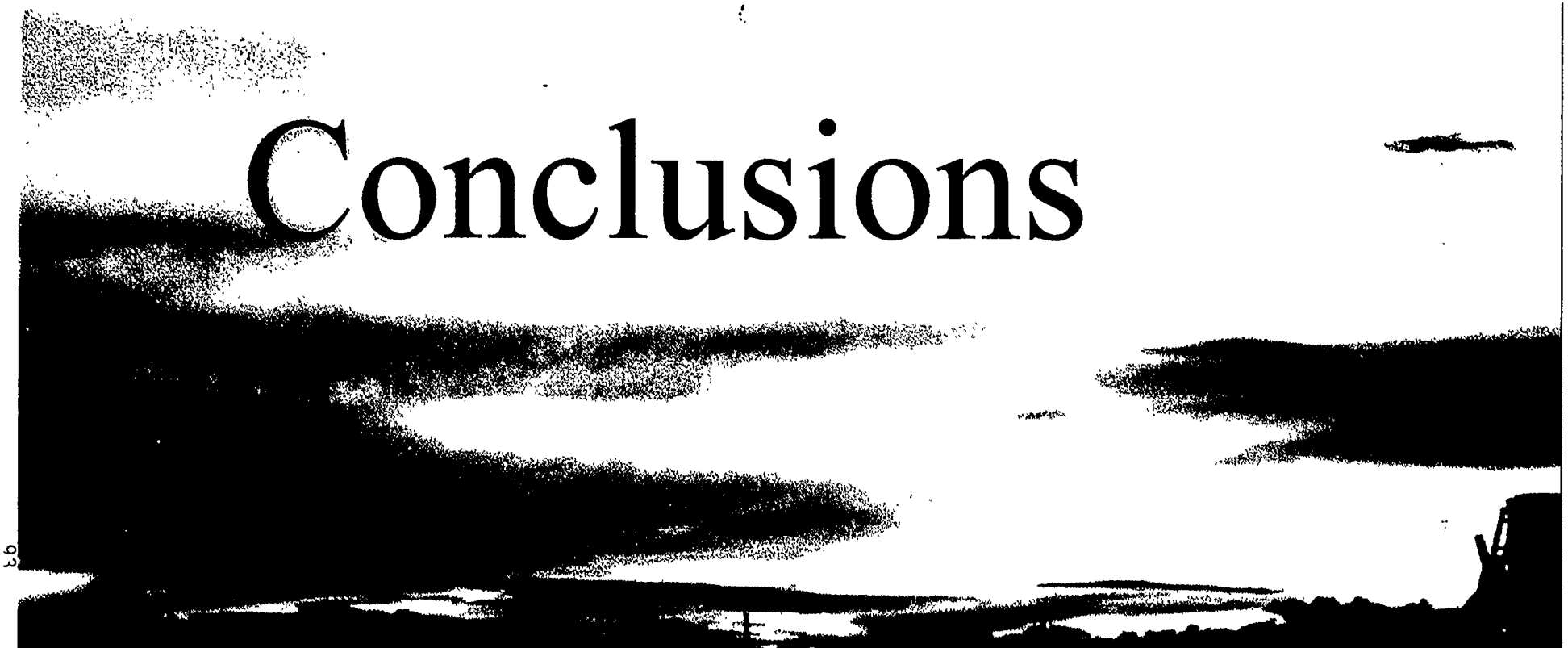

- Inner Survey Showed Two Types of Pathways:
  - Very Rapid Infiltration
  - Slower (Permeation?) Paths
- There Were Cumulative Long Term Changes from Experiment to Experiment Primarily in the Slower Pathways

Survey Results

Location of Planes for Large Scale Survey Images

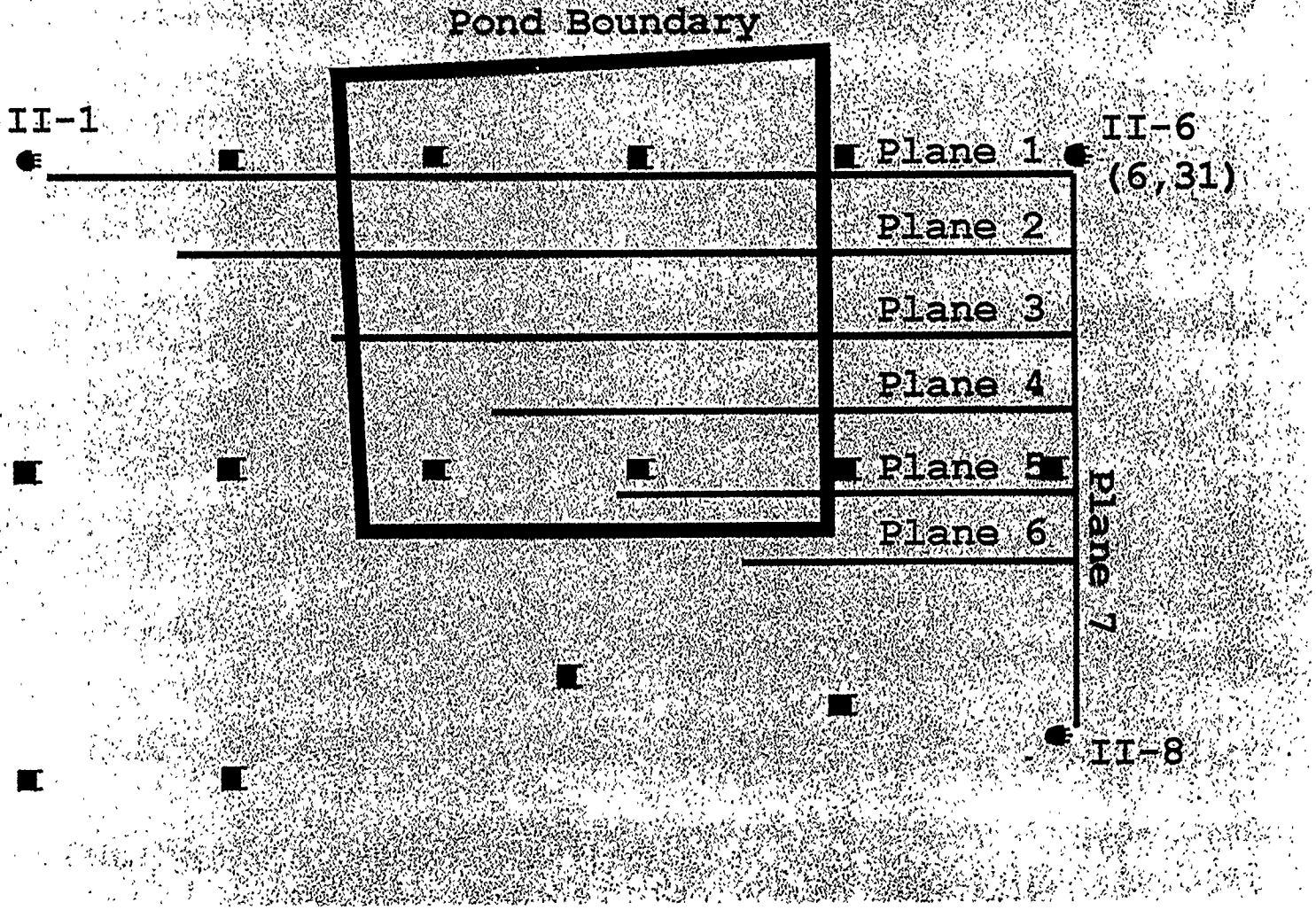

Outer Survey 9/11/97 9:00 hours
Pre-Injection Resistivity

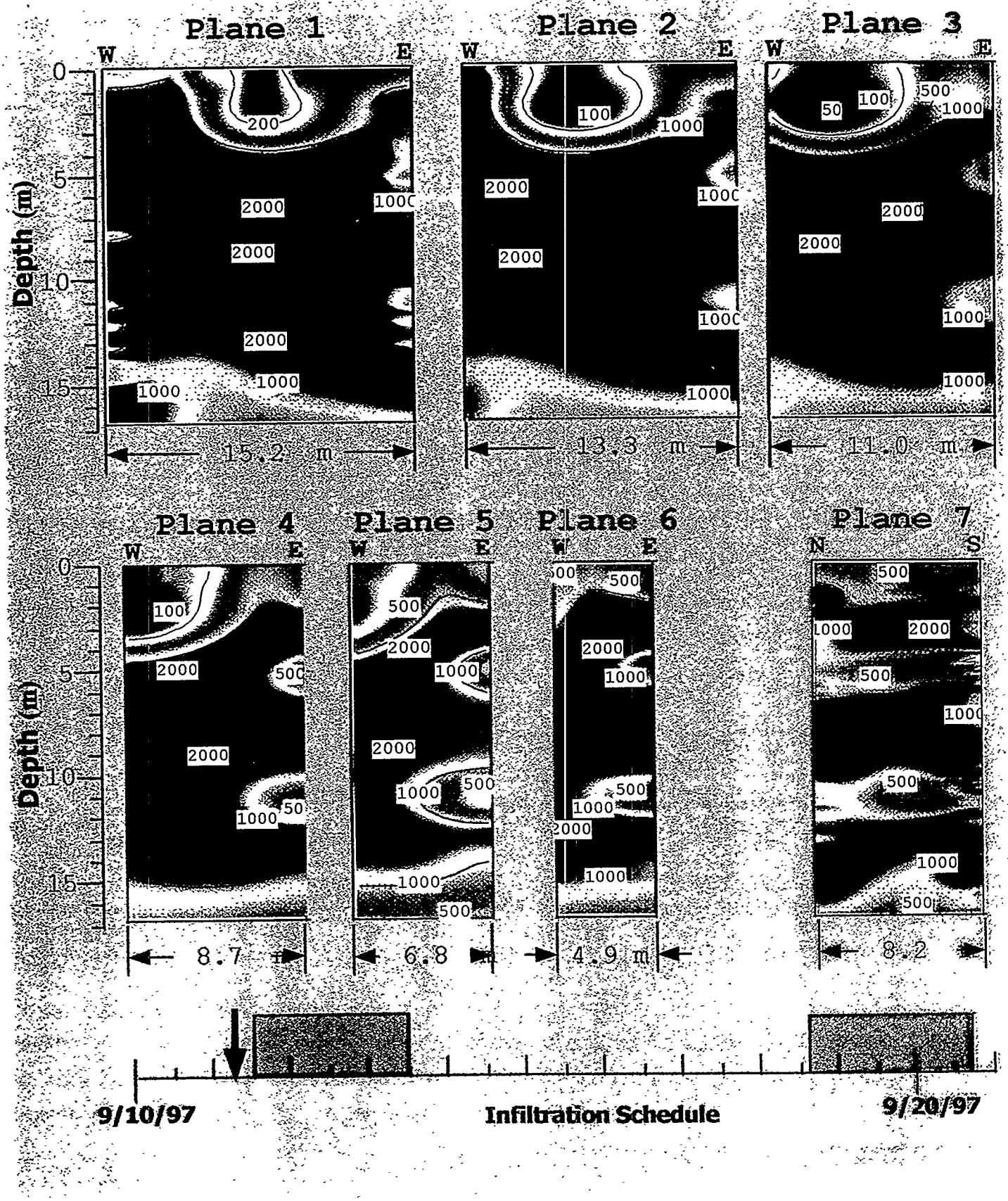

Outer Survey 9/13/97 9:00 Hours
Percent Difference from 9/11/97 9:00 Hours

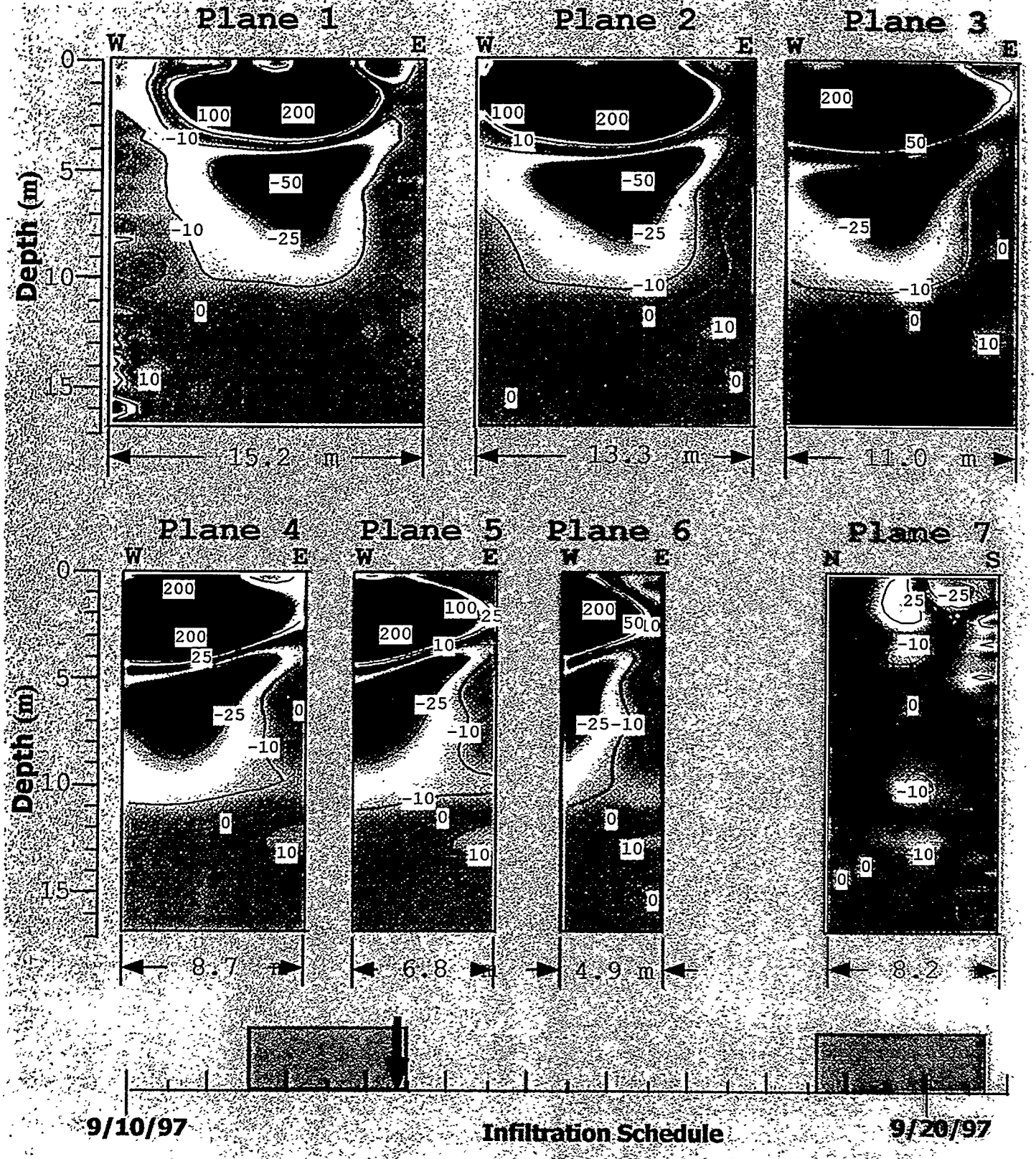

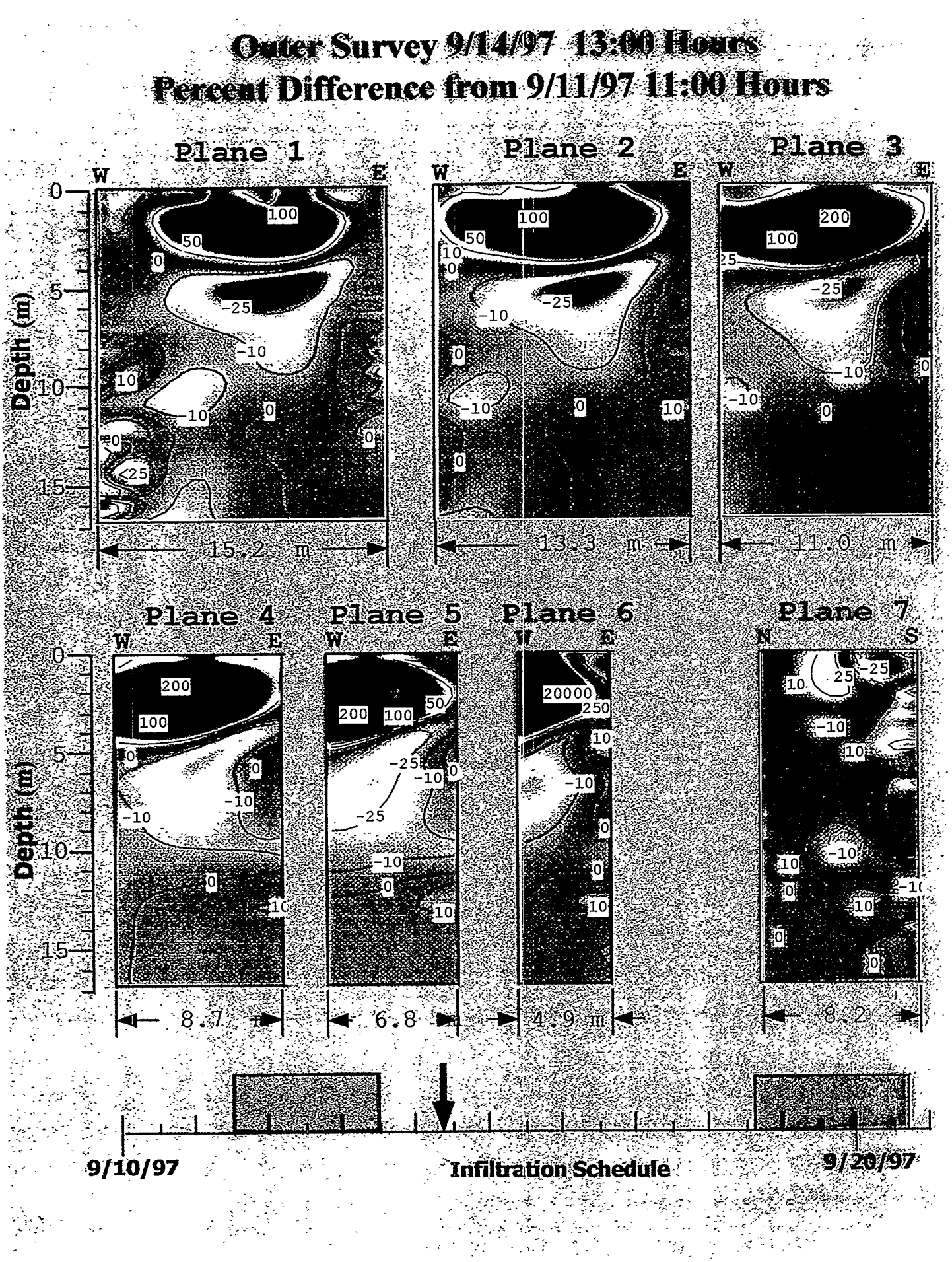
Outer Survey 9/14/97 13:00 Hours
Percent Difference from 9/11/97 11:00 Hours
Plane 1
Plane 2
Plane 3
Plane 4
Plane 5
Plane 6
Plane 7
W
E
N
S
Depth (m)
0
5
10
15
15.2 m
13.3 m
11.0 m
8.7 m
6.8 m
4.9 m
8.2 m
9/10/97
Infiltration Schedule
9/20/97

Outer Survey 9/25/97 13:00 Hours
Percent Difference from 9/11/97 9:00 Hours

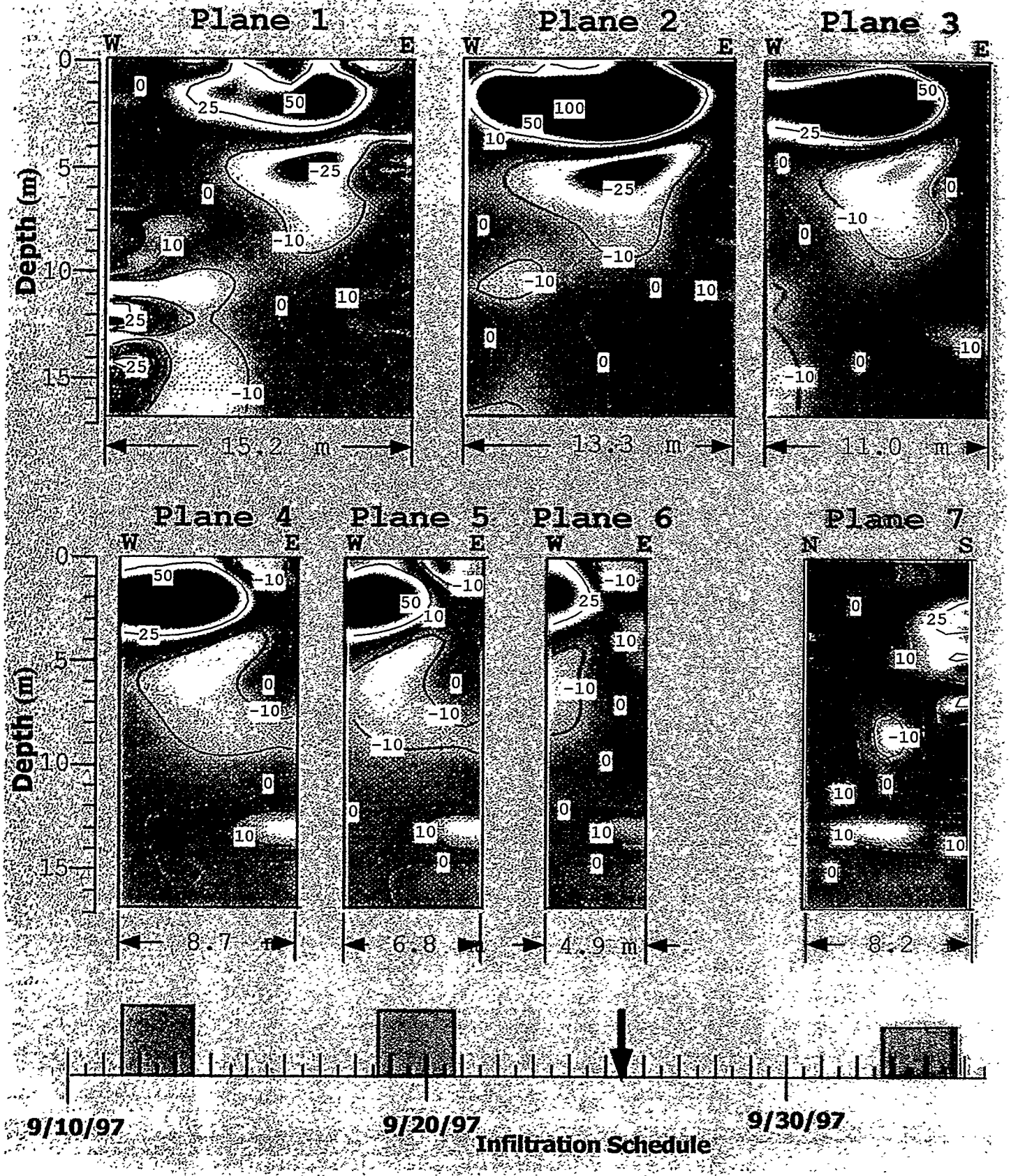

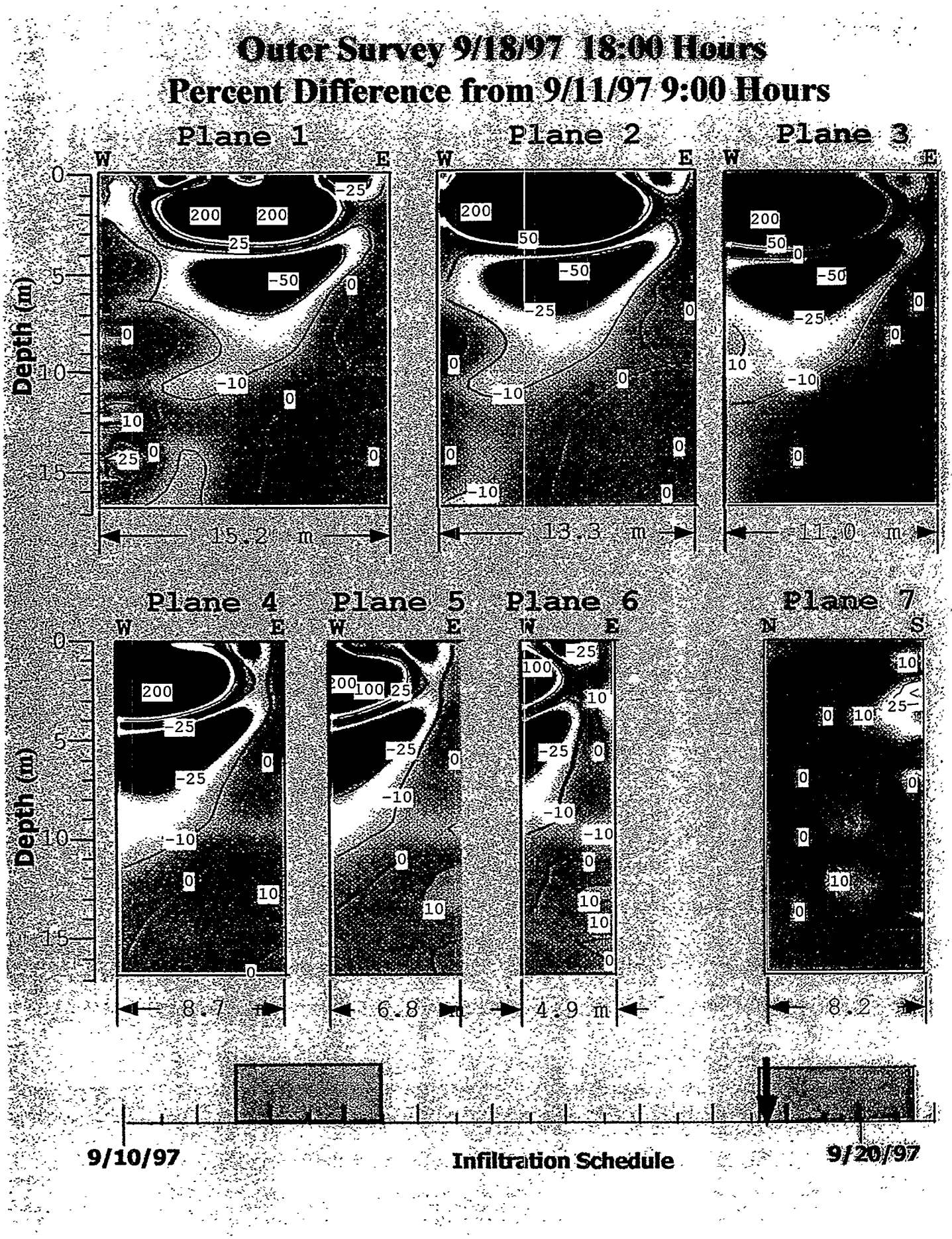
Outer Survey 9/18/97 18:00 Hours
Percent Difference from 9/11/97 9:00 Hours
Plane 1
Plane 2
Plane 3
Plane 4
Plane 5
Plane 6
Plane 7
W
E
N
S
Depth (m)
0
5
10
15
15.2 m
13.3 m
11.0 m
8.7 m
6.8 m
4.9 m
8.2 m
9/10/97
Infiltration Schedule
9/20/97

Outer Survey 9/20/97 14:00 Hours
Percent Difference from 9/11/97 9:00 Hours

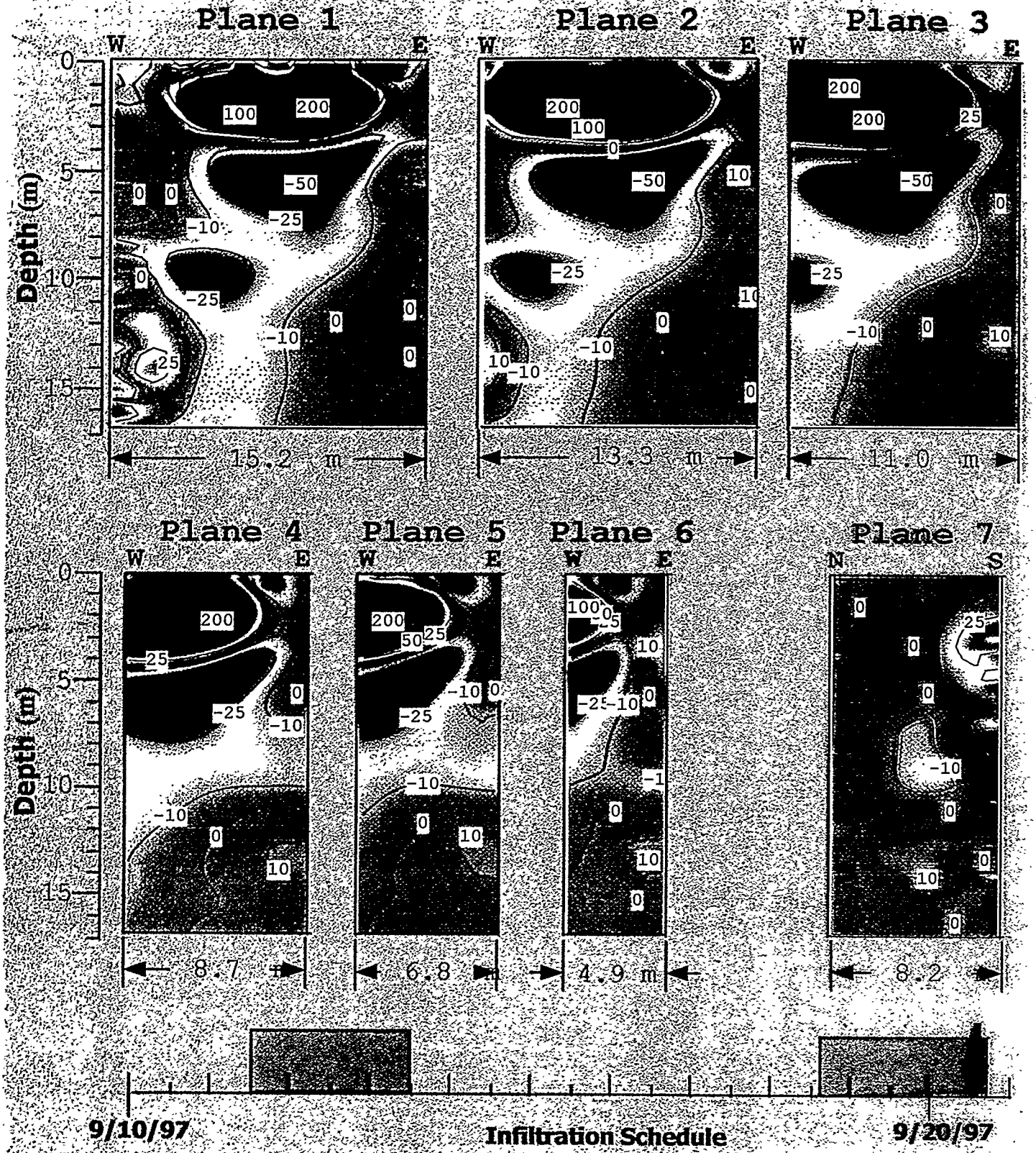

Conclusions

- Large Scale Survey Results Were Disappointing
  - Substantial Artifacts Indicate a "Blind Spot" Below the Pond
  - ObservedChanges at Depths Were Small ~10 to 20%
- It is Not Clear if the Changes Are Small or if We Just Missed the Major Flow Paths

INEEL
A Chaotic-Dynamical Conceptual Model to Describe Fluid Flow and Contaminant Transport in a Fractured Vadose Zone

Outcrop Infiltration Experiments-1997

Project Status

T.R. Wood, Field Team Leader

R.K. Podgorney

T.S. Stoops, Manager

Outline for Project Status Summary Meeting with DOE-ID 12/2/97

- Purpose and Benefits of Chaos Research
- Achievements of Project To-Date
- Current Project Life-Cycle Status
- Activities Scheduled for FY-98

Benefits of a Chaotic-Dynamical Model of Flow and Transport in a Fractured Vadose Zone

- Traditional methods and paradigms describe systems in parameters which reflect average behavior - not adequate for complex geometries and time-dependent processes
- New algorithms will improve our ability to determine what is knowable and thus may have a significant impact on regulatory issues
- The system attractor can be used to predict the long-term bounds on fluid flow and transport

Highlights of INEEL Dynamical-Chaos Project Achievements

- Successful completion of meso-scale fractured rock field test at Hell's Half Acre
- Collection of over 300,000 data points for chaotic analysis
- Observed chaotic behavior in fractured basalt flow
- Papers/Presentations: 2 at GSA; 1 at AGU
- Patent applications:
  - Radial Laser Surveyor
  - Remote Leak Detector
  - Structural Integrity Evaluation System

A Chaotic-Dynamical Conceptual Model to Describe Fluid Flow and Contaminant Transport in a Fractured Vadose Zone

Outcrop Infiltration Experiments-1997

R.K. Podgorney

T.S. Stoops, Manager

T.R. Wood, Team Leader

Objectives

- Quantify hydraulic properties of fractures at the scale of investigation of approximately 1 meter
- Collect datasets which can be analyzed in a chaotic-dynamical fashion
  - Drip interval
  - Tension time series
  - Temporal and spatial variation of outflow
- Provide analogous dataset to previous chaotic analysis (e.g., Shaw, 1984)
- Determine if an attractor exists that describes the behavior of the system

Overview of Activities

- Test Conceptualization
- Instrument Development
- Site Selection
- Site Preparation
- Test Execution
- Data Reductions and Dissemination
- Data Analysis

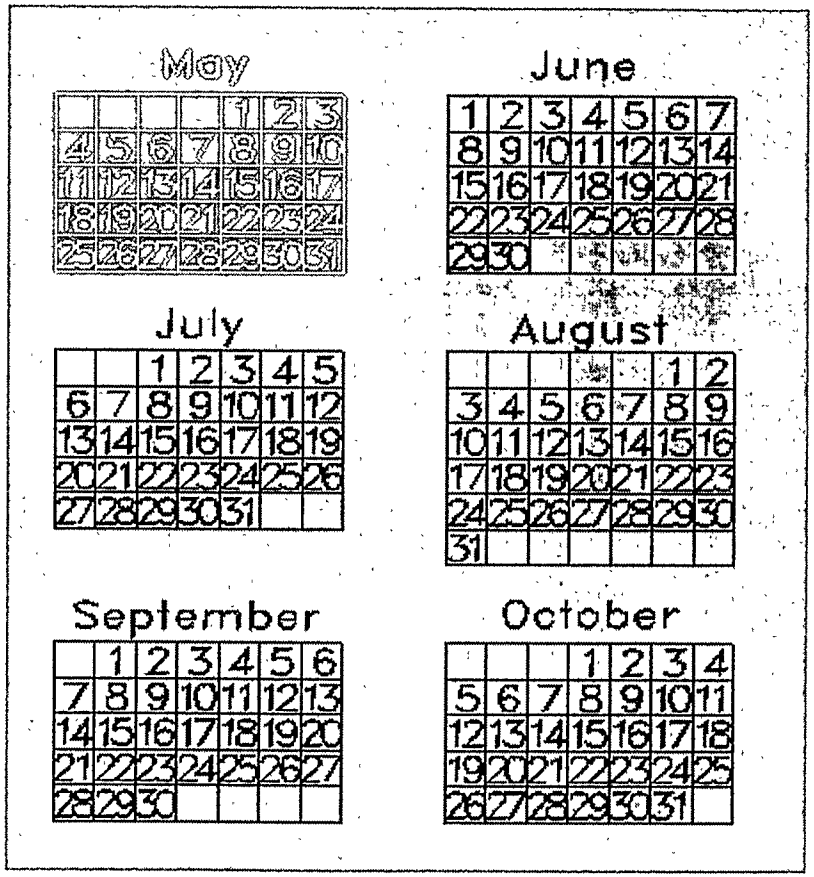

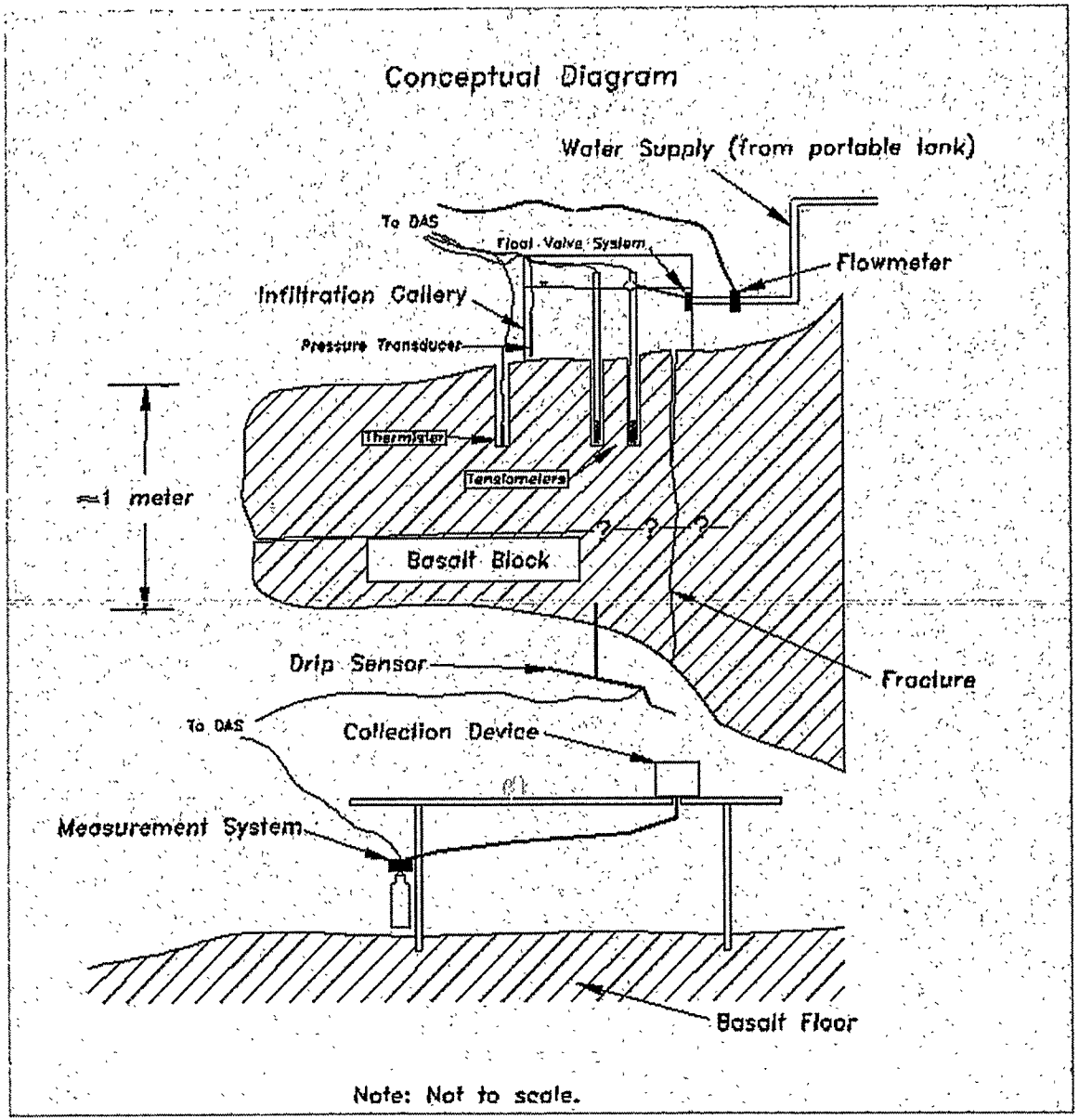
Conceptual Diagram
Water Supply (from portable tank)
To DAS
Float Valve System
Flowmeter
Infiltration Gallery
Pressure Transducer
≈1 meter
Thermister
Tensiometers
Basalt Block
Drip Sensor
Fracture
To DAS
Collection Device
Measurement System
Basalt Floor
Note: Not to scale.

Overview of Activities

- Test Conceptualization
- Instrument Development
- Site Selection
- Site Preparation
- Test Execution
- Data Reductions and Dissemination
- Data Analysis

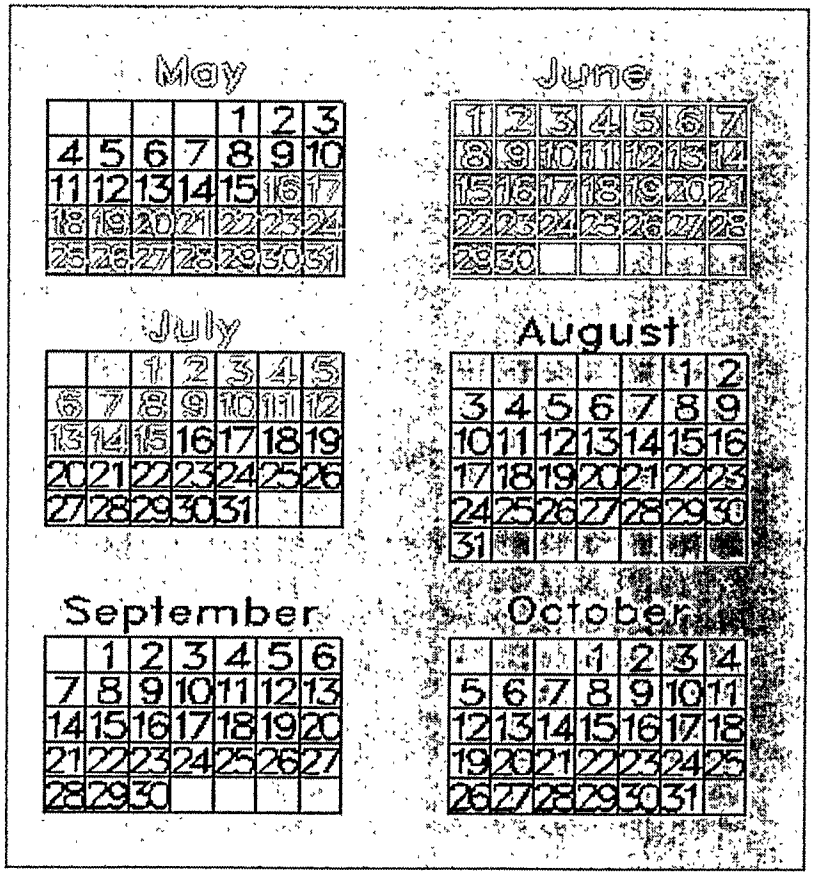

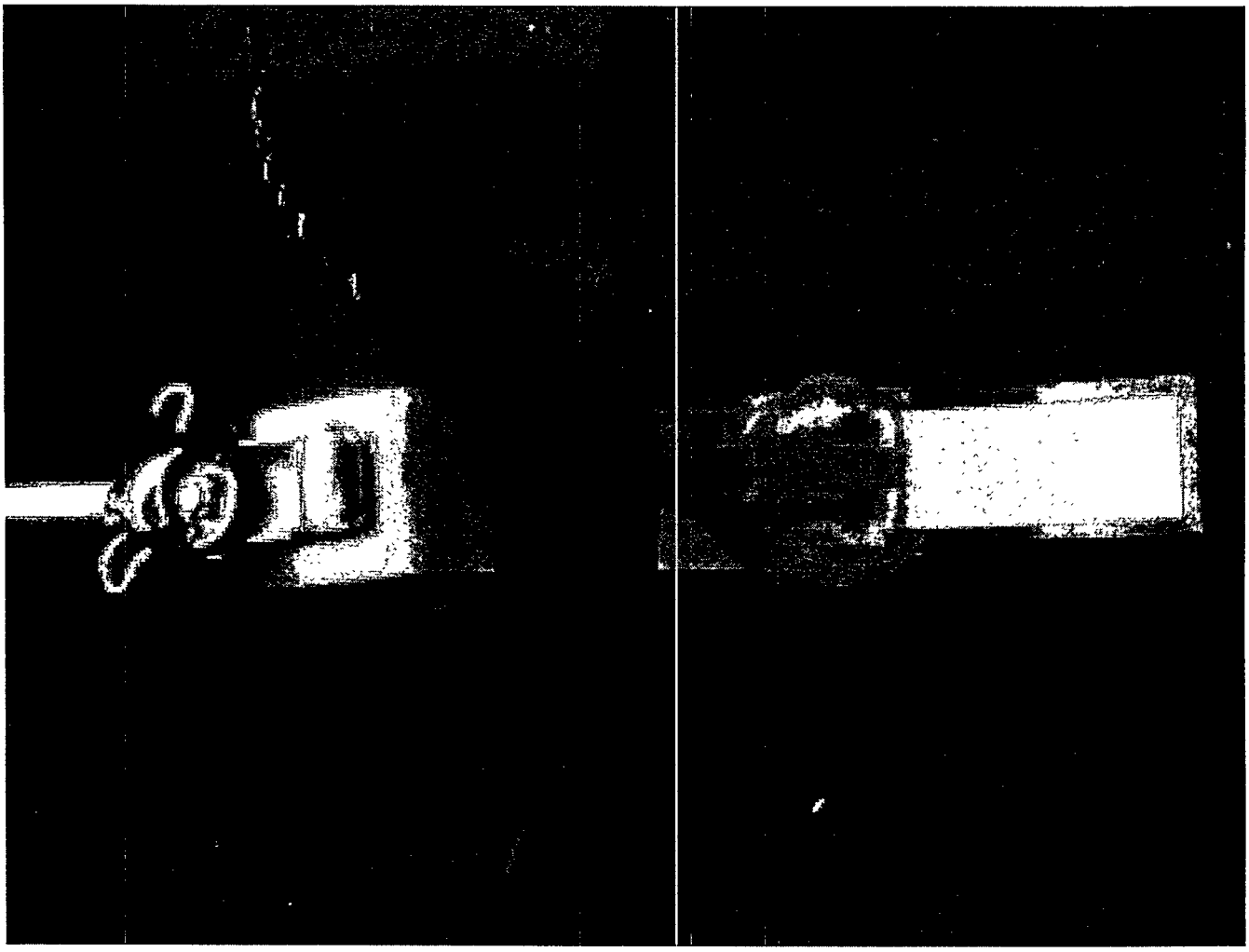

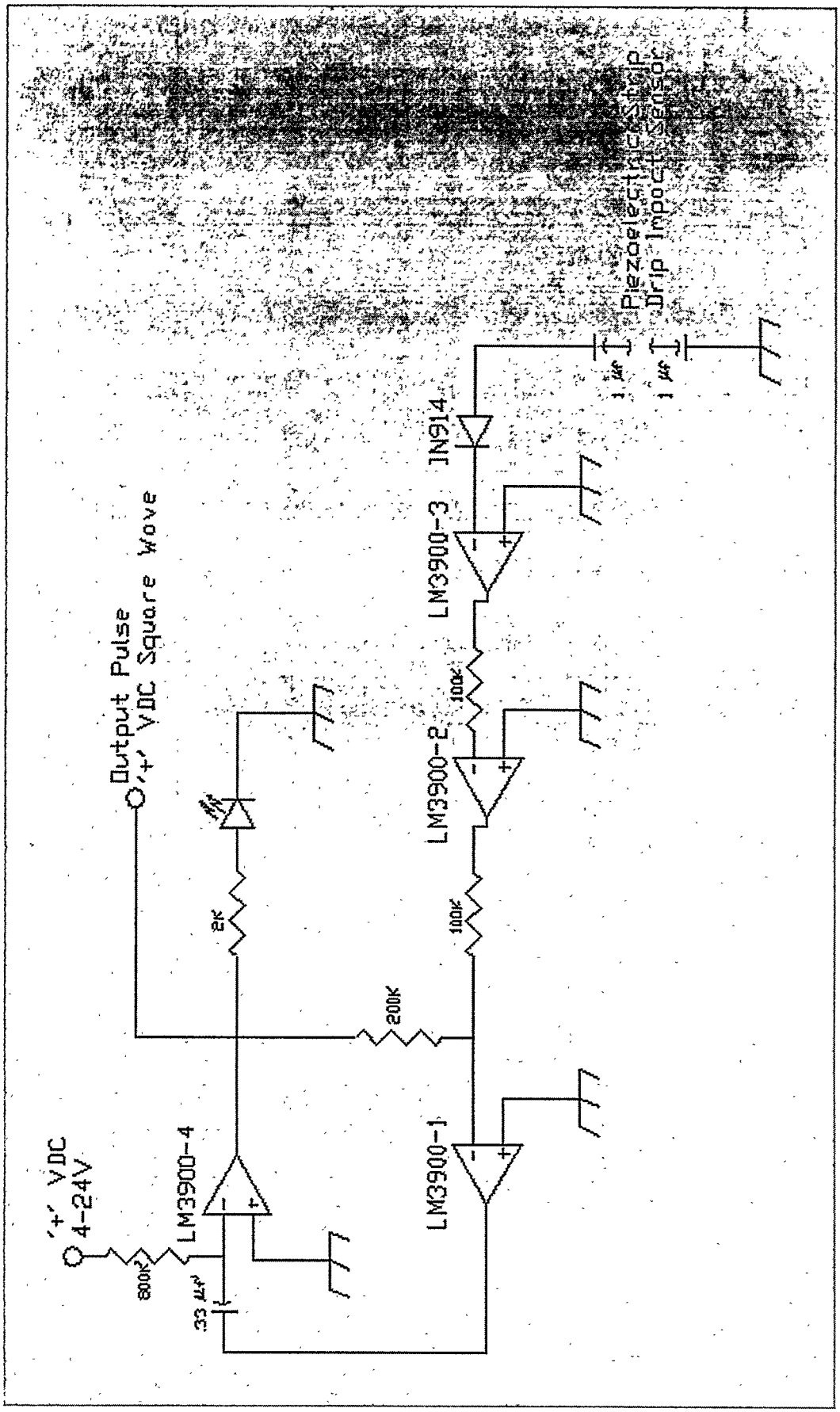
'+' VDC
4-24V
800K
.33 µF
LM3900-4
LM3900-1
LM3900-2
LM3900-3
1N914
2K
100K
100K
200K
Output Pulse
'+' VDC Square Wave
1 µF
1 µF
Piezoelectric Strip
Drip Impact Sensor

Overview of Activities

- Test Conceptualization
- Instrument Development
- Site Selection
- Site Preparation
- Test Execution
- Data Reductions and Dissemination
- Data Analysis

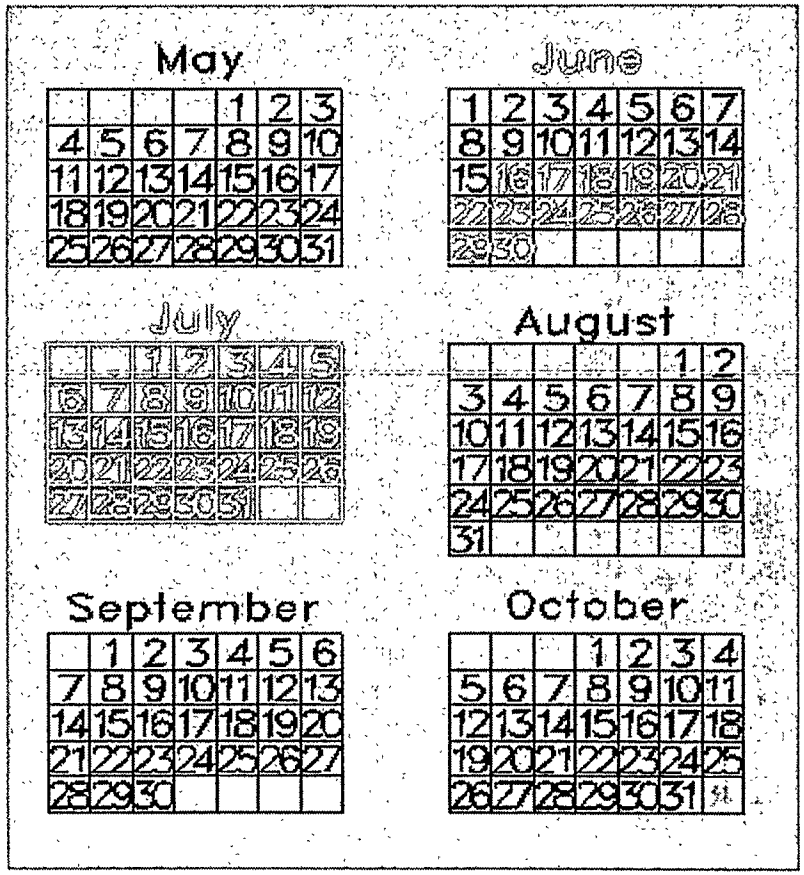

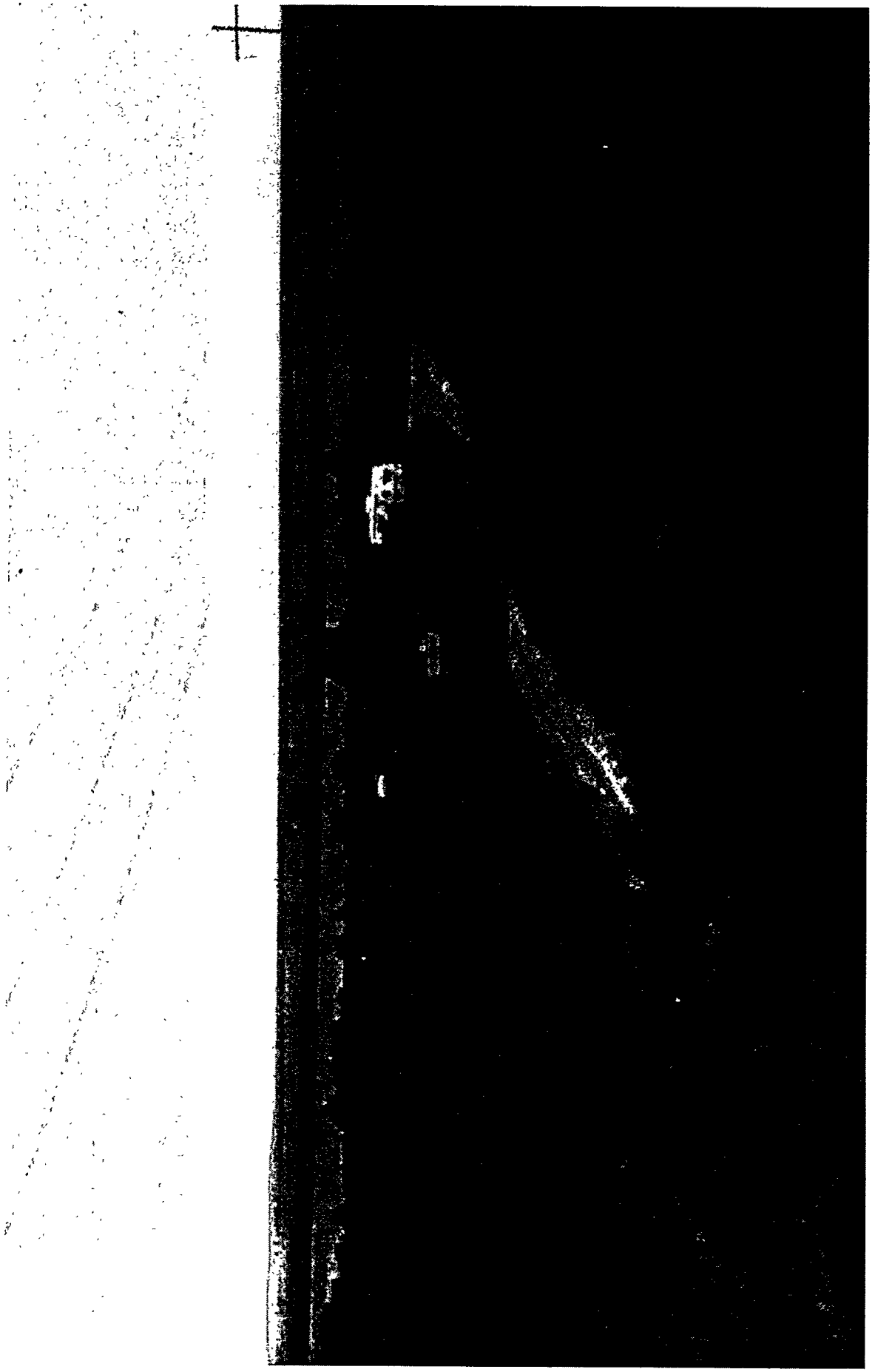

Overview of Activities

- Test Conceptualization
- Instrument Development
- Site Selection
- Site Preparation
- Test Execution
- Data Reductions and Dissemination
- Data Analysis

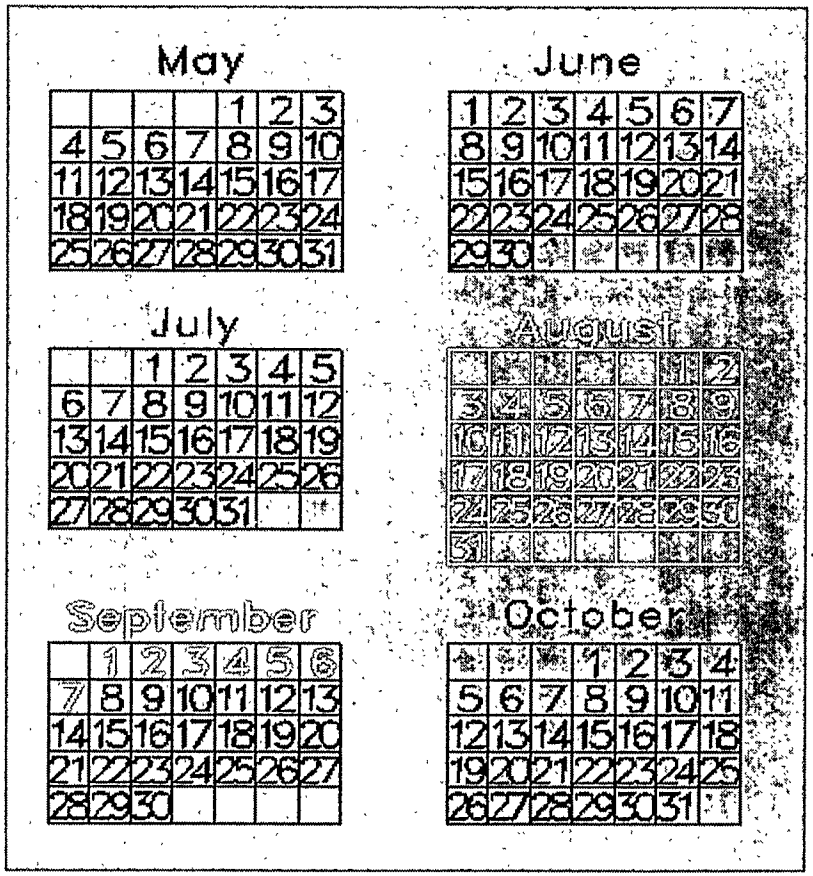

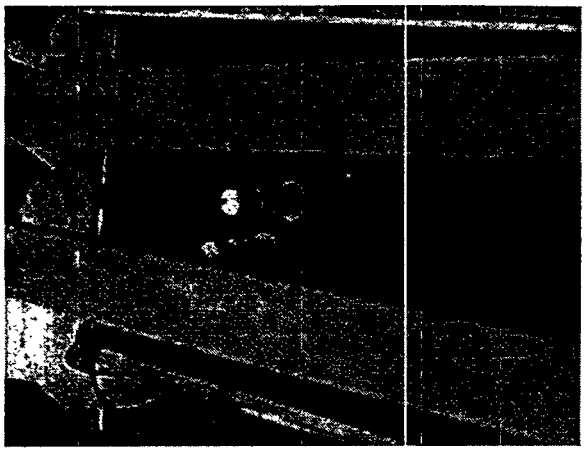

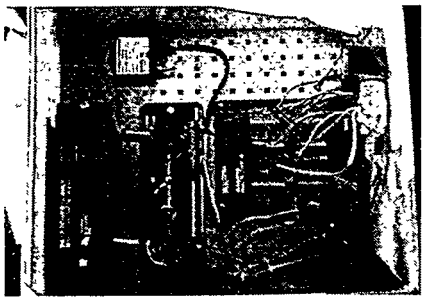

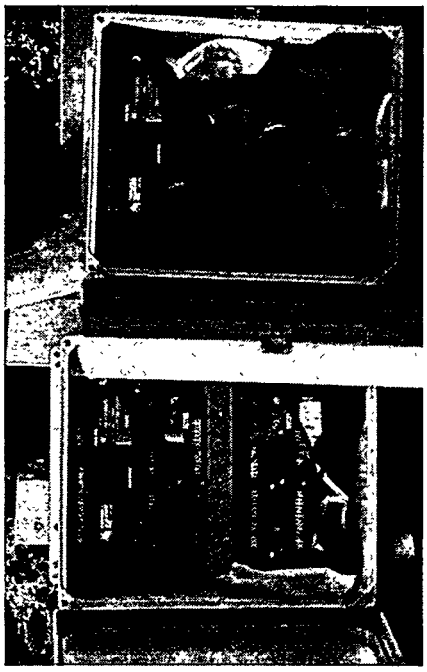

Overview of Activities

- Test Conceptualization
- Instrument Development
- Site Selection
- Site Preparation
- Test Execution
- Data Reductions and Dissemination
- Data Analysis

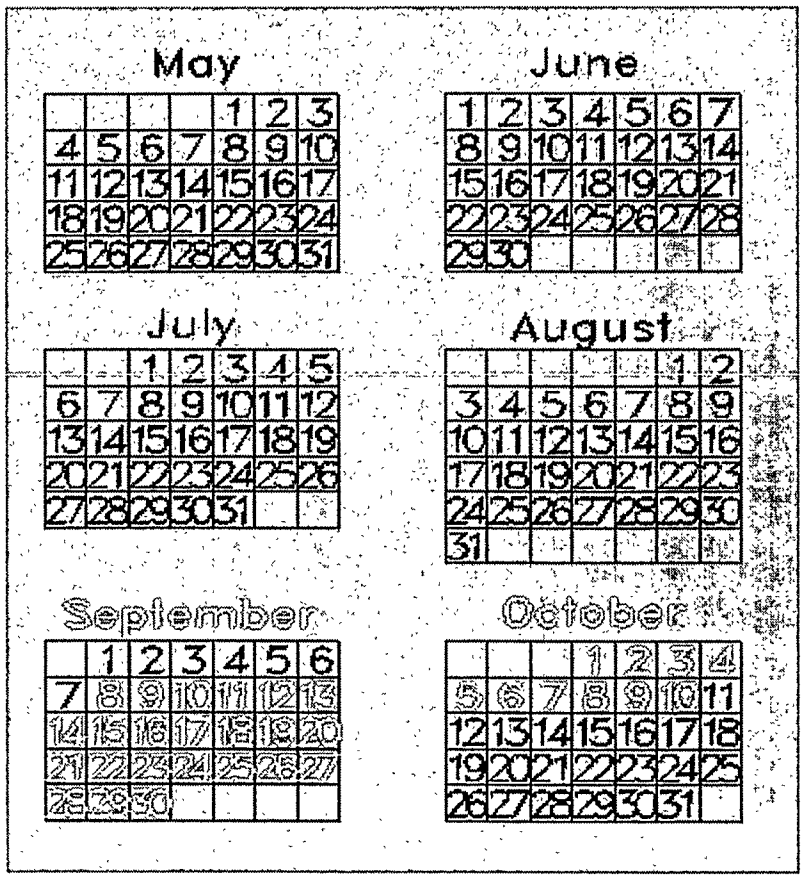

Overview of Activities

- Test Conceptualization
- Instrument Development
- Site Selection
- Site Preparation
- Test Execution
- Data Reductions and Dissemination
- Data Analysis

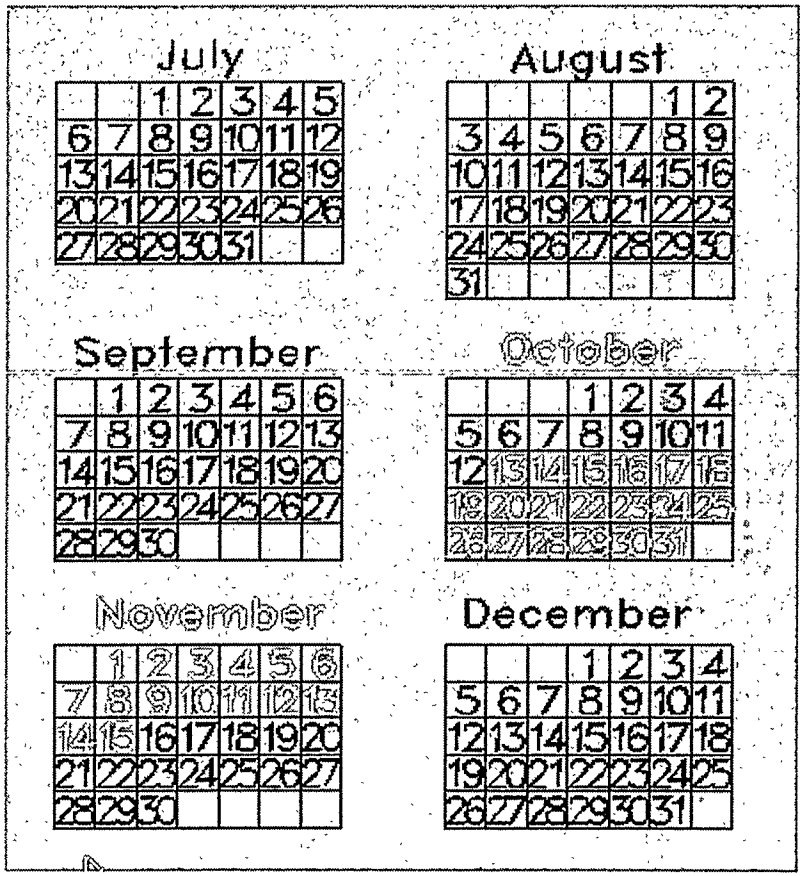

Drip Interval, Test 3, Location 7

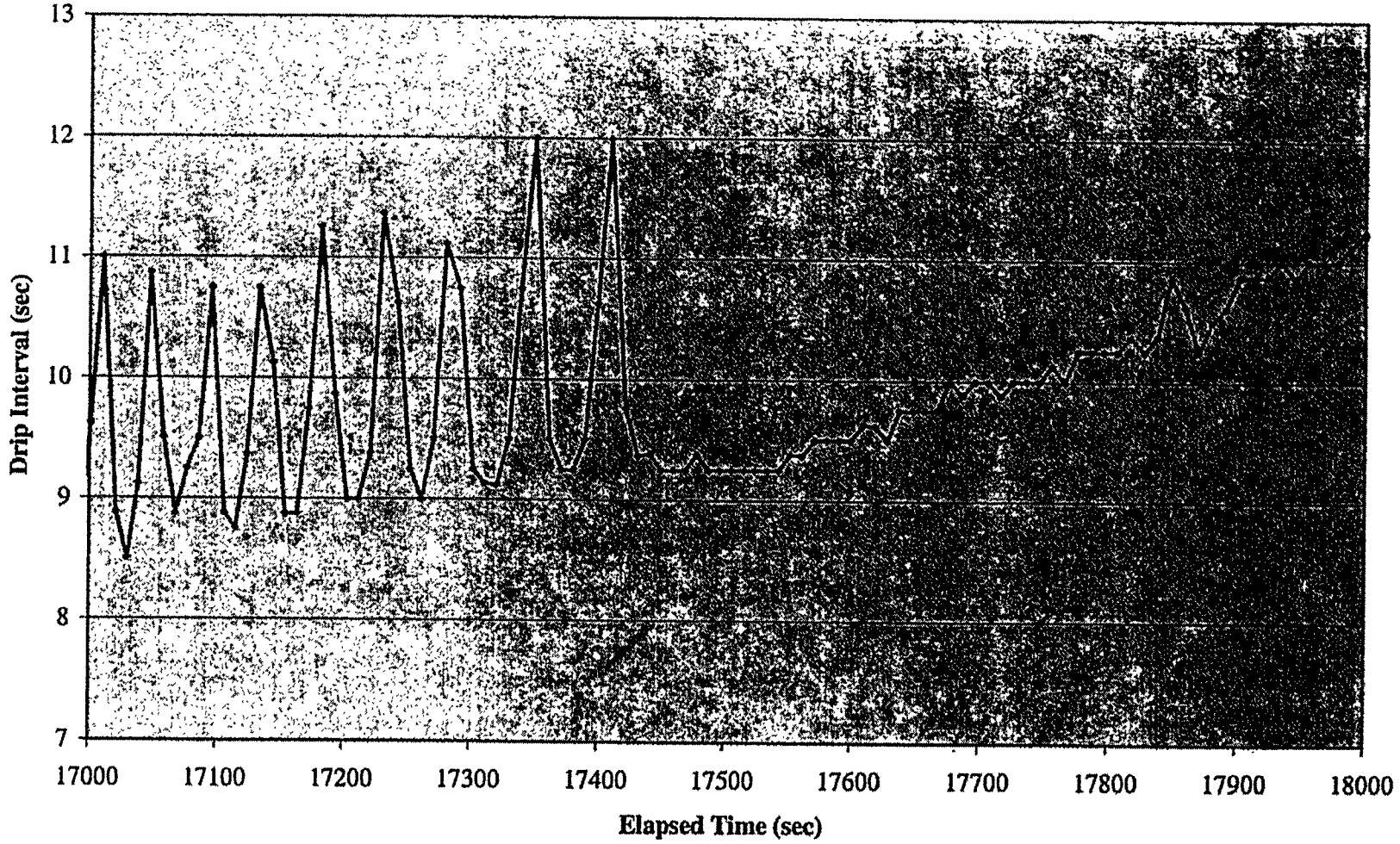

Overview of Activities

- Test Conceptualization
- Instrument Development
- Site Selection
- Site Preparation
- Test Execution
- Data Reductions and Dissemination
- Data Analysis

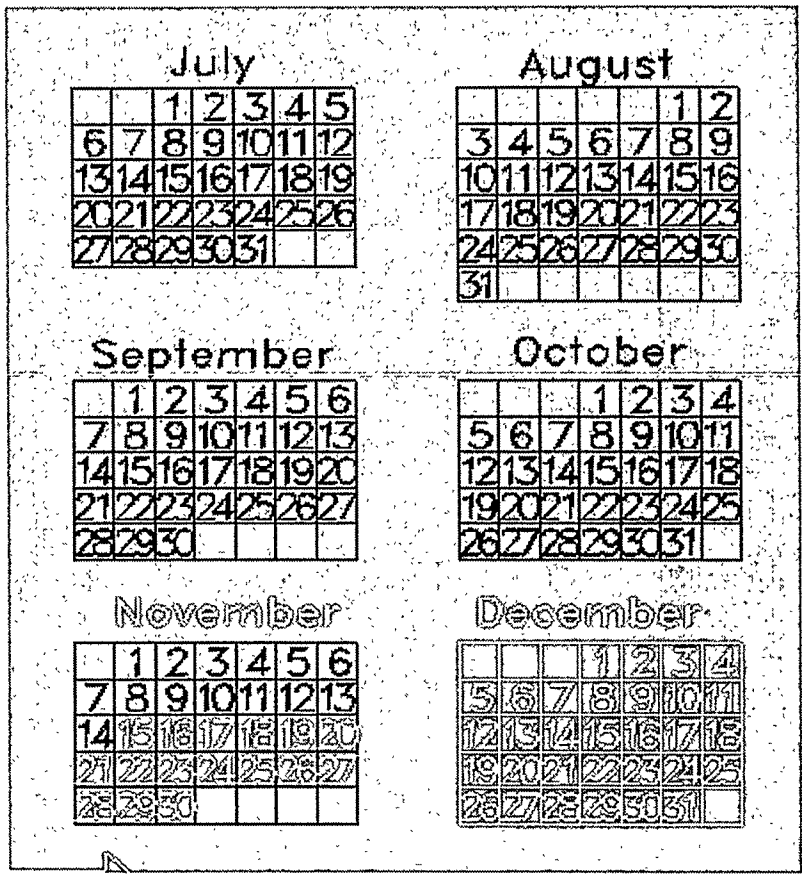

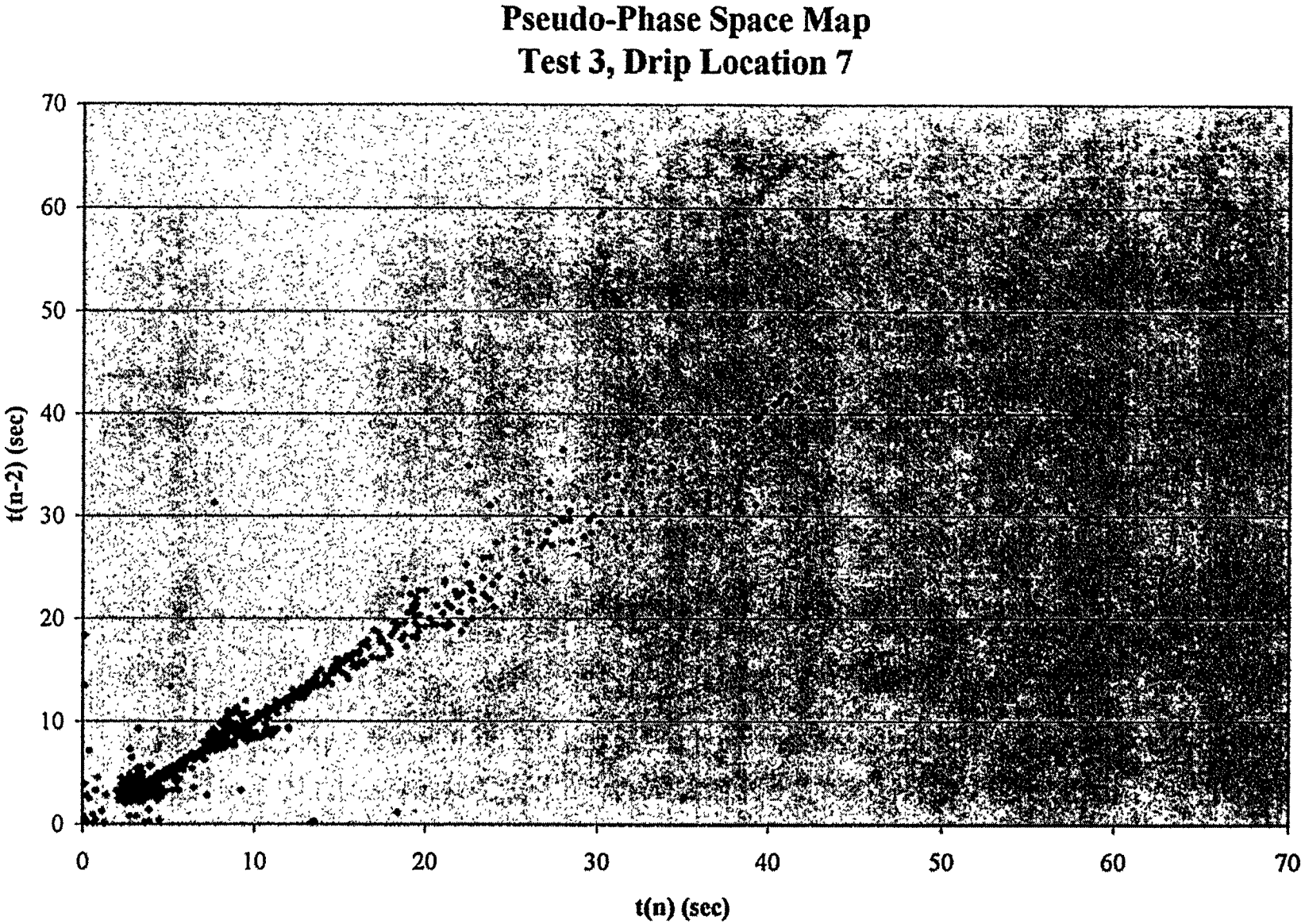
Pseudo-Phase Space Map
Test 3, Drip Location 7
t(n-2) (sec)
t(n) (sec)
0
10
20
30
40
50
60
70

Dynamical-Chaos is Currently in its second year

- First year activities were focused on collecting a data set of sufficient size and quality to perform chaotic analysis
- Second year will analyze data and focus and refine equipment and approach for second year of intermediate scale testing in fractured basalt
- Third year of project will build ties from the micro-, meso- and macro-scale for full scale

FY-98 Scheduled Activities

- Team meeting December 3-5 to summarize results of summer field work
- Winter of 1998 will focus on data analysis and development of instruments for measuring in moisture movement in fractures
- Summer 1998 will focus again on meso-scale testing at Hell's Half Acre (new site(s) and monitoring equipment

II.5

Laboratory Studies

Jil Geller & Sharon Borglin

- Consider drips in parallel plates as an analog to water seepage in fractures
- Extension of the "dripping faucet" model to drips in parallel plates under influence of capillary forces
- Obtain records of the pressure signal to monitor drip behavior
- Vary flow rates, surface texture and angle of inclination

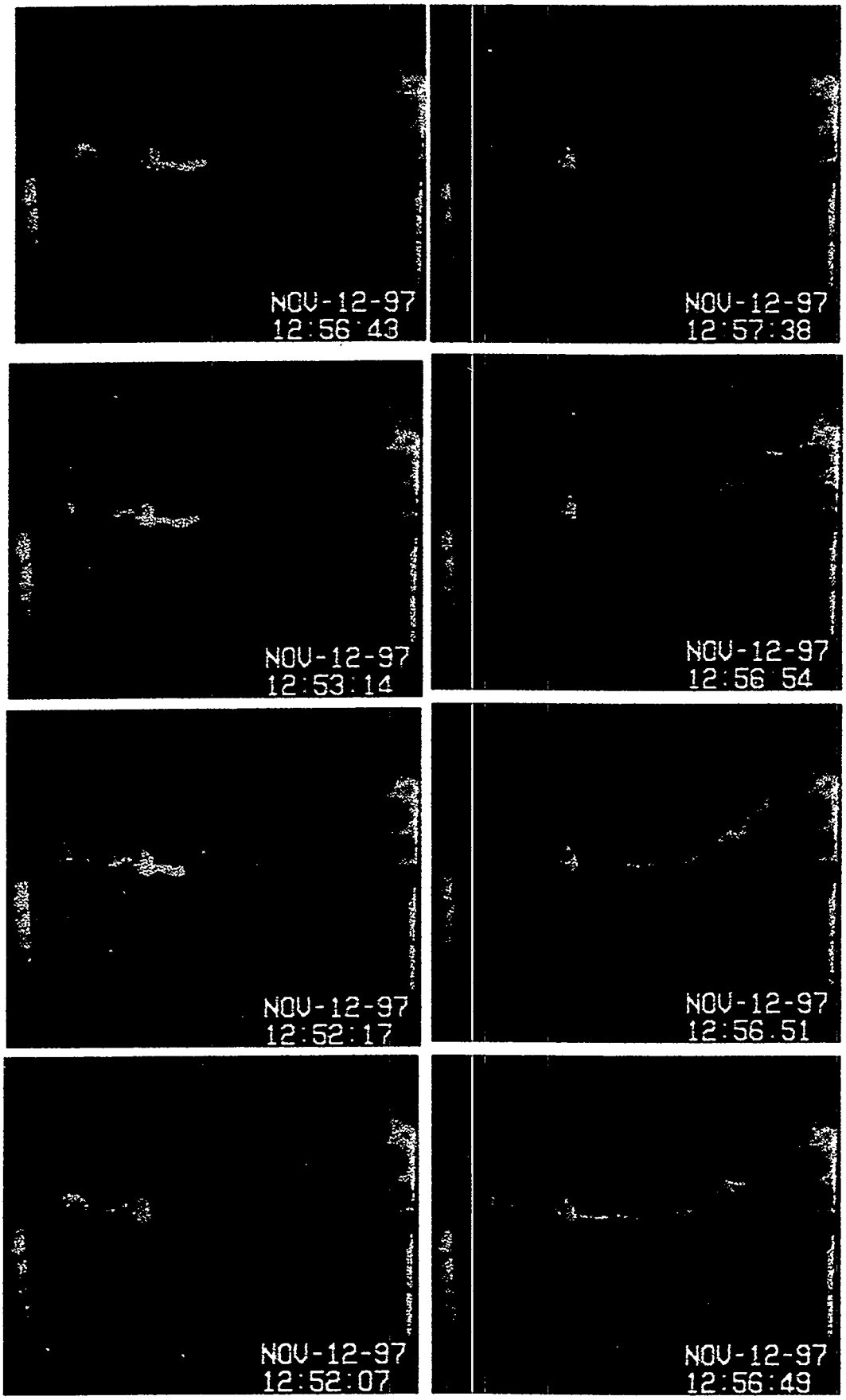
NOV-12-97
12:56:43
NOV-12-97
12:57:38
NOV-12-97
12:53:14
NOV-12-97
12:56:54
NOV-12-97
12:52:17
NOV-12-97
12:56:51
NOV-12-97
12:52:07
NOV-12-97
12:56:49

Behavior of Dripping Water in Parallel Plates

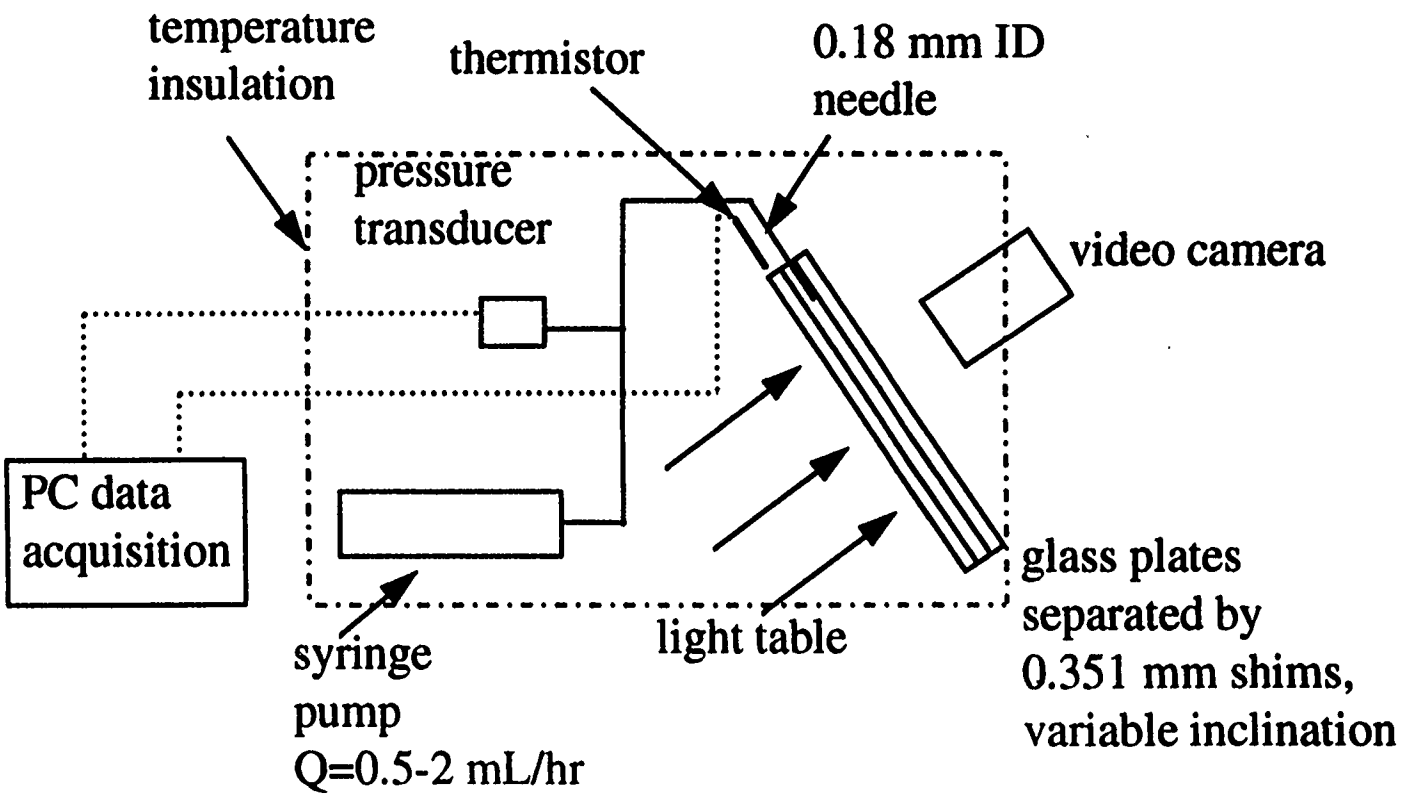

Use of Pressure Record as Indicator of Drip Behavior

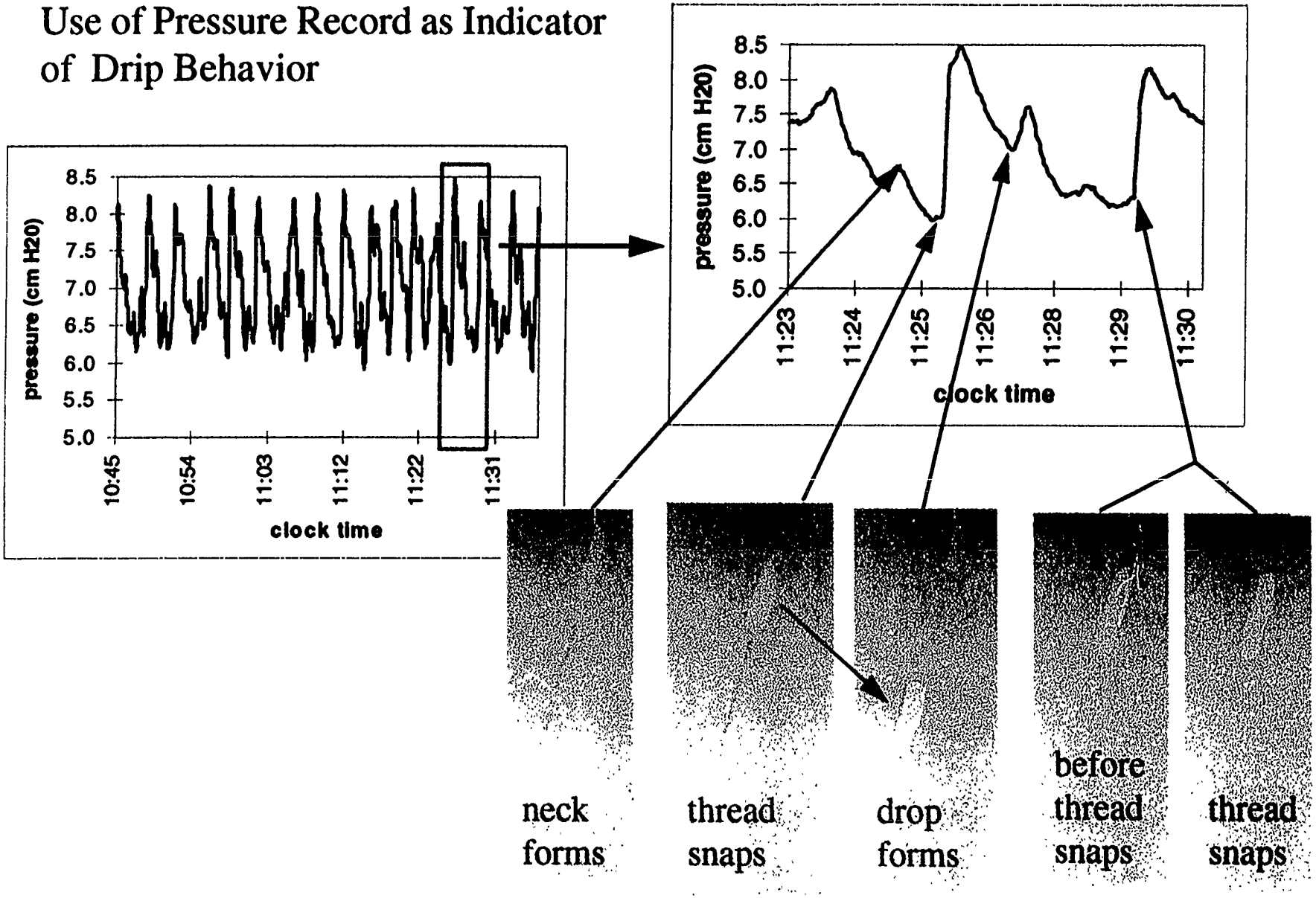

Record of Experiments

Smooth Parallel Plates		
date	flowrate (mL/hr)	estimated # snaps
6/4/97#	0.5	676
6/5/97	0.5	648
6/7/97	1	853
6/7/97	0.5	512
9/5/97*	2	109
9/5/97	1	93
9/8/97	0.5	49
9/9/97	1	202
9/11/97	1	233
9/22/97*	1	112
9/23/97	1	584
9/24/97	0.5	636
9/25/97#	0.25	406
9/26/97#	2	659
9/29/97	1.5	440
9/30/97	3	512
10/6/97	1	148
10/7/97#	1.5	150

*initially dry plates

video taped

Open Drips		
date	flowrate (mL/hr)	estimated # snaps
6/18/97	1	1133
6/20/97	0.5	3823
10/9/97	0.25	1403

Obscure Glass Plates		
date	flowrate (mL/hr)	estimated # snaps
7/29/97*	0.5	448
7/30/97	0.5	433
7/31/97	0.5	544
8/25/97	0.25	186

Baseline	
date	flowrate (mL/hr)
10/7/97	1.5
10/8/97	0.5
10/8/97	1
10/9/97	2
10/9/97	3
10/9/97	0.25

FIGURE 7: Pressure fluctuation from open drips and smooth parallel glass plates, 0.25 ml/hr flow rate

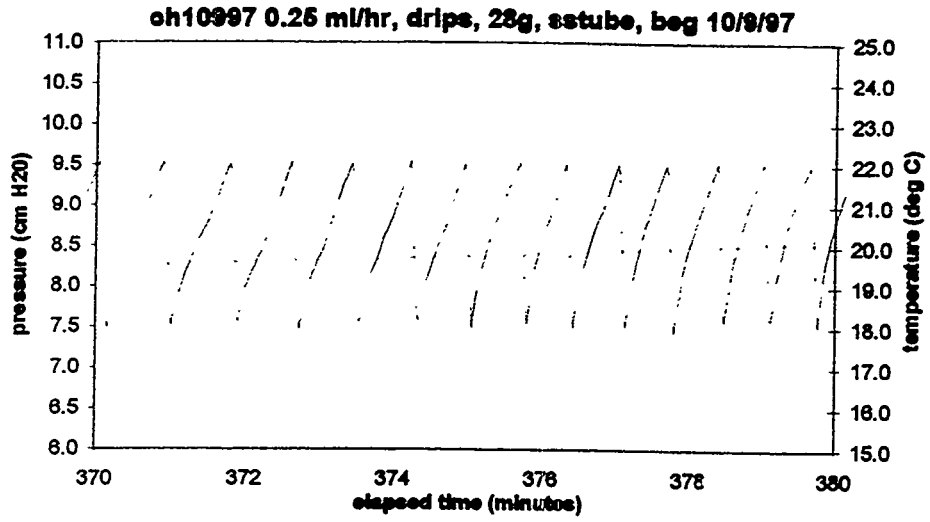

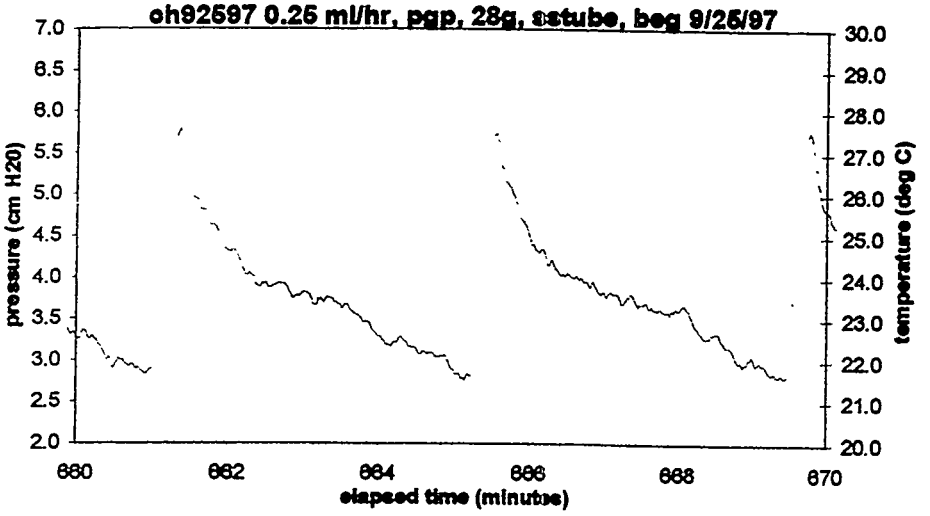

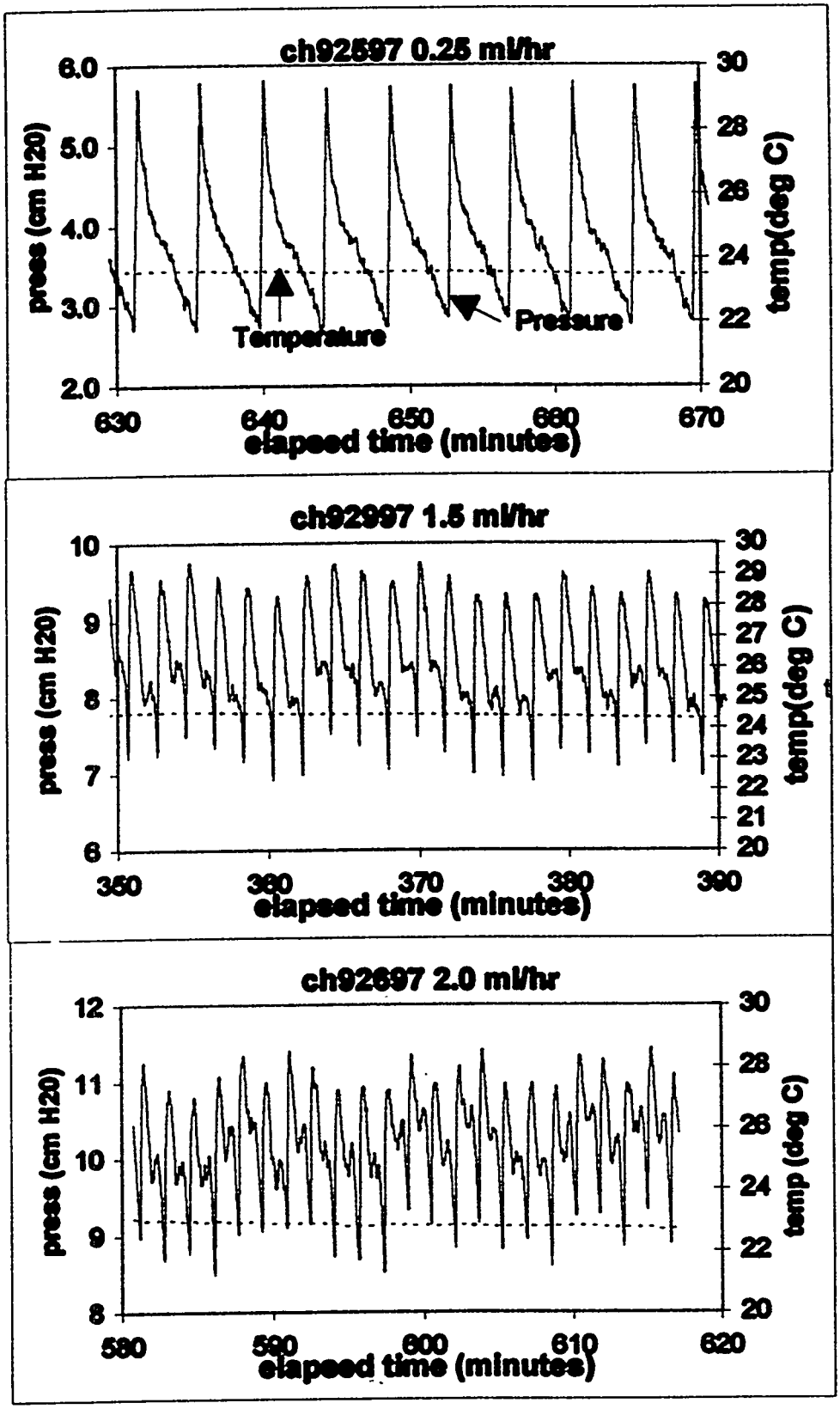

Smooth Parallel Glass Plates

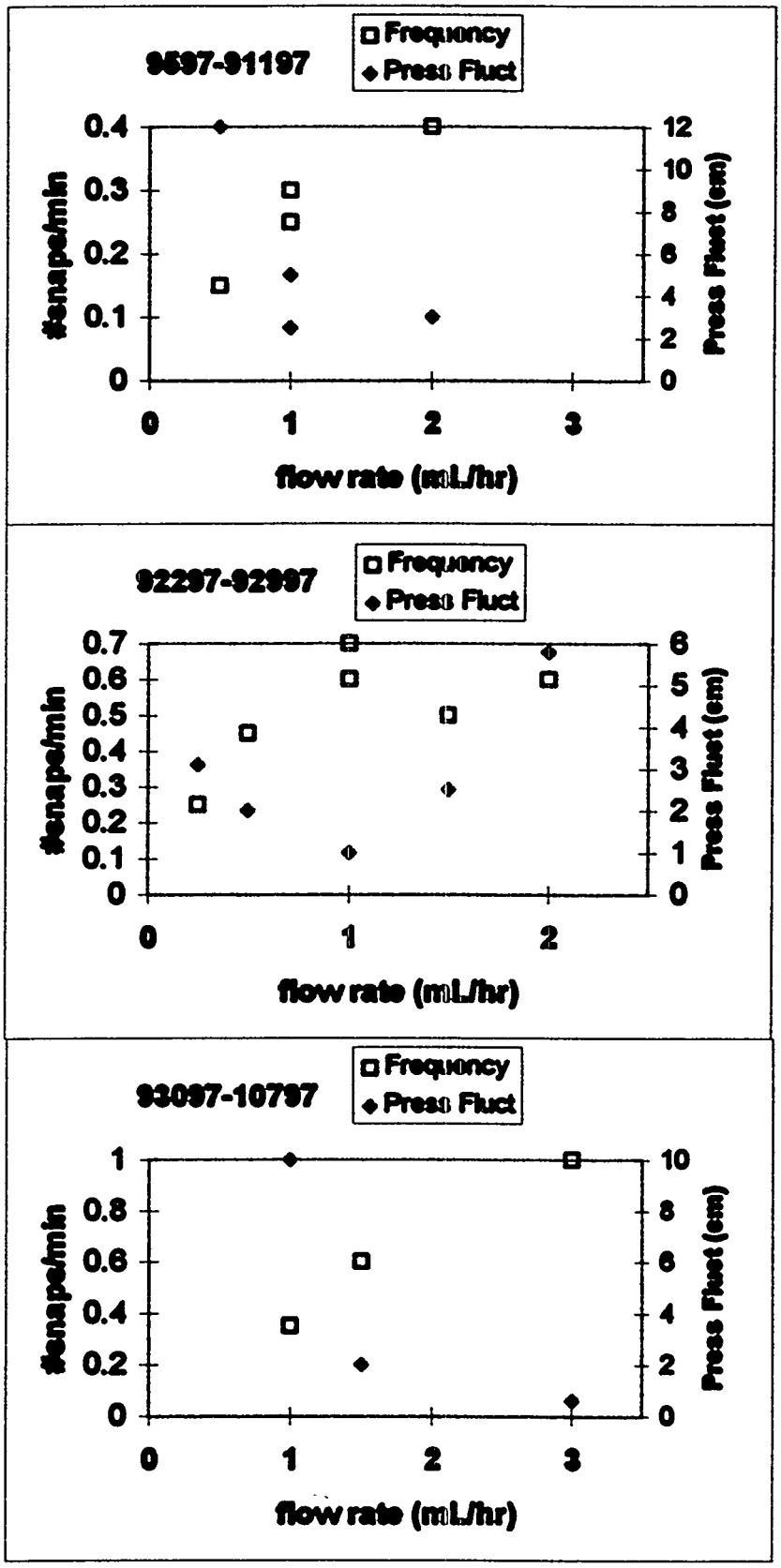
9697-91197
Frequency
Press Fluct
#snapshots/min
Press Fluct (cm)
flow rate (mL/hr)
92297-92997
Frequency
Press Fluct
#snapshots/min
Press Fluct (cm)
flow rate (mL/hr)
93097-10797
Frequency
Press Fluct
#snapshots/min
Press Fluct (cm)
flow rate (mL/hr)

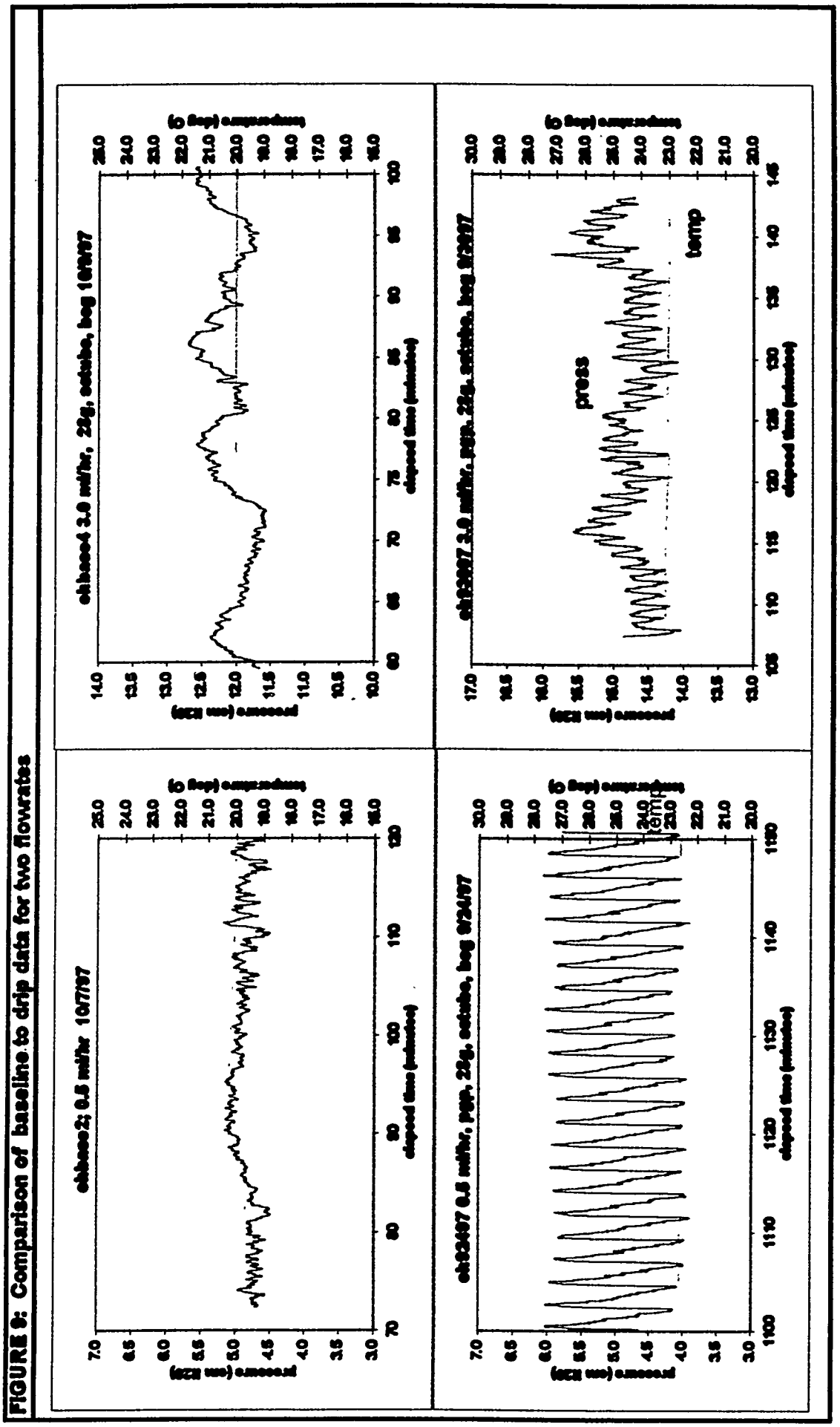

FIGURE 8: Comparison of baseline to drip data for two flowrates

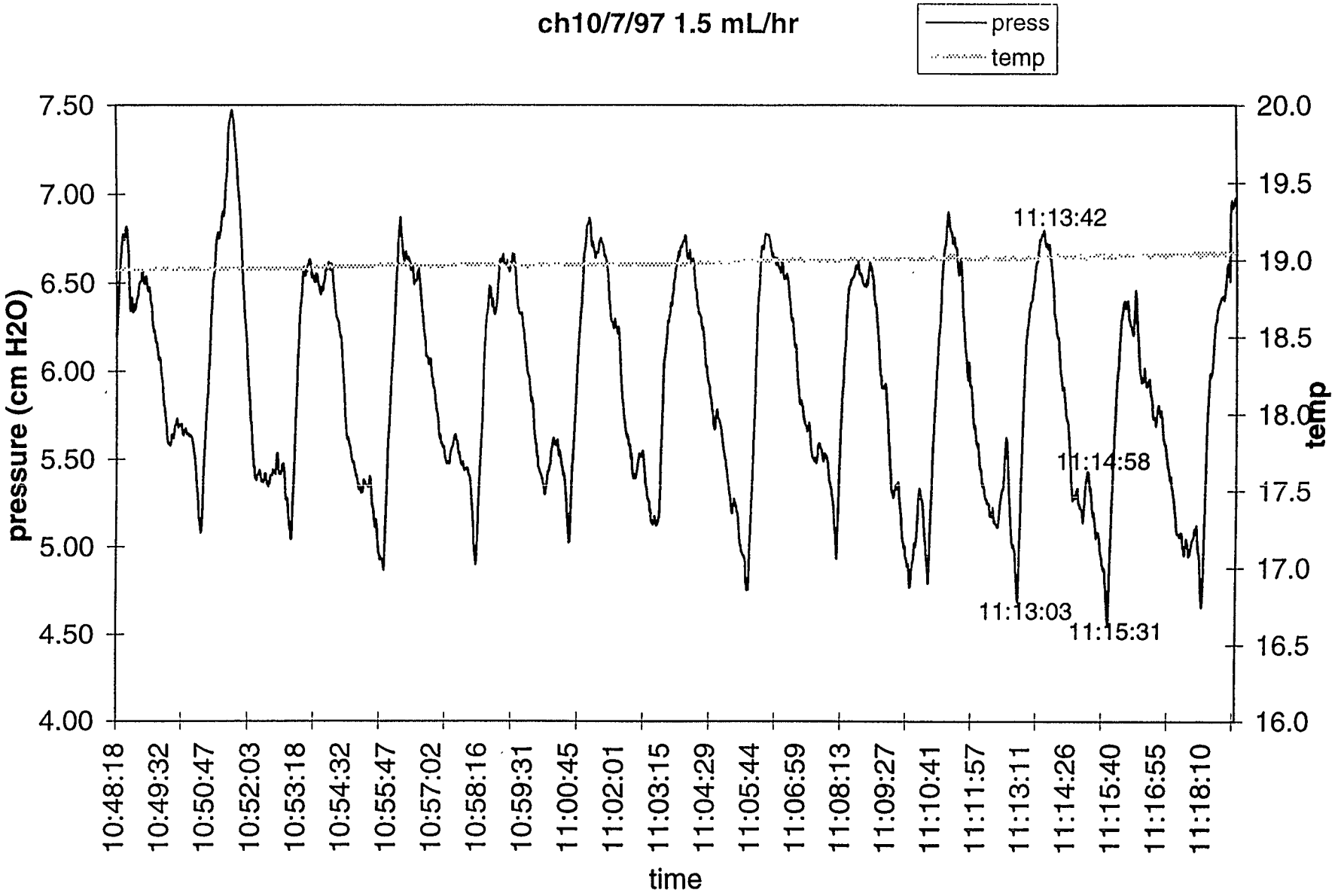
ch10/7/97 1.5 mL/hr
press
temp
pressure (cm H2O)
temp
time
7.50
7.00
6.50
6.00
5.50
5.00
4.50
4.00
20.0
19.5
19.0
18.5
18.0
17.5
17.0
16.5
16.0
11:13:42
11:14:58
11:13:03
11:15:31
10:48:18
10:49:32
10:50:47
10:52:03
10:53:18
10:54:32
10:55:47
10:57:02
10:58:16
10:59:31
11:00:45
11:02:01
11:03:15
11:04:29
11:05:44
11:06:59
11:08:13
11:09:27
11:10:41
11:11:57
11:13:11
11:14:26
11:15:40
11:16:55
11:18:10

Ch10797

FIGURE 6: Parallel shower-door glass plates, 0.5 and 0.25 ml/hr.

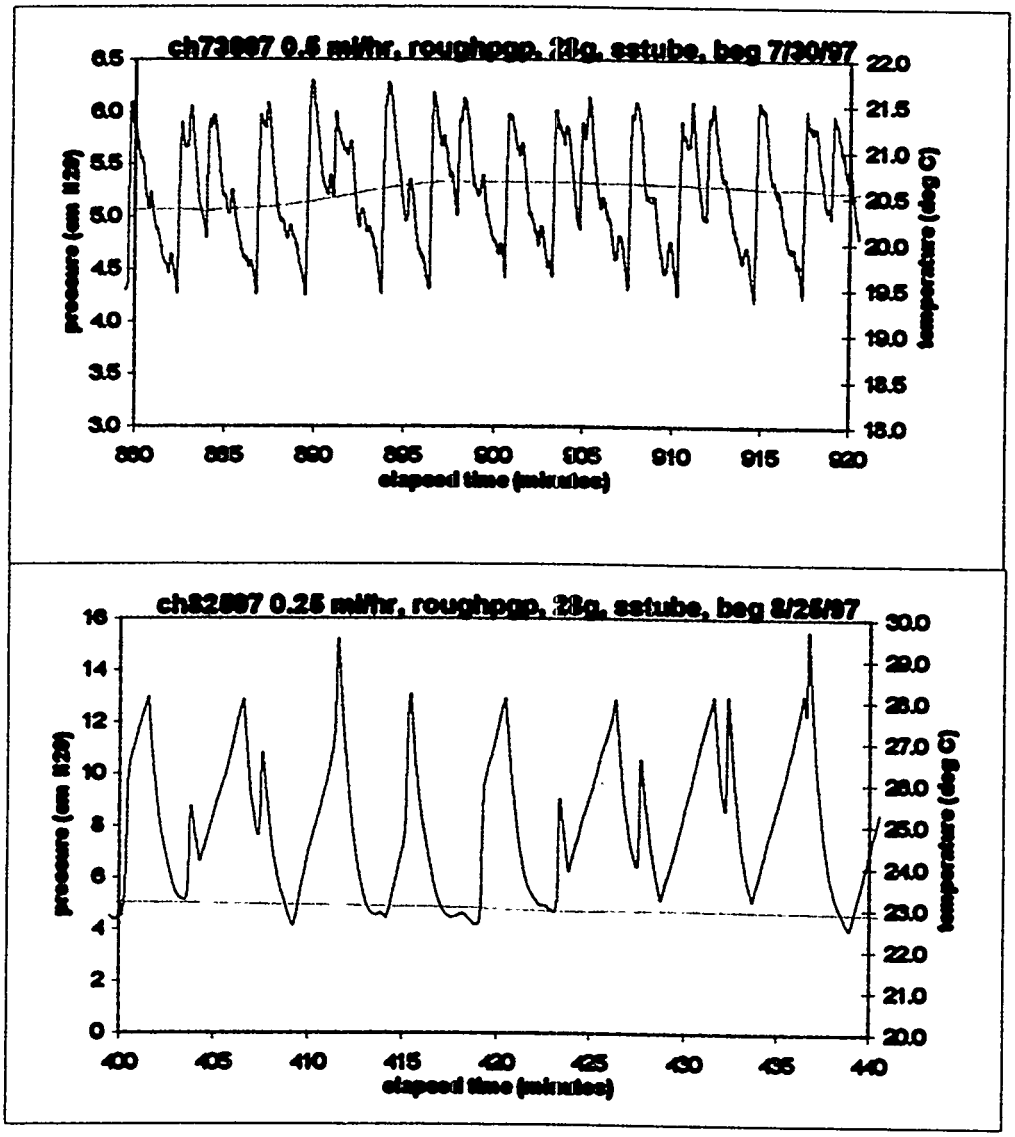

Modes of dripping in "shower-door" plates

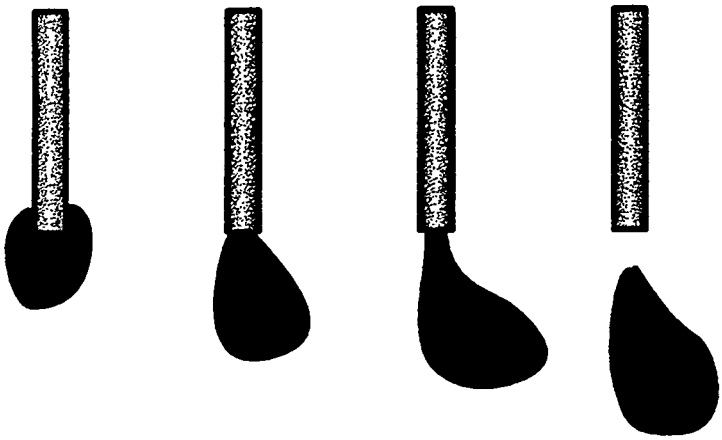

Initially dry plates

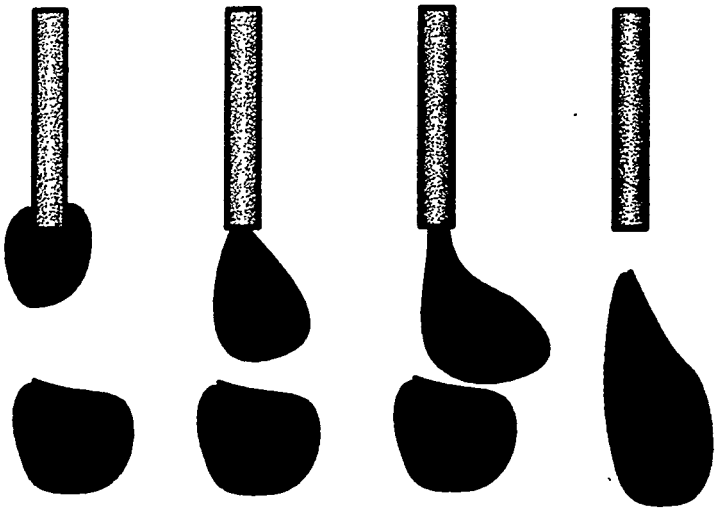

Coalescing w/ trapped water

General Observations in Parallel Plates

- Drips follow pre-wetted paths and path varies with each new assembly
- Frequency of snaps and magnitude of pressure fluctuations increase with flow rate, although absolute values vary from "non-contiguous" runs
- Systematic baseline pressure fluctuations at higher flow rates
- No pressure fluctuations beyond baseline for film flow in sand-blasted glass plates (need higher flow rate)
- Drop coalescence in "shower-door" glass drives snapping from needle due to water-trapping near needle (no observed threads)

Transition to Chaotic Behavior: What affects initial conditions of drop formation?

Drips in open air

- "sawtooth" pattern for small needle diameter - systematically increase needle diameter? needle angle?

Drips in smooth glass parallel plates

- length of thread a function of flow rate - expect transition at higher flow rates (until limit of continuous thread)
- "meandering" thread - at higher flow rates, lower angles of inclination, variable surface texture, needle angle and opening
- partial thread snaps - ???

II.6
TOUGH2 Modeling

Christine Doughty
Berkeley Lab

Objective: Use traditional, non-chaotic models of subsurface flow and transport to identify features of real behavior that can be captured this way, and hence do not require a chaotic explanation

- Spatial distributions
- Time series

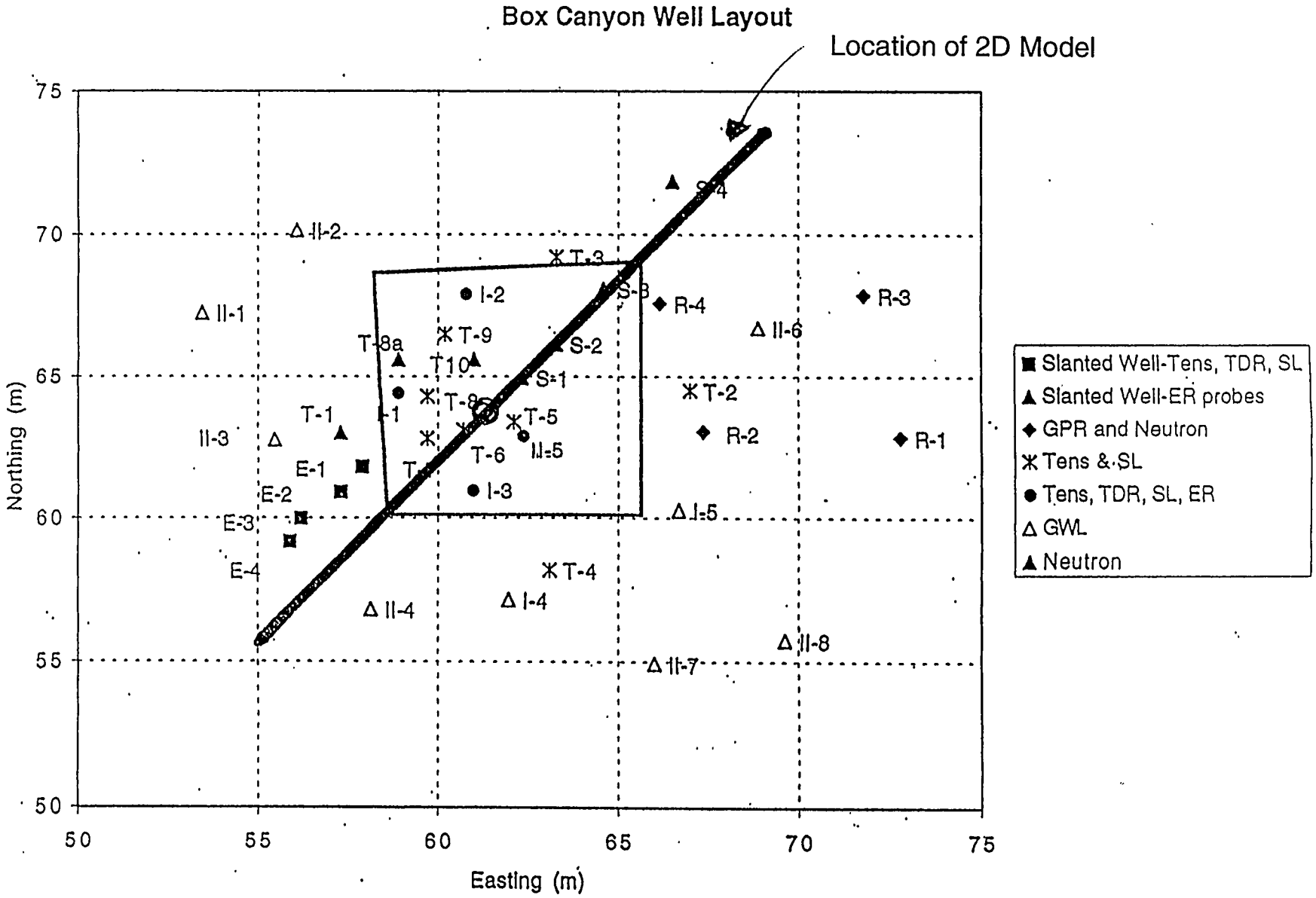
Box Canyon Well Layout
Location of 2D Model
Northing (m)
Easting (m)
75
70
65
60
55
50
50
55
60
65
70
75
II-2
T-3
I-2
S-3
R-4
R-3
II-1
T-9
S-2
II-6
T-8a
T10
S-1
T-2
T-1
I-1
T-8
T-5
II-3
R-2
R-1
T-6
II-5
E-1
E-2
I-3
E-3
I-5
E-4
T-4
I-4
II-4
II-8
II-7
Slanted Well-Tens, TDR, SL
Slanted Well-ER probes
GPR and Neutron
Tens &SL
Tens, TDR, SL, ER
GWL
Neutron

Geologic Cross-Section at Model Location

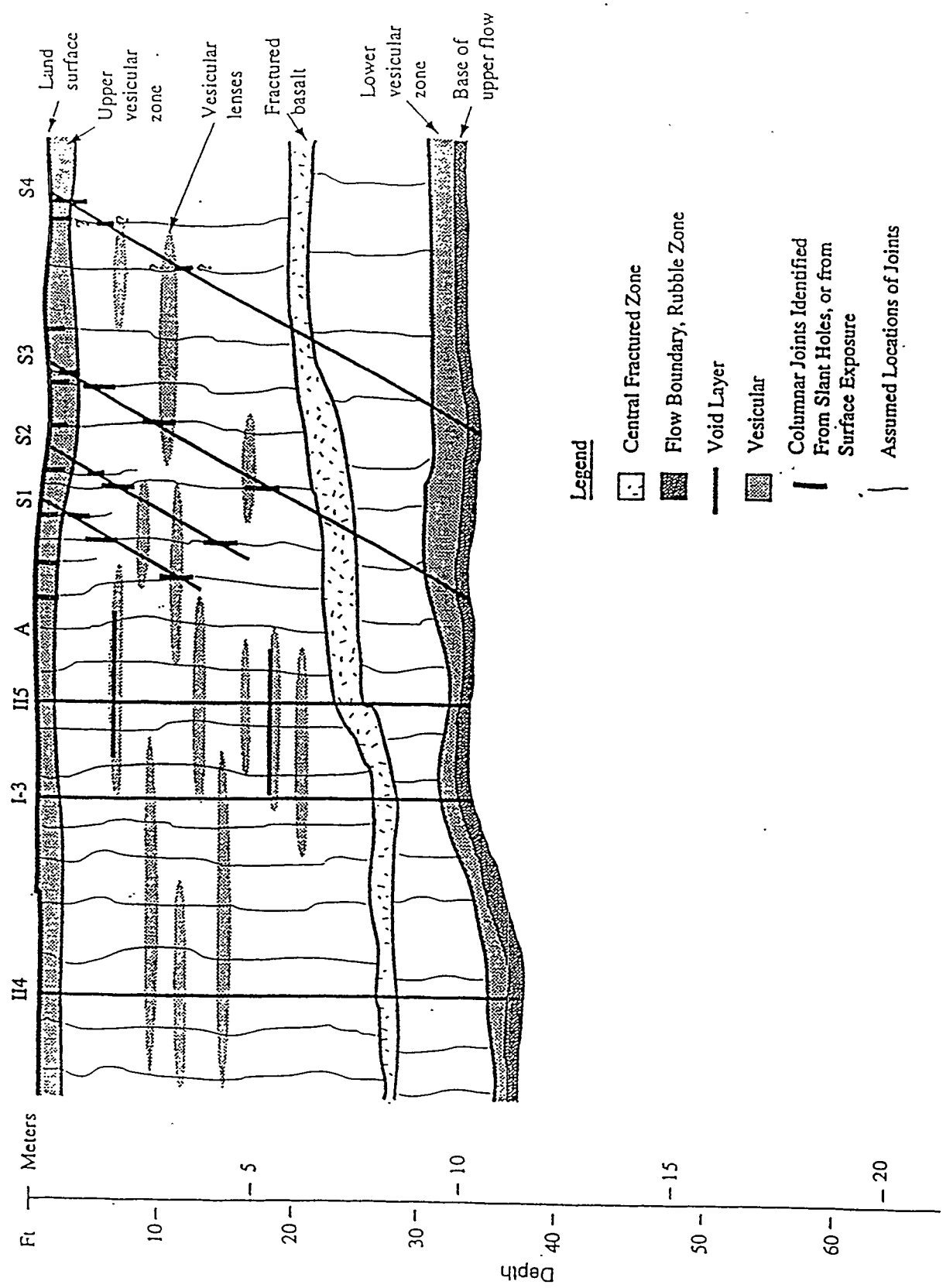

Fracture Map at Box Canyon Cliff Face

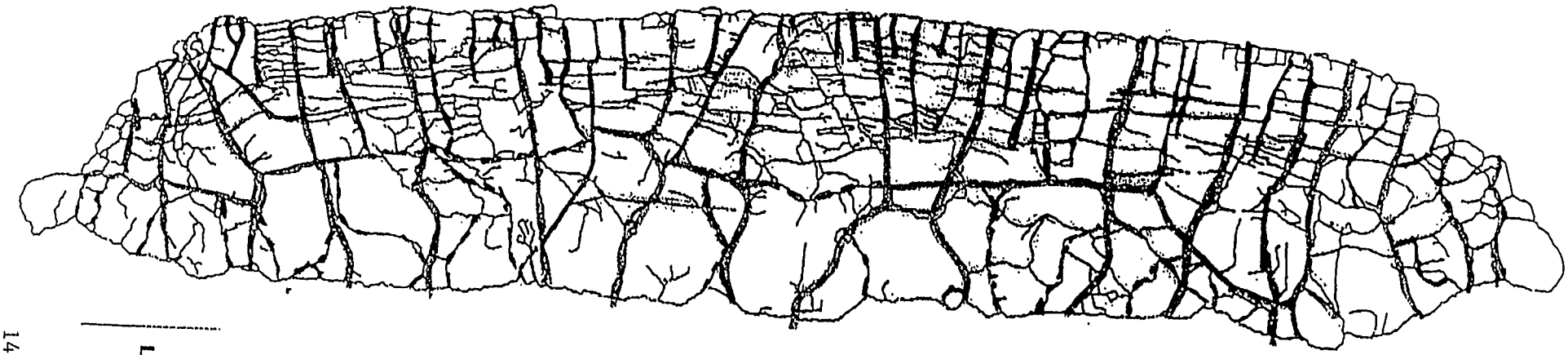

Geometrical Classification of the Fracture System Exposed at the Box Canyon Cliff Face

H0 - central zone horizontal fracture
H1 - central visicular zone
H2 - connect V0 with V1 and V2
H3 - connect V2
H4 - dead-end

V0 - connect top and bottom of basalt flow
V1 - connect top of basalt flow with V0
V2 - connect top of basalt flow with horizontal fractures
V3 - internal vertical fractures (betwen #3)
V4 - connect bottom of flow with horizontal fractures
V5 - dead-end

Numerical Model

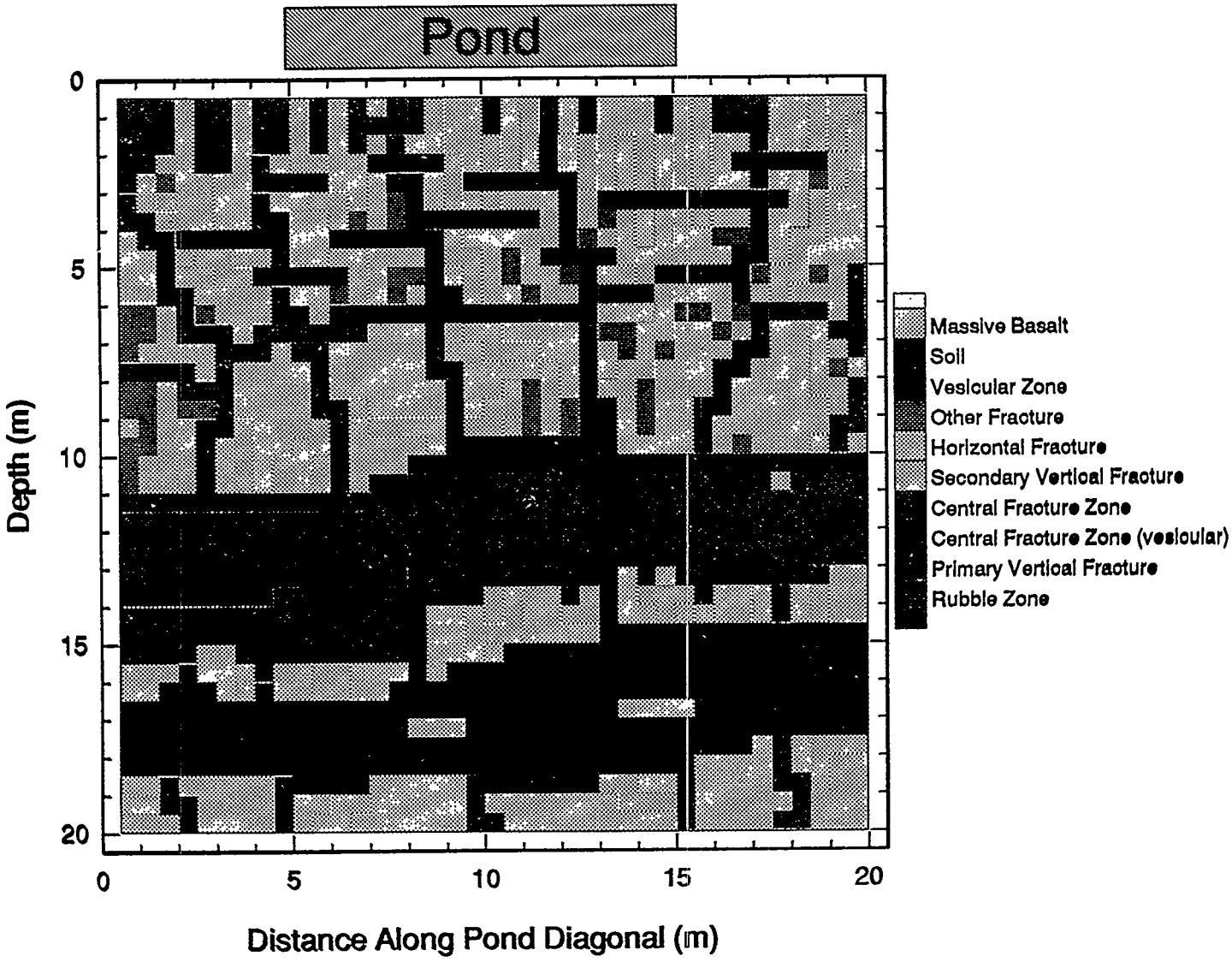

Ponded Infiltration Results
Model with No Air Entrapment

One Week Infiltration

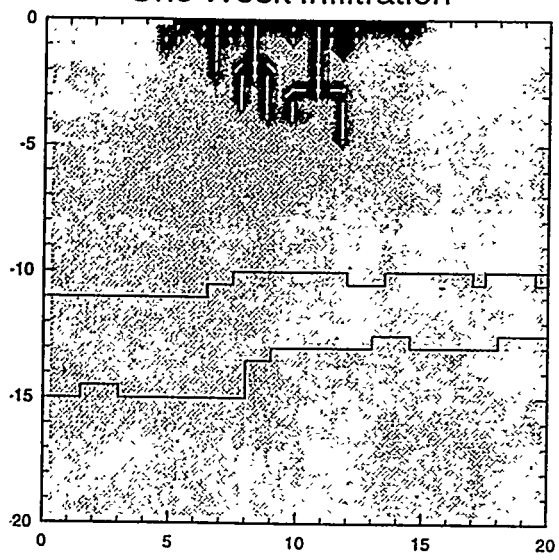

Two Weeks Infiltration

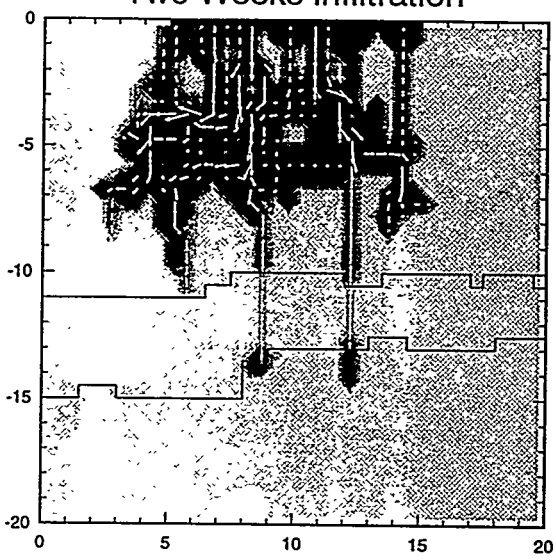

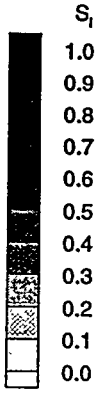

Three Weeks Infiltration

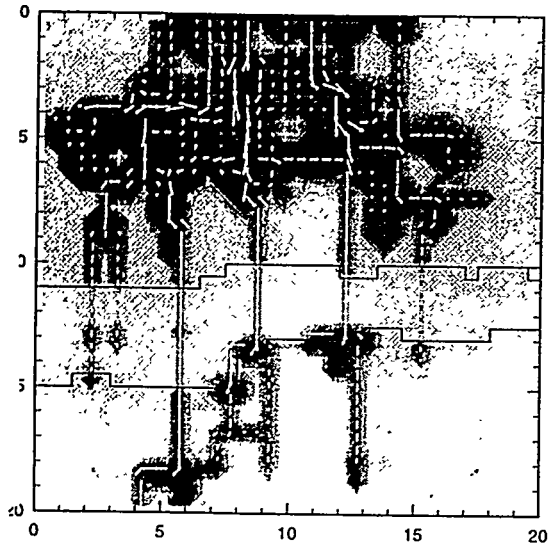

Four Weeks Infiltration

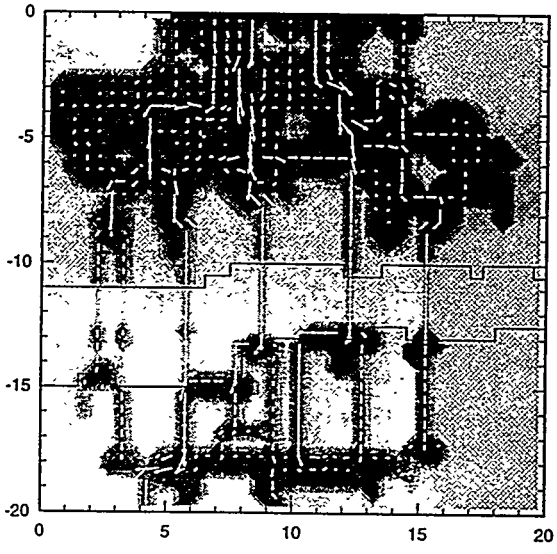

Ponded Infiltration Results
Model with Entrapped Air

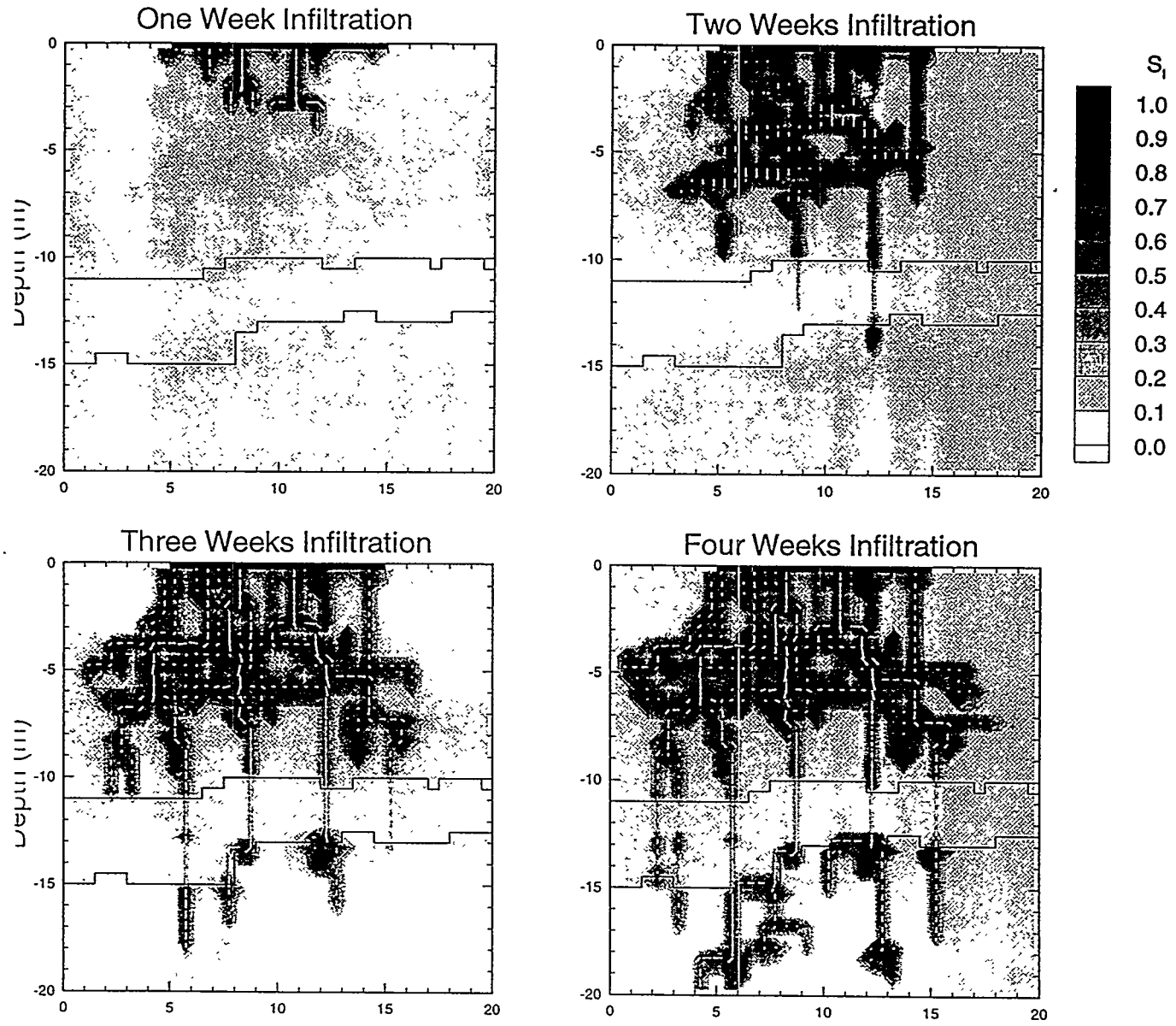

Natural State

Model with Capillary Pressure and Background Infiltration

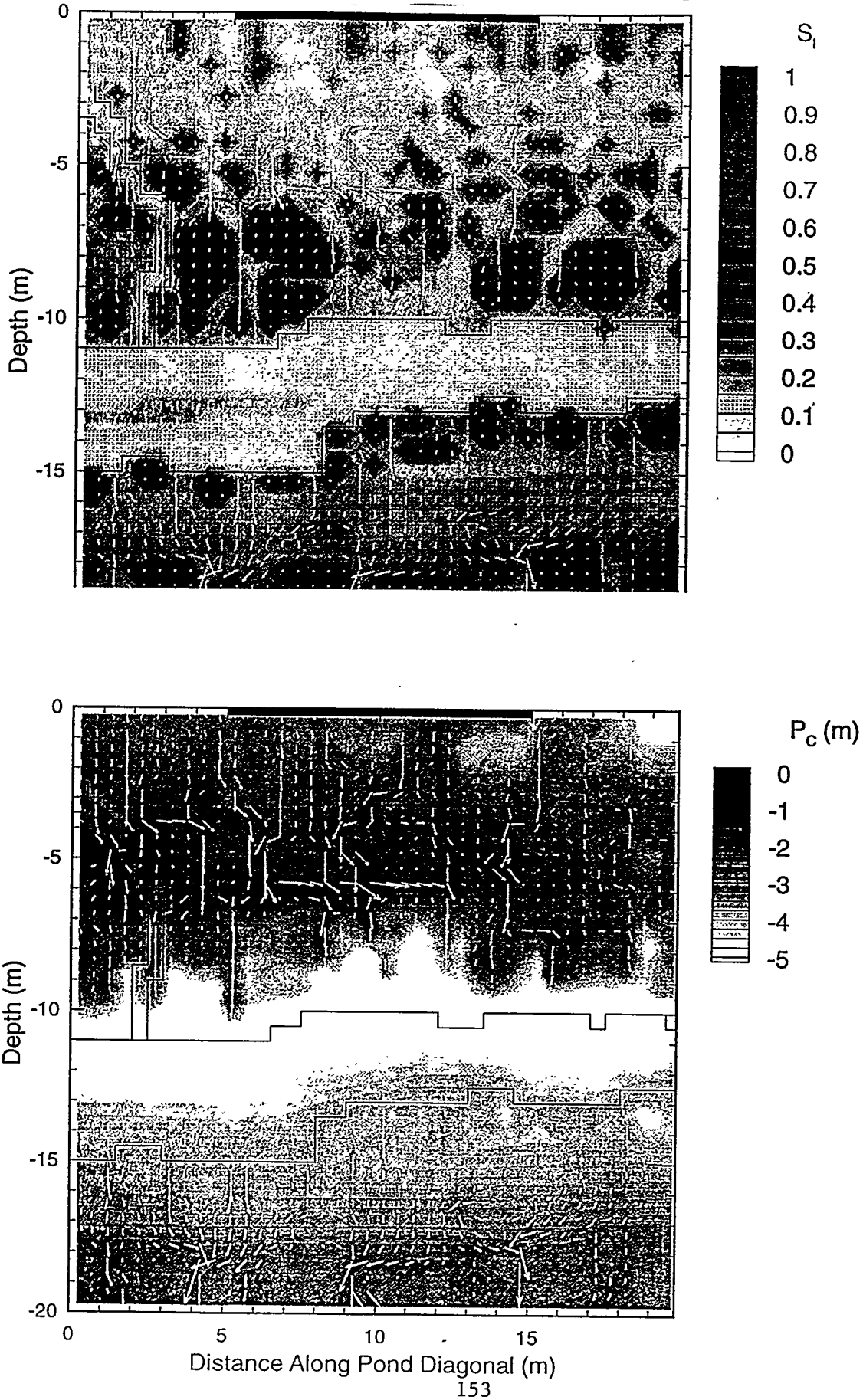

Ponded Infiltration Results

Model with Capillary Pressure and Background Infiltration

Initial Conditions

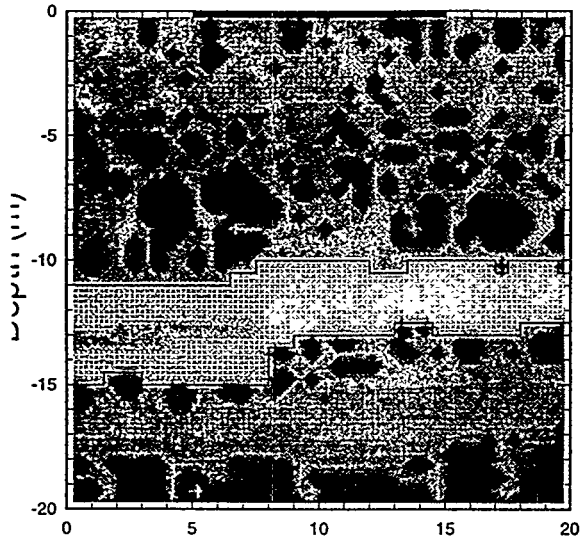

One Week Infiltration

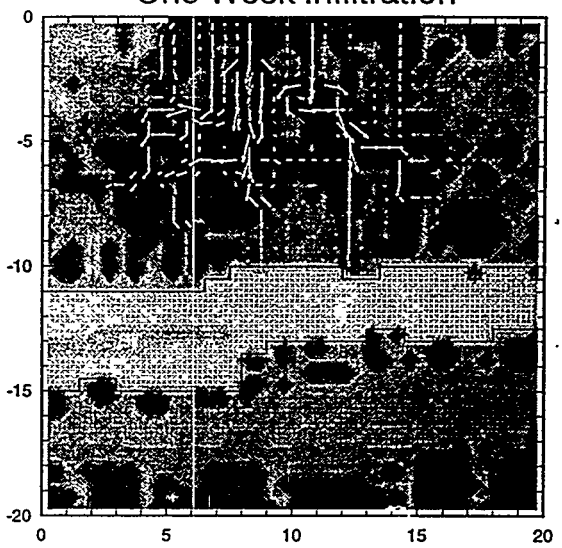

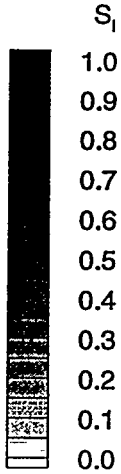

Two Weeks Infiltration

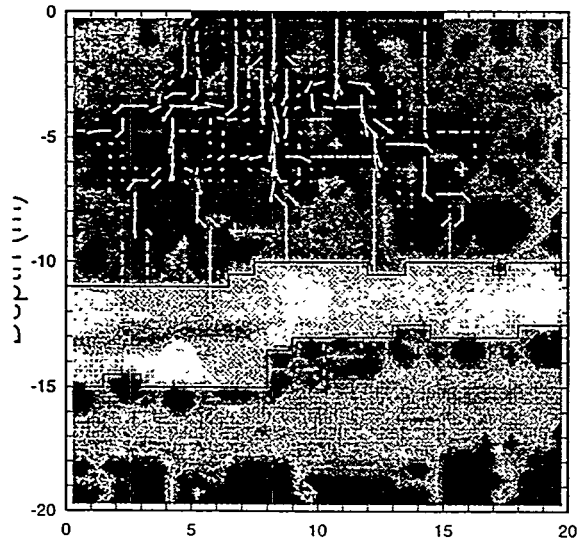

Four Weeks Infiltration

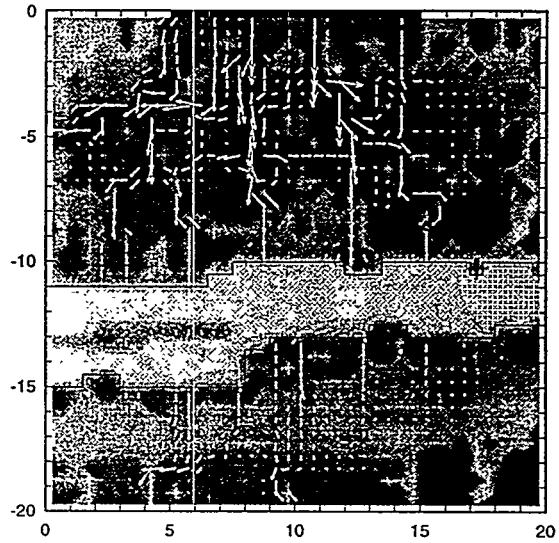

Liquid Flow Field

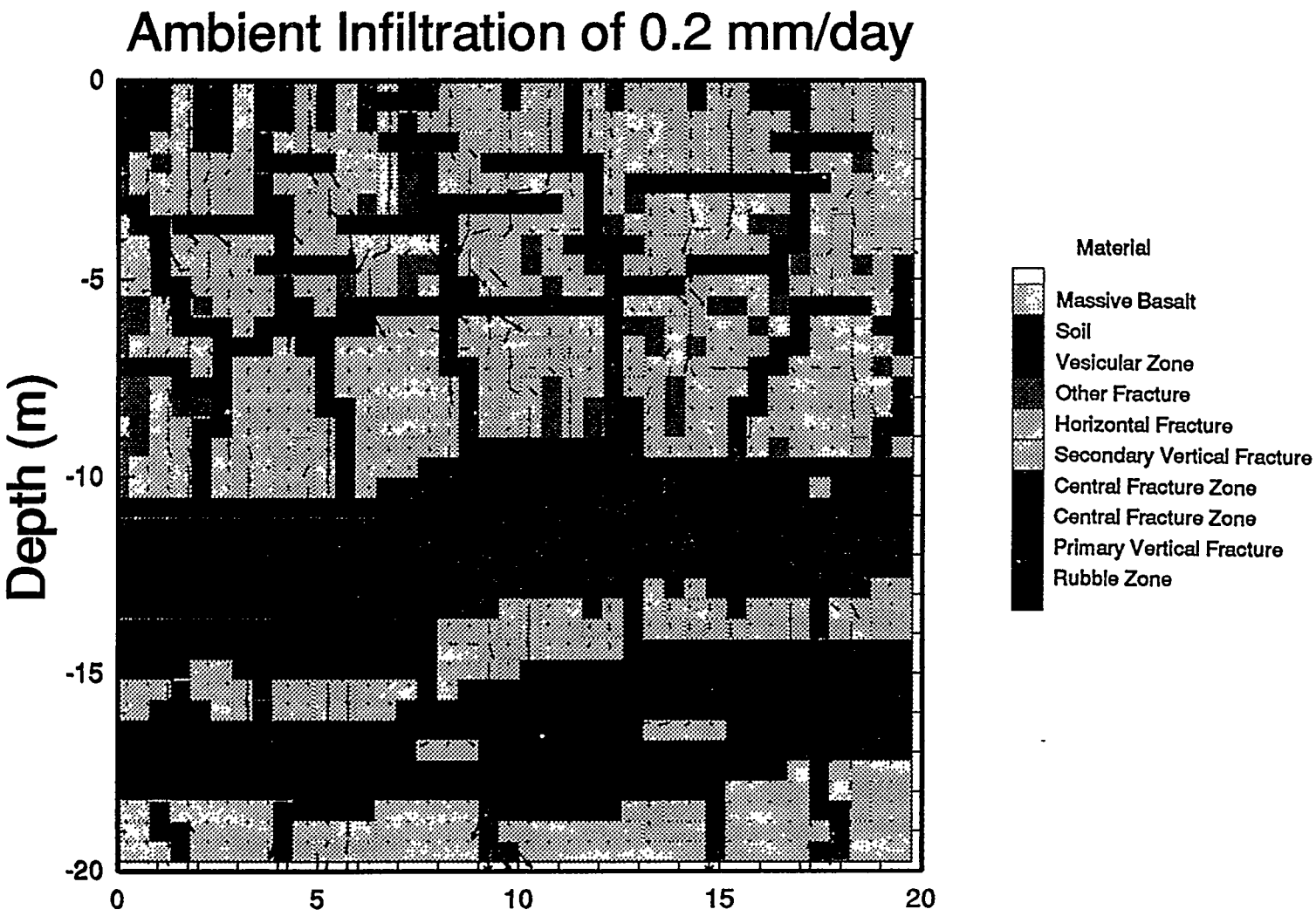

Liquid Flow Field

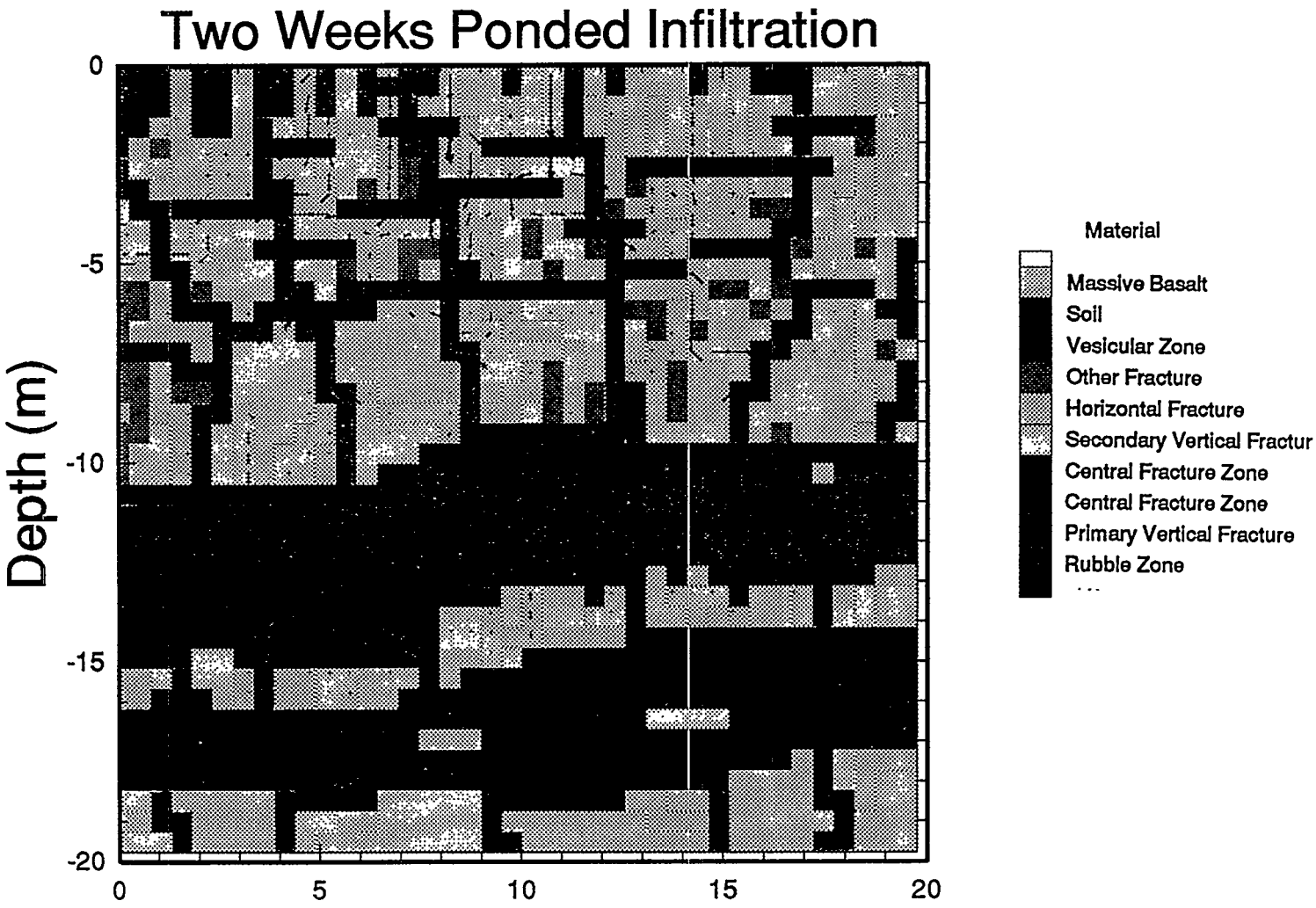

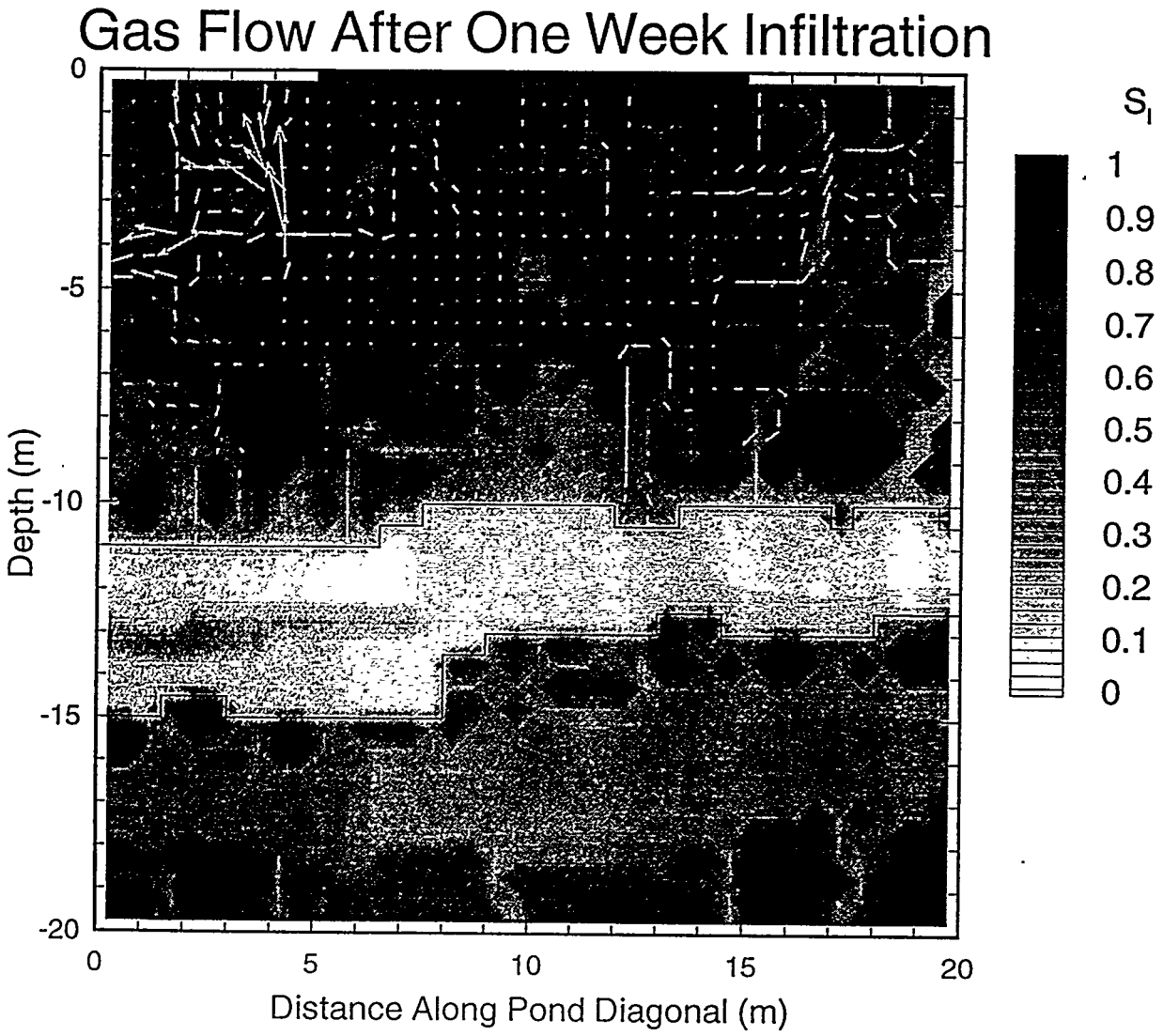
Gas Flow After One Week Infiltration
Depth (m)
0
-5
-10
-15
-20
0
5
10
15
20
Distance Along Pond Diagonal (m)
S_l
1
0.9
0.8
0.7
0.6
0.5
0.4
0.3
0.2
0.1
0

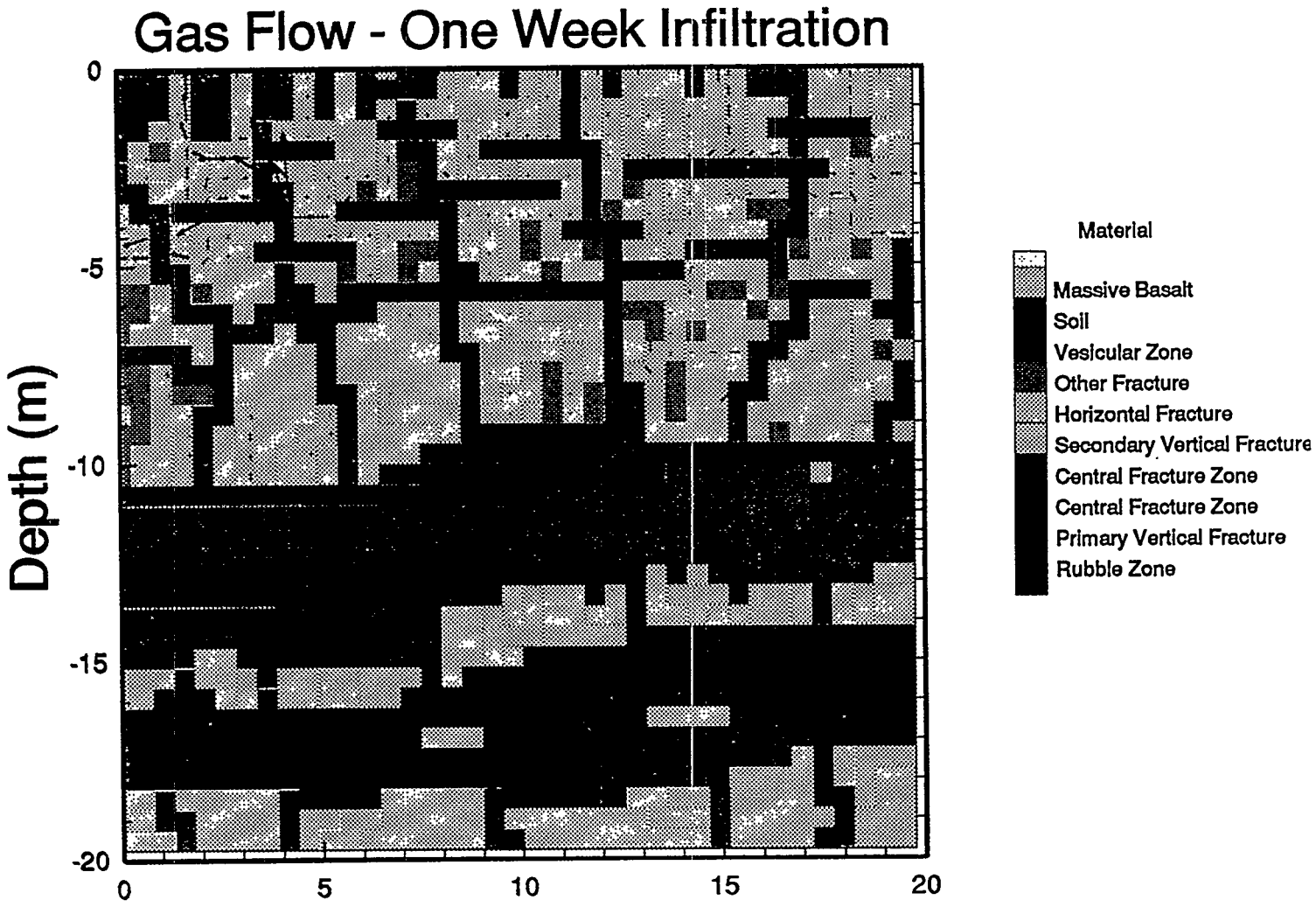
Gas Flow - One Week Infiltration
Depth (m)
0
-5
-10
-15
-20
0
5
10
15
20
Material
Massive Basalt
Soil
Vesicular Zone
Other Fracture
Horizontal Fracture
Secondary Vertical Fracture
Central Fracture Zone
Central Fracture Zone
Primary Vertical Fracture
Rubble Zone

Model with Entrapped Air

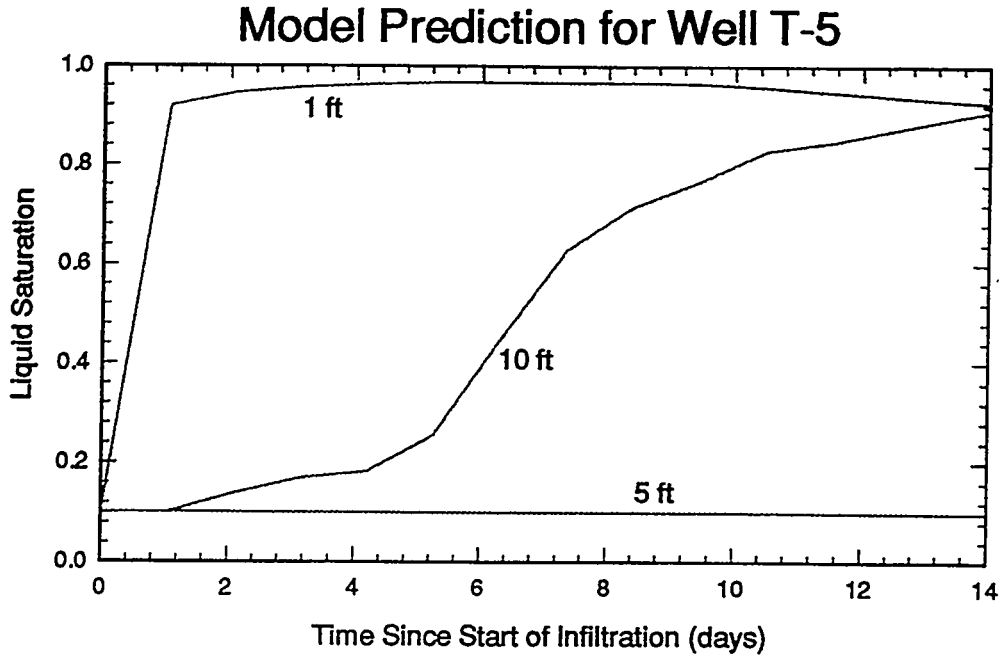

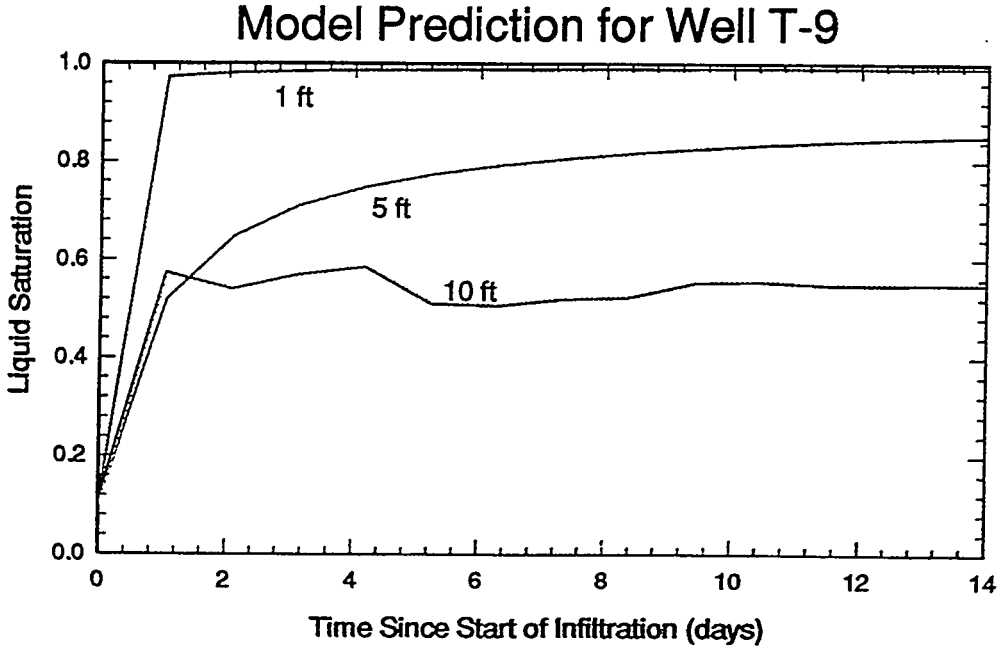

BC116_OBS.PLT
SL_OB59.STY
SL_OB55.STY

(2D) || Print || 04 Aug 1997 || bci16d.plt ||

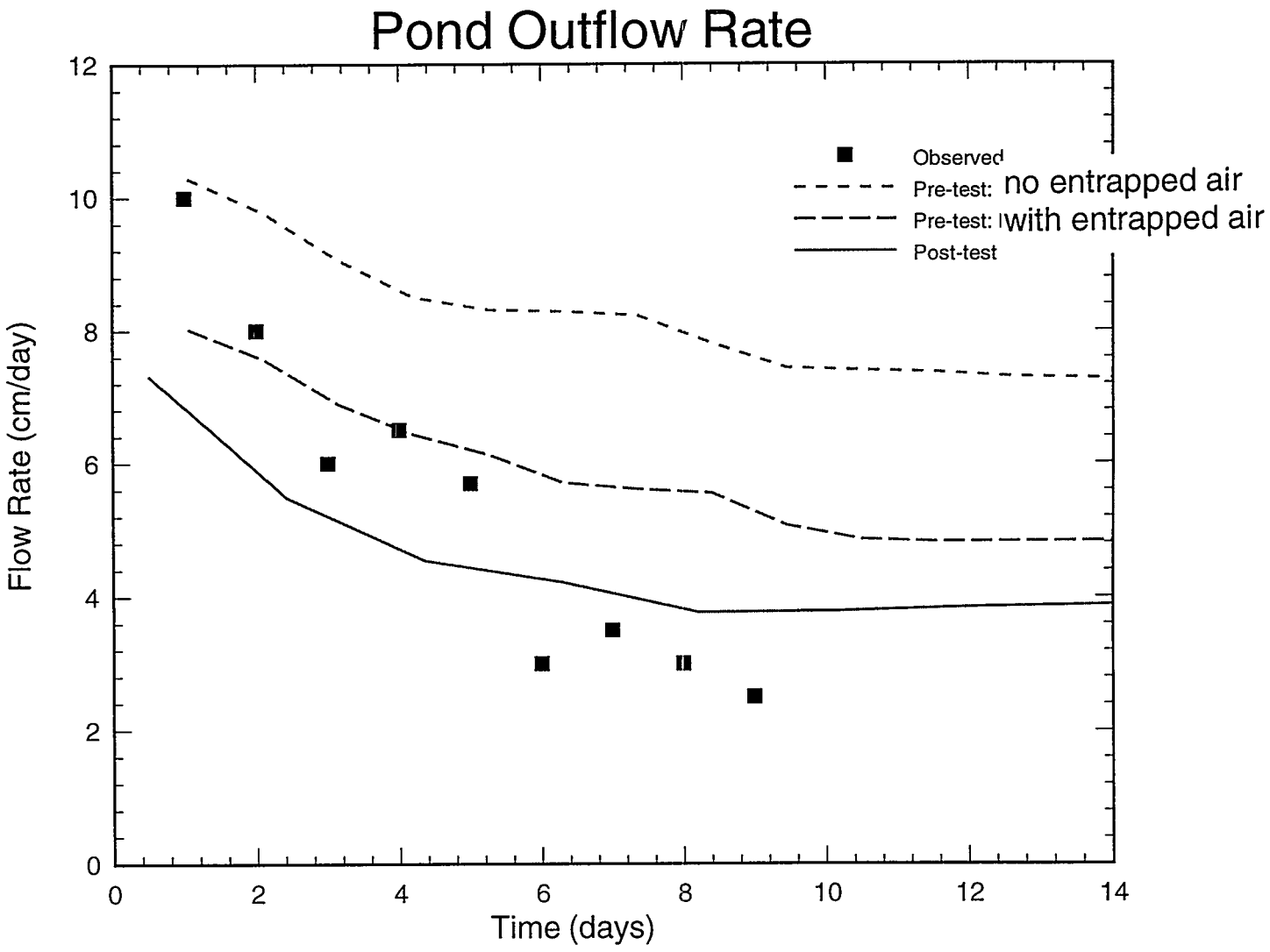

Long-term Flow Rates

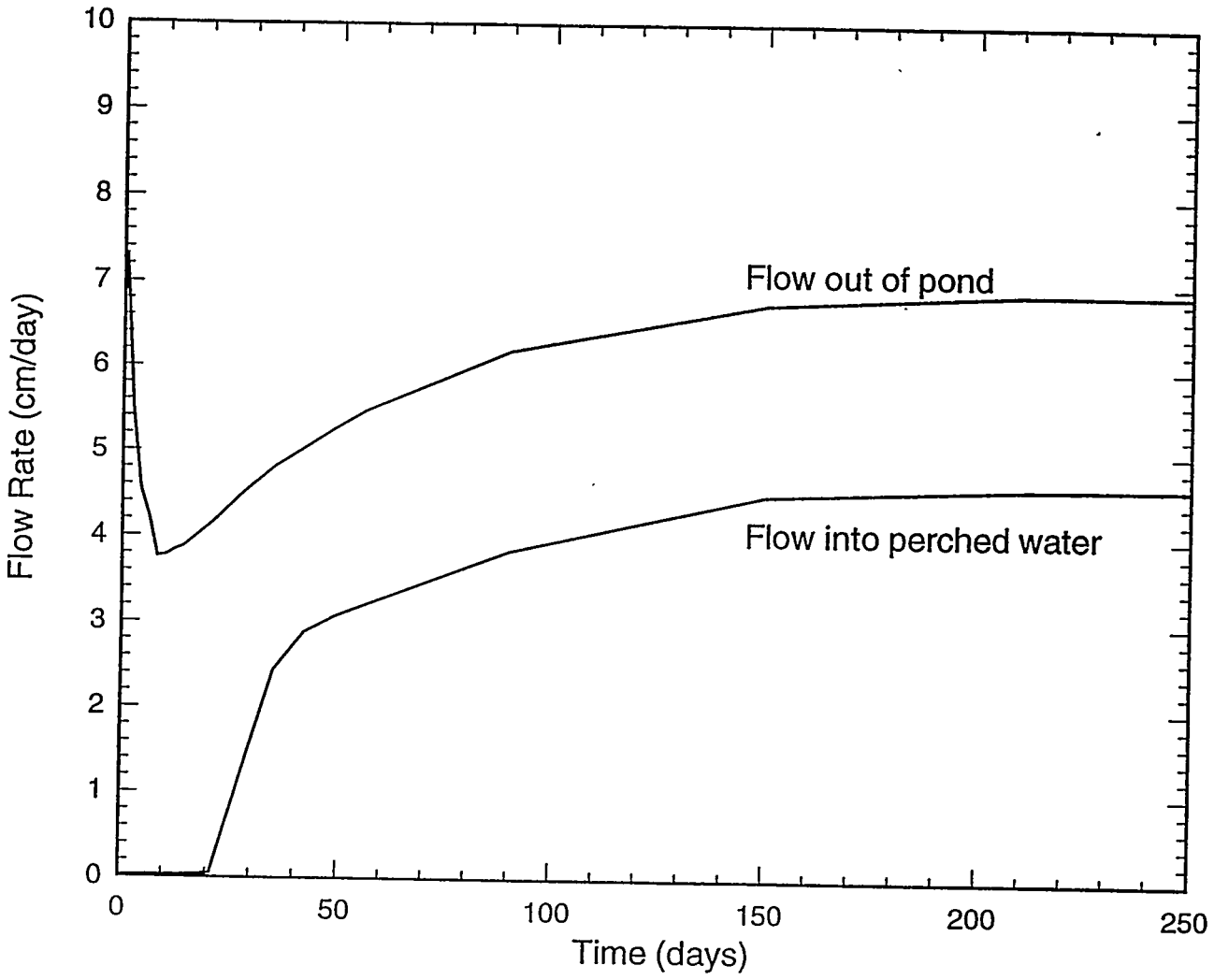

Comparison Between Continuous and Pulsed Ponding

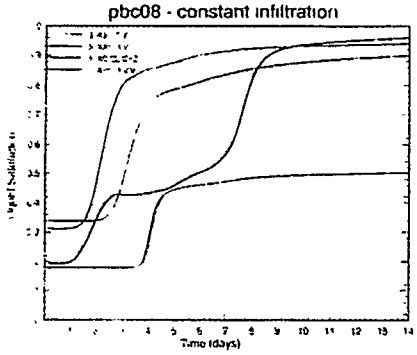

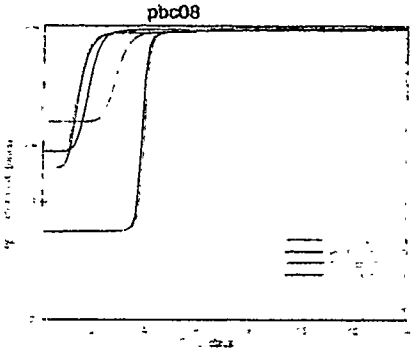

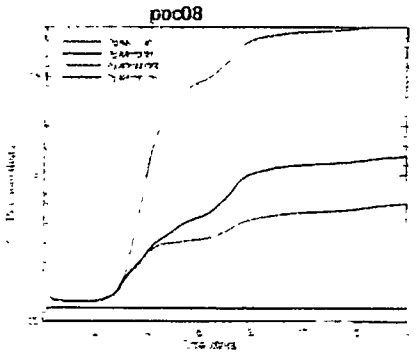

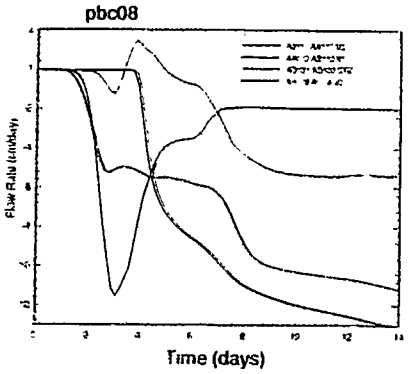

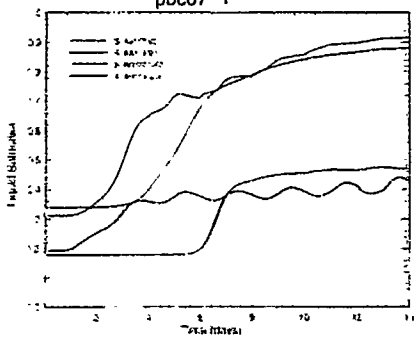

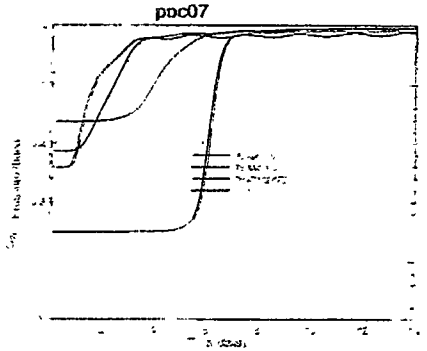

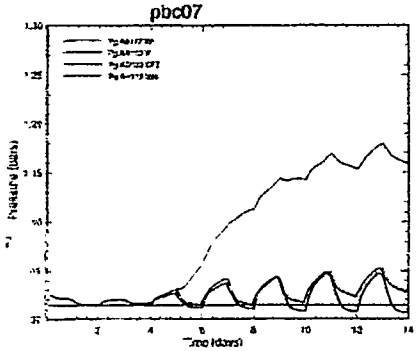

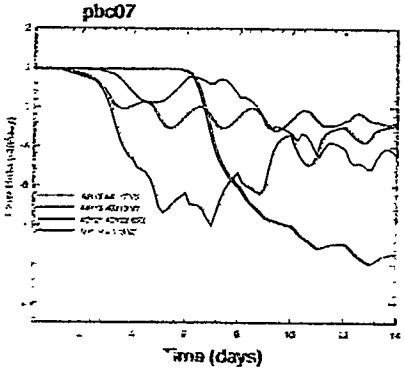

II.7

Estimating Total Mass of Contaminant Plumes from Sparse Well Data

Masoud Nikravesh, Lea Cox, Boris Faybishenko

Lawrence Berkeley National Laboratory, Berkeley, CA

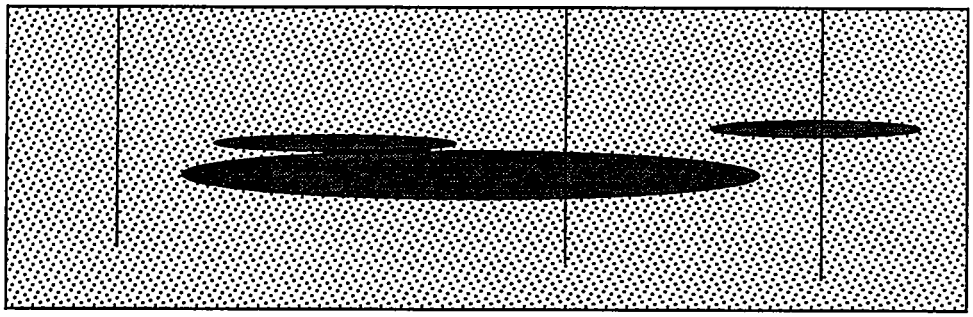

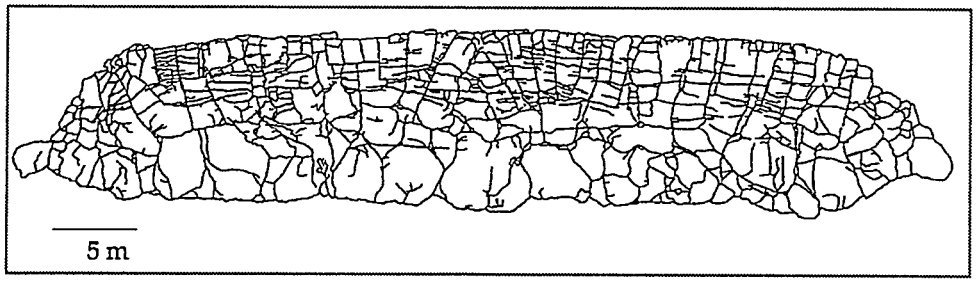

Objectives

- test and compare different methods for interpolating distribution of contaminants

  1) simple averaging

  2) fractal methods

  3) neural network

- minimize number of wells needed to estimate the total mass of contaminant

Generation of Fractal Plume

- fractal surface generator software (Russ, 1995) with midpoint displacement option
- fractal dimension of 2.5
- 256 x 256 pixels
- cutoff of 50 to simulate detection limit

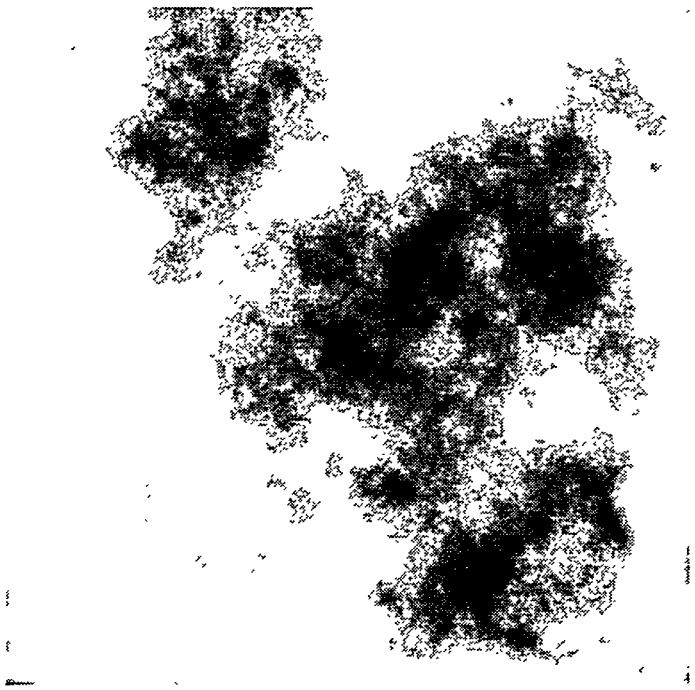

Simple Averaging: Case 1

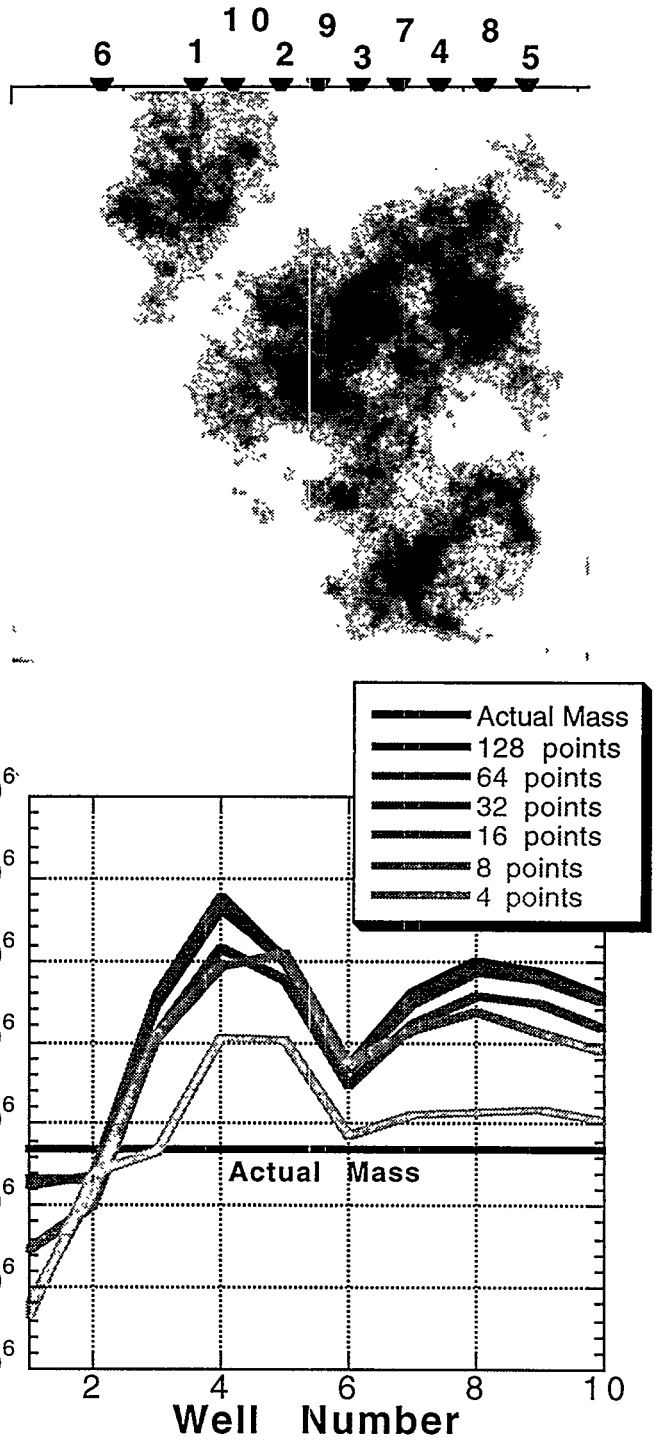

Simple Averaging: Case 2

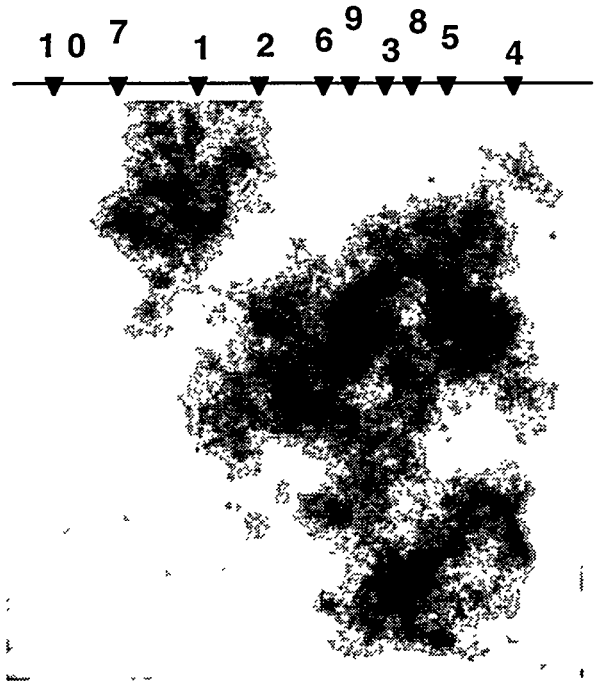

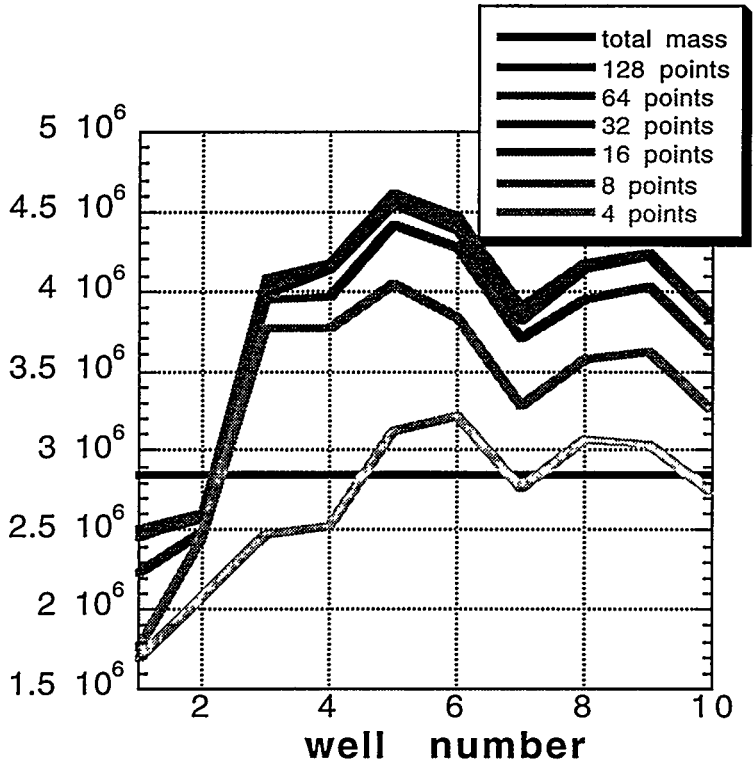

Simple Averaging: Case 3

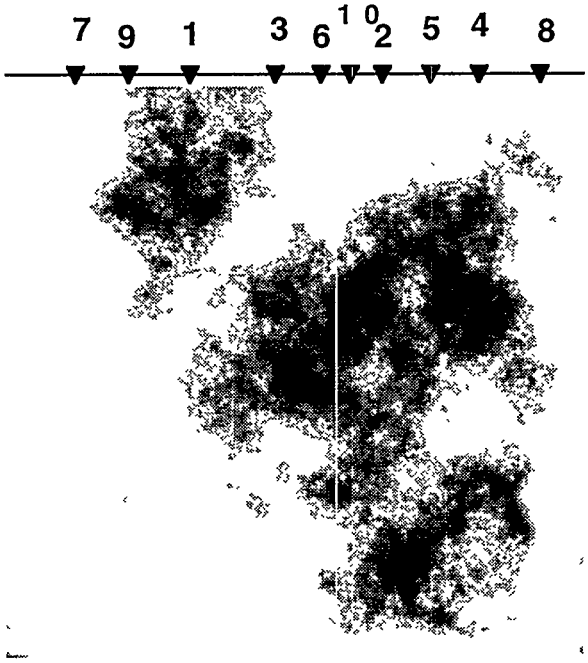

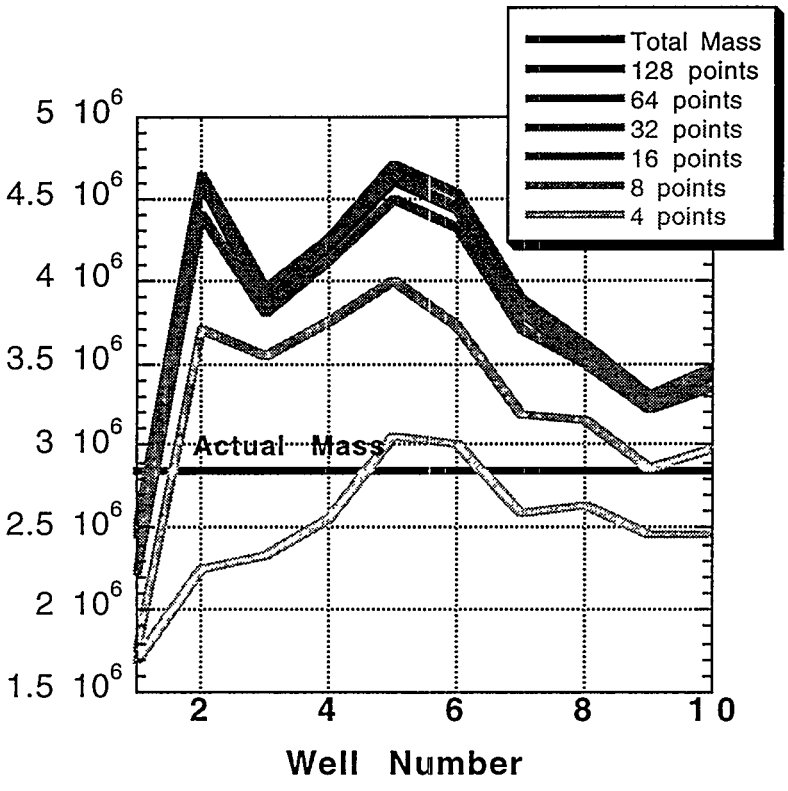

Fractal Plume #2, D=2.75

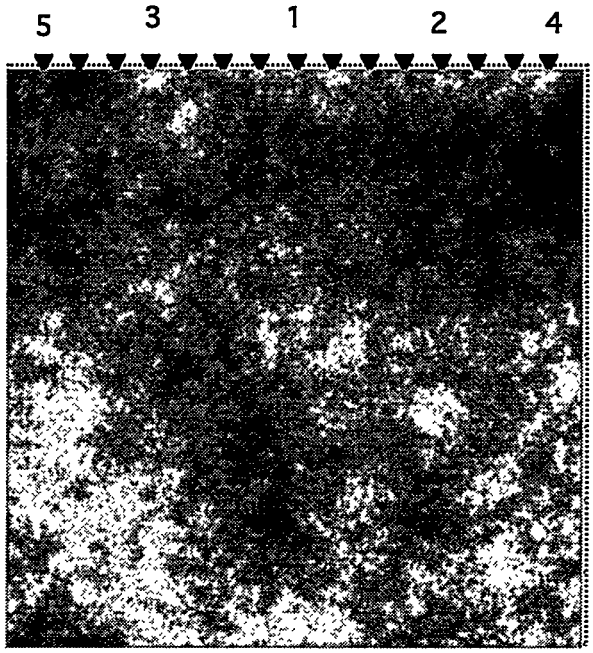

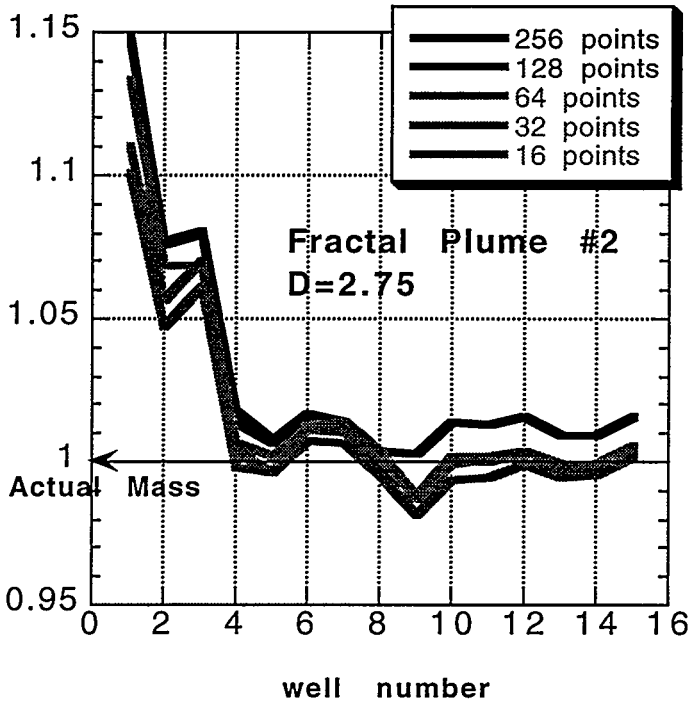

Yucca Mountain Fracture

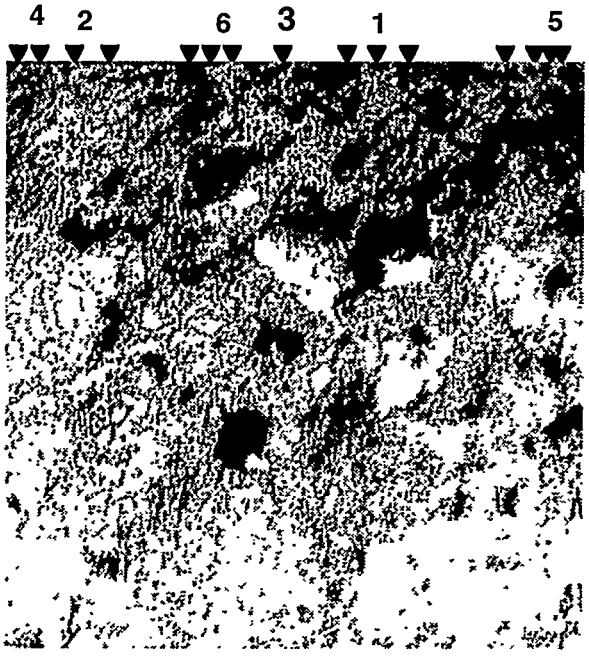

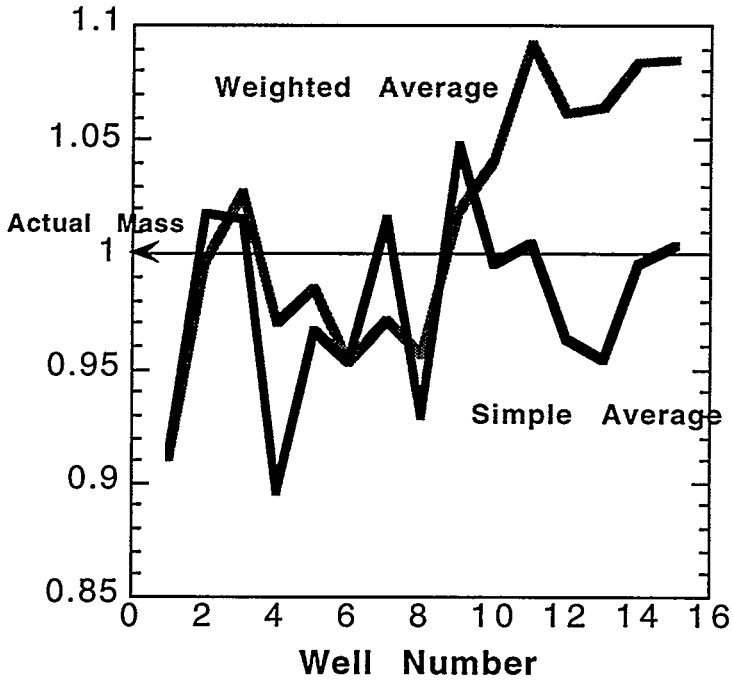

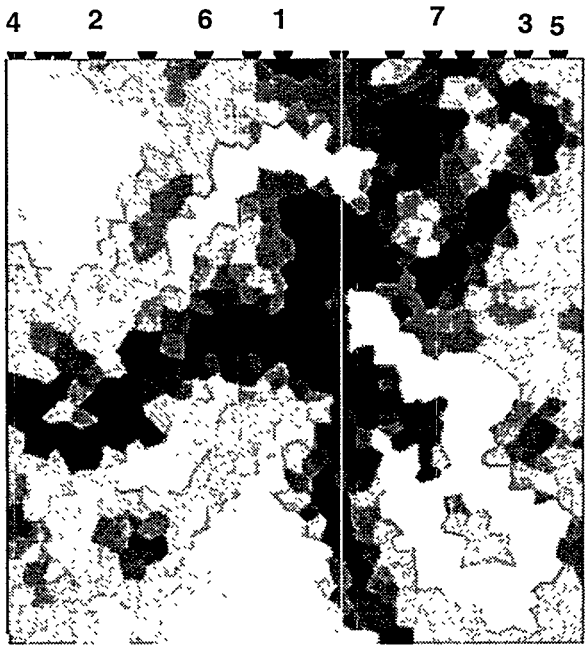
4
2
6
1
7
3
5

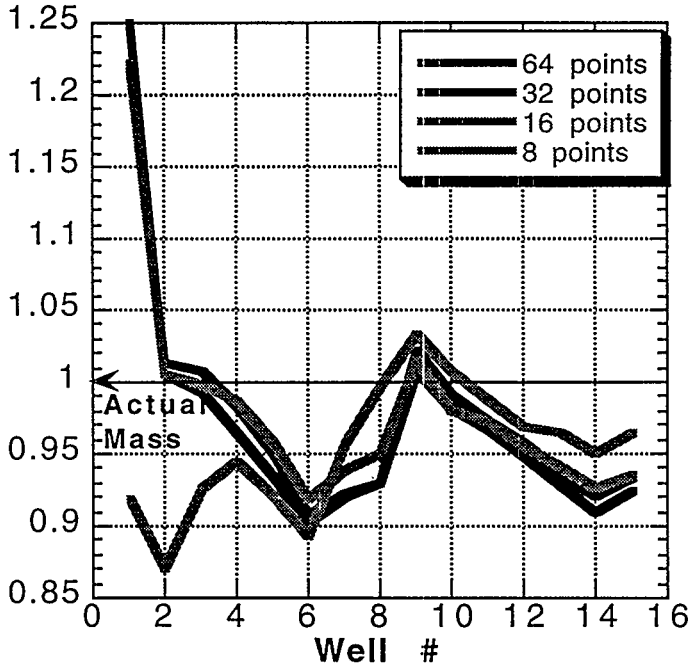
1.25
1.2
1.15
1.1
1.05
1
0.95
0.9
0.85
0
2
4
6
8
10
12
14
16
64 points
32 points
16 points
8 points
Actual
Mass
Well #

Fractal Methods

- Total Mass ~ (a) $(r)^D$
- Uncertainty in "a" and in "D"

  sparse data

  variations with each well

  methods of measurement

Conclusion: Fractal Methods not useful for this type of problem

Method of Measurement	Case #1 (D=2.5)	Case #2 (D=2.75)	Case #3 (D=2.25)
Slit Island	2.31	2.60	2.14
Kolmogorov Box	2.49	2.68	2.37
RMS versus Area	2.19	2.37	2.17
Minkowski Cover	2.19	2.42	2.10
Hurst	2.57	2.67	2.36

Why Neural Network?

- Structure Free
- Nonlinear Mapping
- Multivariable Systems
- Train Easily Based on Historical Data
- Ability to Learn
- Ability to Predict
- Parallel Processing
- Fault Tolerance

Much Like Human Brain

Neural Network Model

- each node is a processing unit and manipulates the input vector to give output
- utilizes weighting factors, internal thresholds and transfer functions
- prespecify the topology of the node connections
- use statistics and probability to reduce the output error
- interpolation and extrapolation confined to the region defined by the measurements
- no sharp boundaries

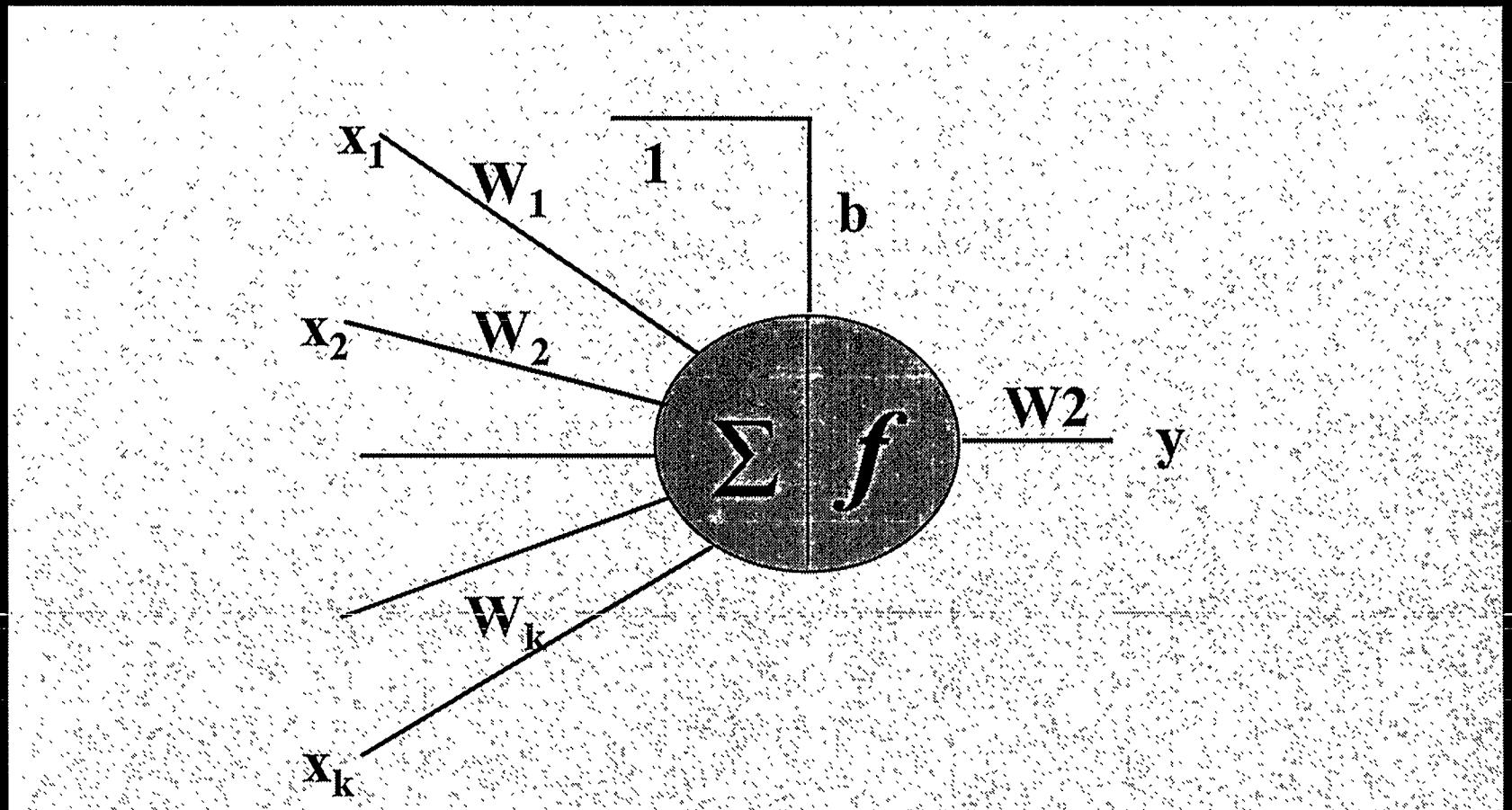

$$y = f\,[\,b + w_1 x_1 + w_2 x_2 + \cdots + w_k x_k\,] \cdot w_2$$

Typical Neural Network

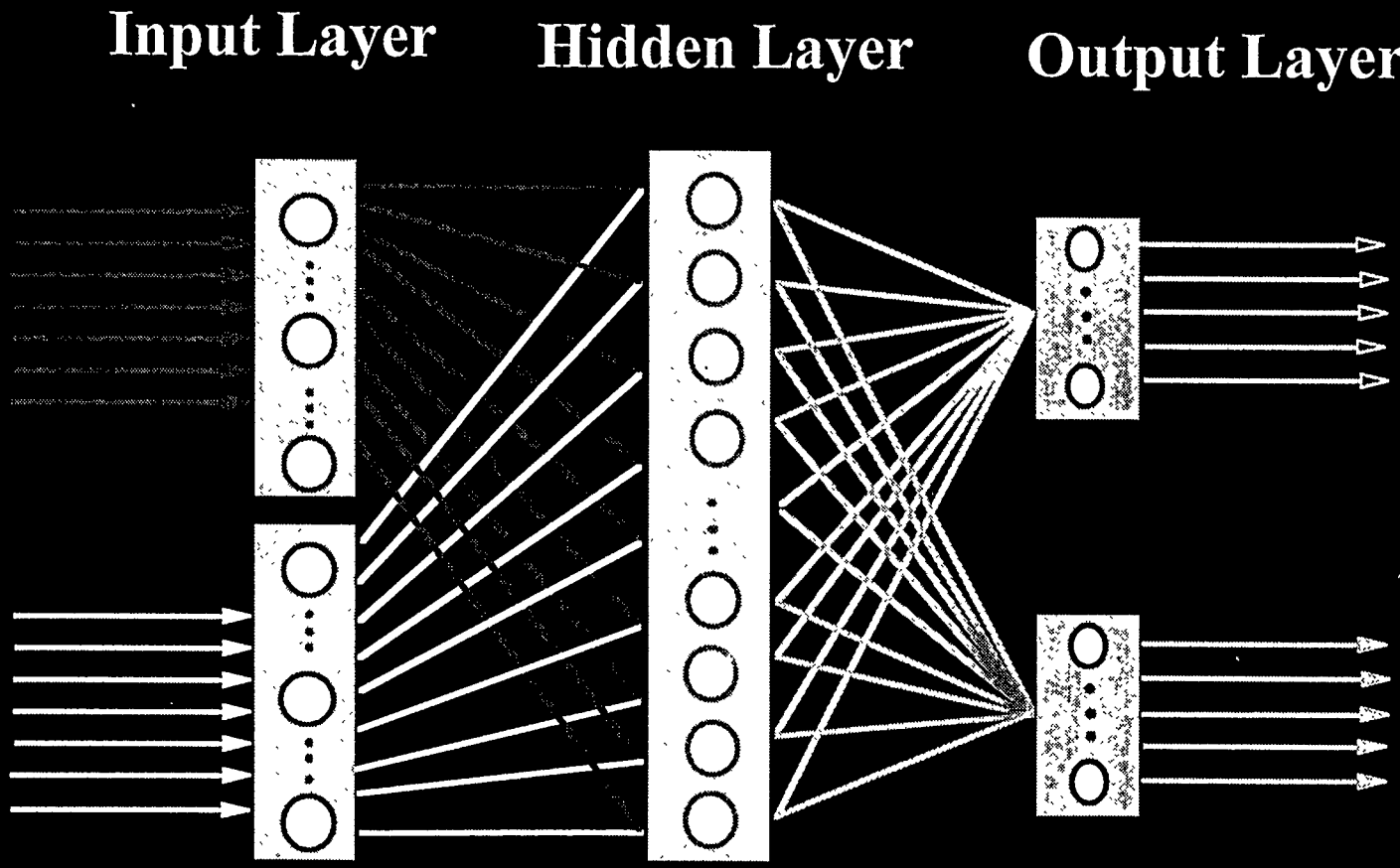

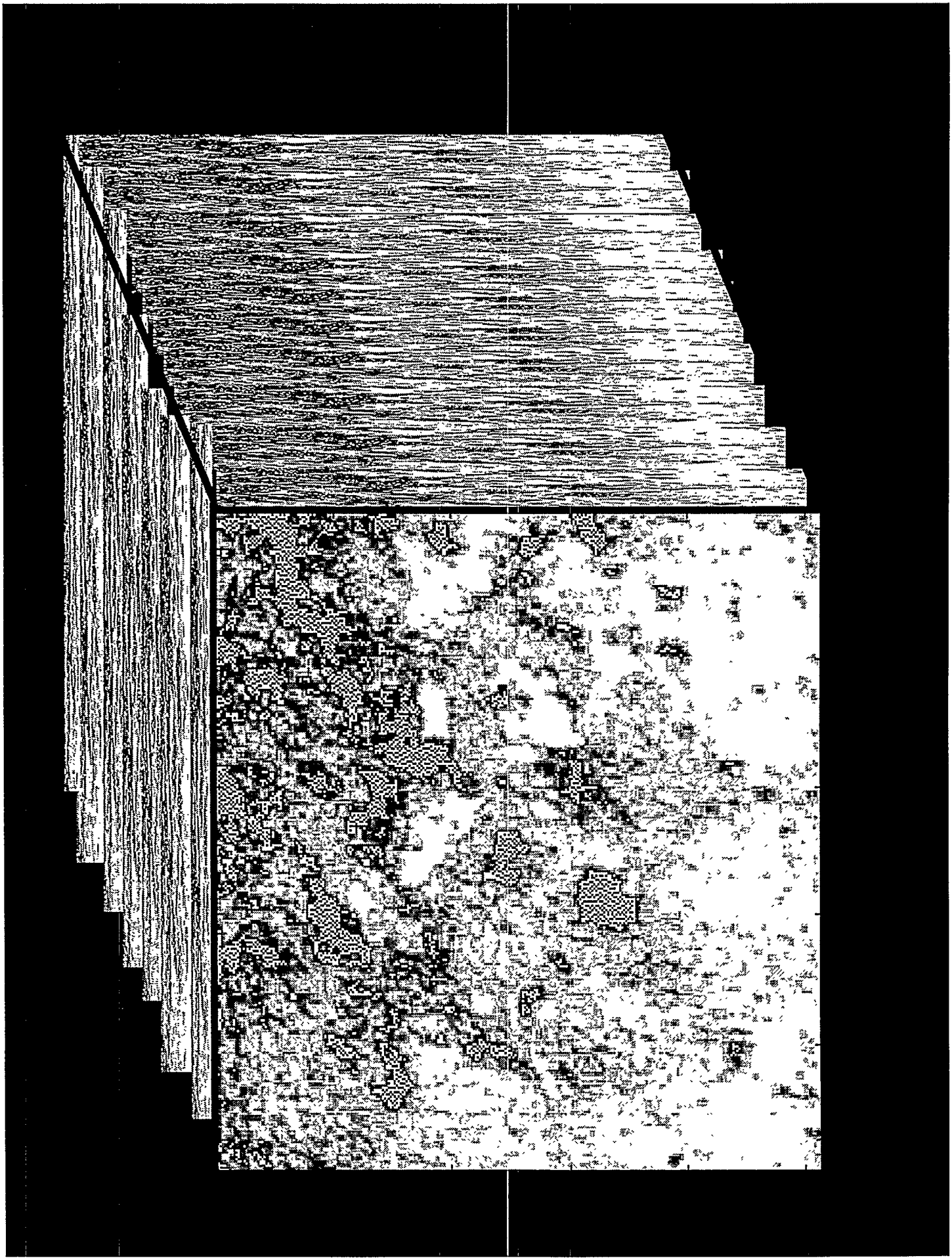

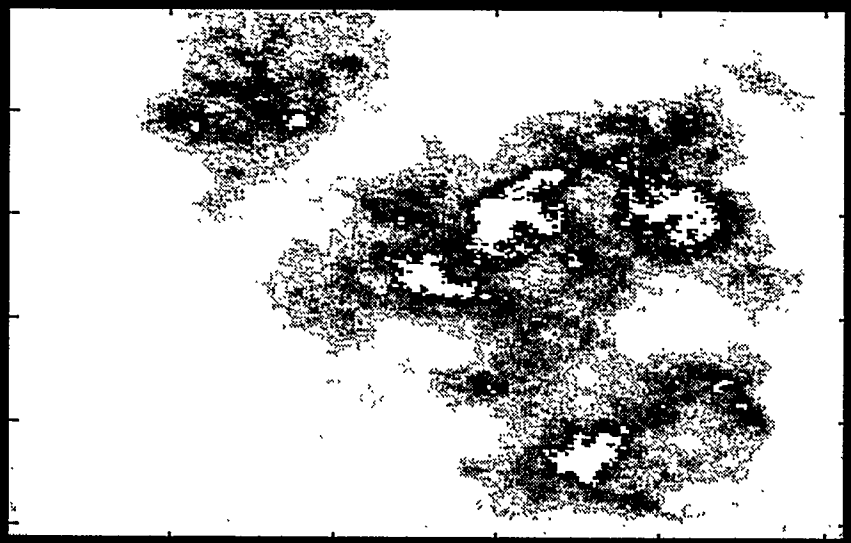

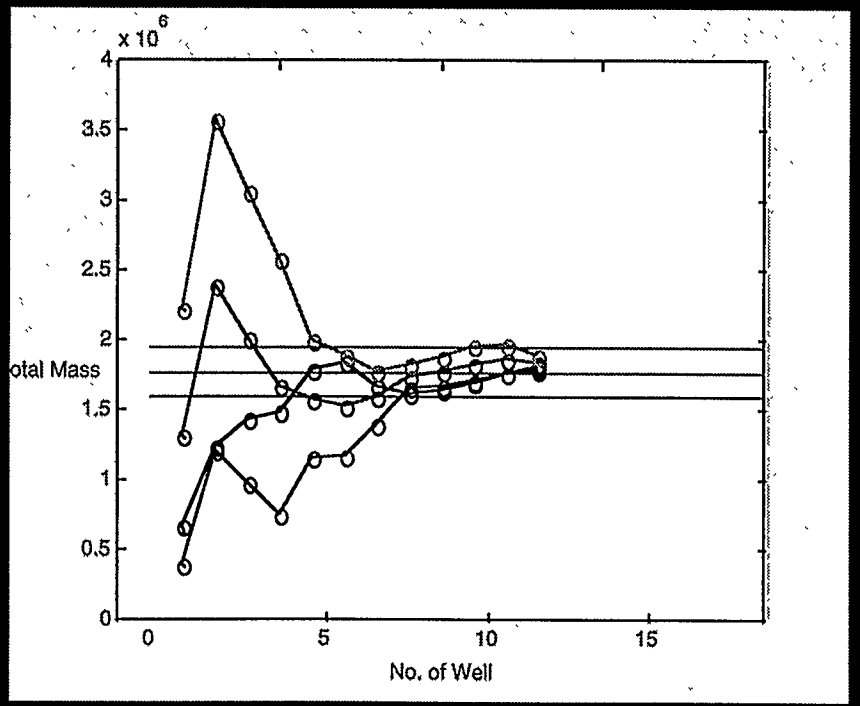
x 10^6
4
3.5
3
2.5
2
1.5
1
0.5
0
otal Mass
0
5
10
15
No. of Well

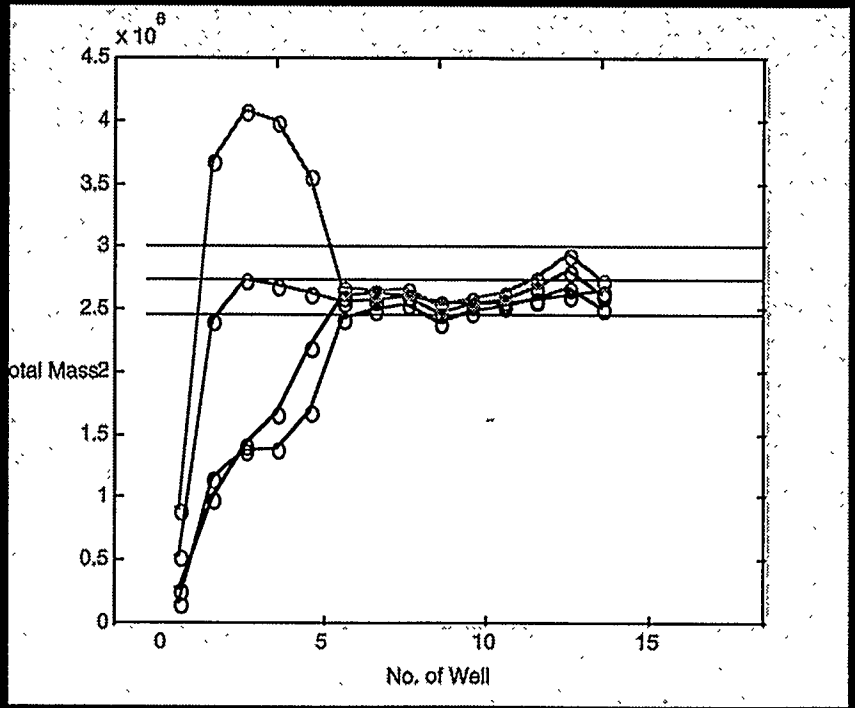
x 10^6
4.5
4
3.5
3
2.5
2
1.5
1
0.5
0
otal Mass2
0
5
10
15
No. of Well

Conclusions

- simple averaging predictions show sensitivity to initial wells selected
- higher resolution sampling does not always lead to a better prediction
- simple averaging predictions did not improve after 5 wells were drilled
- fractal methods not applicable to this type of problem
- neural network approach can help optimize the location and number of wells

Pathfinder Code

- very simple and fast approach to simulating infiltration into complex geometries
- complementary to more complex codes such as TOUGH2
- easy to modify parameters and initial conditions
- given a map of permeabilities, finds the channel of least resistance

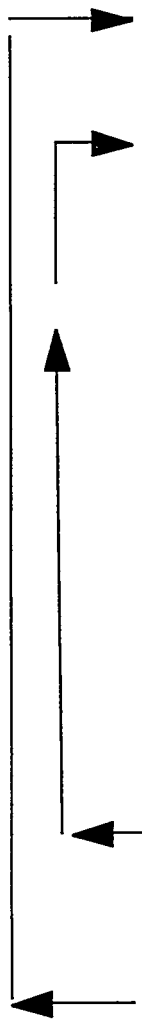

- **Find largest aperture with no water at top boundary(active site); fill with water**
- **identify nearest neighbors to active site**
  - compute capillary pressures between active site and nearest neighbors
  - compute gravity pressure between active site and nearest neighbors
  - summation of pressures between active site and nearest neighbors
  - identify new active site(the neighbor with the maximum combined capillary and gravity force); fill with water
- **calculation of area and volume; repeat steps until flow stops (trapping or bottom boundary)**
- **Return to top boundary; select next largest aperture; continue until no more paths are available or until a designated infiltration volume is exceeded**

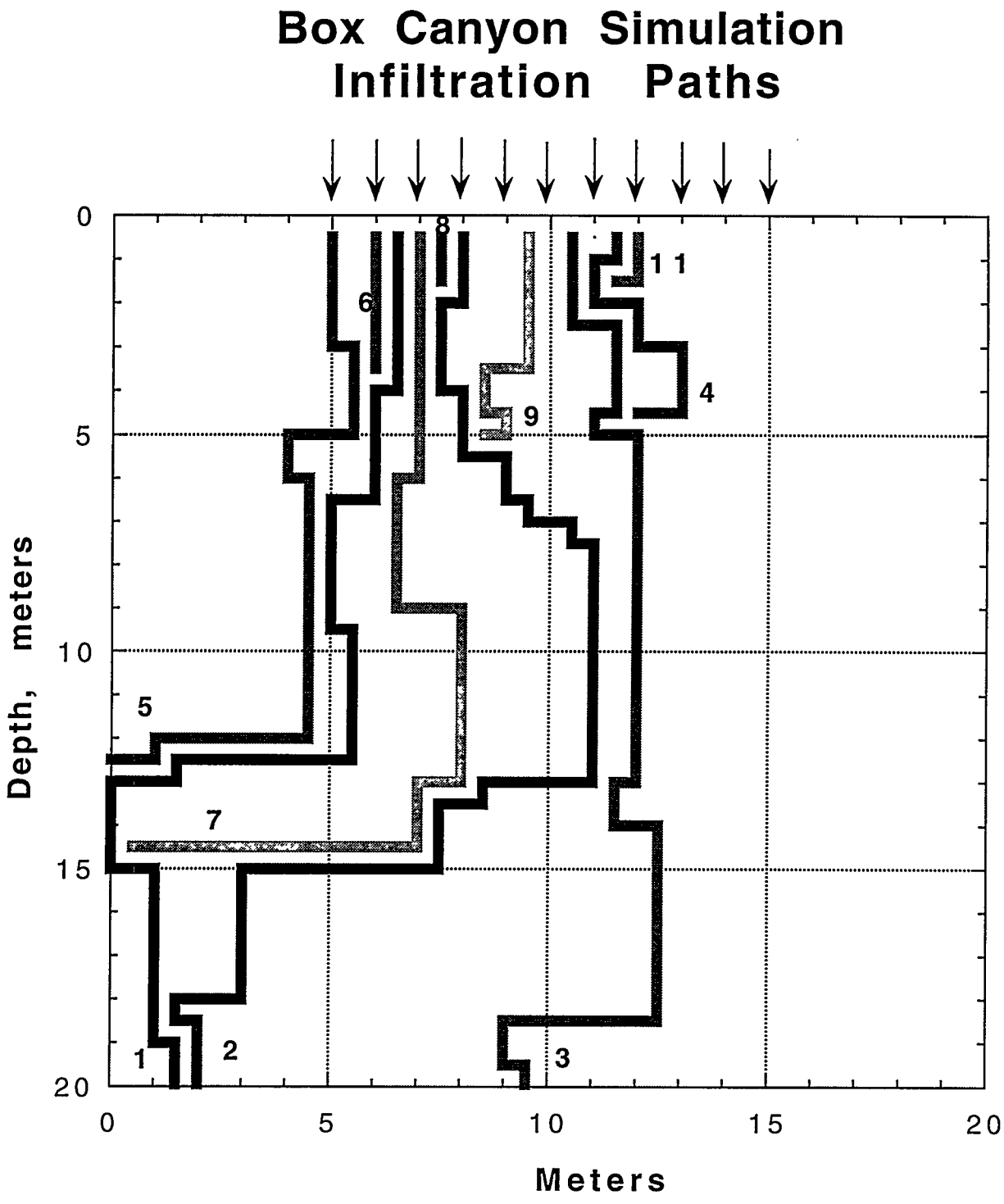
Box Canyon Simulation
Infiltration Paths
Depth, meters
Meters
0
5
10
15
20
1
2
3
4
5
6
7
8
9
11

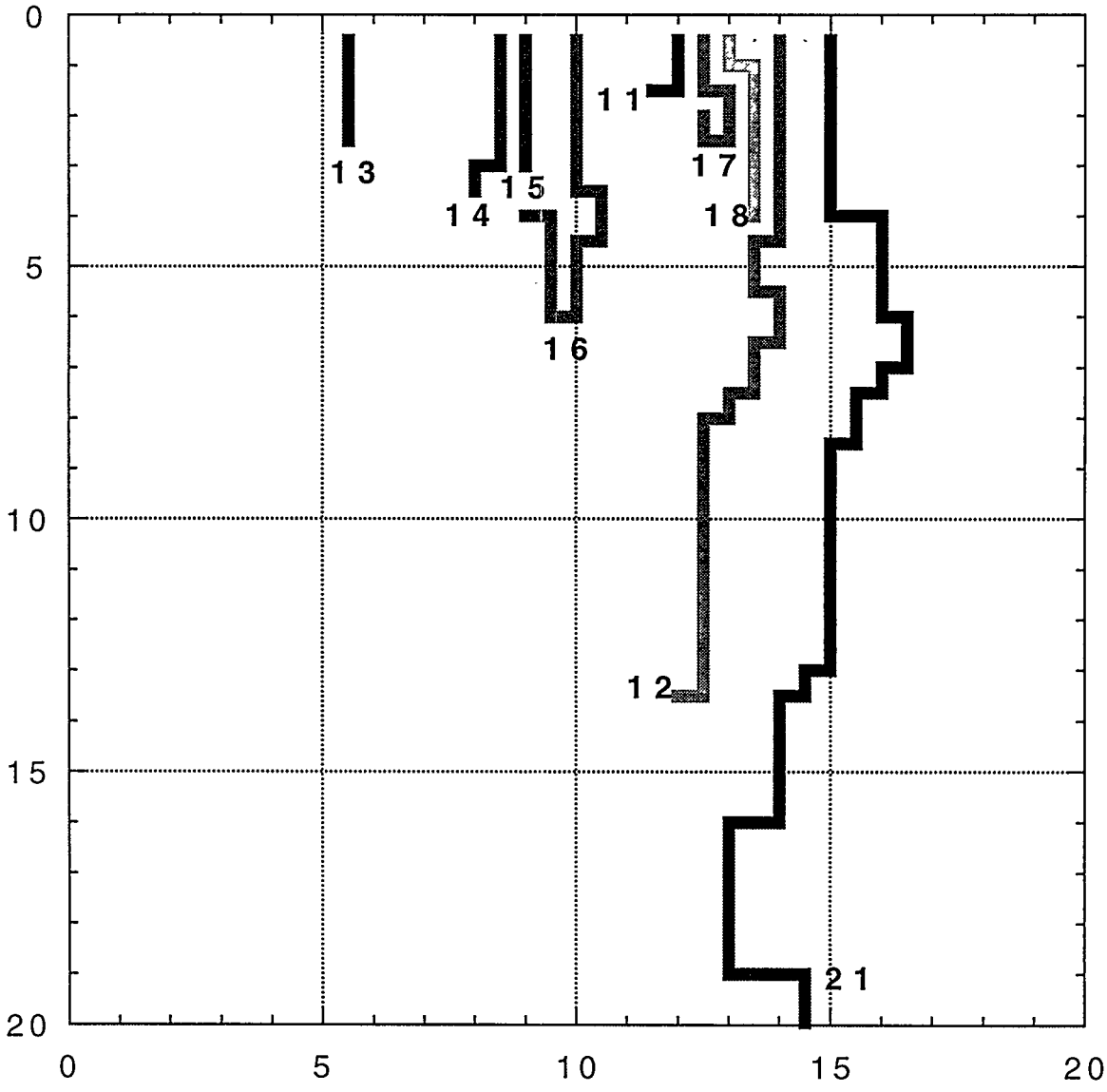
0
5
10
15
20
0
5
10
15
20
11
12
13
14
15
16
17
18
21

II.8

Tensiometers in Fractured Rock: Experiment and Modeling

S. Finsterle, B. Faybishenko, and P. Persoff

Earth Sciences Division

Lawrence Berkeley National Laboratory

Outline

- Introduction
- Design Calculations
- Experimental Results
- Concluding Remarks

Motivation

- Fractures are pathways for fast and preferential flow of contaminants.
- Direct measurements of the transient hydraulic response of fracture-matrix systems are needed.
- The interaction between tensiometer and formation should be studied.

Problems

- Tensiometer tip in fractured rock contacts both fracture and matrix.
- Fracture and matrix are not in equilibrium during transient flow events.
- Gauge water pressure includes matrix and fracture pressure components.
- Porous tip of tensiometer may lead to local redistribution of water.

Objectives

- Study the performance of the tensiometer installed in unsaturated fractured rock under draining and wetting conditions
- Explore the possibilities of deconvolving the observed tensiometer pressure into fracture and matrix components

Methods

- Analyze field data from tensiometers in fractured formations
- Perform laboratory experiments on fractured core
- Perform numerical simulations of unsaturated flow in fracture-matrix system, including interaction with tensiometer

Field Experiment

- Tensiometer measurements at three different depths prior to and during ponded infiltration experiment in fractured basalt (Box Canyon Site, INEEL)
- Immediate pressure response to infiltration at all deph
- Slow pressure response to drainage

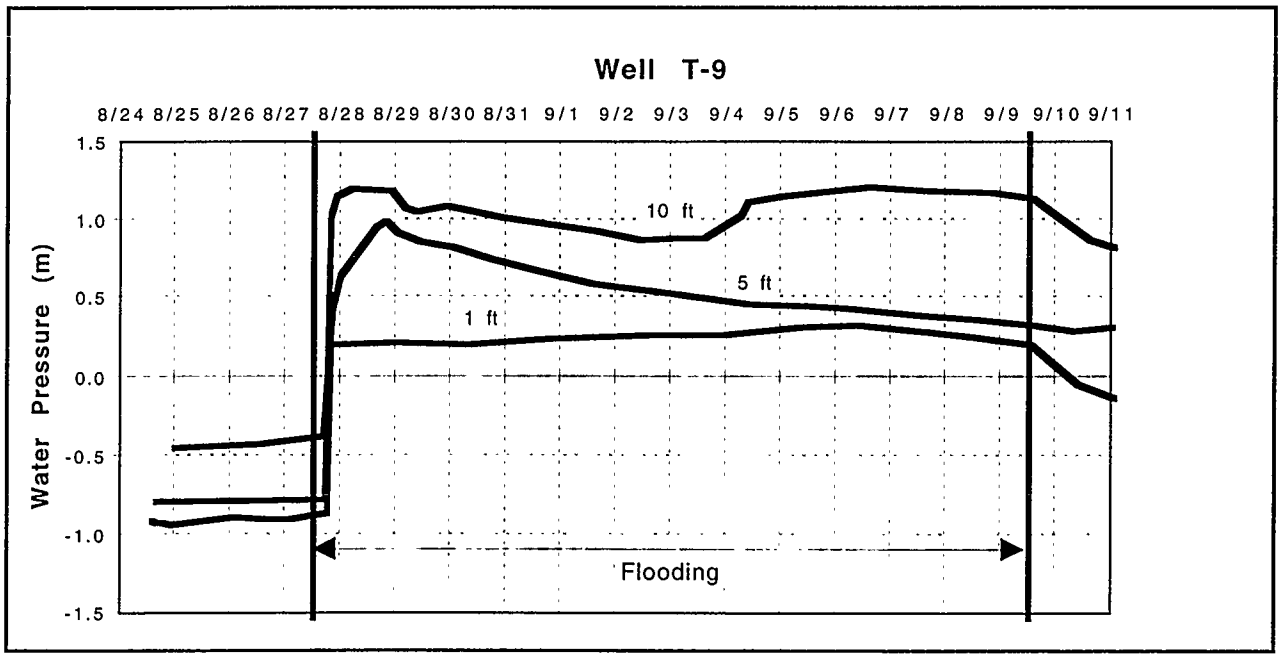

Laboratory Experiment

- Fractured core in flow cell for drainage and imbibition experiment
- Tensiometers installed in matrix and intersecting fracture at two levels

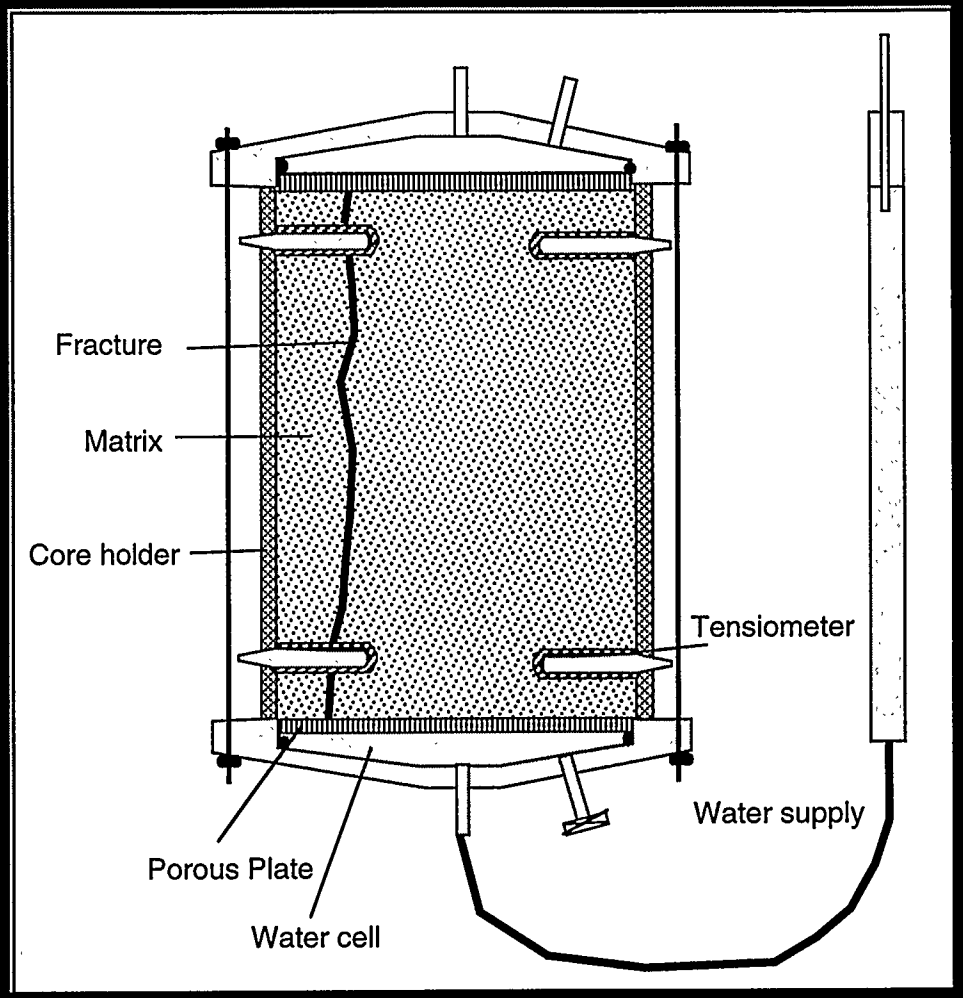

Imbibition and Drainage in Fractured Basalt Core

- During imbibition, the response of the fracture tensiometers is fast, followed by transient effects caused by water imbibition into the matrix. During drainage, the responses of the fracture and matrix tensiometers are identical because the fracture is drained immediately.
- The presence of a fracture leads to a strong hysteretic behavior in the observed water pressure.

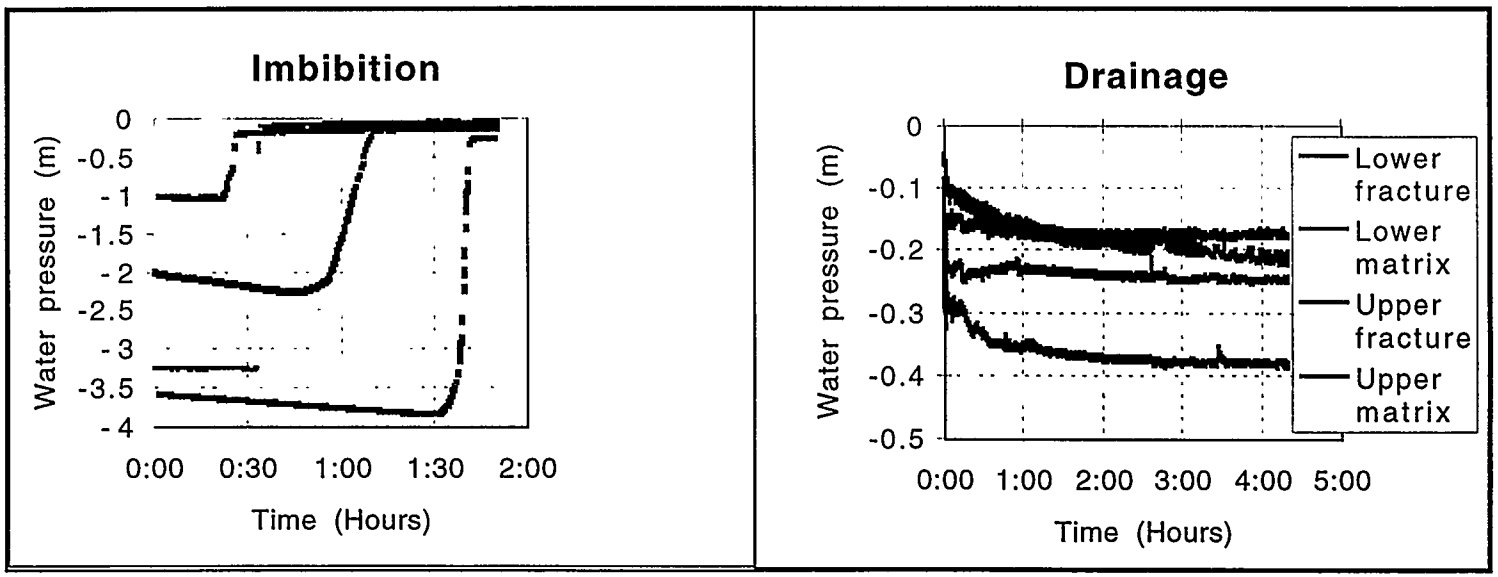

Tensiometer in Fracture-Matrix System During Imbibition

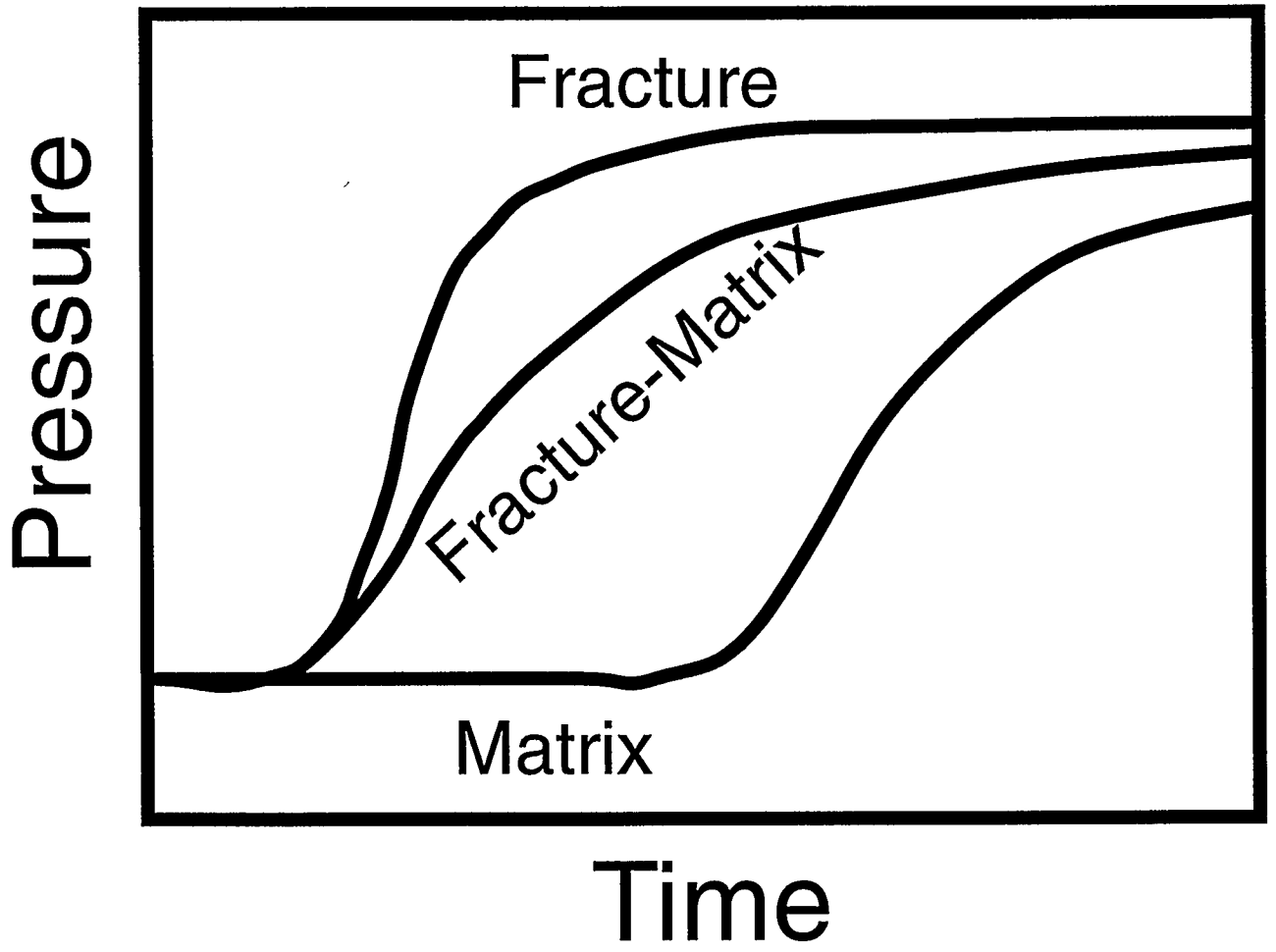

Modeling Approach

- Simulation of two-phase flow (gas and liquid) in fracture-matrix system.
- Accurate representation of air-pocket tensiometer (ceramic cup, water-filled tubing, air bubble)
- Initial drainage from both sides for ten days under -0.9 bars of suction, followed by ponded imbibition from top for ten days.

Discretization of Tensiometer

Modeling Approach (cont.)

- Examination of saturation distribution and flow patterns during drainage and imbibition.
- Examination of pressure in fracture and matrix; comparison with pressure in tensiometer air bubble.
- The calculations were performed with the TOUGH2 simulator for multi-phase, multi-component flow in porous media.

Parameter Set

Parameter	Matrix	Fracture
permeability k, m^2	5.00E-17	1.00E-12
matrix porosity	0.23	-
fracture aperture, μm	-	1.00E+02
van Genuchten α, Pa^{-1}	3.84E-04	5.43E-02
van Genuchten n	1.47	1.47

Drainage

The fracture drains immediately. Drying progresses inward from both ends. The flow field is slightly affected by the presence of the tensiometer.

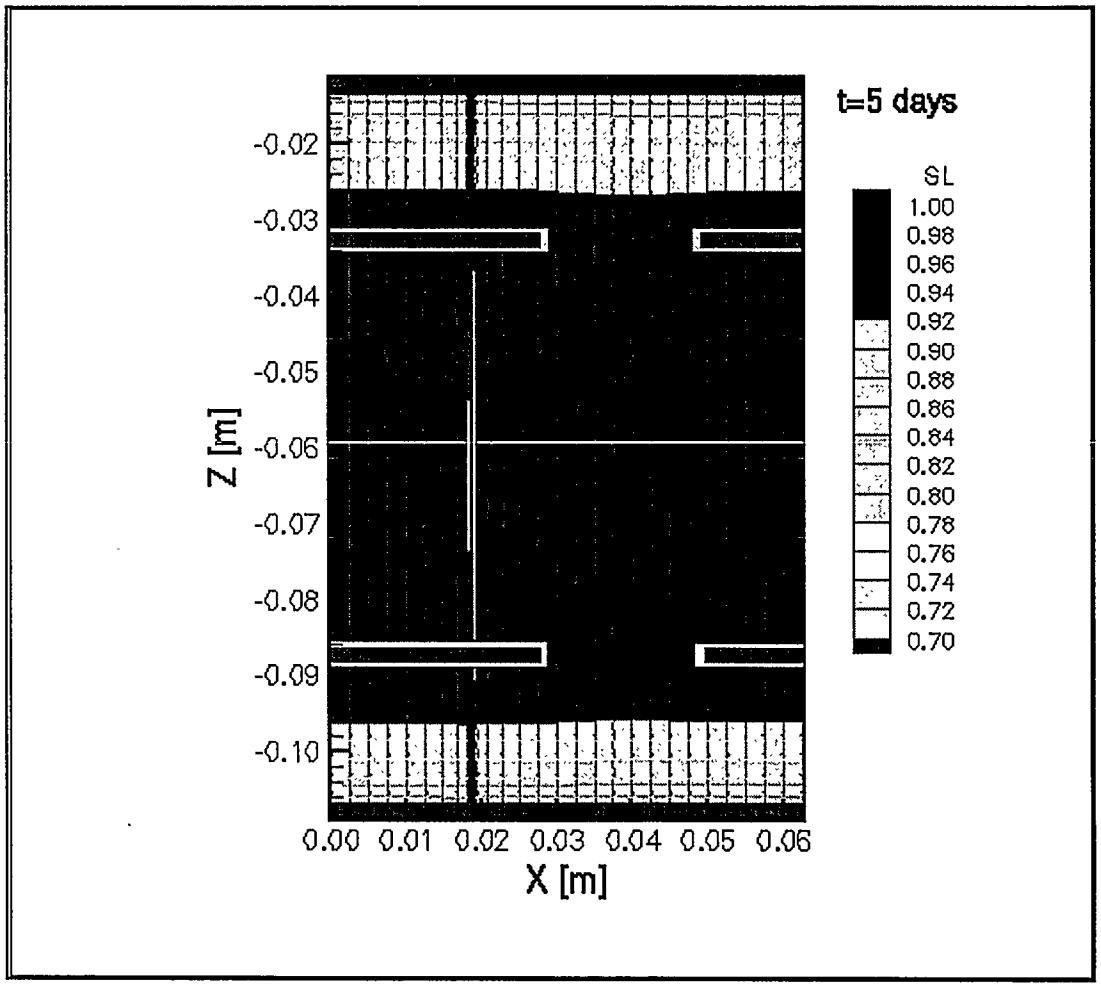

Imbibition

Imbibition progresses from the fracture into the matrix and axially from the top. The flow field is slightly affected by the presence of the tensiometer.

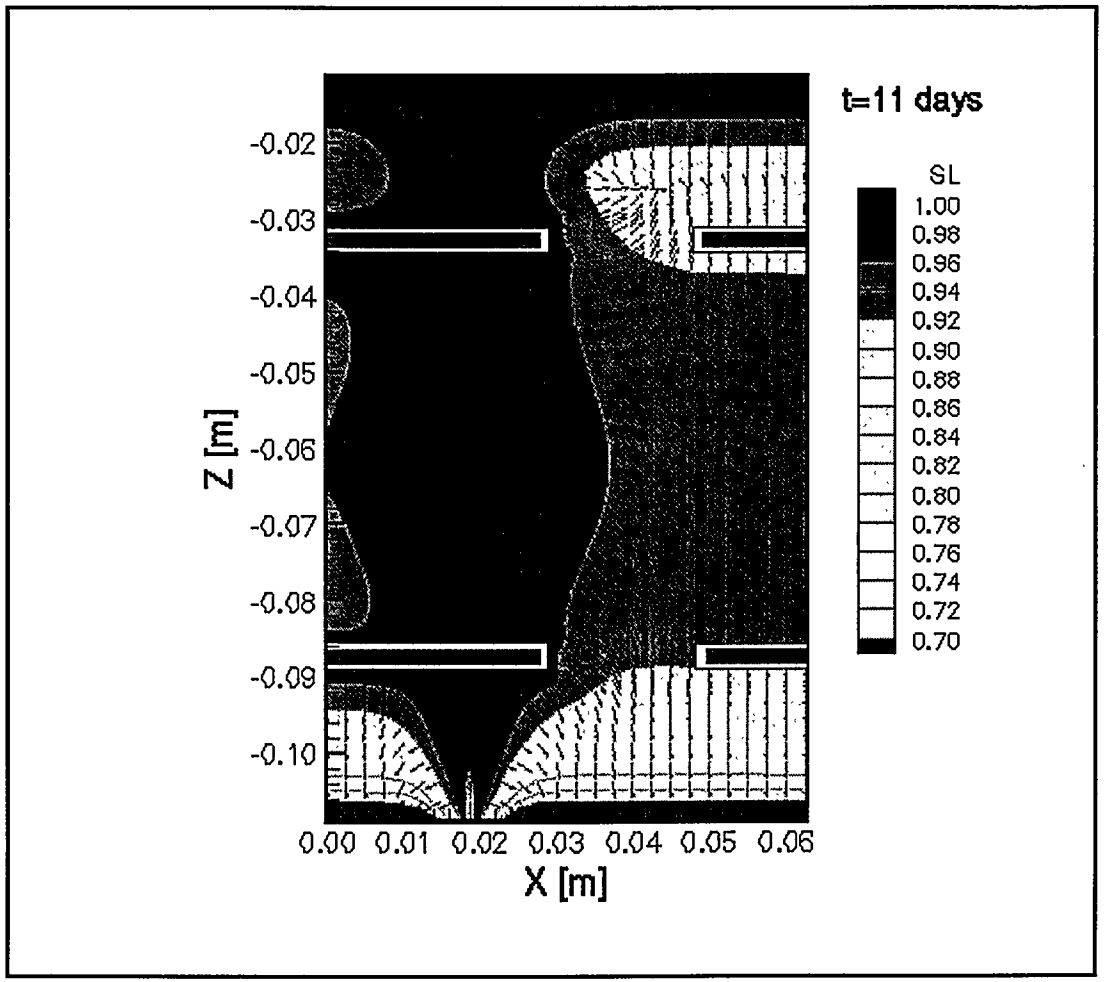

Fracture, Matrix, and Tensiometer Pressure

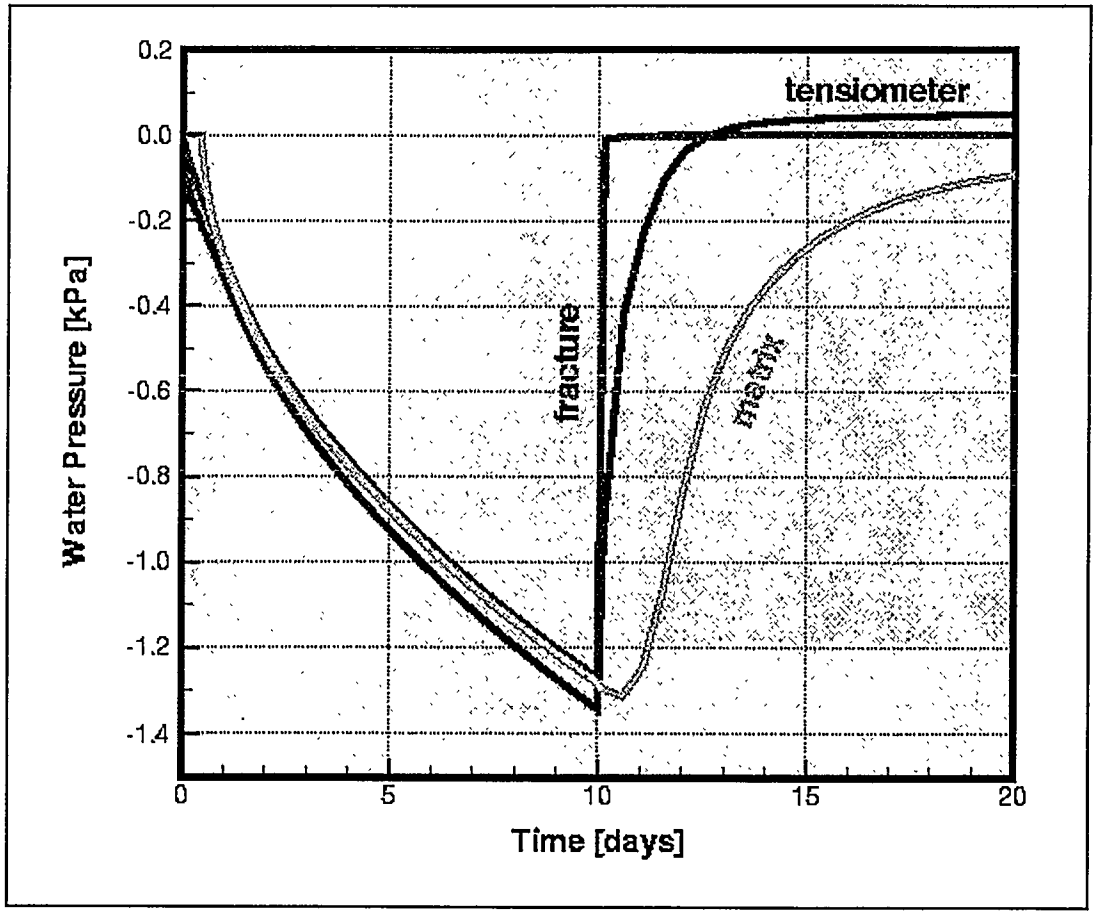

Conclusions

- The presence of a measuring device in a formation affects the system behavior to be monitored.
- It is therefore necessary to study the interaction between the sensor and the formation to correctly interpret the observed pressure.

Conclusions (cont.)

- The gauge pressure is primarily affected by the conducting component that transmits water into or out of the ceramic cup of the tensiometer.
- During drying, the gauge pressure is mostly affected by the matrix pressure; during wetting, it is dominated by the fracture pressure.
- The presence of a fracture leads to hysteresis

II.9

2-D modeling of the ERT performance to predict fracture geometry

Jeong-Seok Yang

Purpose of this research:

fracture imaging

resolution of result

different fracture combination modeling

Forward Modeling

Generate Synthetic Data

Background Resistivity Value: 1000 Ohm-m

Conductive Zone Resistivity Value: 50 Ohm-m

Pole-Pole array was used for the Modeling

2-D ERT Modeling

Grid used in the Modeling

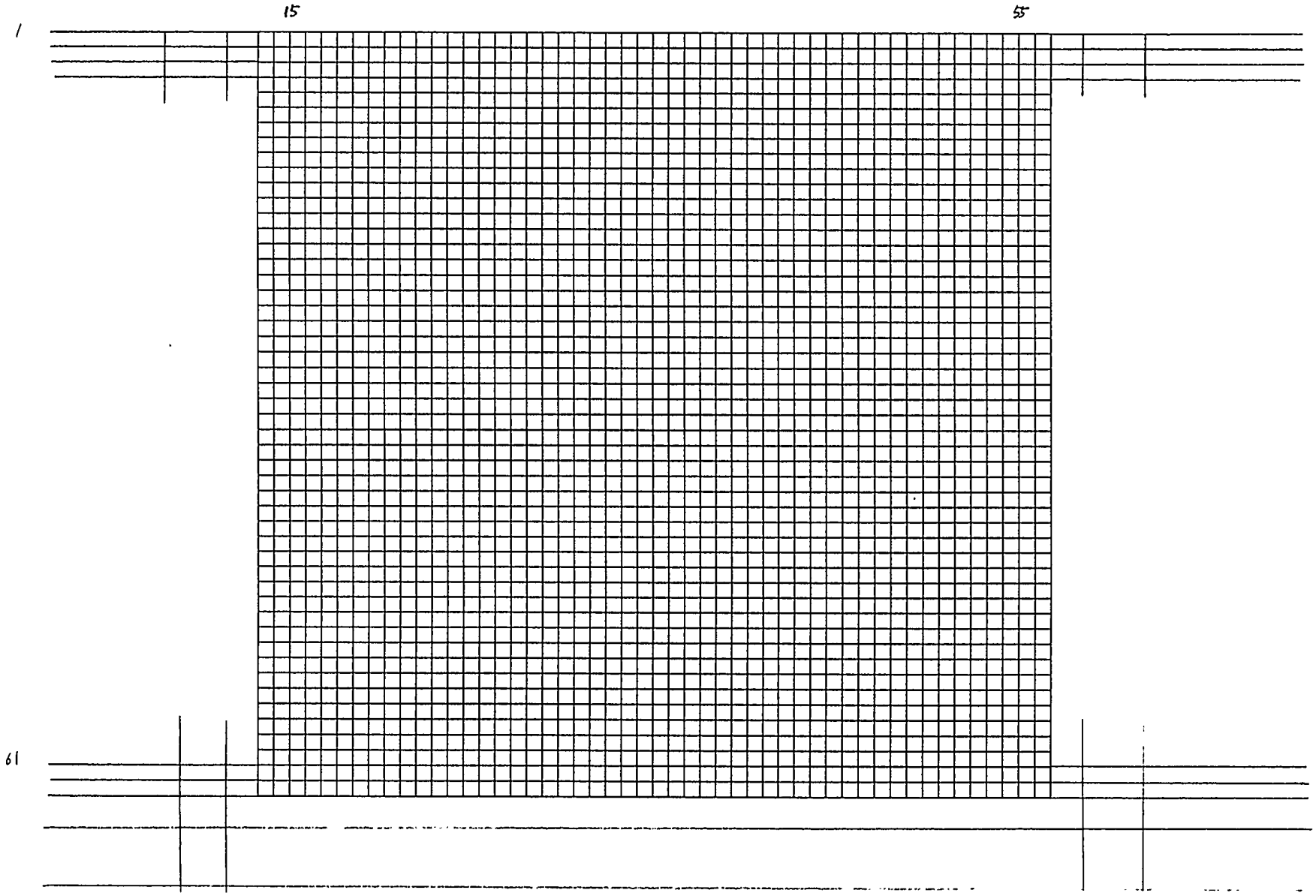

Equivalent Resistivity Values for a Cube contains a Fracture

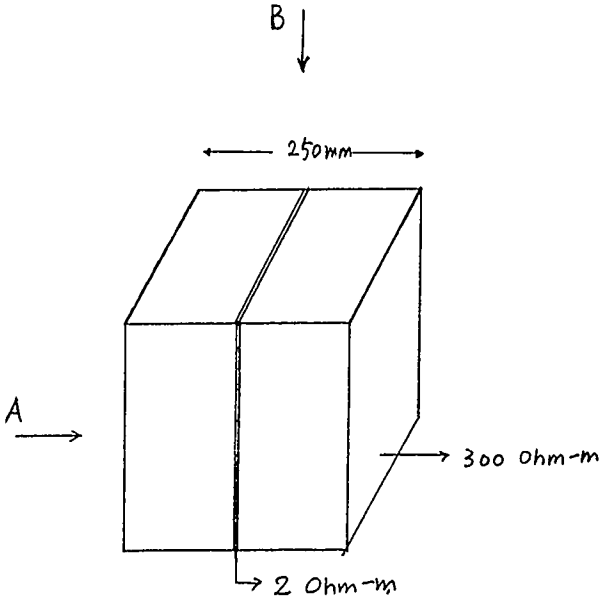

A. ρ_E = 298.8 Ohm-m (1 mm)
288.8 Ohm-m (1 cm)
(arithmetic mean)

B. ρ_E = 188.0 Ohm-m (1 mm)
43.10 Ohm-m (1 cm)
(harmonic mean)

1 mm fracture thickness: normal fracture

1 cm fracture thickness: rubble zone

Conclusion

We can have rough information about fracture geometry.

The prediction of the complex geometry of fracture is difficult.

The resolution for shallow depth is good due to surface electrodes.

The bottom part of the inversion result is not reliable.

p-1.out
(34 36 1 71)

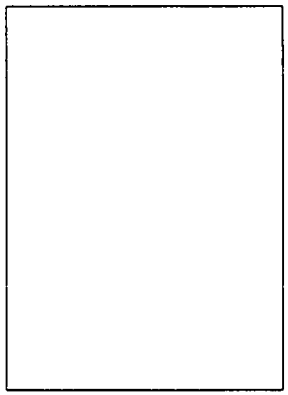

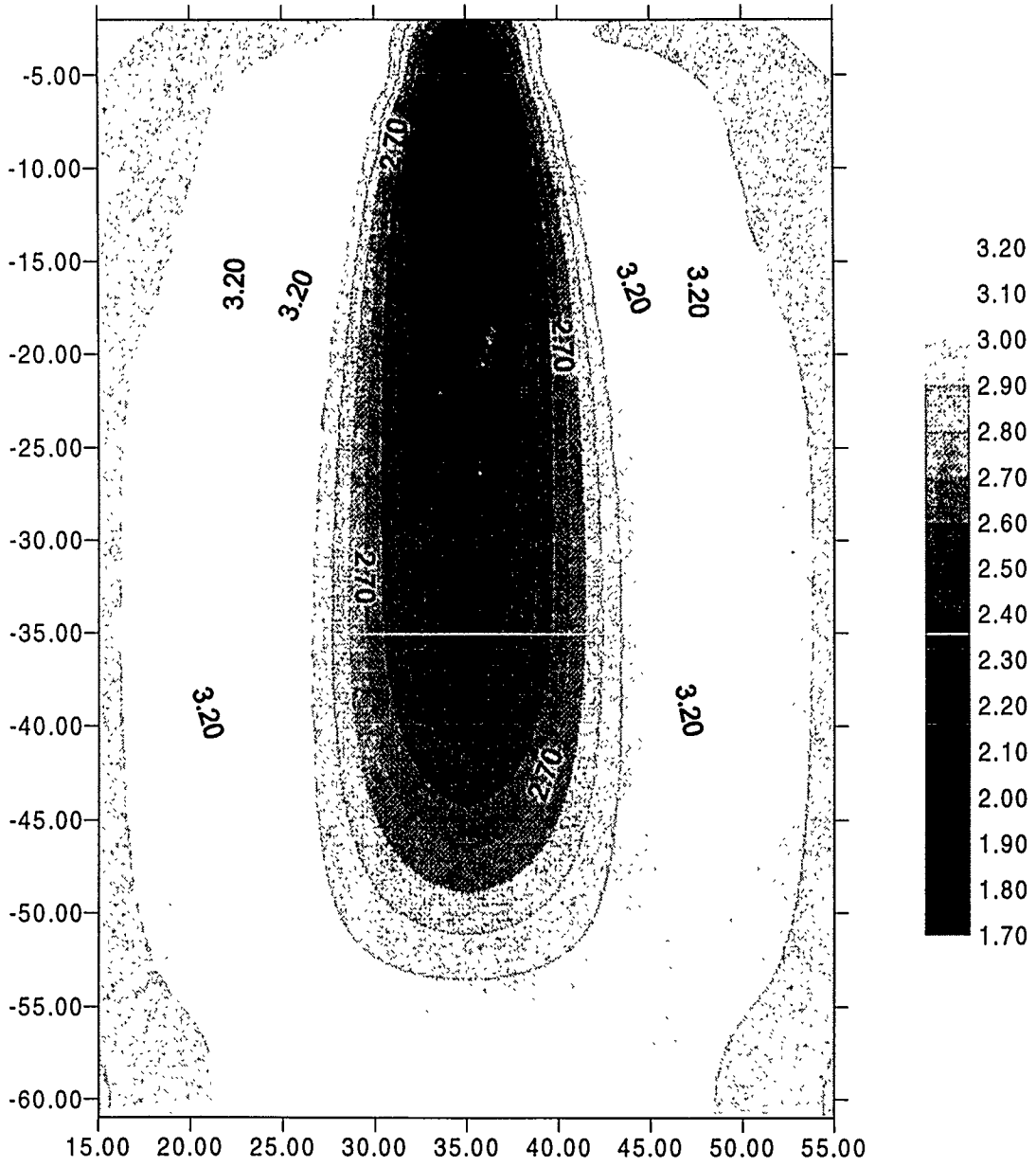

p-2.out
(22 23 1 71)

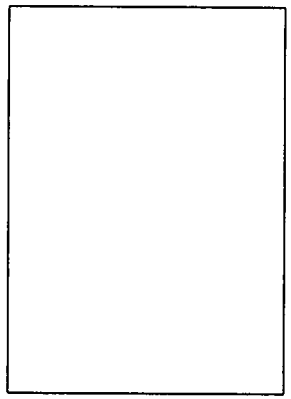

p-3.out
(5 65 9 10)

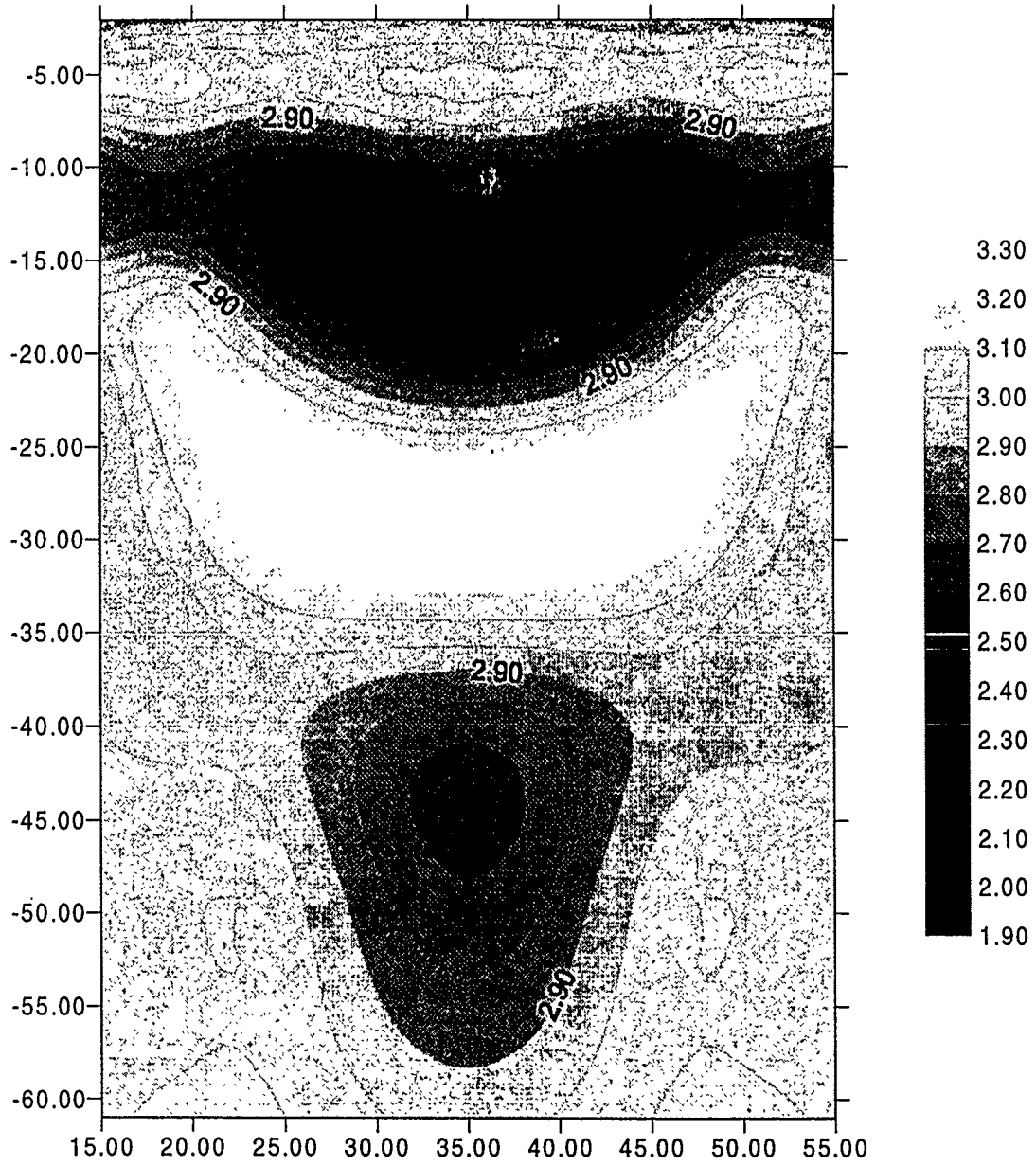

p-4.out
(5 65 20 21)

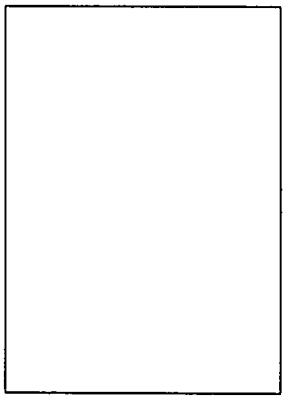

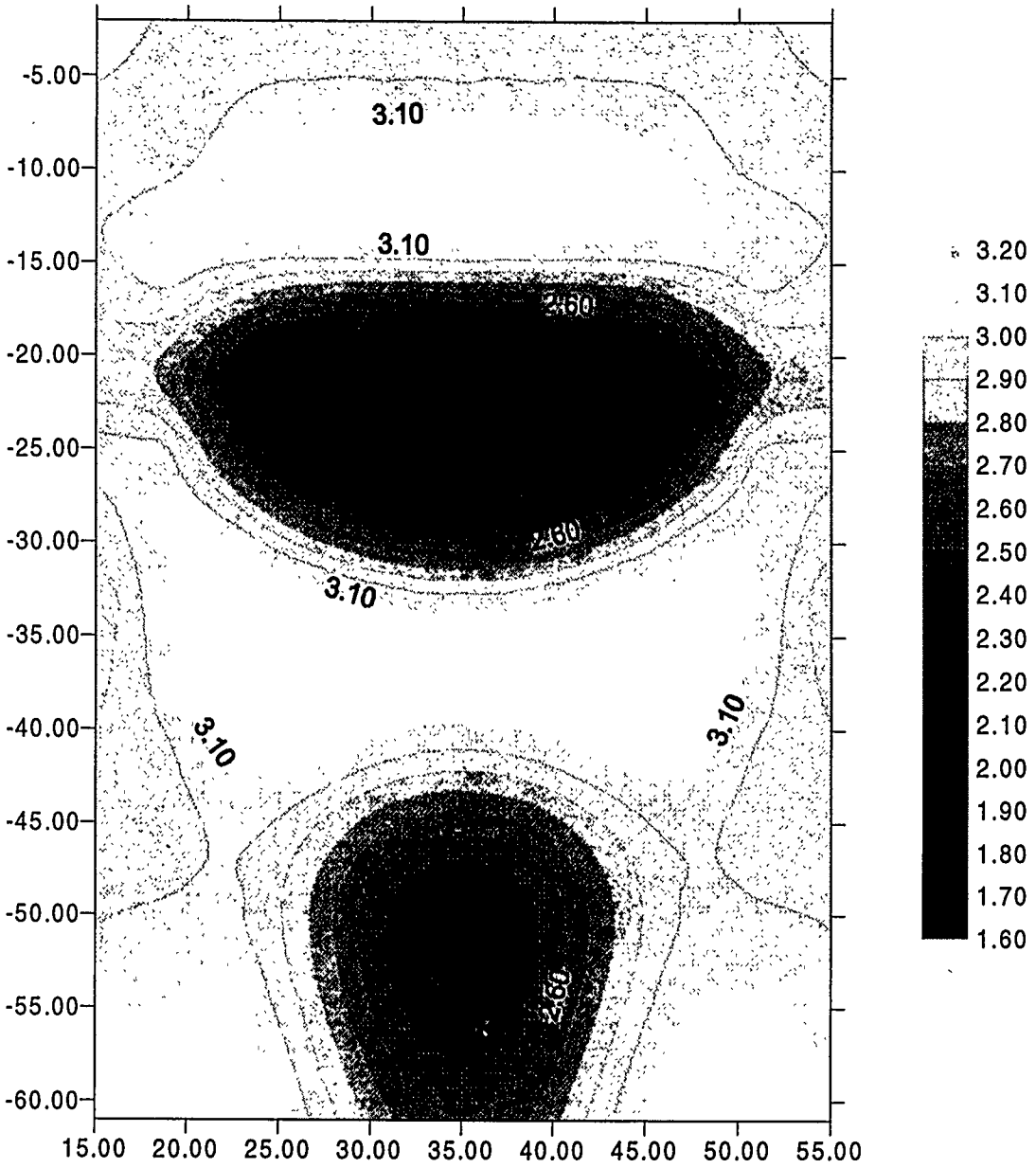

p-5.out
(5 65 29 30)

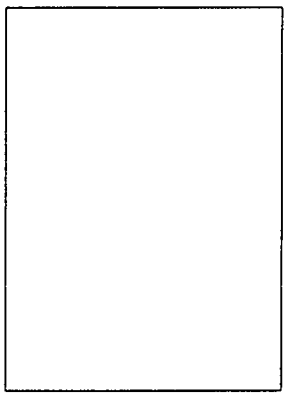

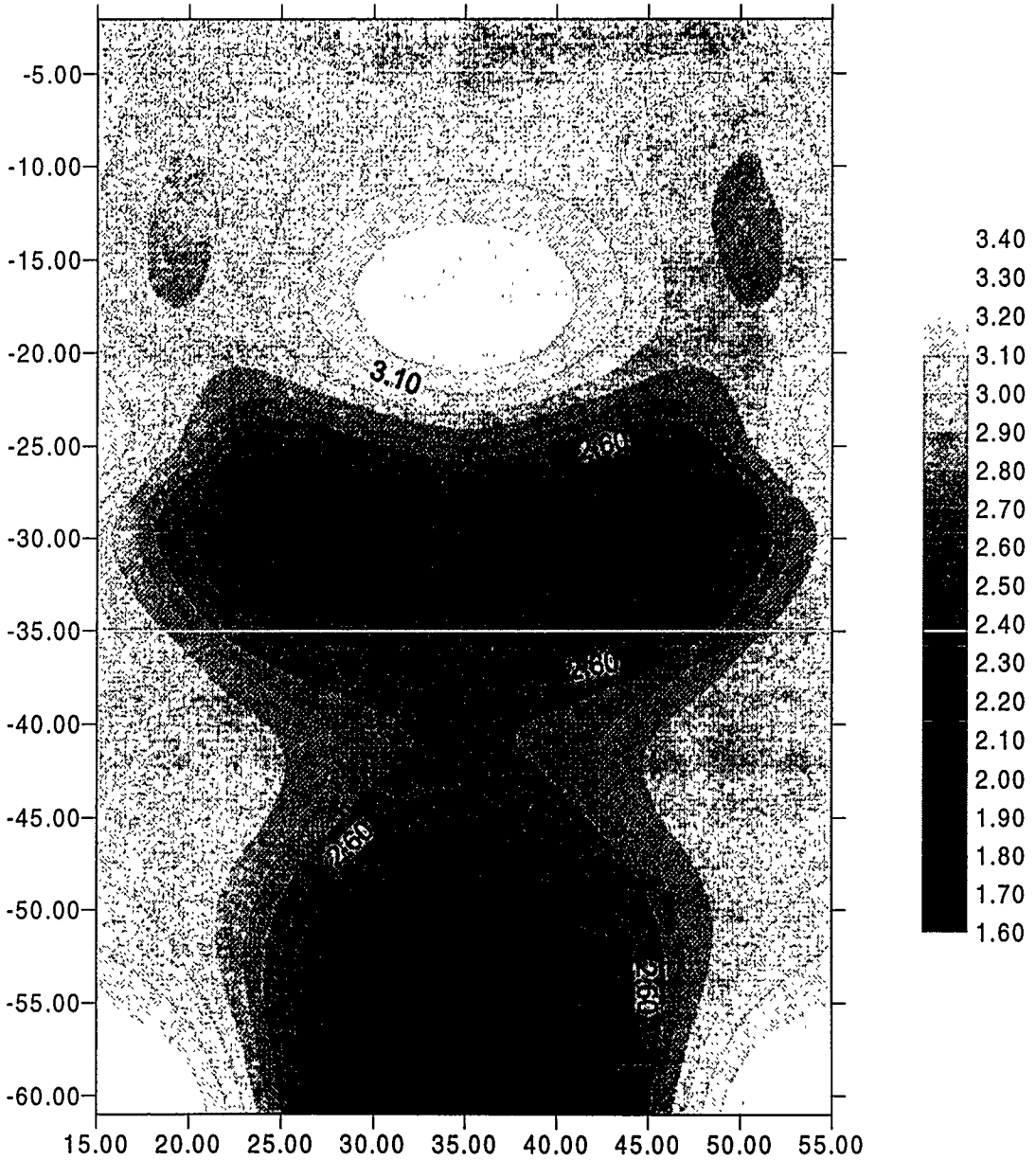

p-6.out
(5 65 40 41)

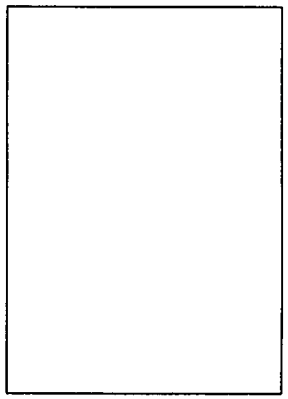

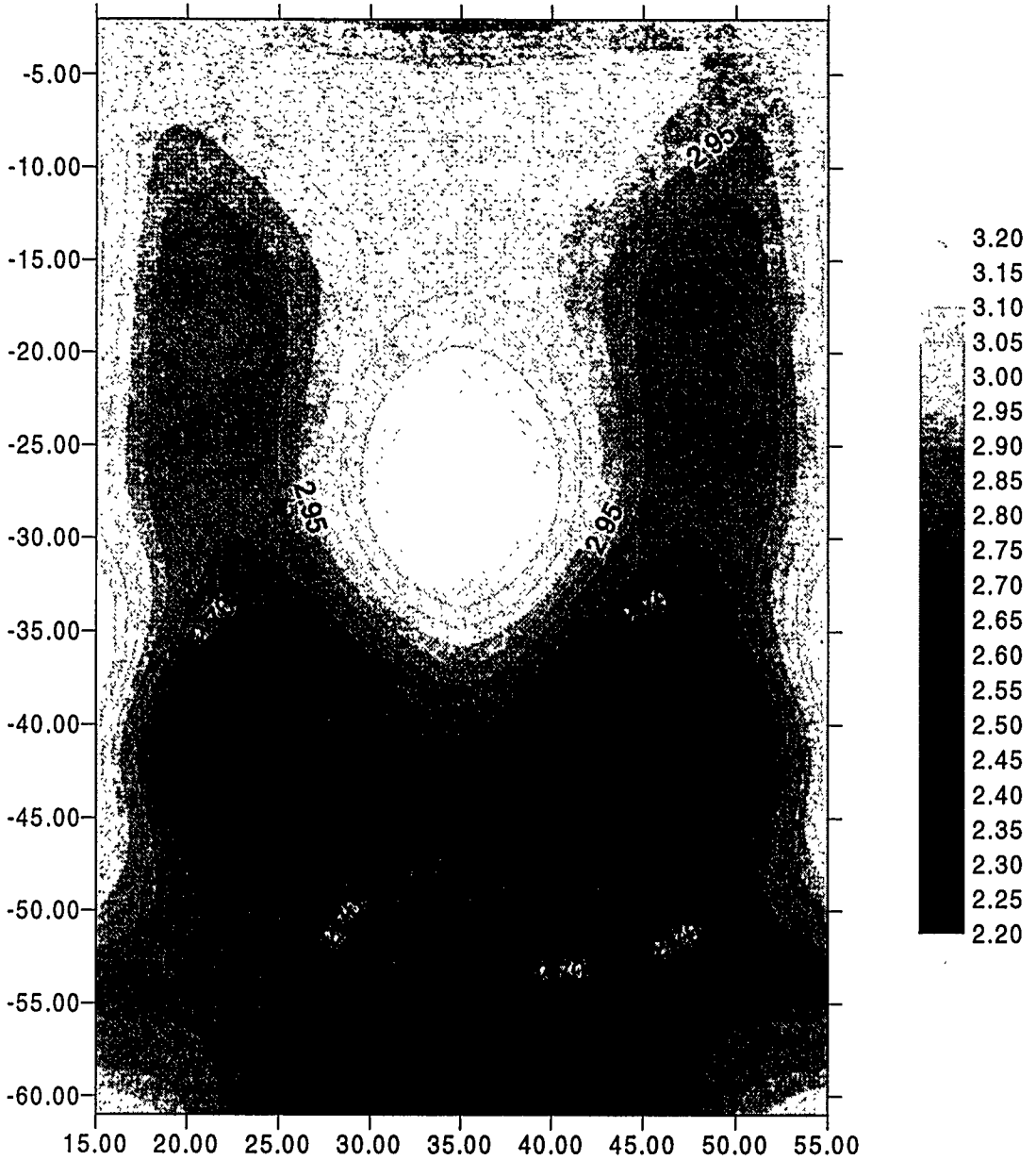

p-7.out
(34 35 1 71)
(22 23 1 71)

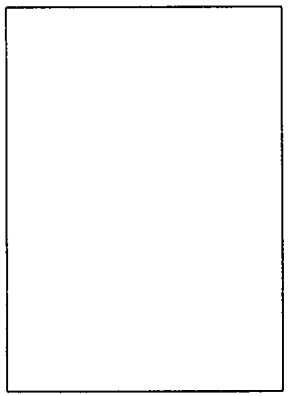

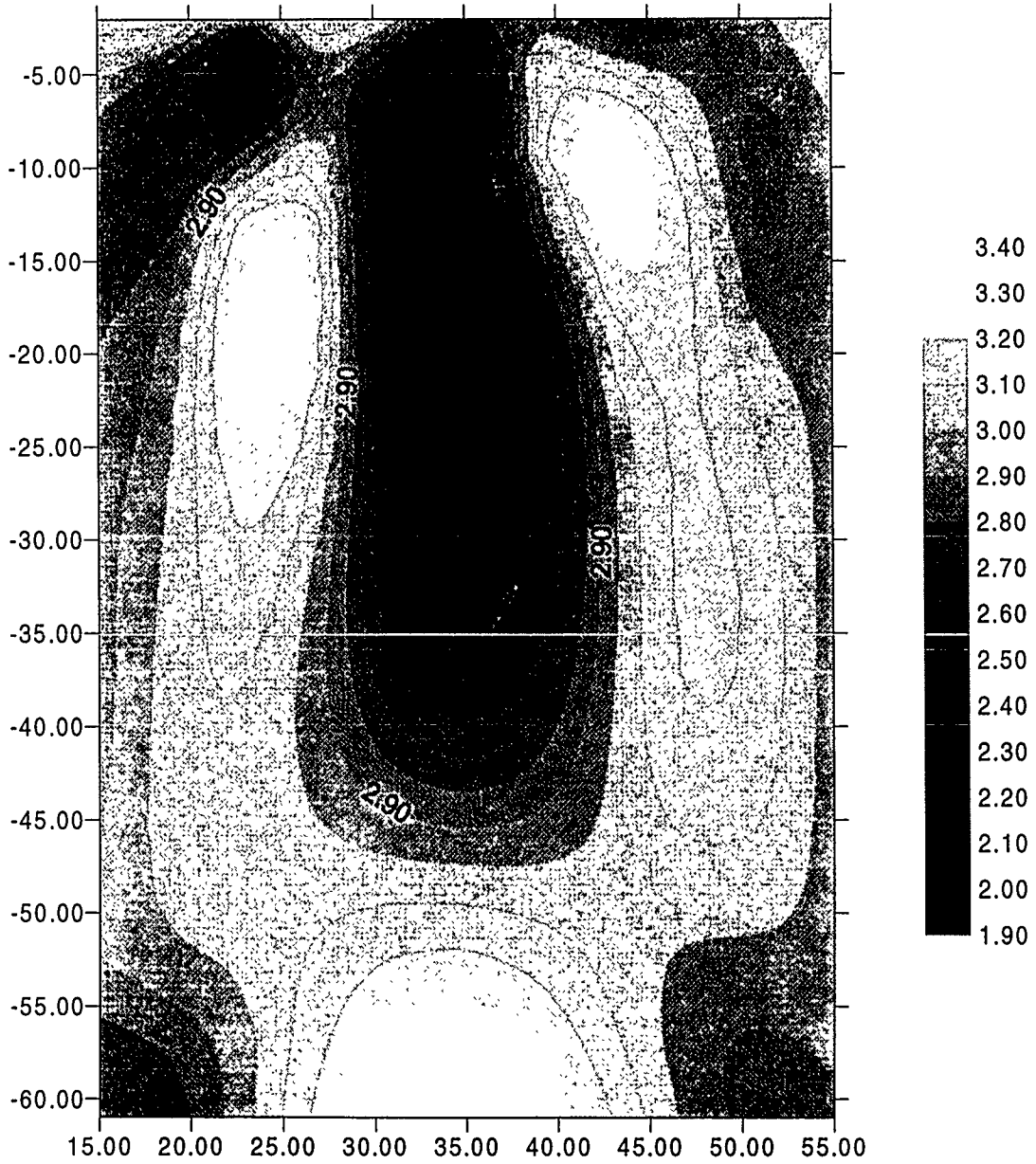

p-8.out
(22 23 1 71)
(47 48 1 71)

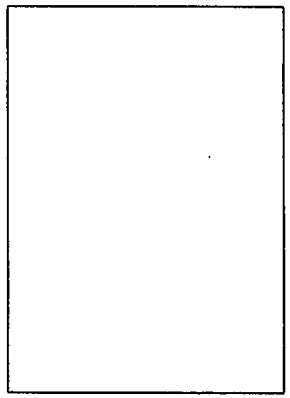

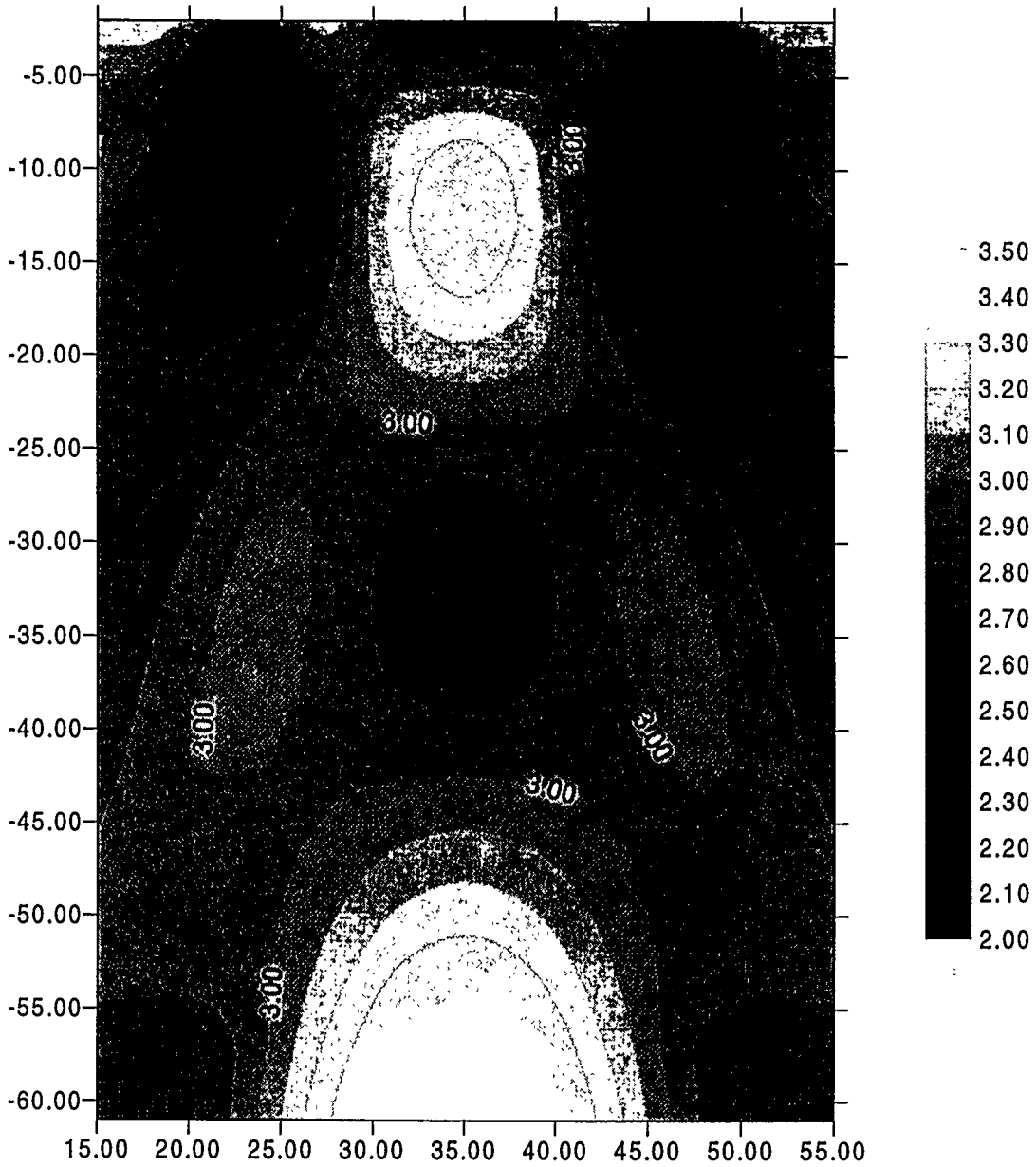

p-9.out
(5 65 9 10)
(5 65 20 21)

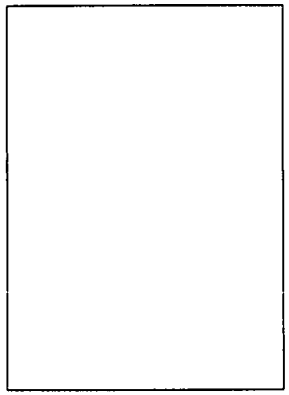

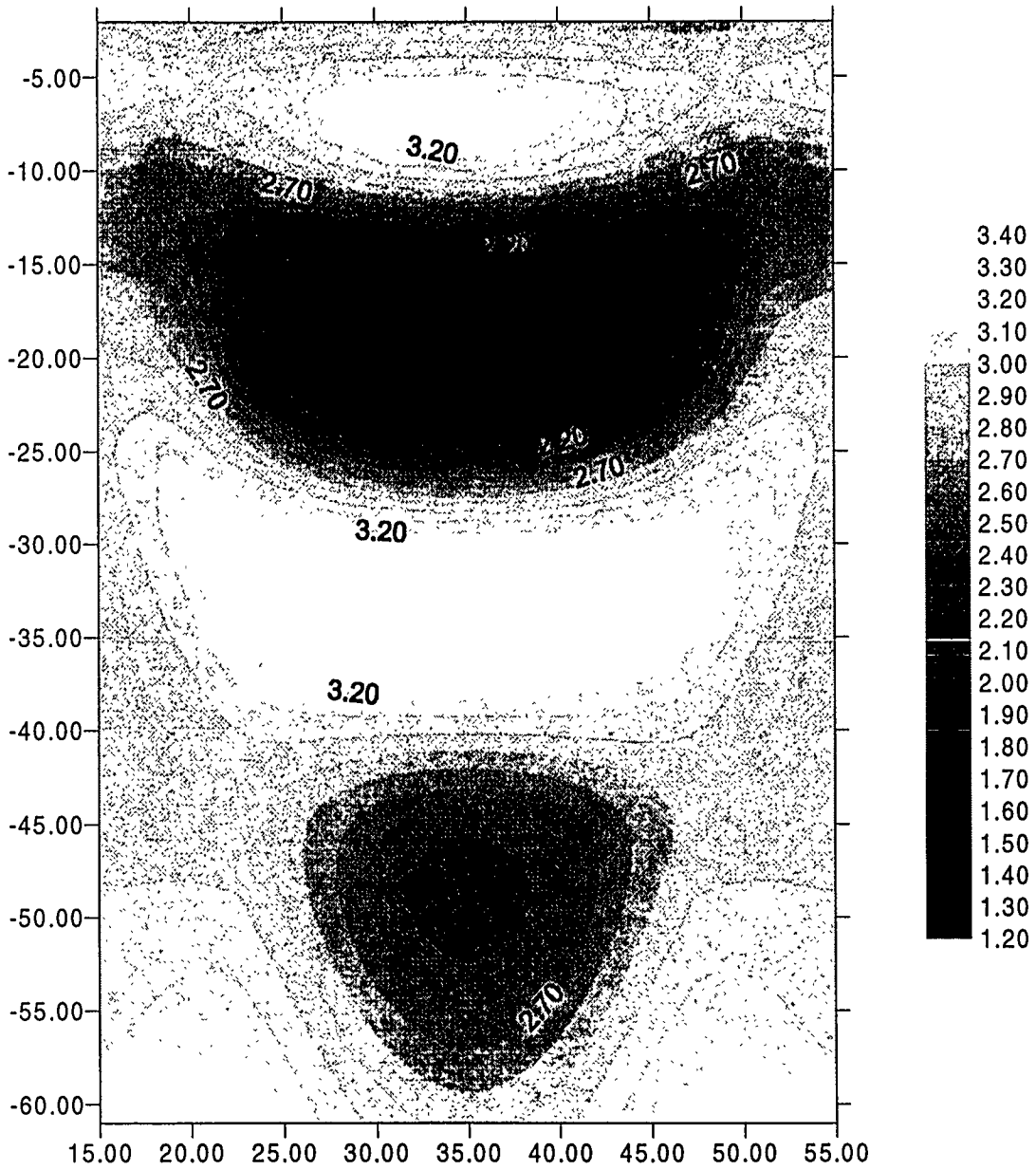

p-10.out
(5 65 20 21)
(5 65 29 30)

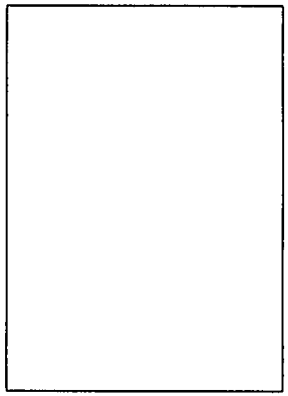

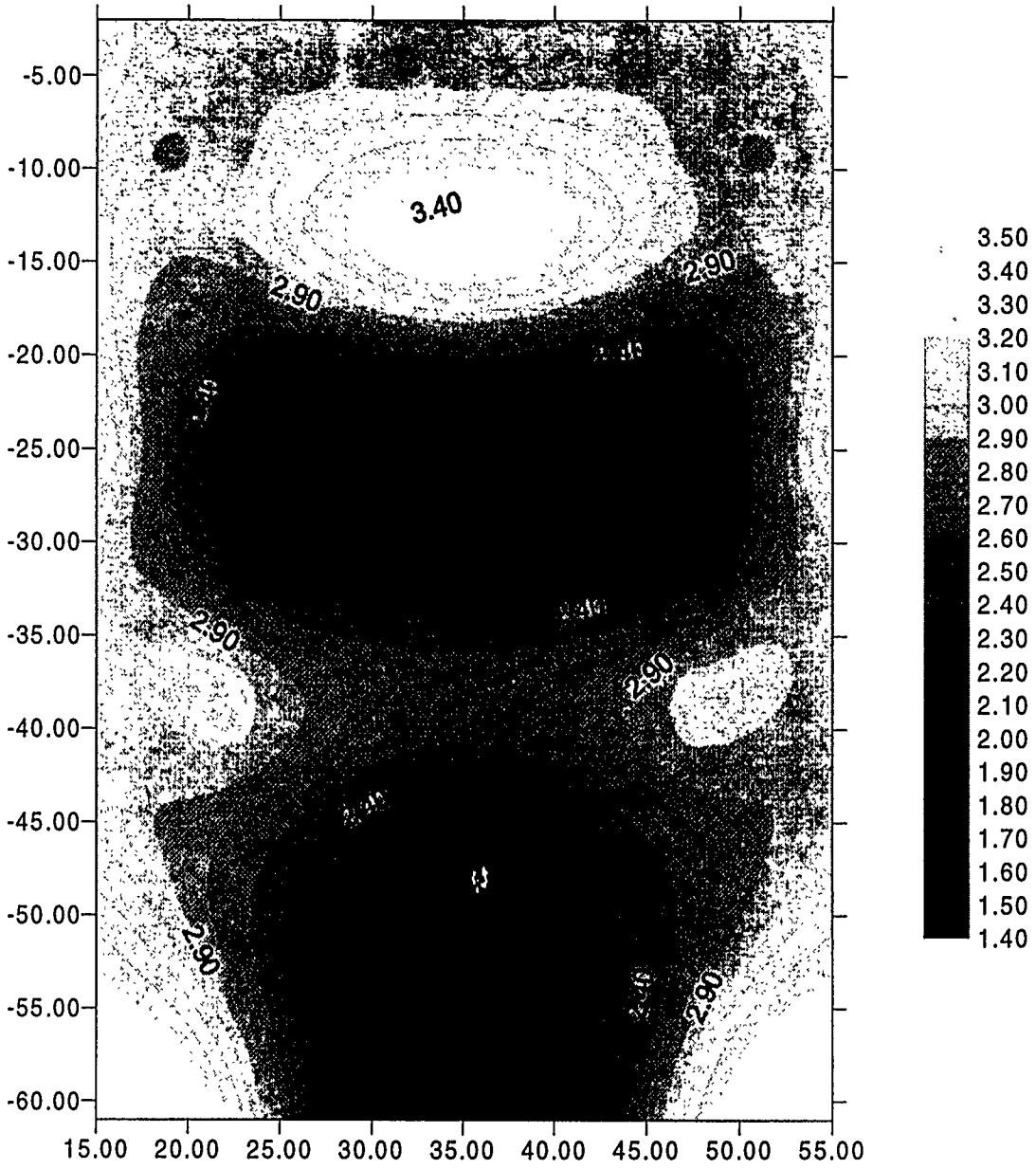

p-11.out
(5 65 9 10)
(5 65 29 30)

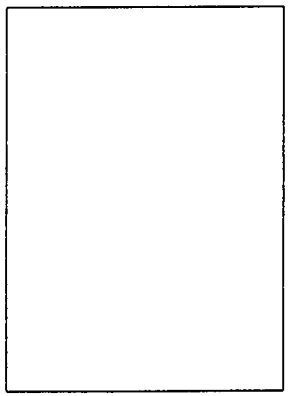

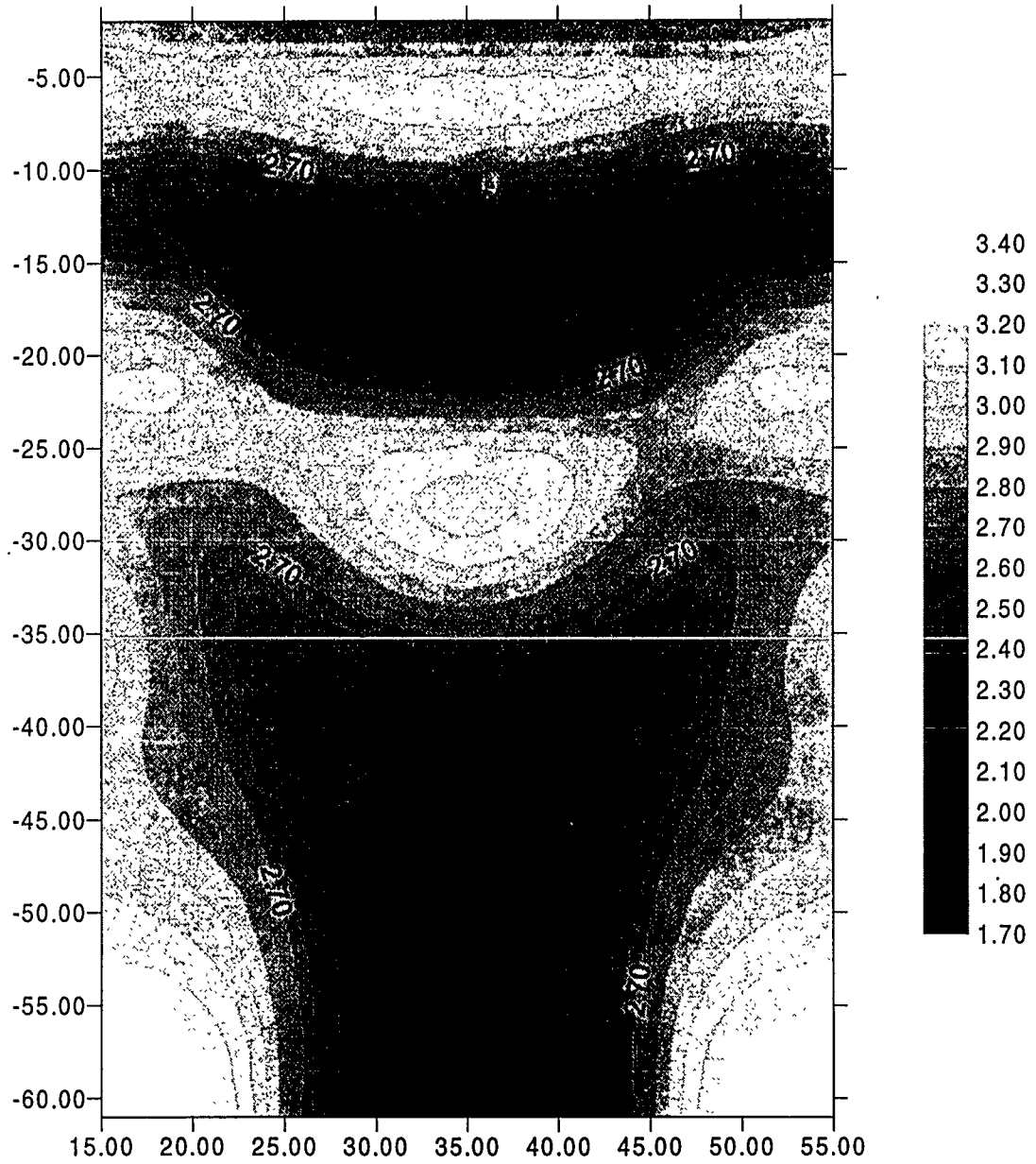

pp1.out
(34 36 1 71)
(5 65 9 10)

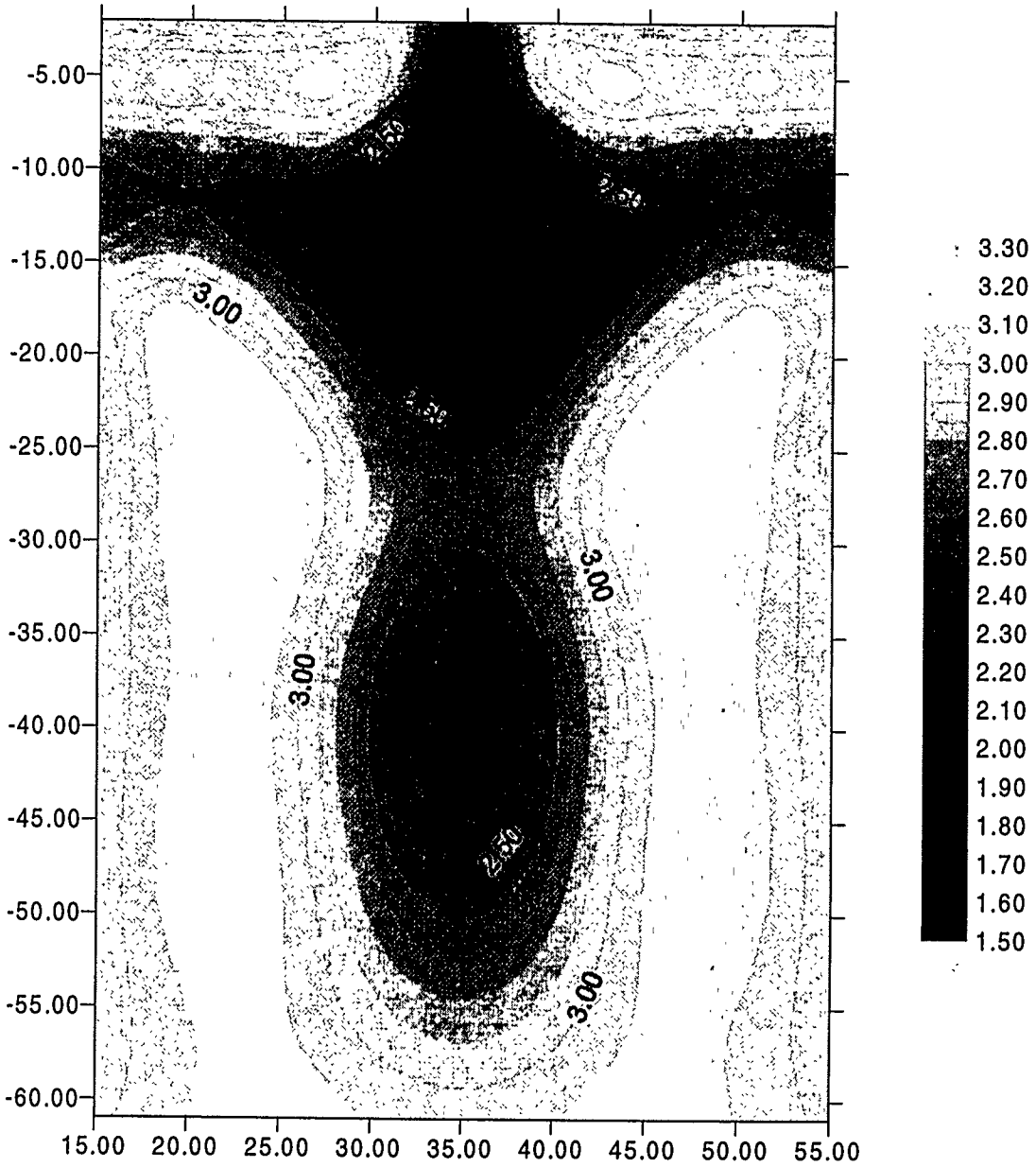

pp2.out
(34 36 1 71)
(5 65 29 30)

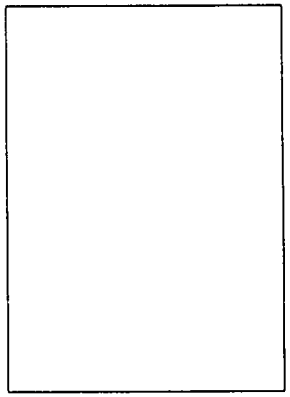

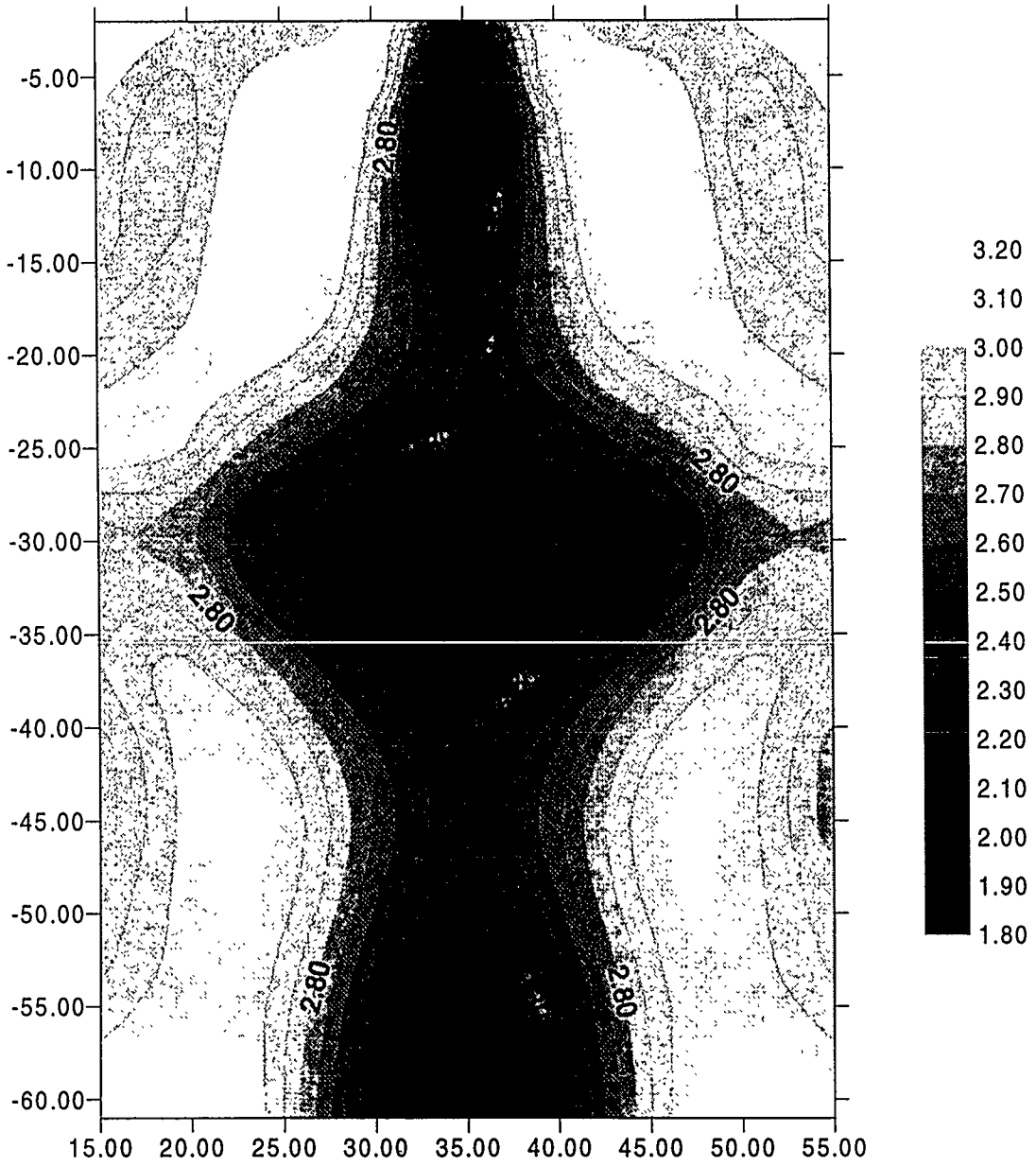

pp3.out
(22 23 1 71)
(5 65 29 30)

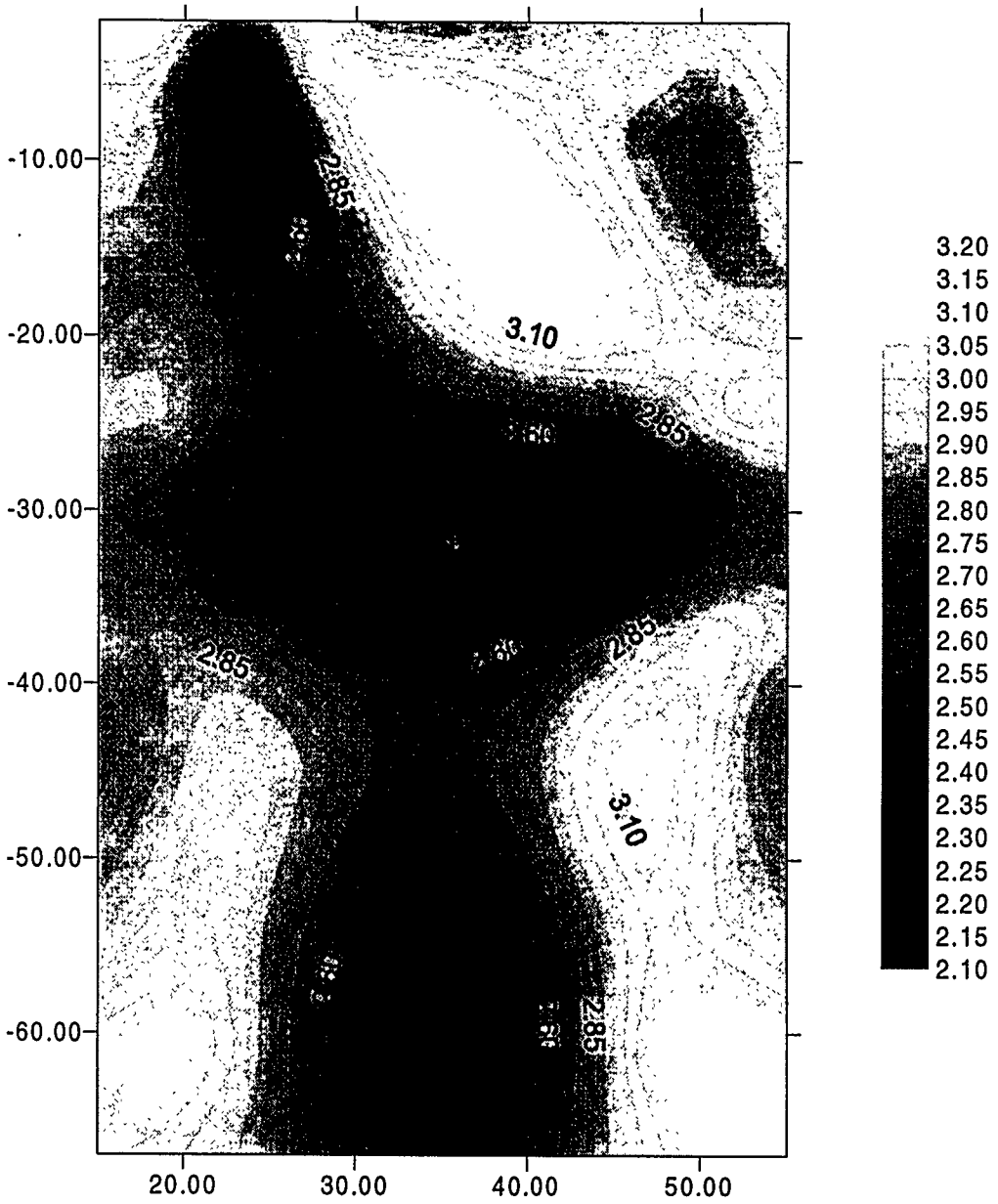

pp4.out
(22 23 1 71)
(47 48 1 71)
(5 65 20 21)

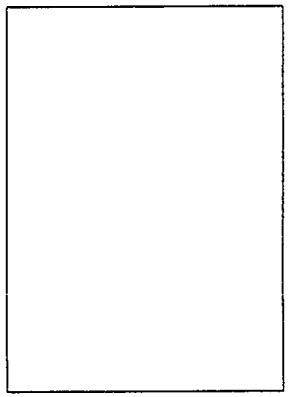

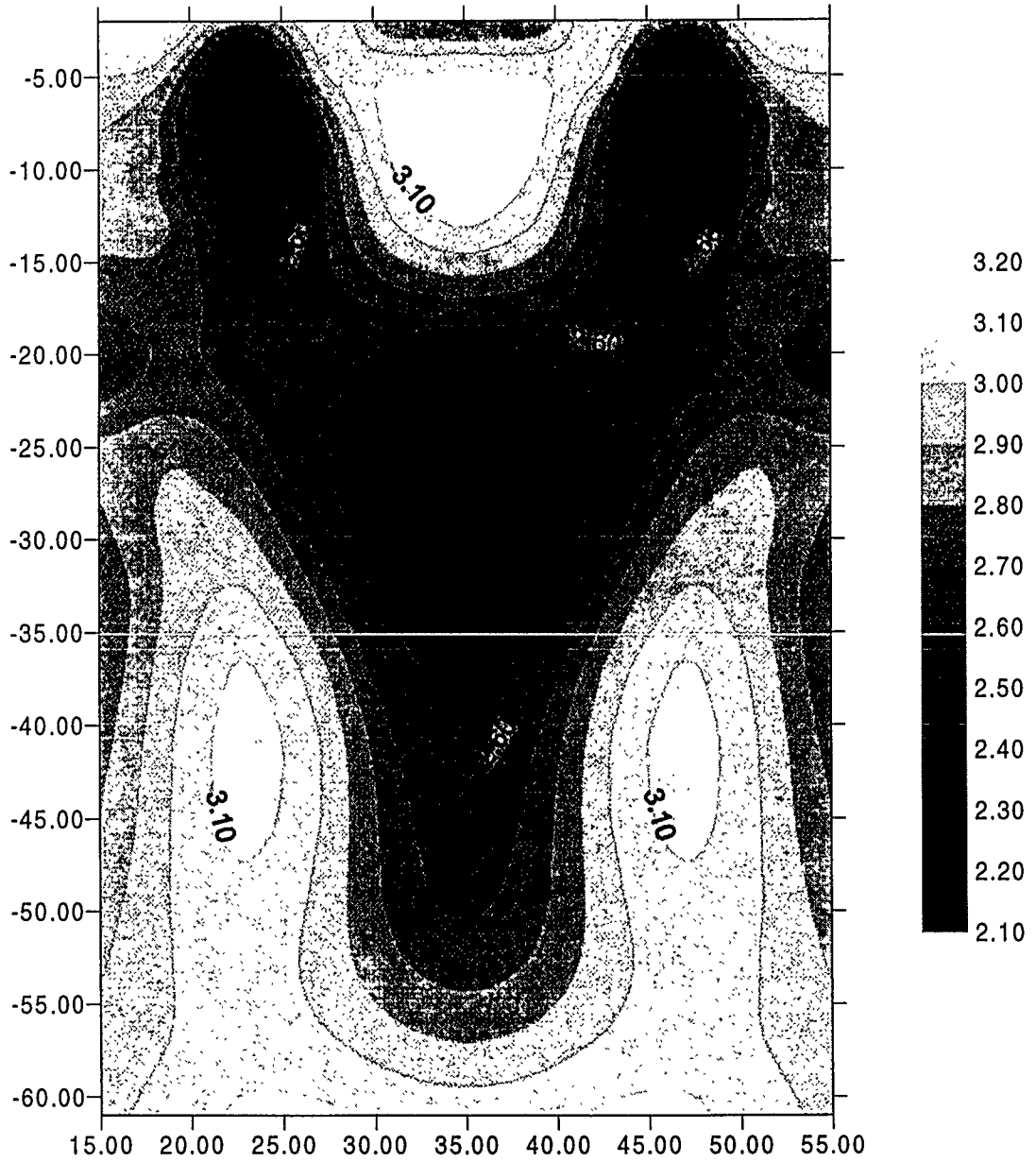

pp5.out
(34 36 1 71)
(5 65 9 10)
(5 65 20 21)

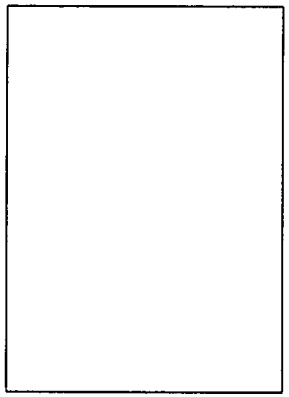

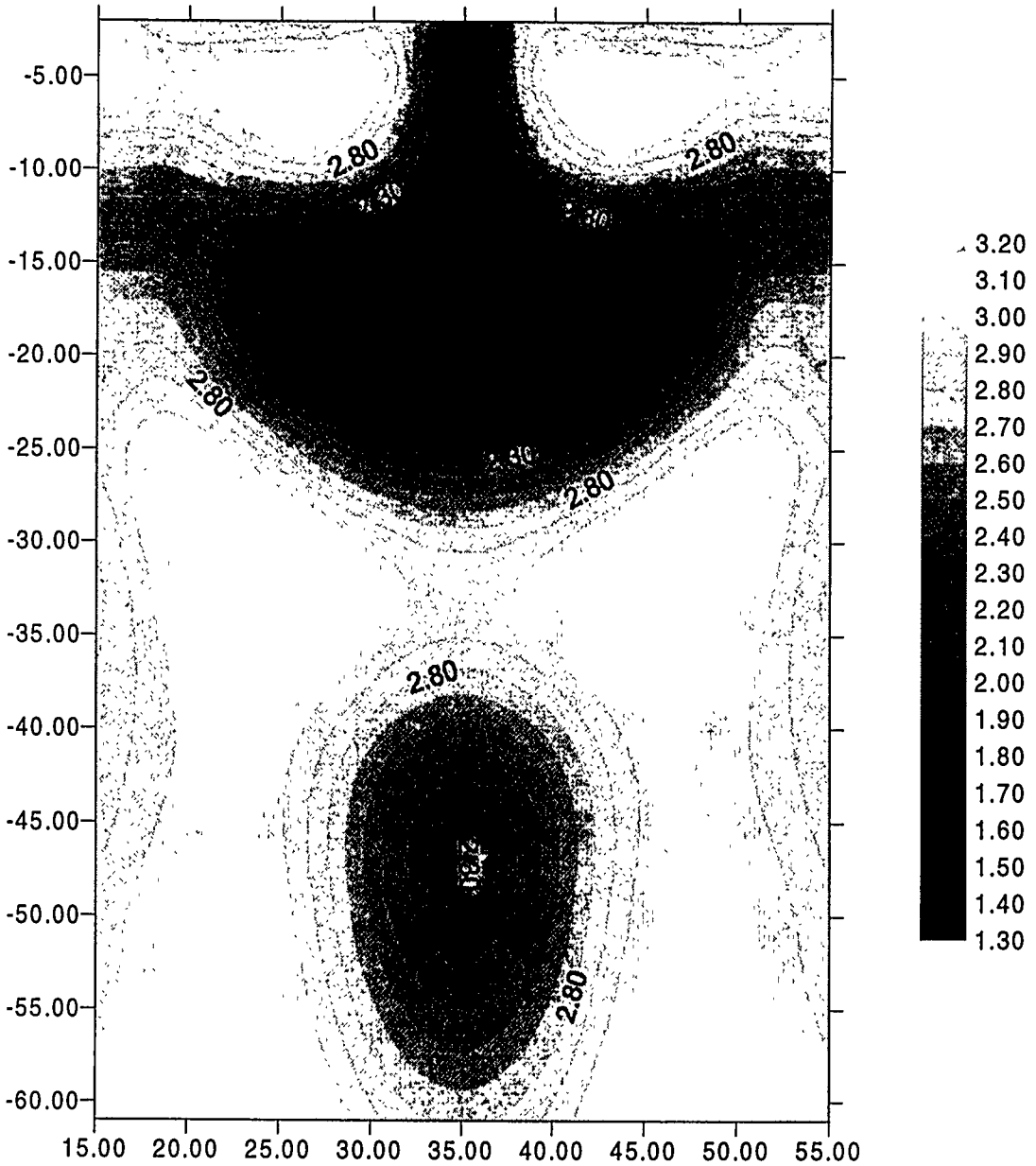

pp6.out
(34 36 1 71)
(5 65 9 10)
(5 65 29 30)

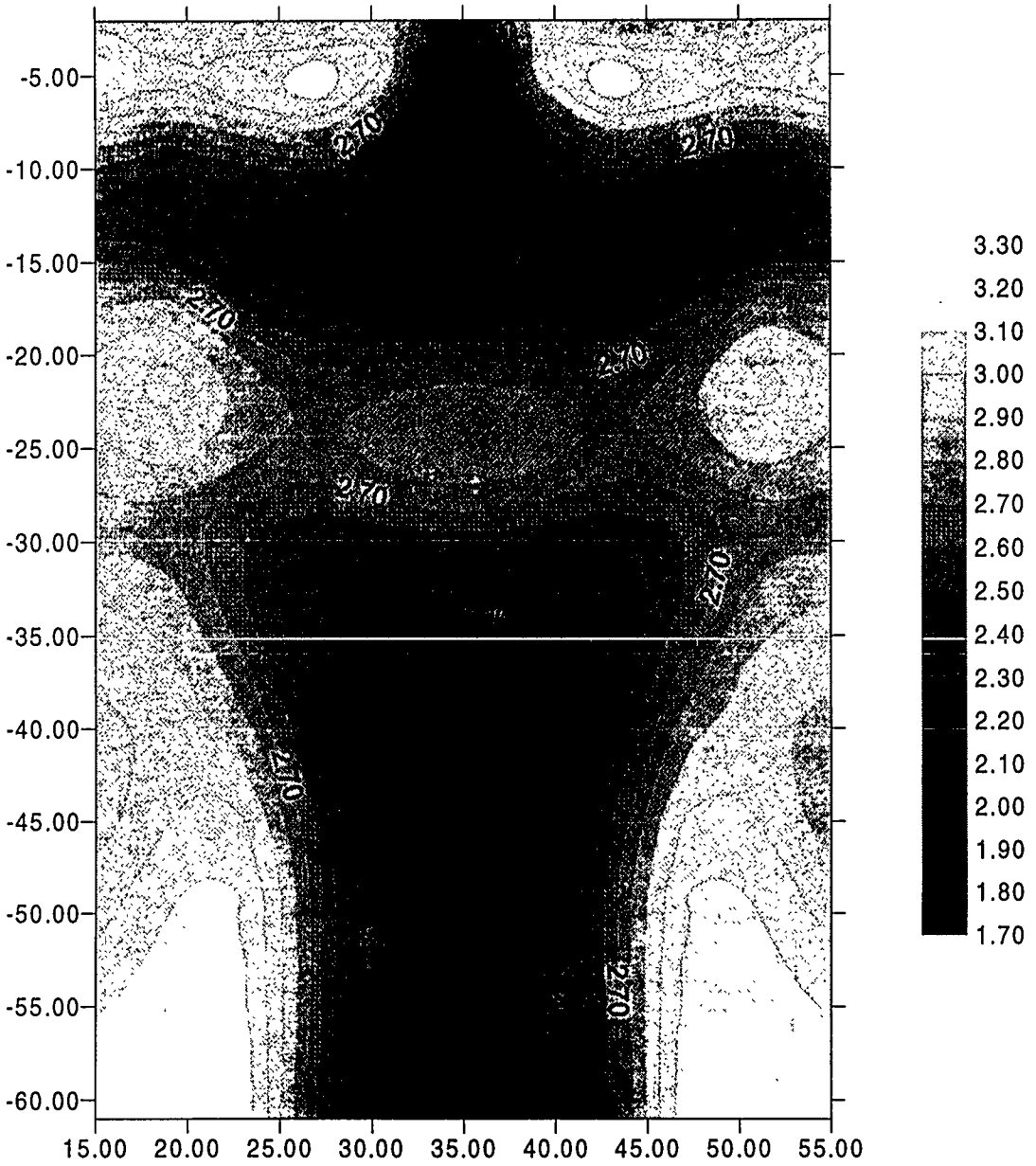

pp7.out
(22 23 1 71)
(5 65 9 10)
(5 65 29 30)

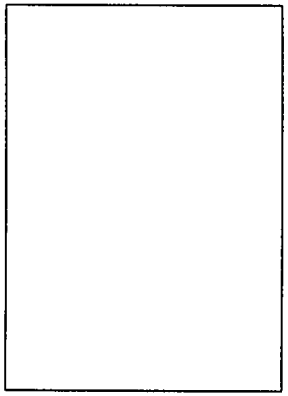

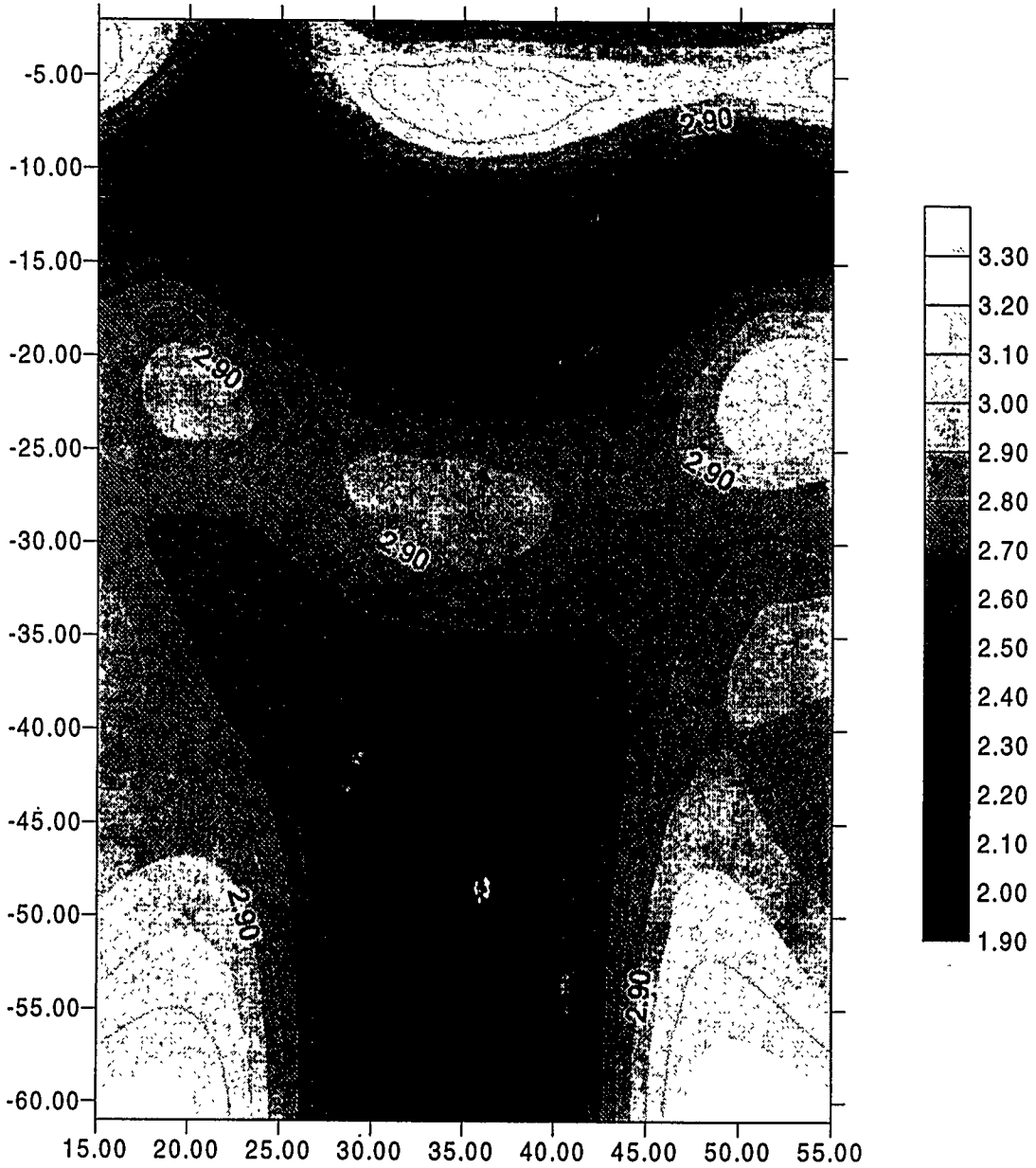

pp8.out
(5 23 9 10)
(47 65 9 10)

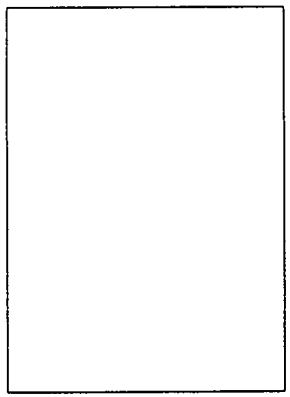

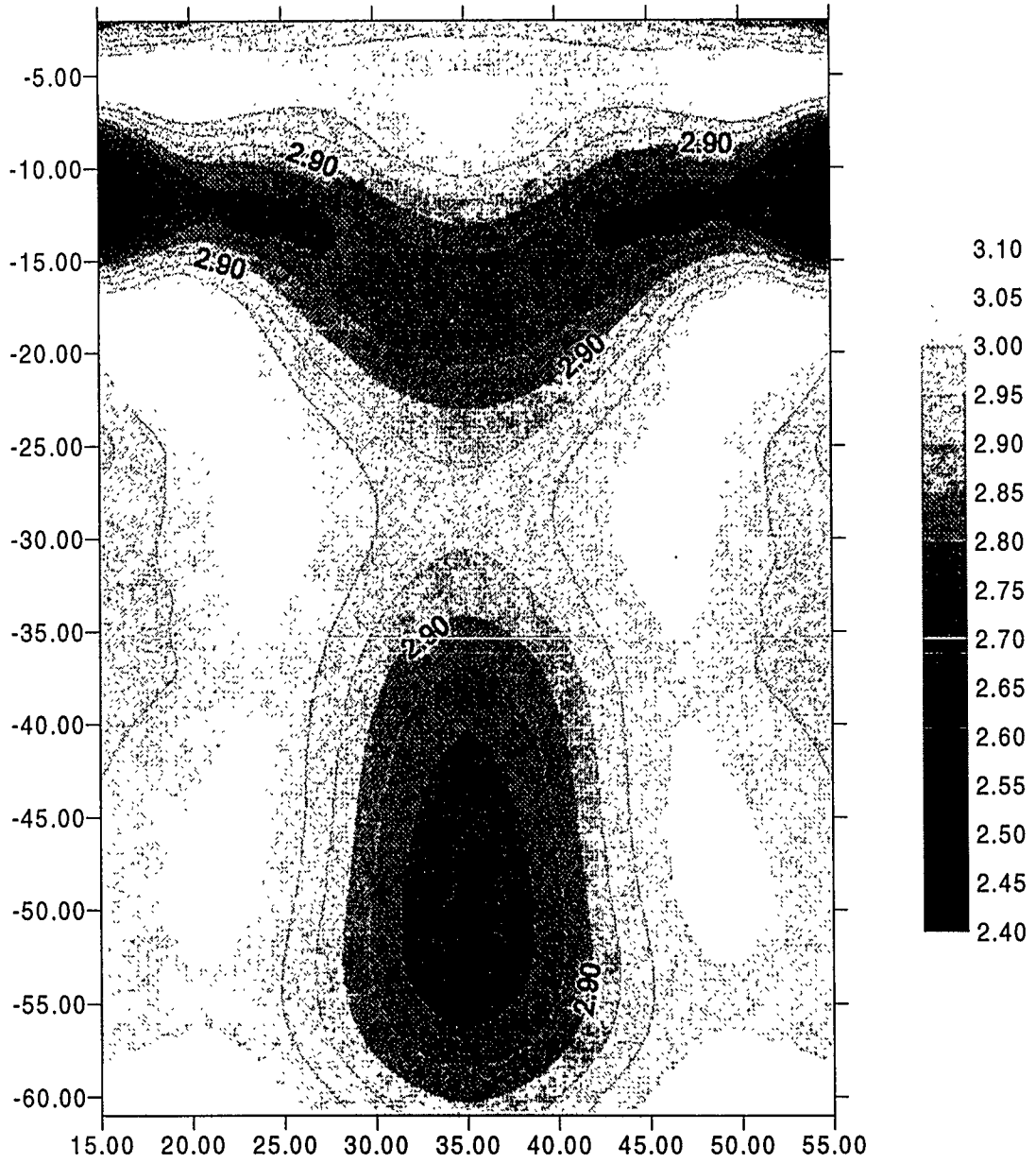

p_2.out
(5 30 9 10)
(40 65 9 10)

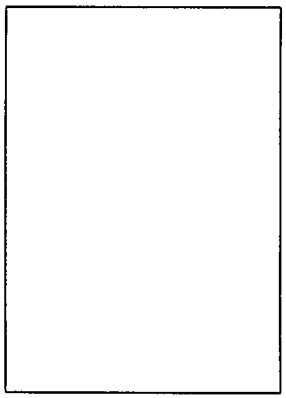

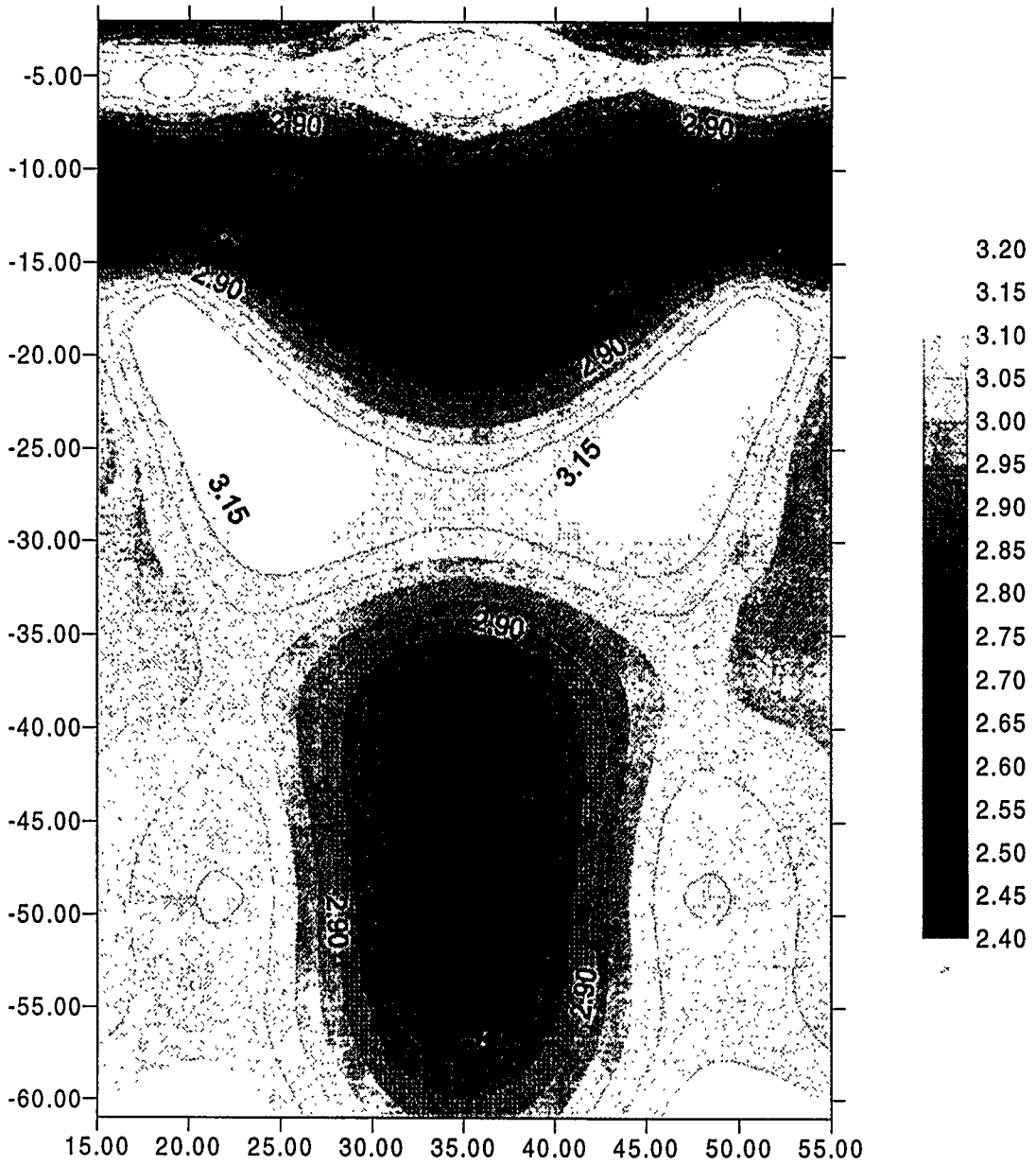

II.10
Theory and numerical evaluation of the parameters of the chaotic behavior of flow

Boris Faybishenko

12/04/97

Introductory Statements

- Random-looking aperiodic behavior may be a product of determinism

- Chaos is mathematically defined as "randomness" generated by simple deterministic systems

- This randomness is a result of the sensitivity to initial conditions

Outline

- Complexity of unsaturated flow in soils and fractured rocks
- What is deterministic chaos?
- Why do we need to know that chaos is involved in time series data?
- Calculations of chaotic parameters

Hierarchy of Tests and Models

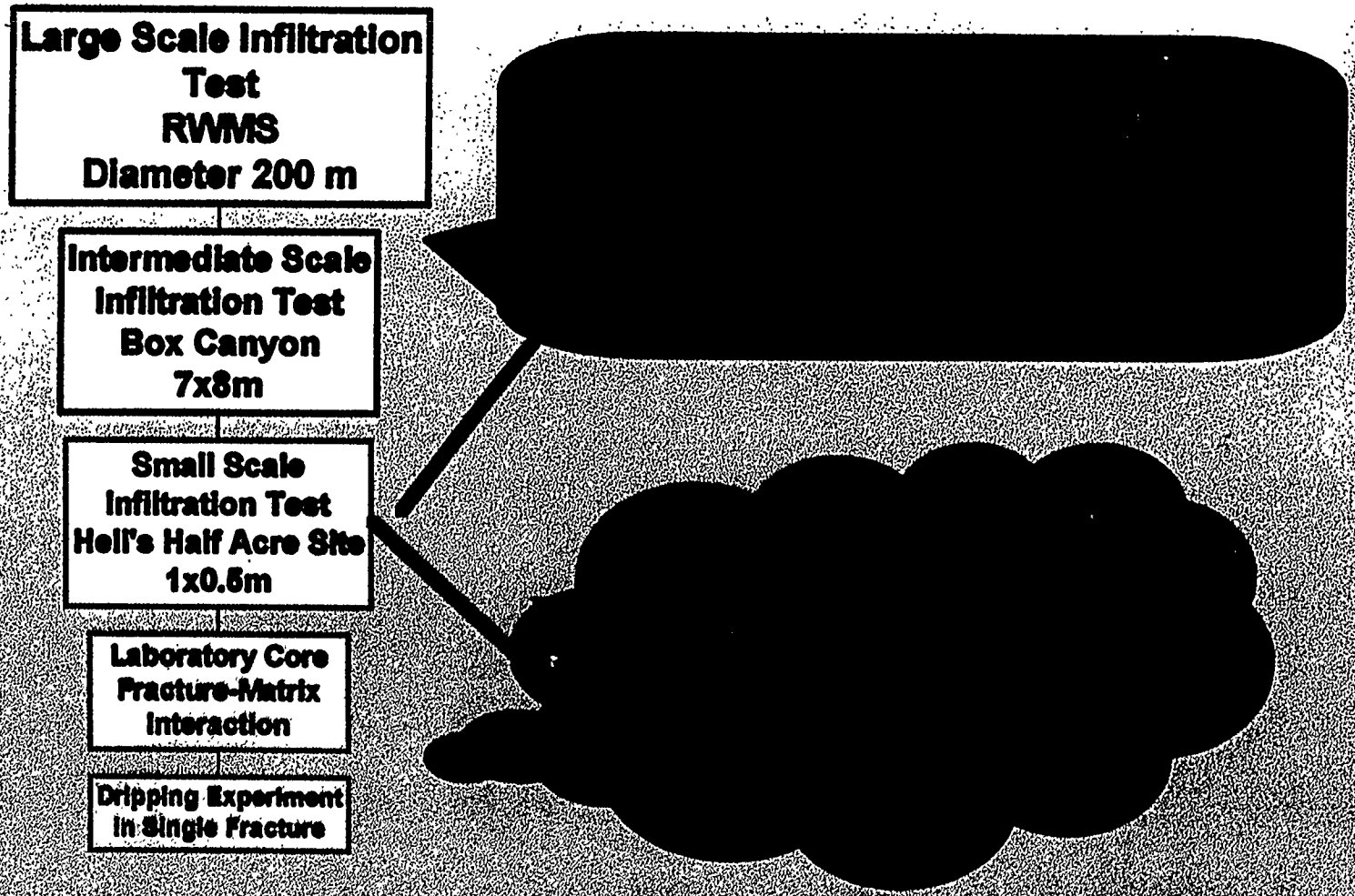

Vadose Zone is an Open Dissipative System

- There is an exchange of energy and flux (water, chemicals, gas) between the VZ and the atmosphere and groundwater

- Processes of energy and mass transfer are irreversible, and the phase-space of the system may contract

Dynamical system

- For a differential equation, the solution is continuous

- For a difference equation, the solution is a map

Chaotic Dynamical System

- The evolution of the system is very sensitive to initial conditions

- The system generates randomness

- The attractor (called chaotic, or strange) is the attracting point set representing the closure of a orbit of the system as the time goes to infinity.

Examples of conservative and dissipative systems

- A conservative system
  - A particle falls with no friction

$$dx/dt = v$$

$$dv/dt = g$$

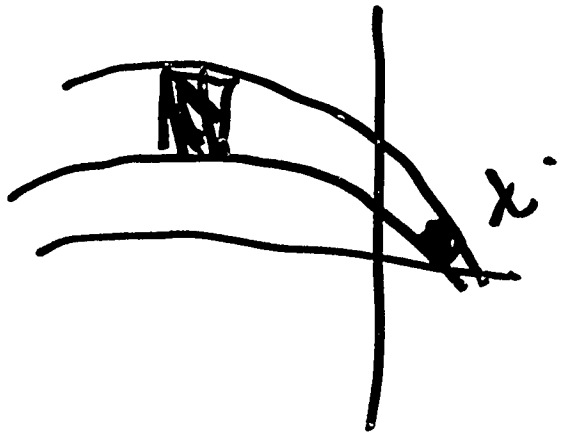

- A dissipative system
  - A particle falls with a friction force, -kv

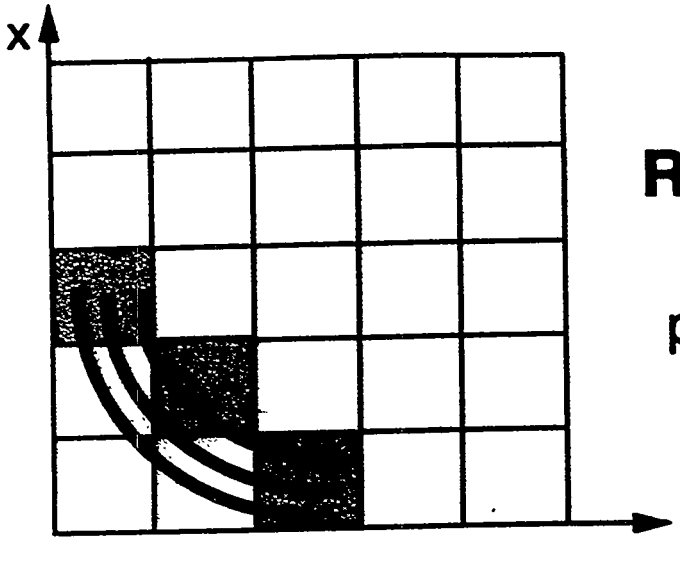

Regular Motion

Initially adjacent points stay adjacent

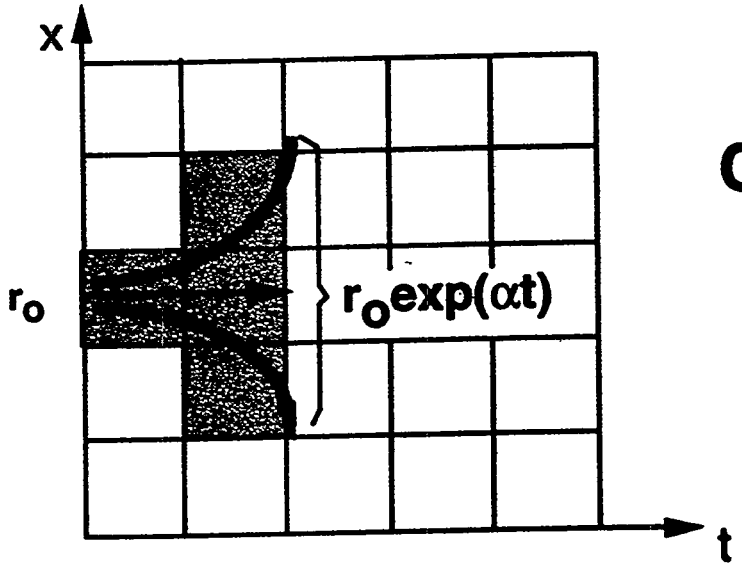

Chaotic Motion

Initially adjacent points become exponentially separated

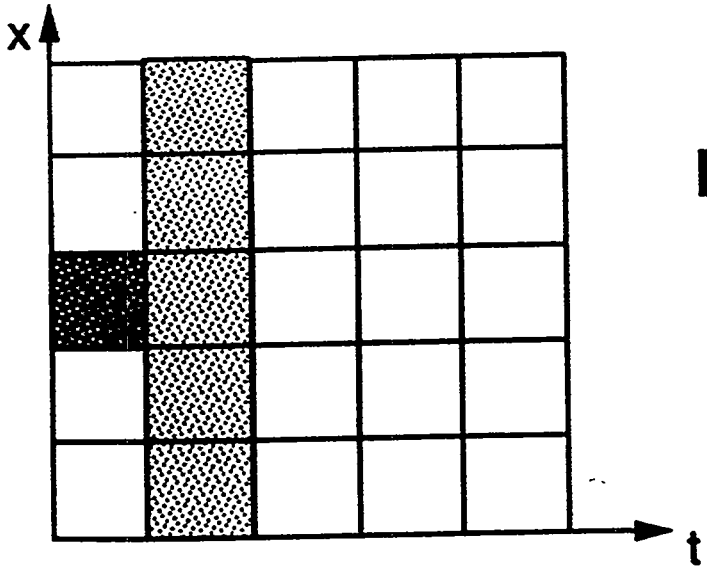

Random Motion

Initially adjacent points are distributed with equal probability

$$T_M \leq \frac{1}{\lambda} \log\left(\frac{1}{r_o}\right)$$

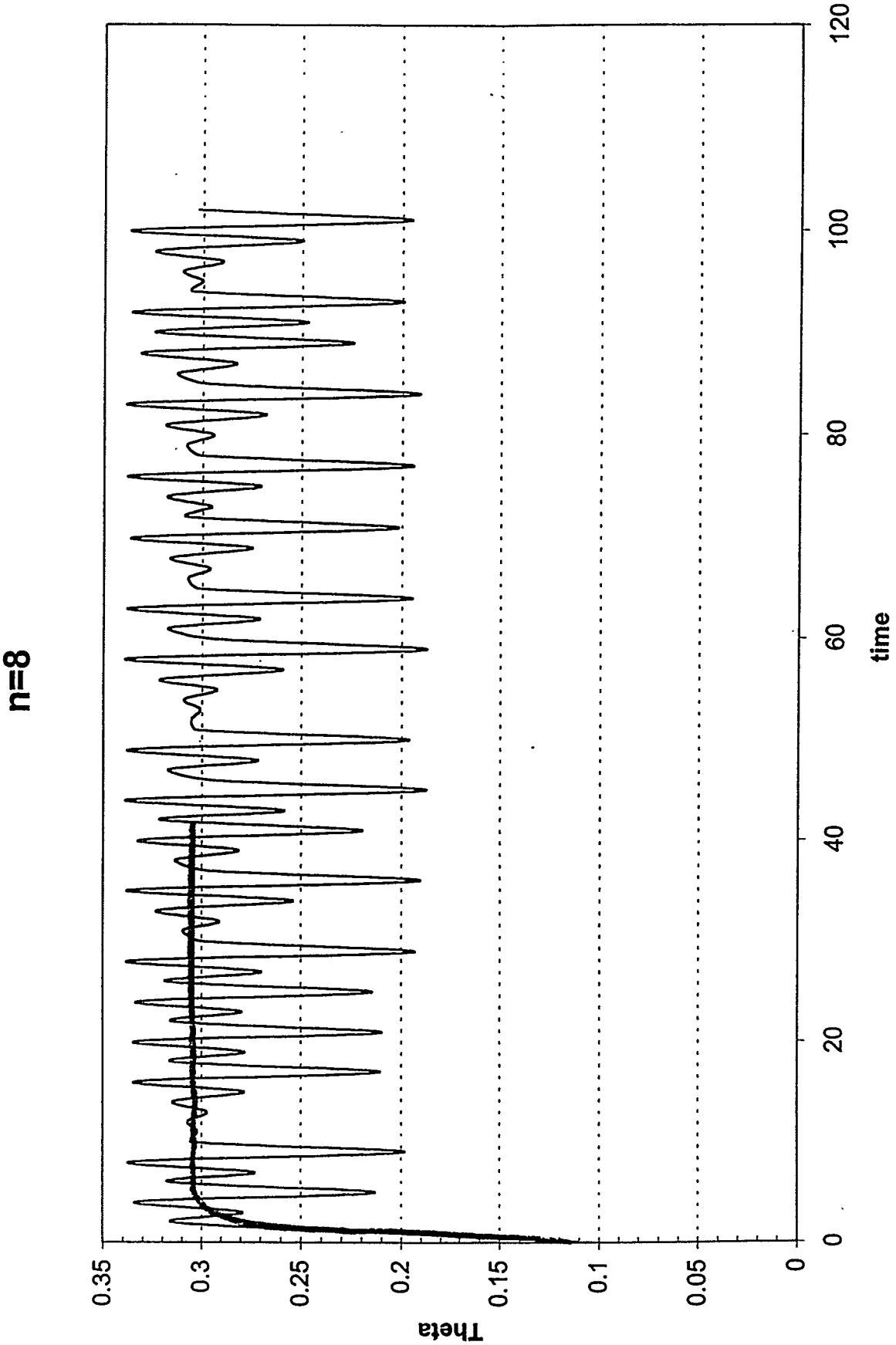
n=8
Theta
time
0.35
0.3
0.25
0.2
0.15
0.1
0.05
0
0
20
40
60
80
100
120

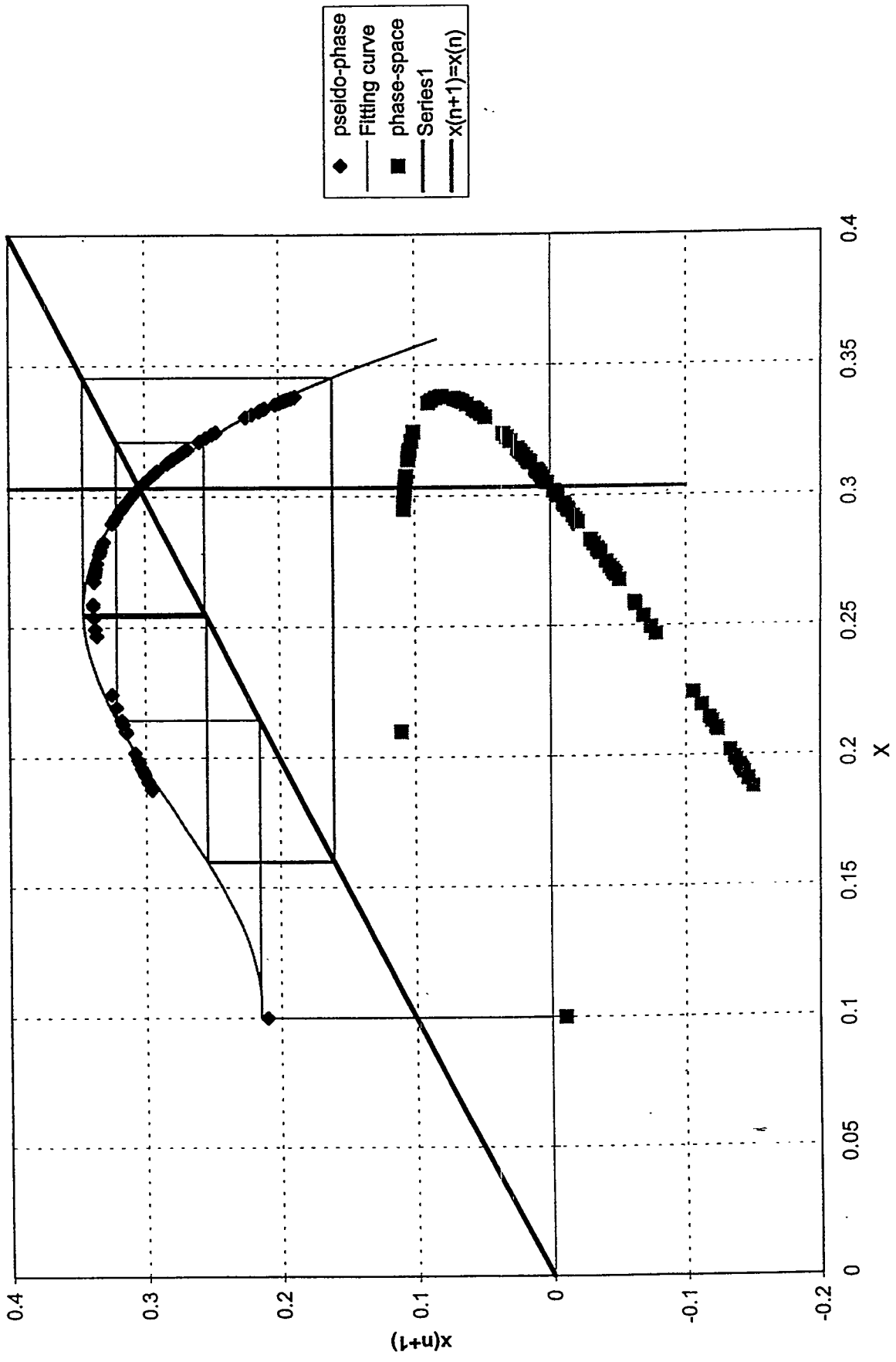
pseido-phase
Fitting curve
phase-space
Series1
x(n+1)=x(n)
0.4
0.3
0.2
0.1
0
-0.1
-0.2
x(n+1)
0
0.05
0.1
0.15
0.2
0.25
0.3
0.35
0.4
X

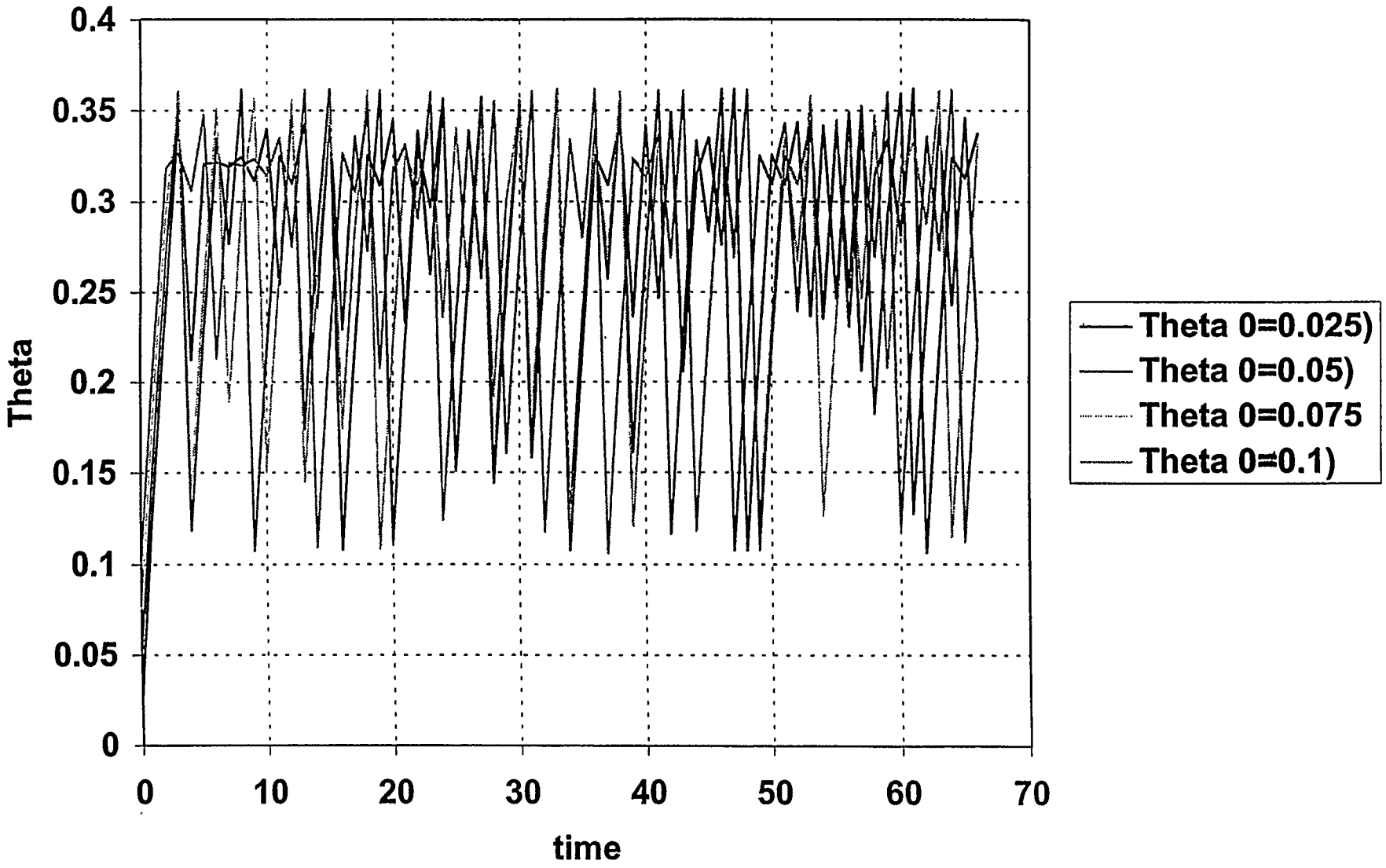
Sensitive dependence to initial conditions of Theta vs. Time
Theta
0.4
0.35
0.3
0.25
0.2
0.15
0.1
0.05
0
0
10
20
30
40
50
60
70
time
Theta 0=0.025)
Theta 0=0.05)
Theta 0=0.075
Theta 0=0.1)

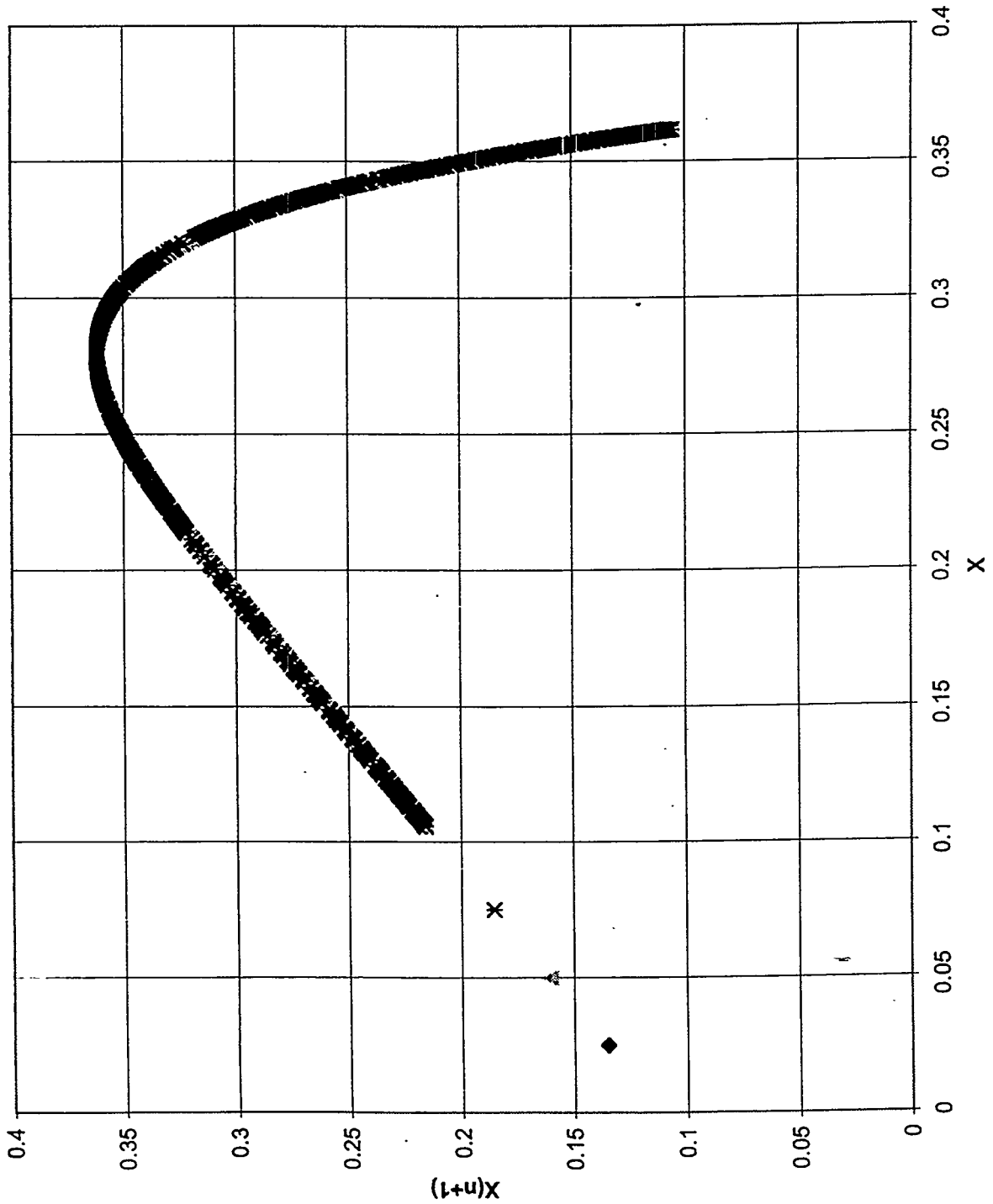
0.4
0.35
0.3
0.25
0.2
0.15
0.1
0.05
0
X(n+1)
0
0.05
0.1
0.15
0.2
0.25
0.3
0.35
0.4
X

Time Series Analysis

- One-dimensional data set, X(t), contains the information about some other physical parameters of the system

- No-prior-model approach to detect key properties of the system

The logistic differential equation

$$\frac{dy}{dt} = ry\left(1-\frac{y}{K}\right) \qquad (1)$$

is analogous to the logistic difference equation

$$y_{n+1} = \rho y_n \left(1-\frac{y_n}{K}\right) \qquad (2)$$

$$\frac{dy}{dt} \approx \frac{y_{n+1}-y_n}{h};$$

$$\rho = 1+hr; \qquad K = (1+hr)K/hr$$

$$u_n = y_n/K$$

$$u_{n+1} = \rho u_n (1-u_n)$$ deterministic case

noisy logistic map

$$u_{n+1} = [\rho + q(n)]\, u_n (1 - u_n)$$

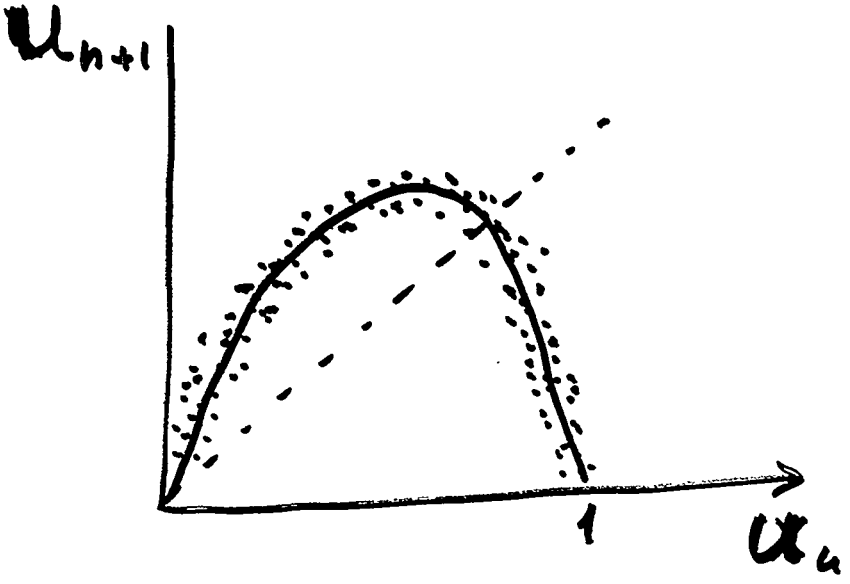

q_n indicates the fluctuations of the ρ parameter

Lyapunov exponent

- The system is evolving from two slightly differing initial states, X, and X+ε:

$$\varepsilon(n) = \varepsilon \exp(\lambda n)$$

λ = average rate of divergance

Lyapunov exponent

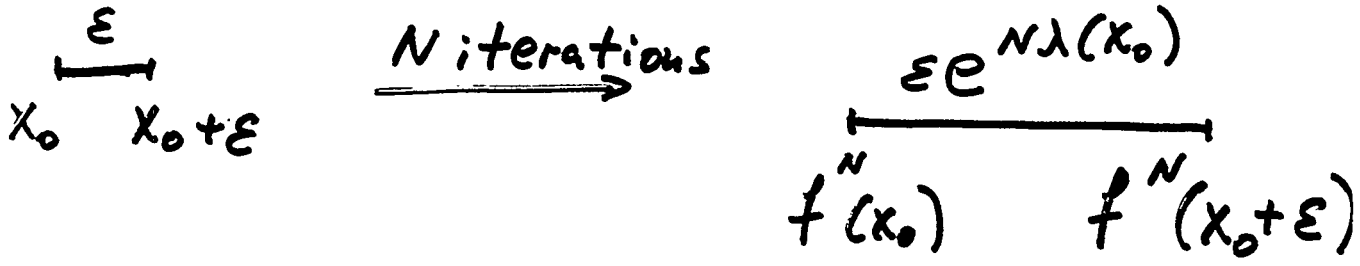

Hurst exponent

$$\Delta X(\lambda \Delta t) = \lambda^H \Delta X(\Delta t)$$

for all $\lambda > 0$ $\quad 0 < H < 1$

$H = \frac{1}{2}$ - Pure Brownian motion

$H = 0$ Position is independent of time because $S \sim t^H$

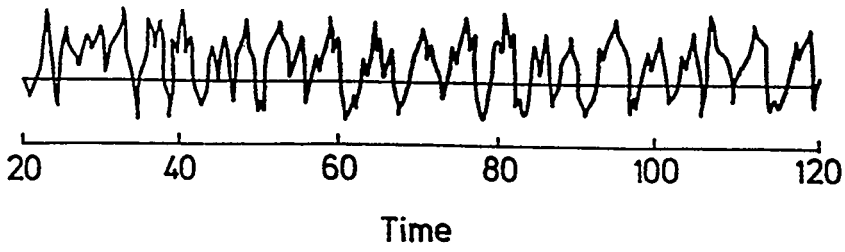

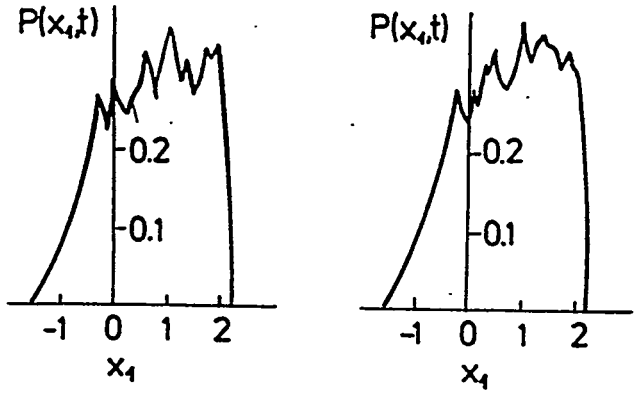

Figure 5.7 : (a) t=80.0 , (b) t=120.0

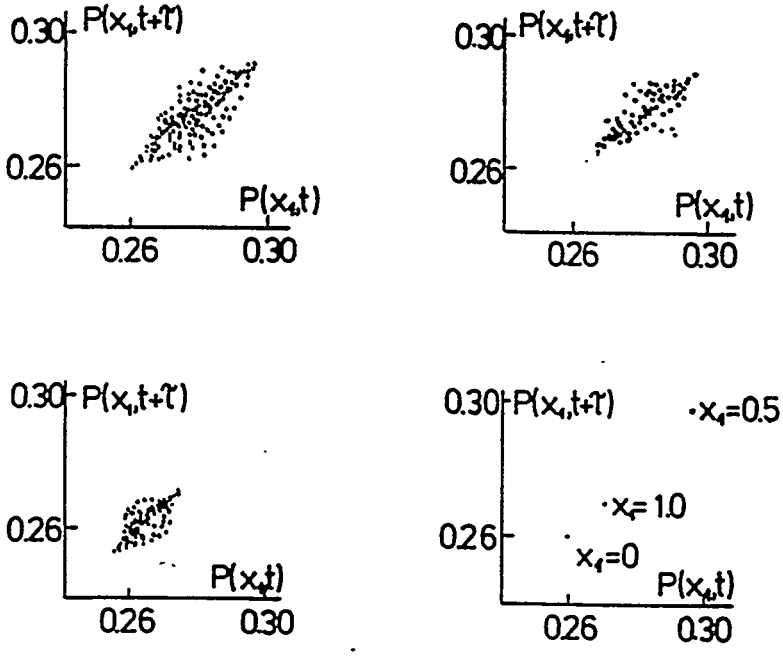

Figure 5.8 : (a) x_1=1.0 , (b) x_1=0.5 , (c) x_1=0 , (a)-(c) chaotic behaviour, (d) regular behaviour, τ=5.

Capacity Dimension

- Called Hausdorff dimension or Fractal dimension

- Box counting method

$$d_c = \lim_{e \to 0} \log N(\varepsilon)/\log(1/\varepsilon)$$

Entropy

- Comparing the results to a statistical system
- A measure of the disorder in the system

$$S = - \Sigma p_i \log_2 p_i$$

- With increasing the degree of chaos, S increases, until it reaches the maximum value for a random system

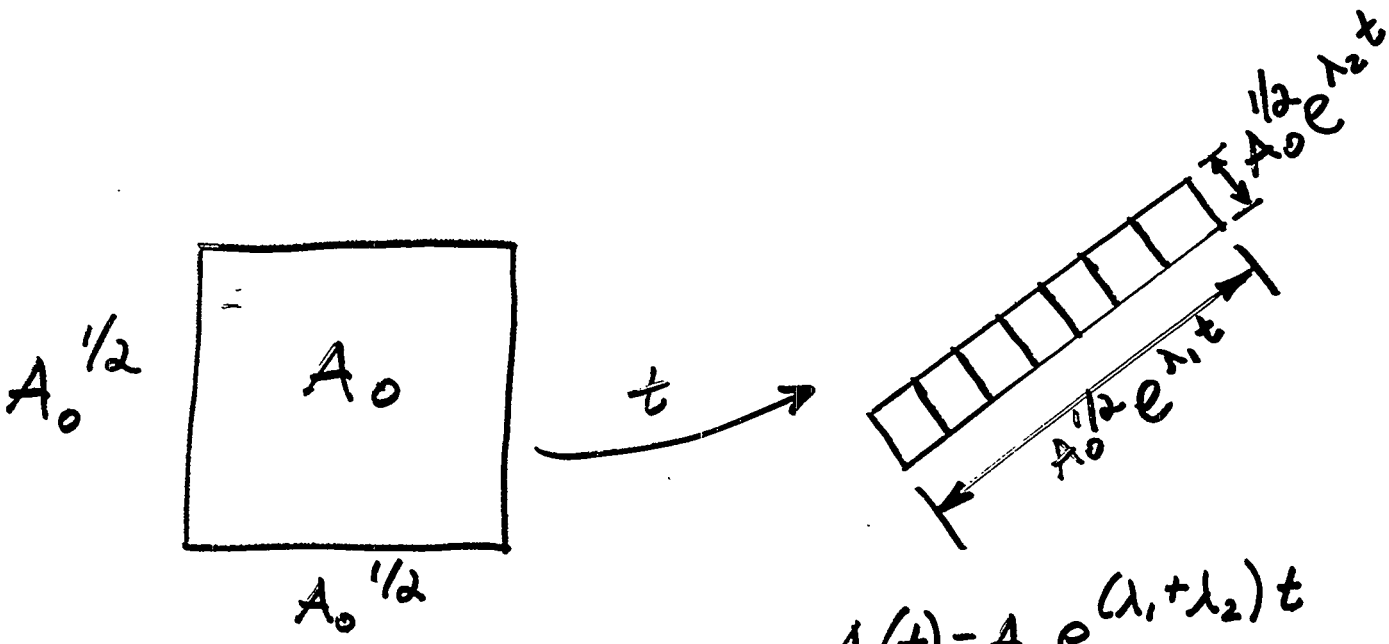

$$A(t) = A_0 e^{(\lambda_1 + \lambda_2) t}$$

λ = Lyapunov exponent

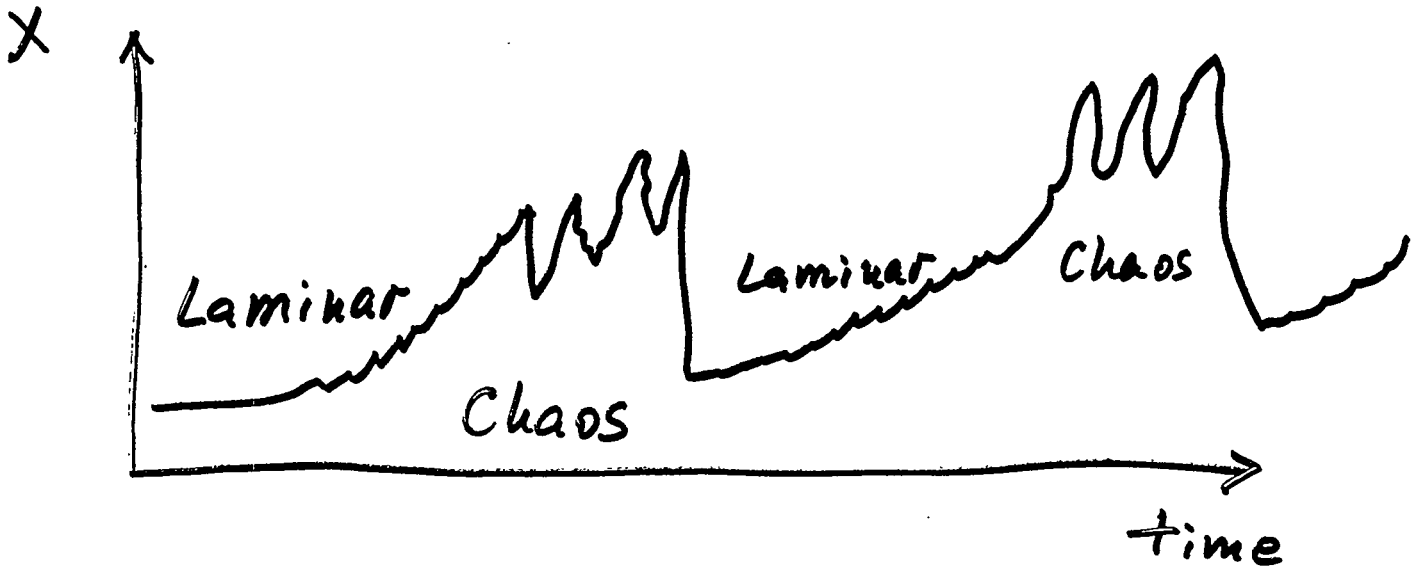
X
Laminar
Chaos
Laminar
Chaos
time

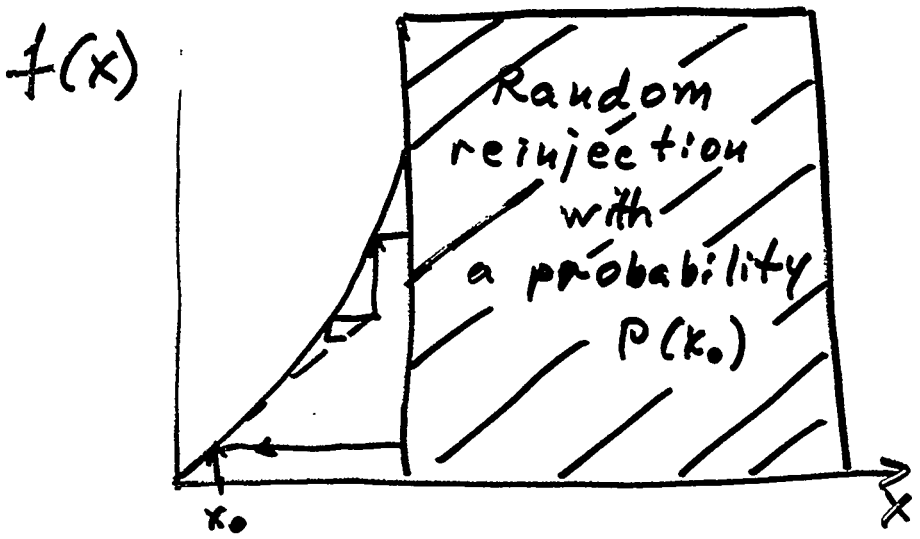
f(x)
Random
reinjection
with
a probability
P(k₀)
x₀
x

	Chaos	Random	Noise	0.25 ml/hr	0.5 ml/hr	1 ml/hr	2 ml/hr		SC3-t7	
No data points	2000	2000		13220	13378	13394	15674		5001	
Minimum value	-17.72337	7.77E-04		2.59	3.64	5.39	8.37		6.65E-05	
Average value	-0.2358849	0.5030416		3.769	4.903713	6.356282	10.58747		7.62E-05	
Maximum value	17.98758	0.9993806		5.84	7.11	7.61	12.3		9.99E-05	
Range of data	35.71095	0.9986031		3.25	3.47	2.22	3.93		3.34E-05	
Resolution	1.26E-02	2.73E-04		1.00E-02	1.00E-02	1.00E-02	1.00E-02		1.00E-07	
Lower quartile	-5.713983	0.2617328		3.24	4.4	6.05	10.2		7.08E-05	
Median value	-0.3580765	0.5082129		3.71	4.87	6.33	10.6		7.23E-05	
Upper quartile	5.163997	0.7541968		4.13	5.35	6.67	11		8.11E-05	
Mode (max probalility)	-0.625	0.796875		3.90625	4.21875	6.09375	10.3125		7.03E-05	
Aver deviation	6.450353	0.2501415		0.5420973	0.4945862	0.3149368	0.5080337		6.78E-06	
Standard deviation	7.916132	0.2886727		0.6915743	0.5860473	0.36666431	0.6420568		8.06E-06	
Variance	62.66514	8.33E-02		0.4782749	0.3434514	0.1344272	0.4122369		6.50E-11	
Skewness	4.91E-02	-3.08E-02		0.7280276	0.2634546	0.1397251	-0.2310608		0.990818	
Kurtosis	-0.6851208	-1.189187		0.1732618	-0.9731036	-0.936166	8.62E-03		-0.333621	
Pearson's correlation	0.9634255	1.73E-02		0.9965331	0.993629	0.9885468	0.98848		0.259216	
									7.08E-05	
Fixed point (estimated)	-0.5625651	0.983019		3.72	4.59	6.72	10.7			
Relative LZ complexity	0.1809354	1.041749	1.04723	0.1253058	0.1465229	0.1903785	0.1929393		0.375938	
Dominant frequency (FFT)	0.015625	0.09375	0.2969	3.91E-03	0.0078125	1.17E-03	0		0.15625	
Dominant frequency (MEM)	0.003	0.0795		0.003	0.0015	0.0055	0			
Dominant period (FFT)	64	10.66667		256	128	85.3333			6.4	
Dominant period (MEM)	333.333	12.557862		333.333	666.6667	181.8182				
Hurst exponent	0.4382105	2.62E-03	-2.93E-03	0.6253539	0.4067501	0.5242398	0.4431641		1.16E-02	
Largest Lyapunov exponent	0.075+-.034	0.895+-0.031	0.78	0.118+-.096	0.242+-0.03	0.392+-0.019	0.322+-0.101		0.560±0.046	
Lyapunov exponent (base e)	0.052+-0.24	0.620+-0.02		.082+-.067	0.168+-0.021	0.272+-0.013	0.223+-0.07		0.388±0.032	
Capacity dimension (appr)	1.807+-0.283		3.145+-0.492	1.437+-0.088	1.453+-0.088	1.391+-0.084	0.944+-0.053		2.926+-.29	
Correlation dimension (appr)	2.002+-0.103		4.555+-0.031	3.699+-.458	3.641+-.765				4.958±0.449	
Entropy (approx)	0.35	0.413	0.527	0.259	0.231				0.548	
BDS statistic	0.334	-16.83684	-11.789	2.031	3.13				6.63E-02	
Correlation time	6.101169	0.6435637	0.622	23.05126	16.54703		12.83941		0.853542	

Deterministic, stochastic, chaotic, and noisy components of data

Outcrop test SC3-T7

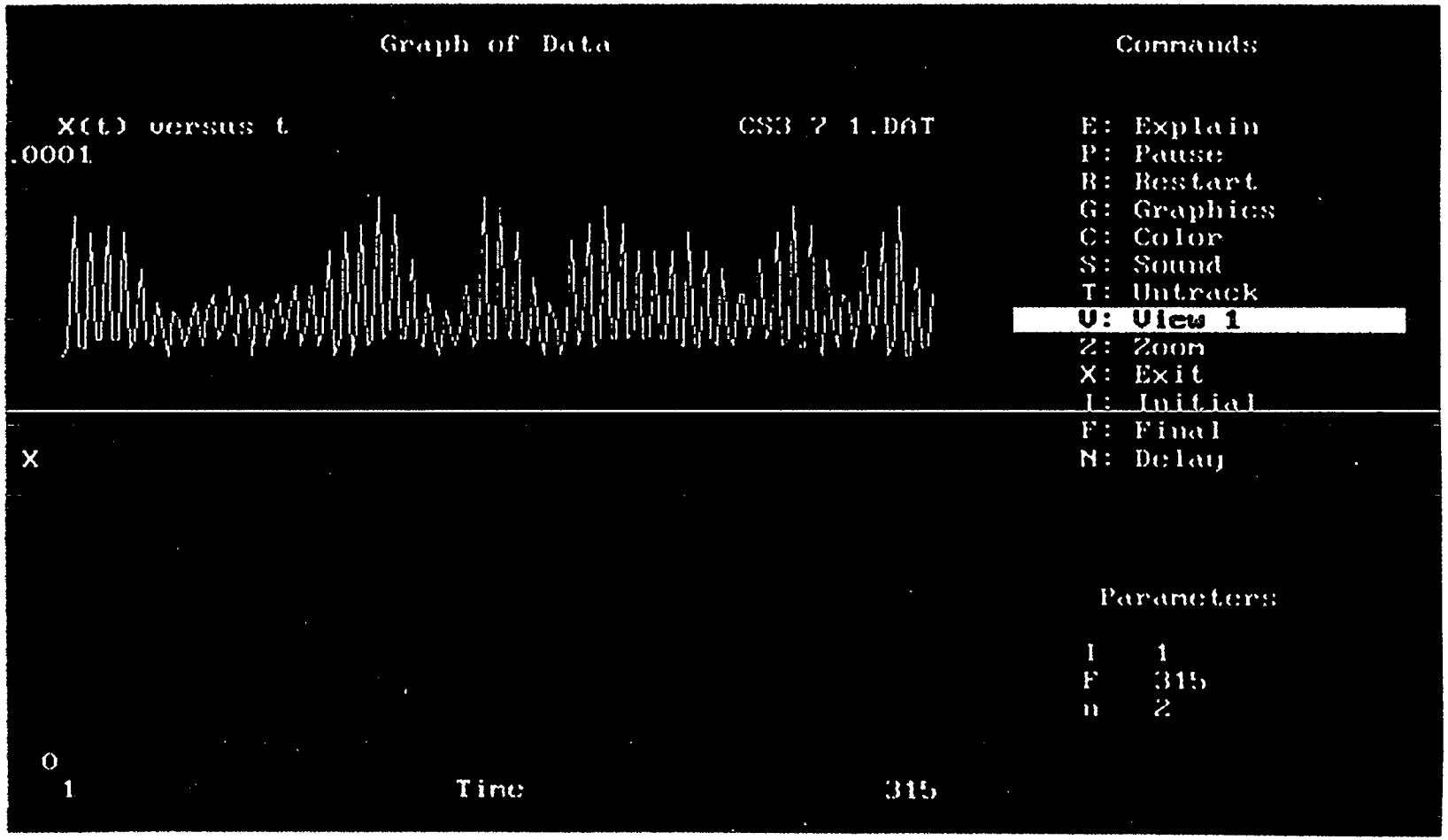

Phase-Space Portrait, SC3-t7

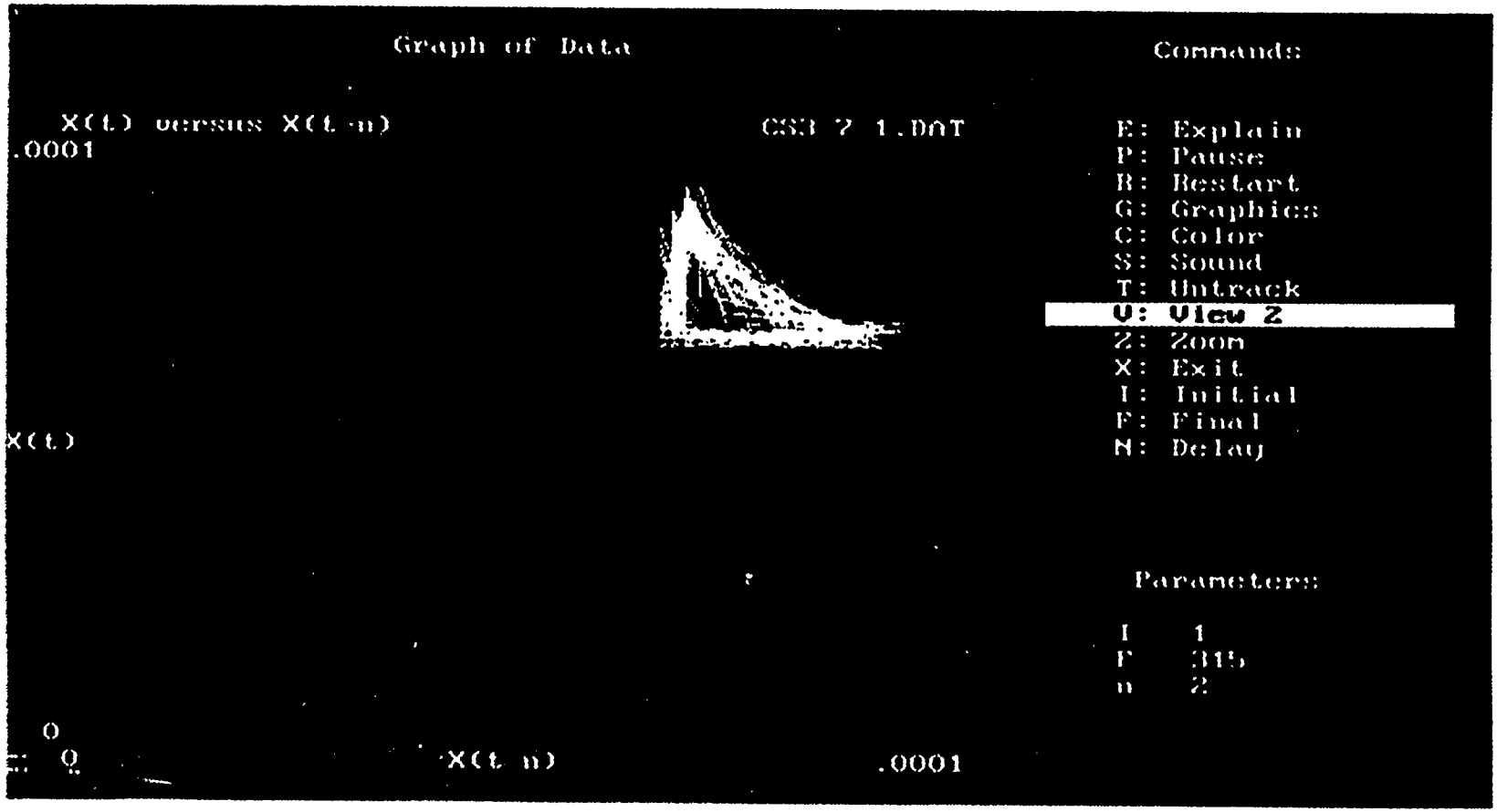

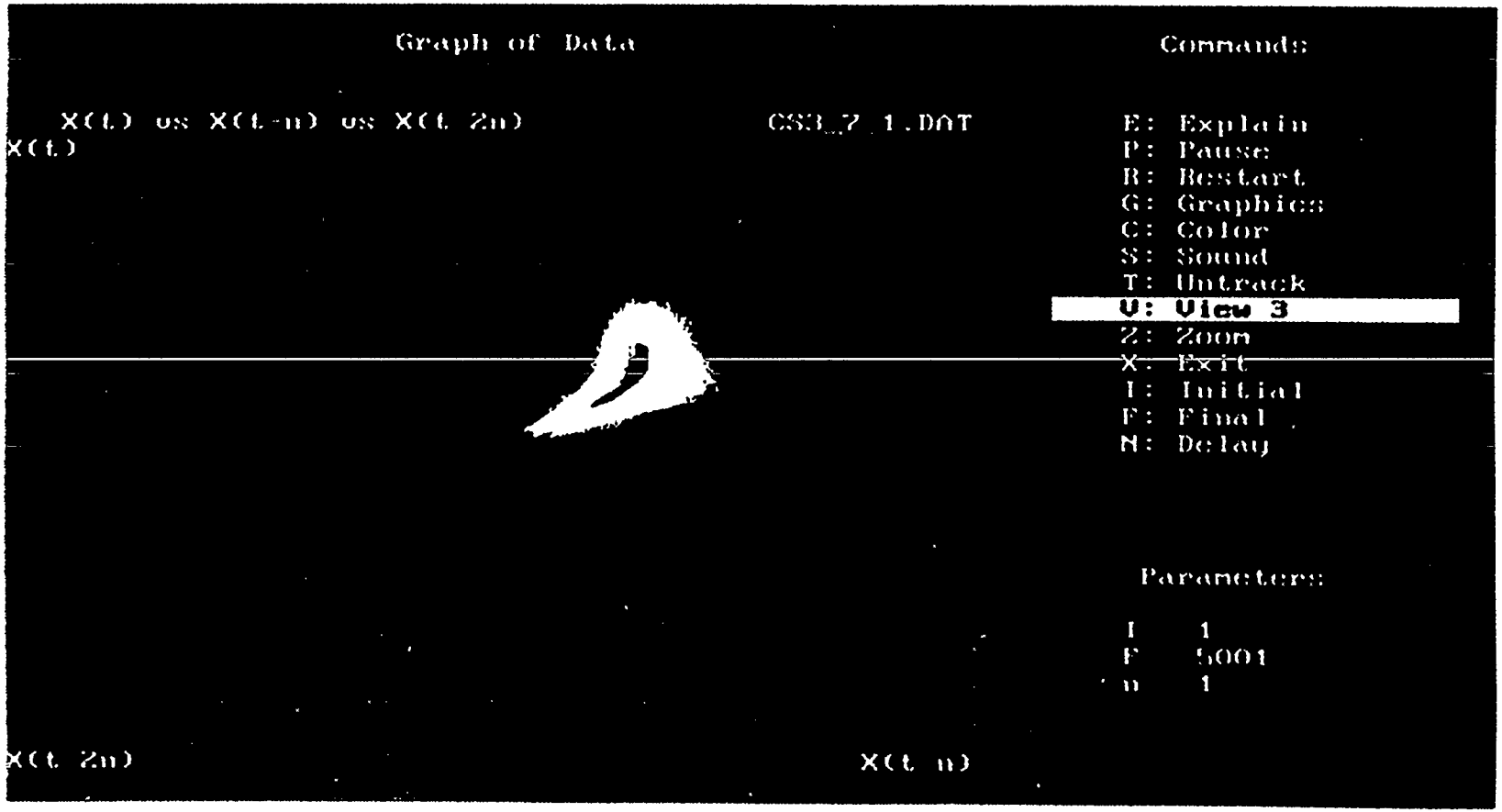
Graph of Data
X(t) vs X(t-n) vs X(t, 2n)
CSC3_7_1.DAT
X(t)
Commands:
E: Explain
P: Pause
R: Restart
G: Graphics
C: Color
S: Sound
T: Untrack
V: View 3
Z: Zoom
X: Exit
I: Initial
F: Final
N: Delay
Parameters:
I 1
F 5001
n 1
X(t, 2n)
X(t, n)

Stereo Plot, SC3-t7

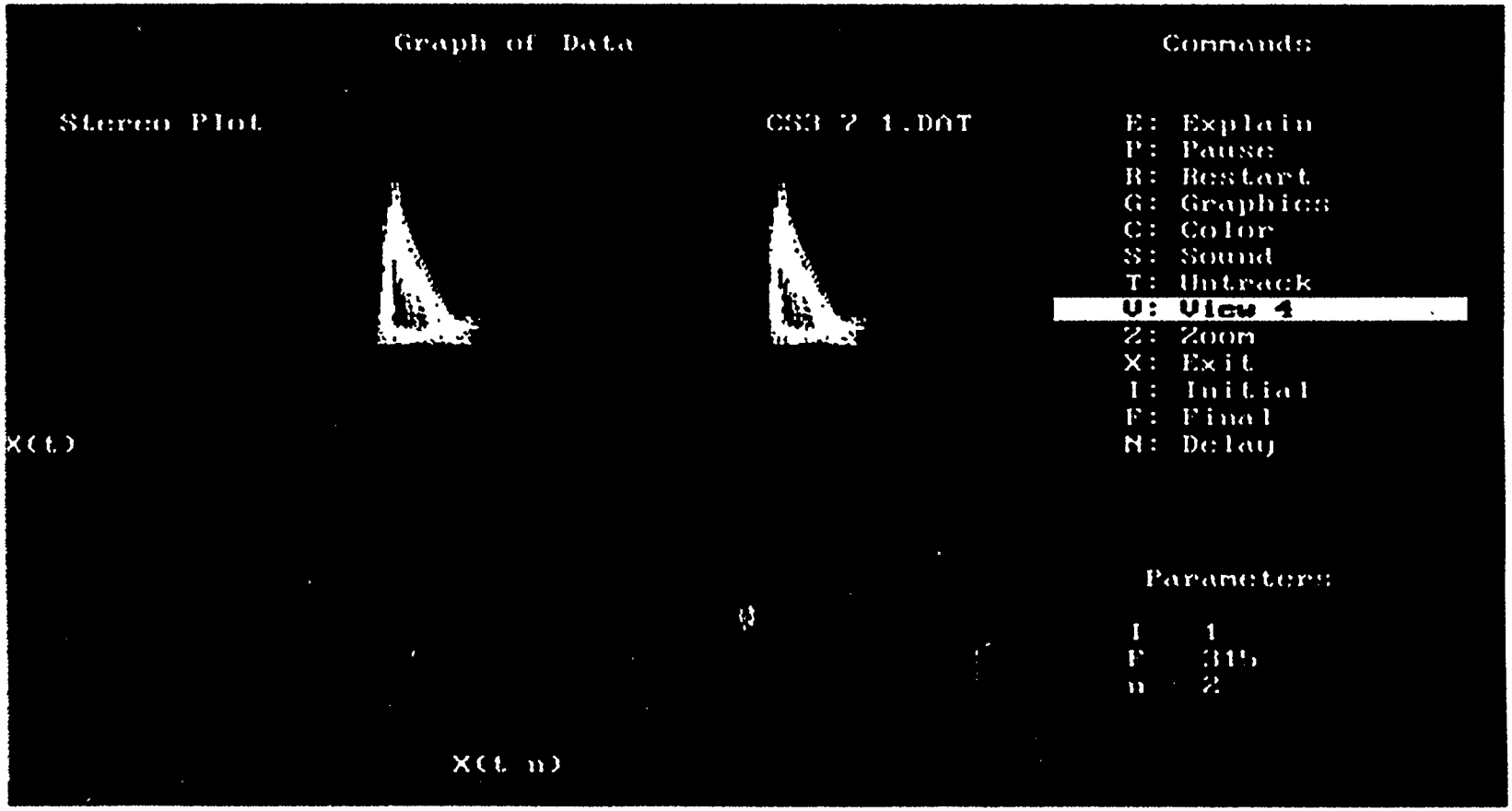

Determining embedding dimension

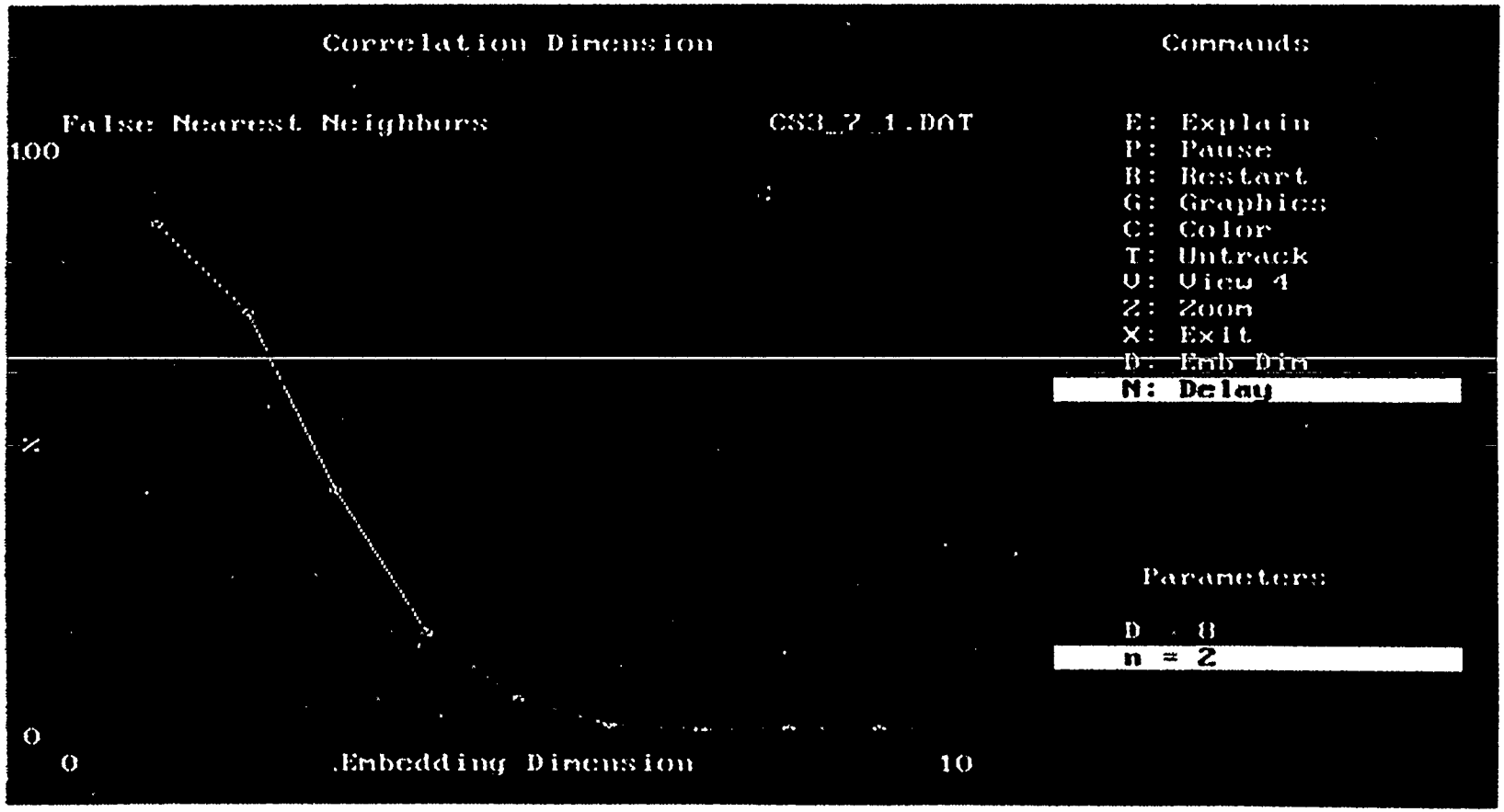

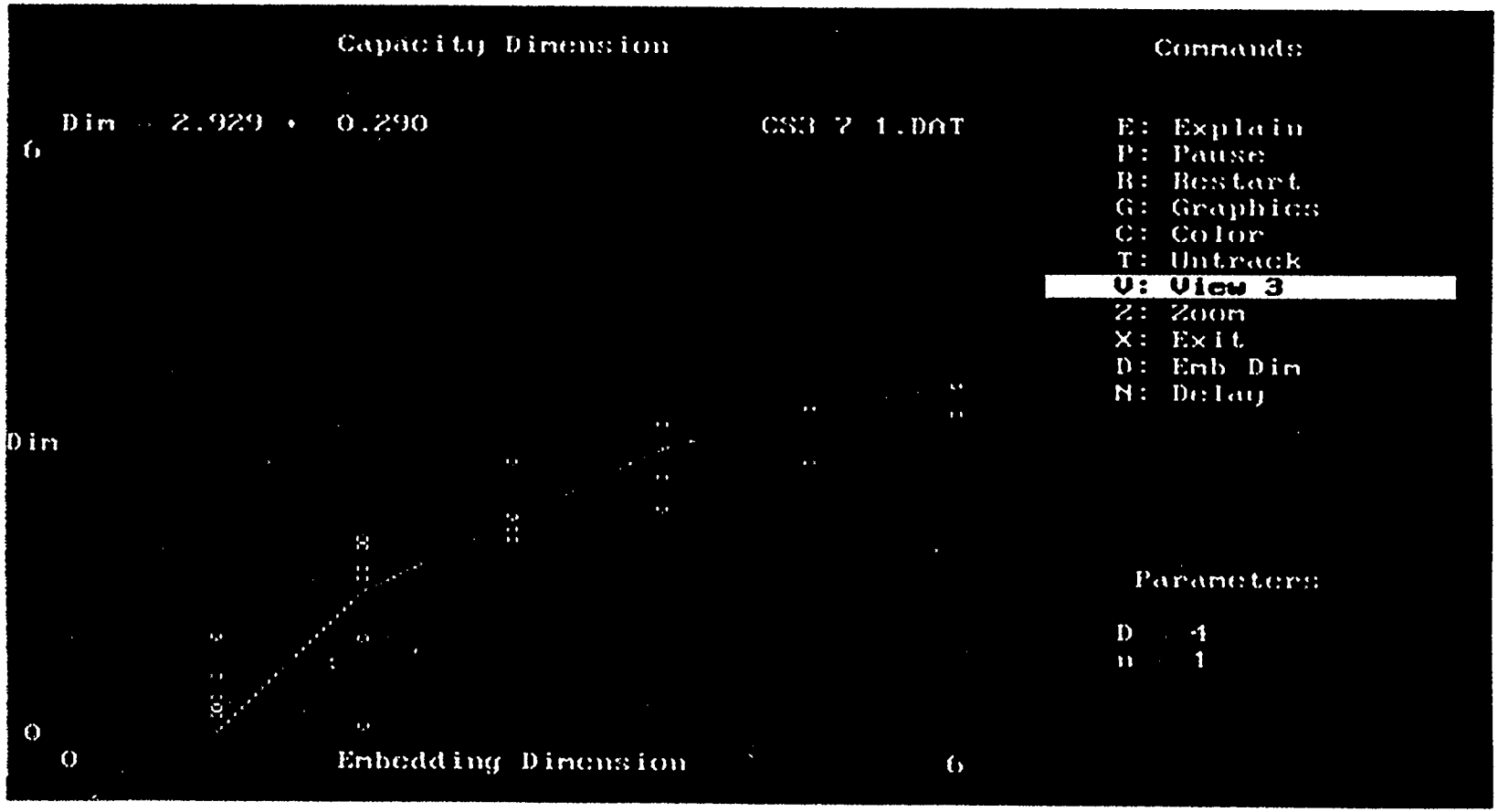
Capacity Dimension
Dim = 2.929 ± 0.290
CSS 7 1.DAT
Commands
E: Explain
P: Pause
R: Restart
G: Graphics
C: Color
T: Untrack
V: View 3
Z: Zoom
X: Exit
D: Emb Dim
N: Delay
Dim
6
0
0
Embedding Dimension
6
Parameters:
D = 4
n = 1

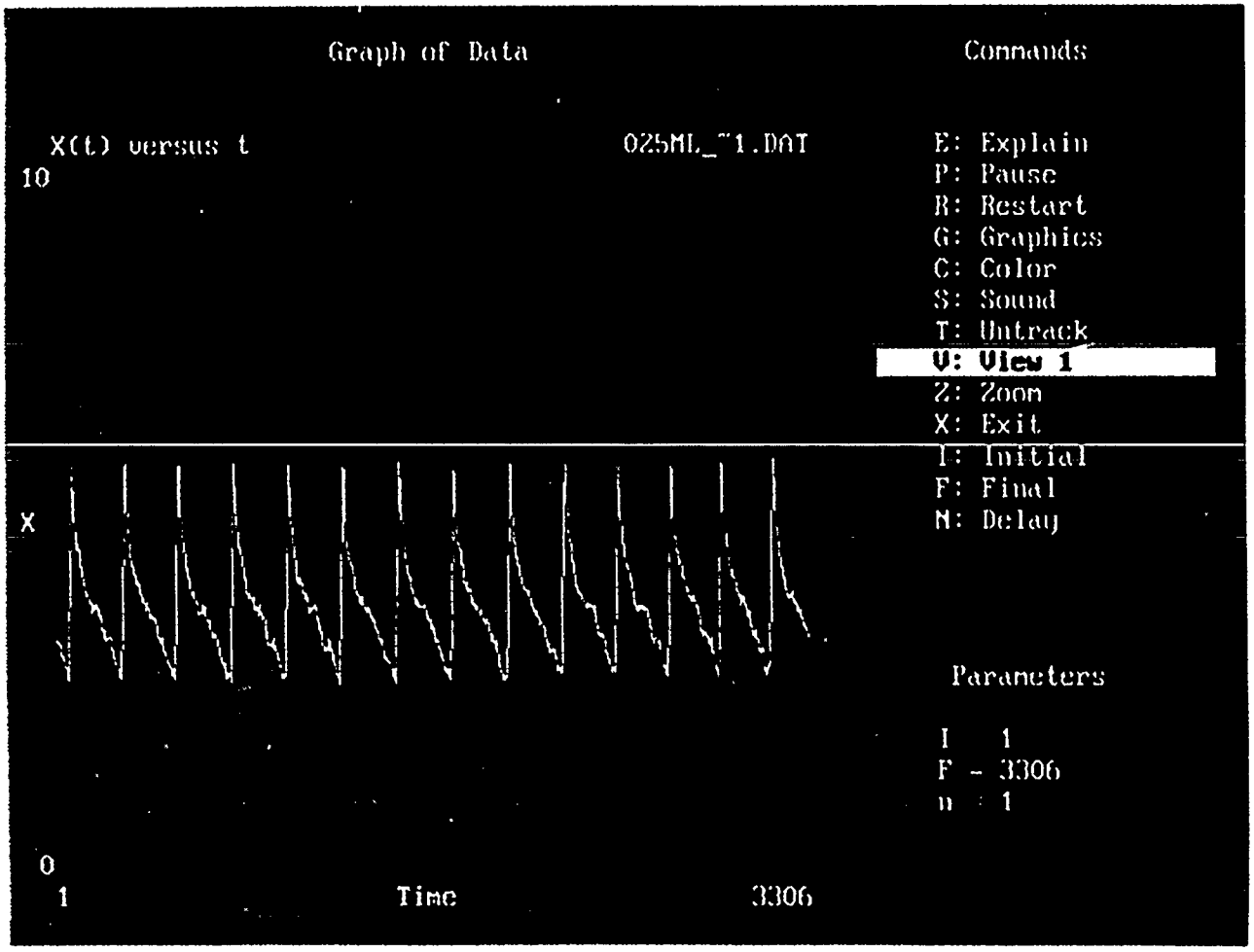
Graph of Data
Commands
X(t) versus t
025ML_~1.DAT
10
E: Explain
P: Pause
R: Restart
G: Graphics
C: Color
S: Sound
T: Untrack
V: View 1
Z: Zoom
X: Exit
I: Initial
F: Final
N: Delay
X
Parameters
I 1
F - 3306
n : 1
0
1
Time
3306

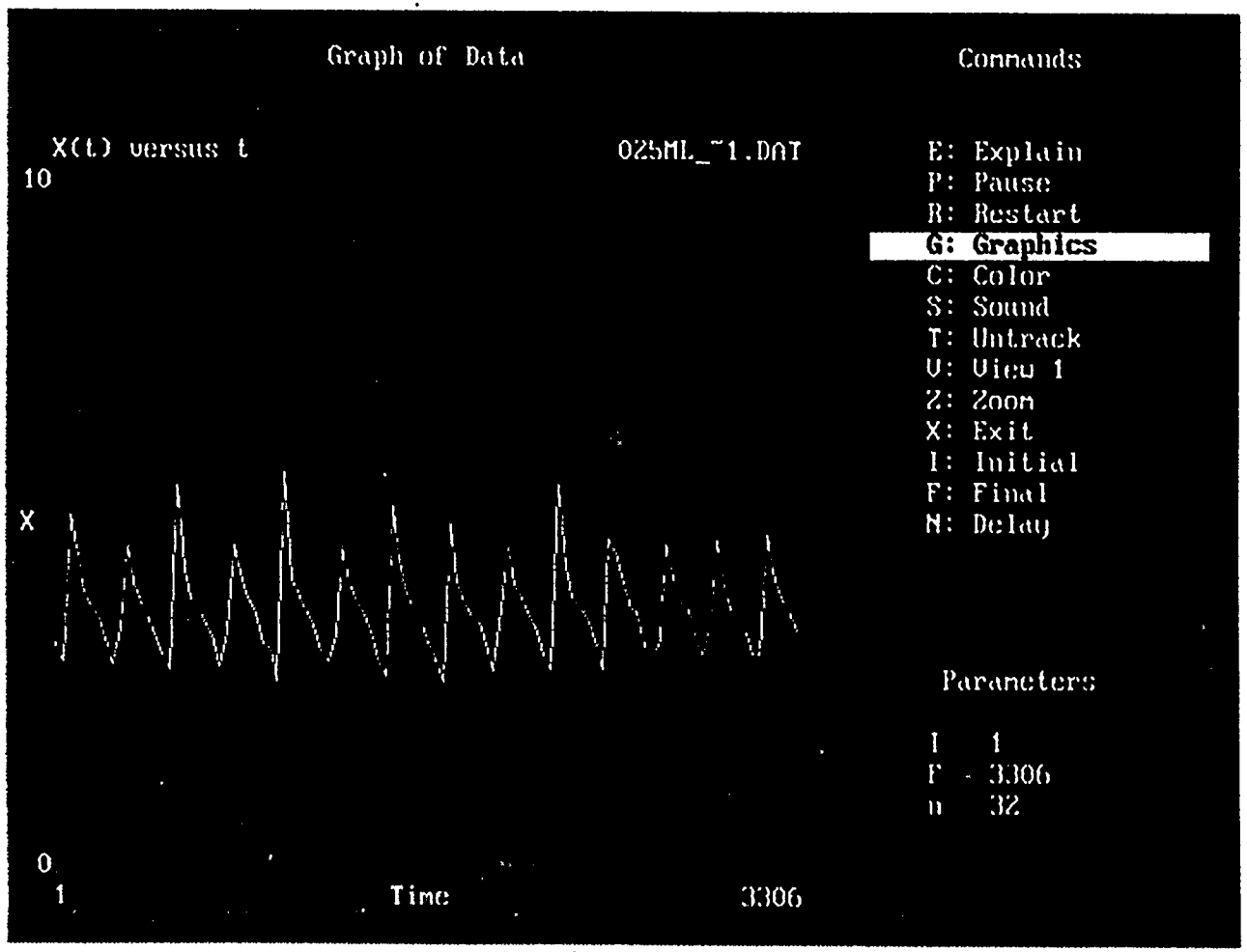
Graph of Data
Commands
X(t) versus t
025ML_~1.DAT
10
E: Explain
P: Pause
R: Restart
G: Graphics
C: Color
S: Sound
T: Untrack
V: View 1
Z: Zoom
X: Exit
I: Initial
F: Final
N: Delay
X
Parameters
I 1
F 3306
n 32
0
1
Time
3306

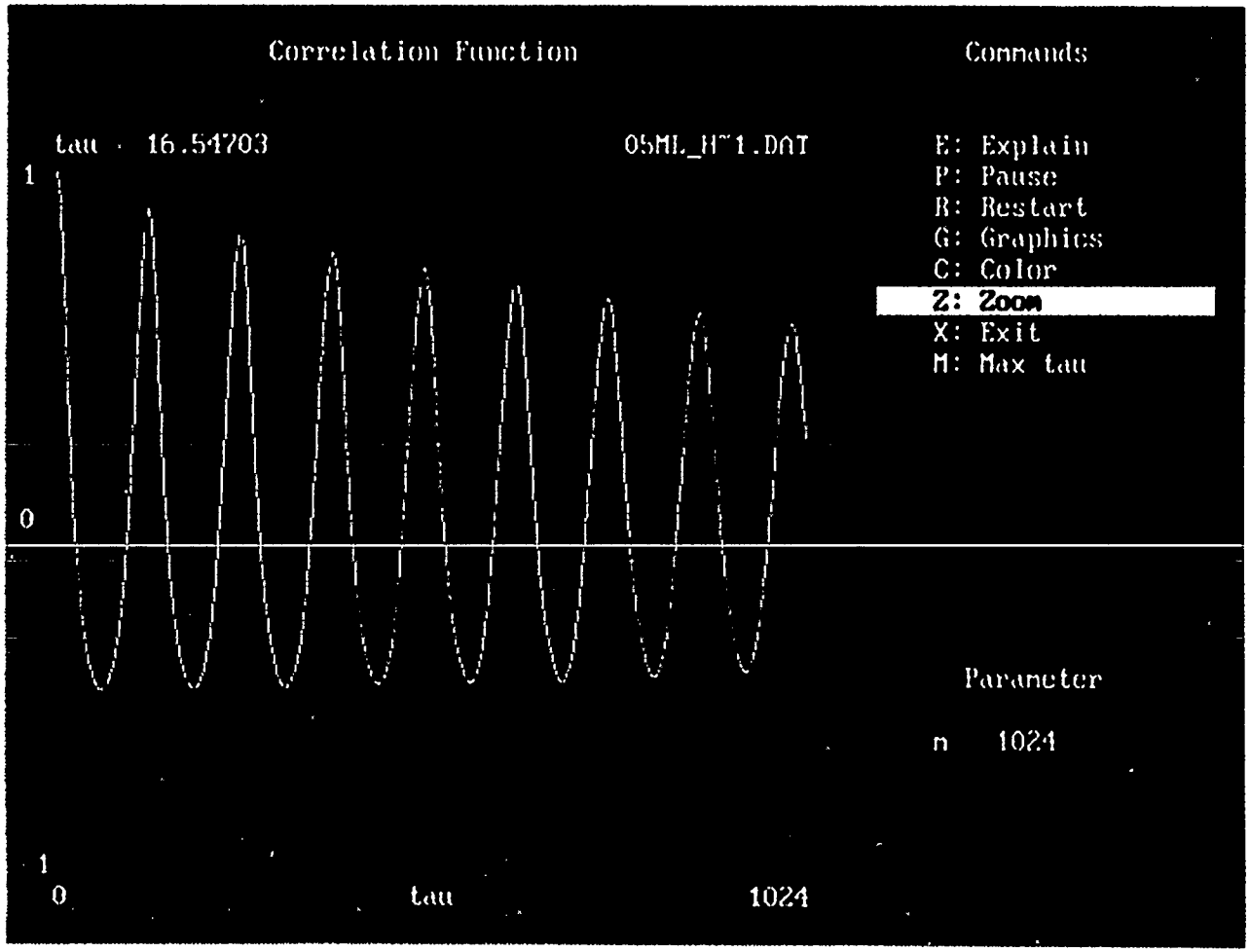
Correlation Function
Commands
tau = 16.54703
05ML_H~1.DAT
E: Explain
P: Pause
R: Restart
G: Graphics
C: Color
Z: Zoom
X: Exit
M: Max tau
1
0
Parameter
n 1024
1
0
tau
1024

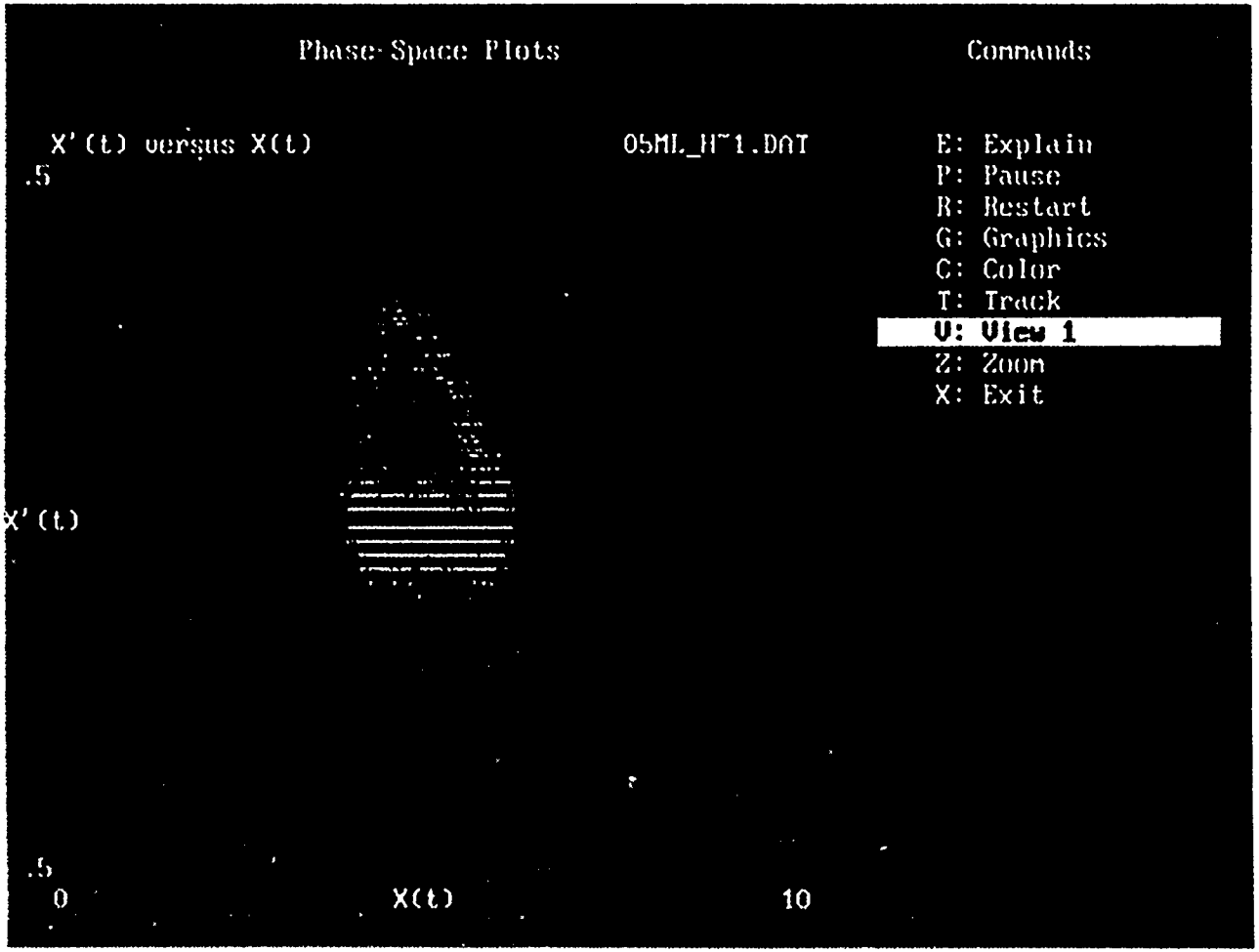
Phase-Space Plots
Commands
X'(t) versus X(t)
05ML_H~1.DAT
E: Explain
P: Pause
R: Restart
G: Graphics
C: Color
T: Track
V: View 1
Z: Zoom
X: Exit
.5
X'(t)
.5
0
X(t)
10

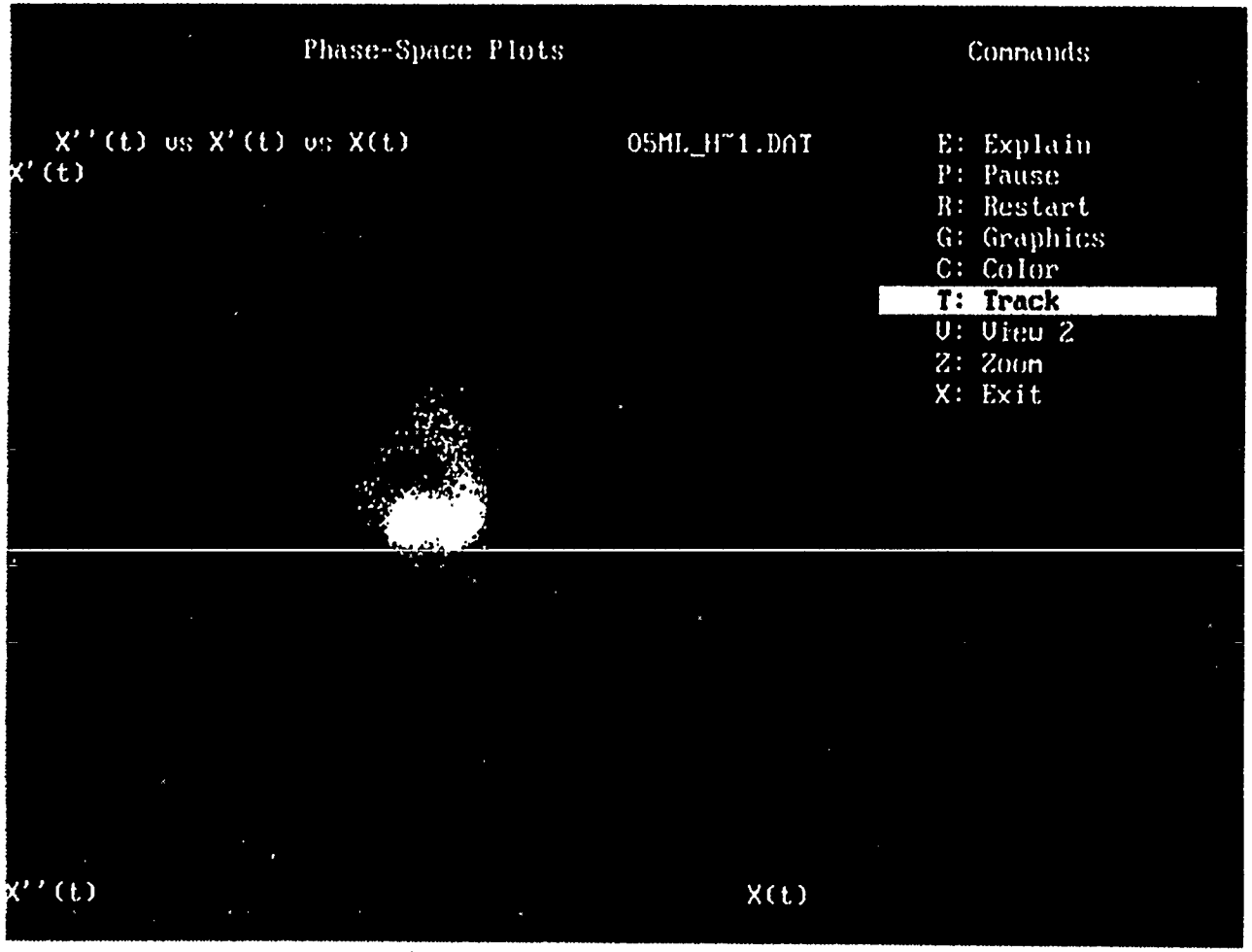
Phase-Space Plots
Commands
X''(t) vs X'(t) vs X(t)
05ML_H~1.DAT
E: Explain
P: Pause
R: Restart
G: Graphics
C: Color
T: Track
V: View 2
Z: Zoom
X: Exit
X'(t)
X''(t)
X(t)

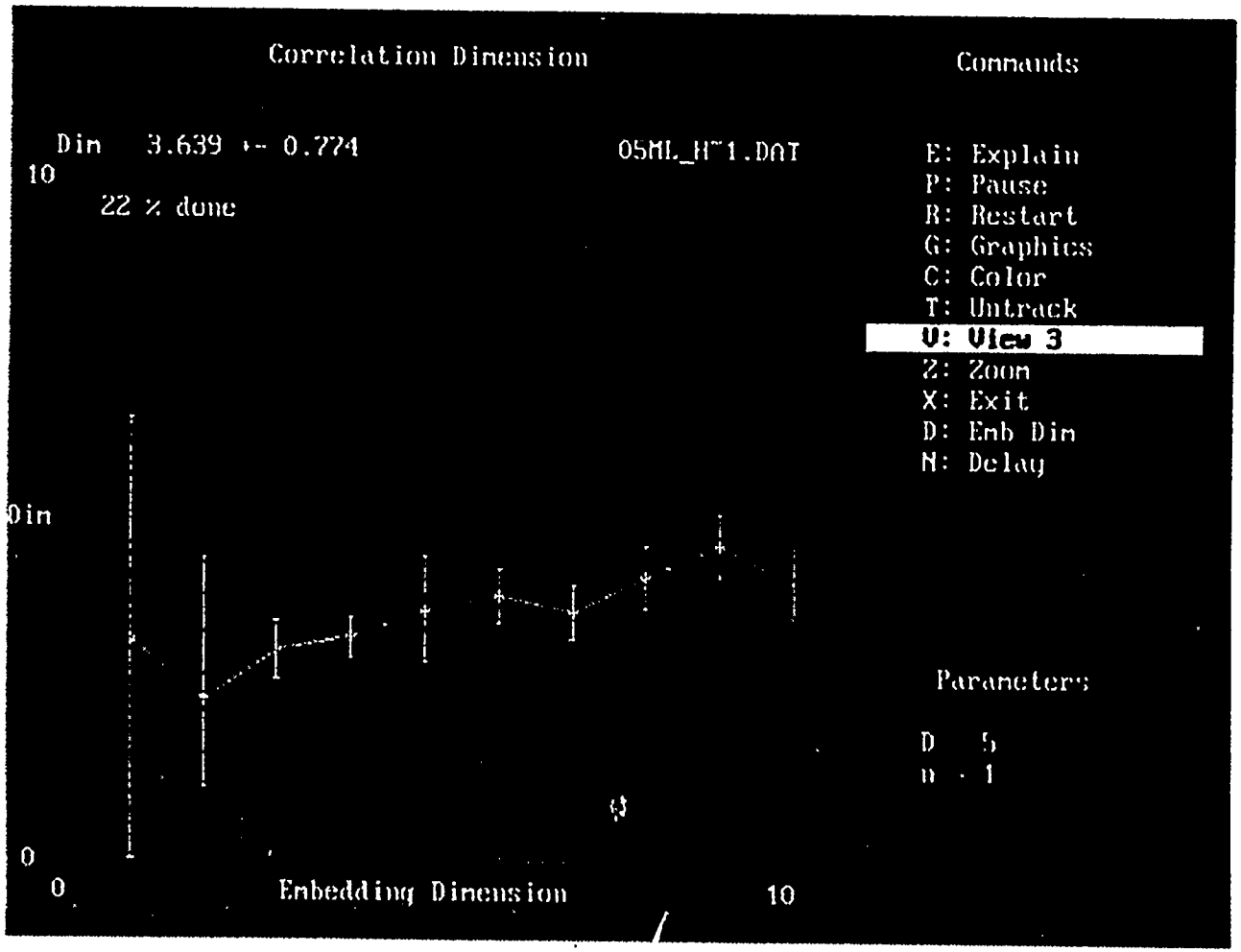
Correlation Dimension
Commands
Din 3.639 +- 0.774
05ML_H~1.DAT
10
22 % done
E: Explain
P: Pause
R: Restart
G: Graphics
C: Color
T: Untrack
V: View 3
Z: Zoom
X: Exit
D: Emb Din
M: Delay
Din
Parameters:
D 5
n 1
0
0
Embedding Dimension
10

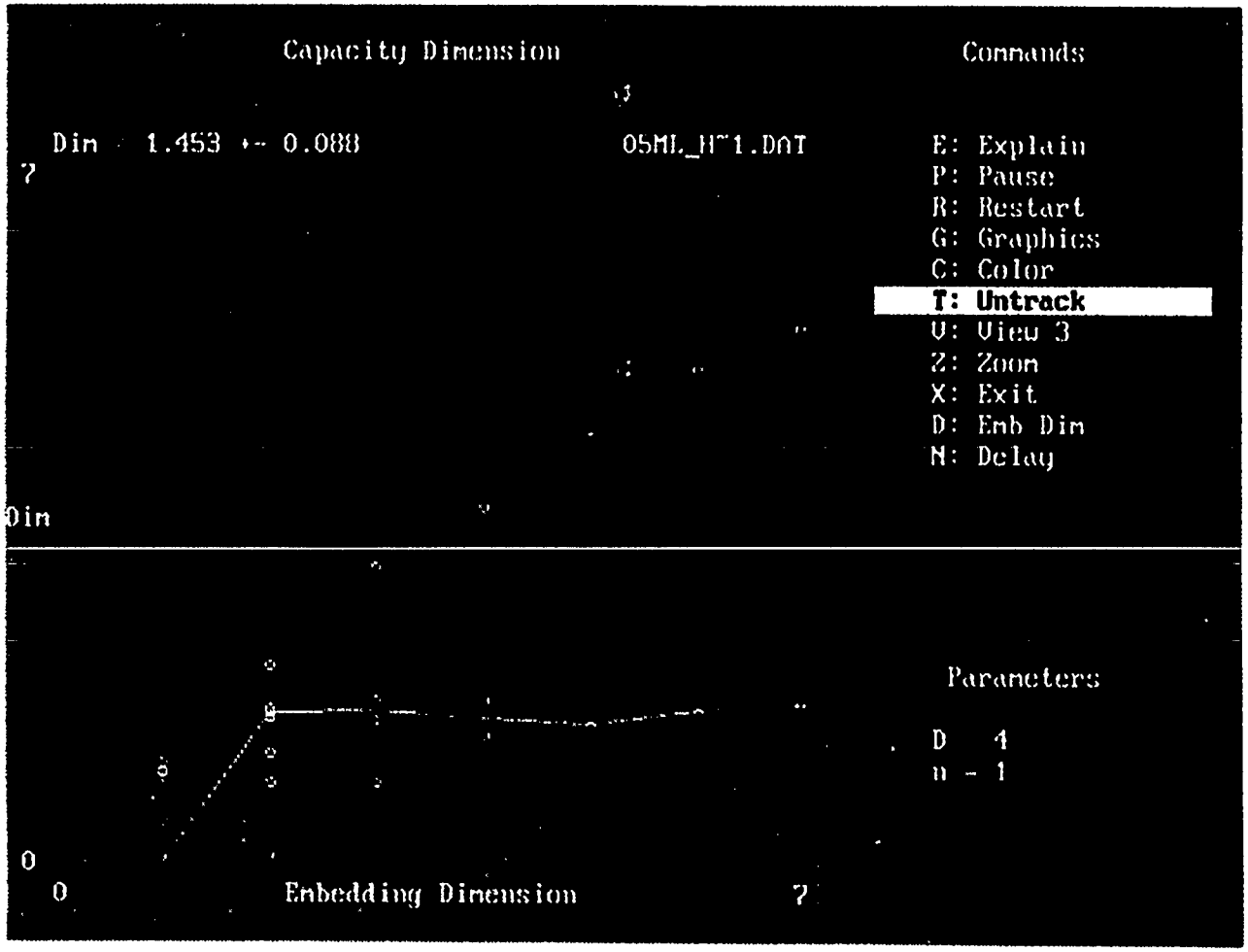
Capacity Dimension
Commands
Din 1.453 +- 0.088
05ML_H~1.DAT
E: Explain
P: Pause
R: Restart
G: Graphics
C: Color
T: Untrack
V: View 3
Z: Zoom
X: Exit
D: Emb Dim
N: Delay
Din
Parameters
D 1
n - 1
0
0
Embedding Dimension

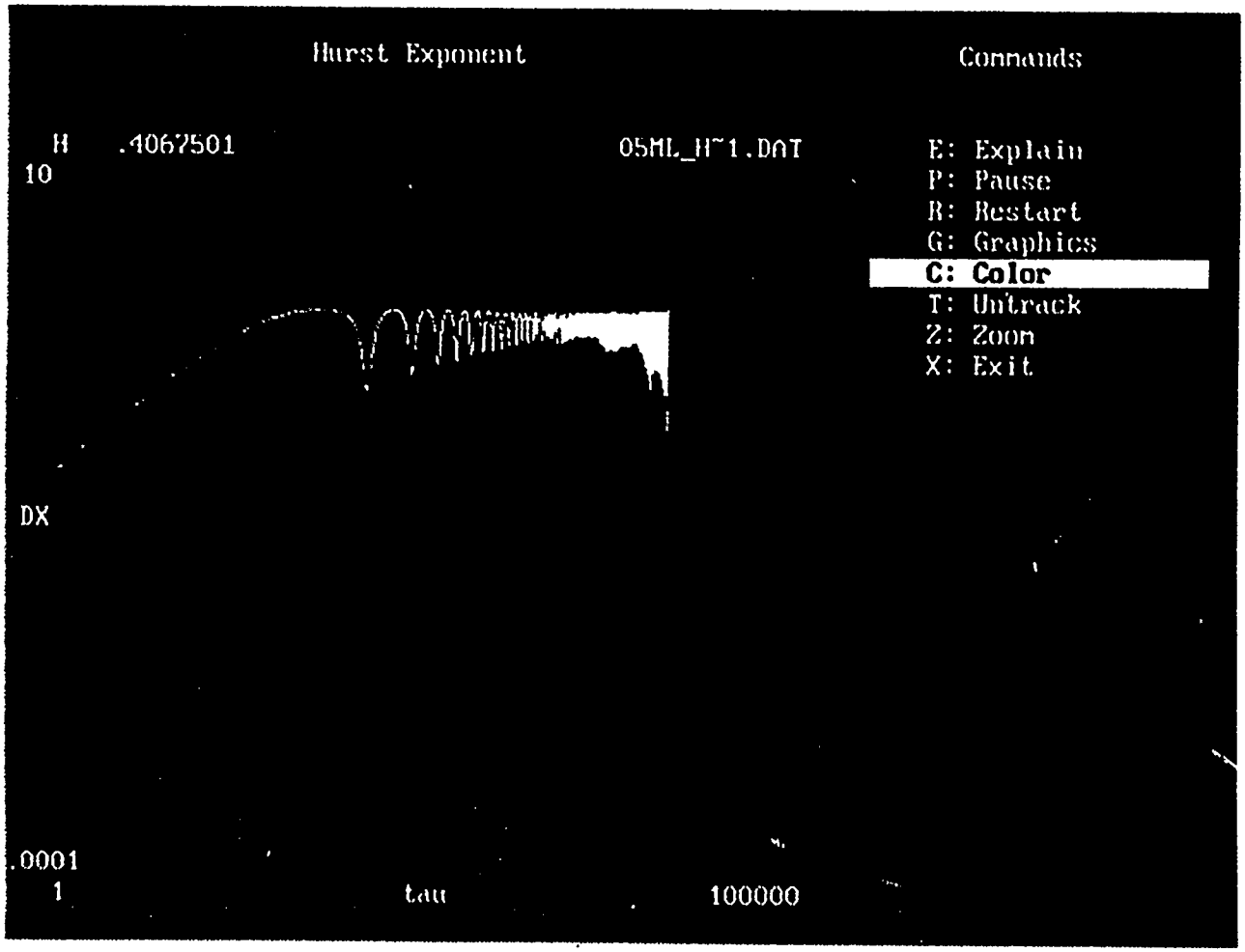
Hurst Exponent
Commands
H .4067501
05ML_H~1.DAT
10
E: Explain
P: Pause
R: Restart
G: Graphics
C: Color
T: Untrack
Z: Zoom
X: Exit
DX
.0001
1
tau
100000

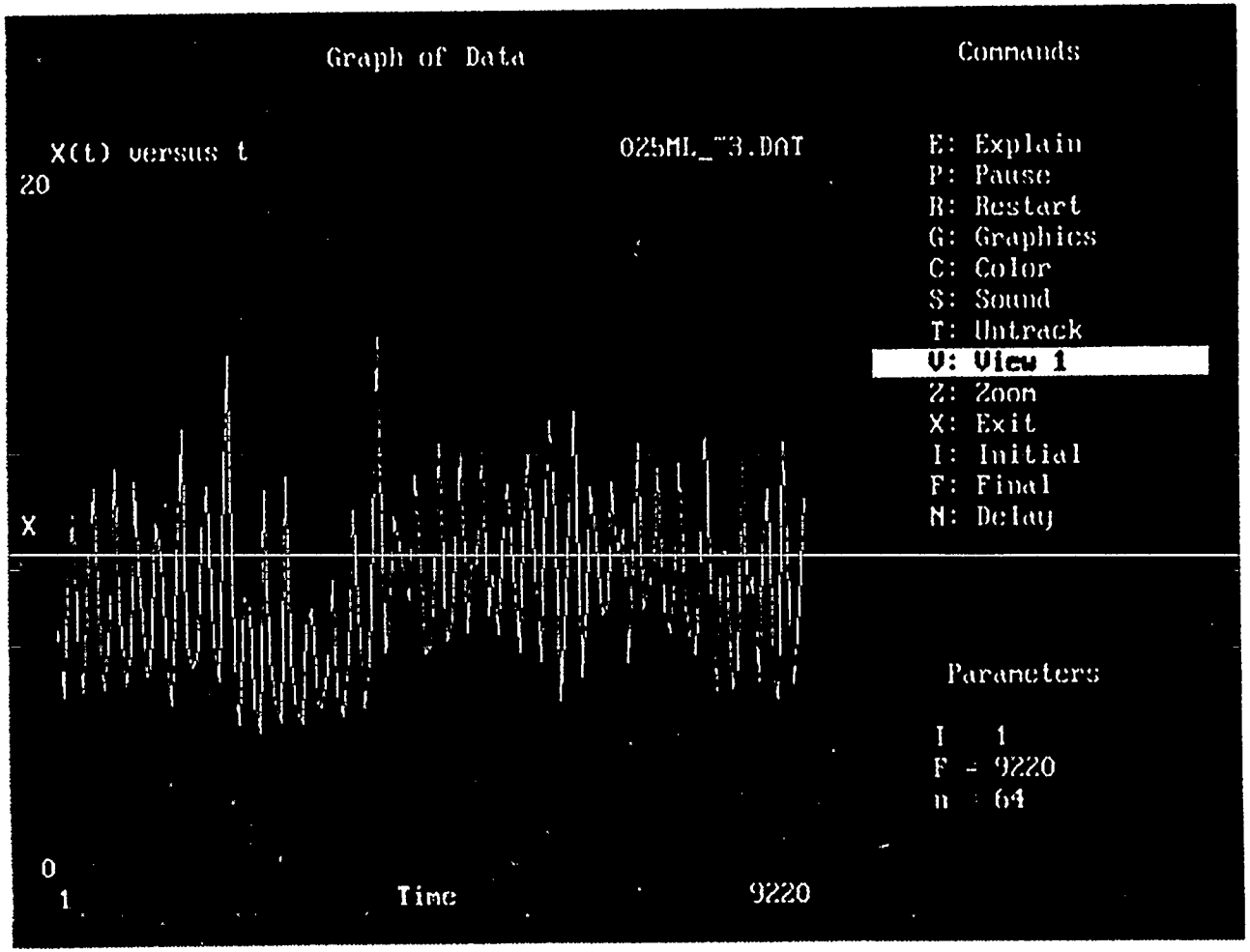
Graph of Data
Commands
X(t) versus t
025ML_~3.DAT
20
E: Explain
P: Pause
R: Restart
G: Graphics
C: Color
S: Sound
T: Untrack
V: View 1
Z: Zoom
X: Exit
I: Initial
F: Final
N: Delay
X
Parameters
I = 1
F = 9220
n = 64
0
1
Time
9220

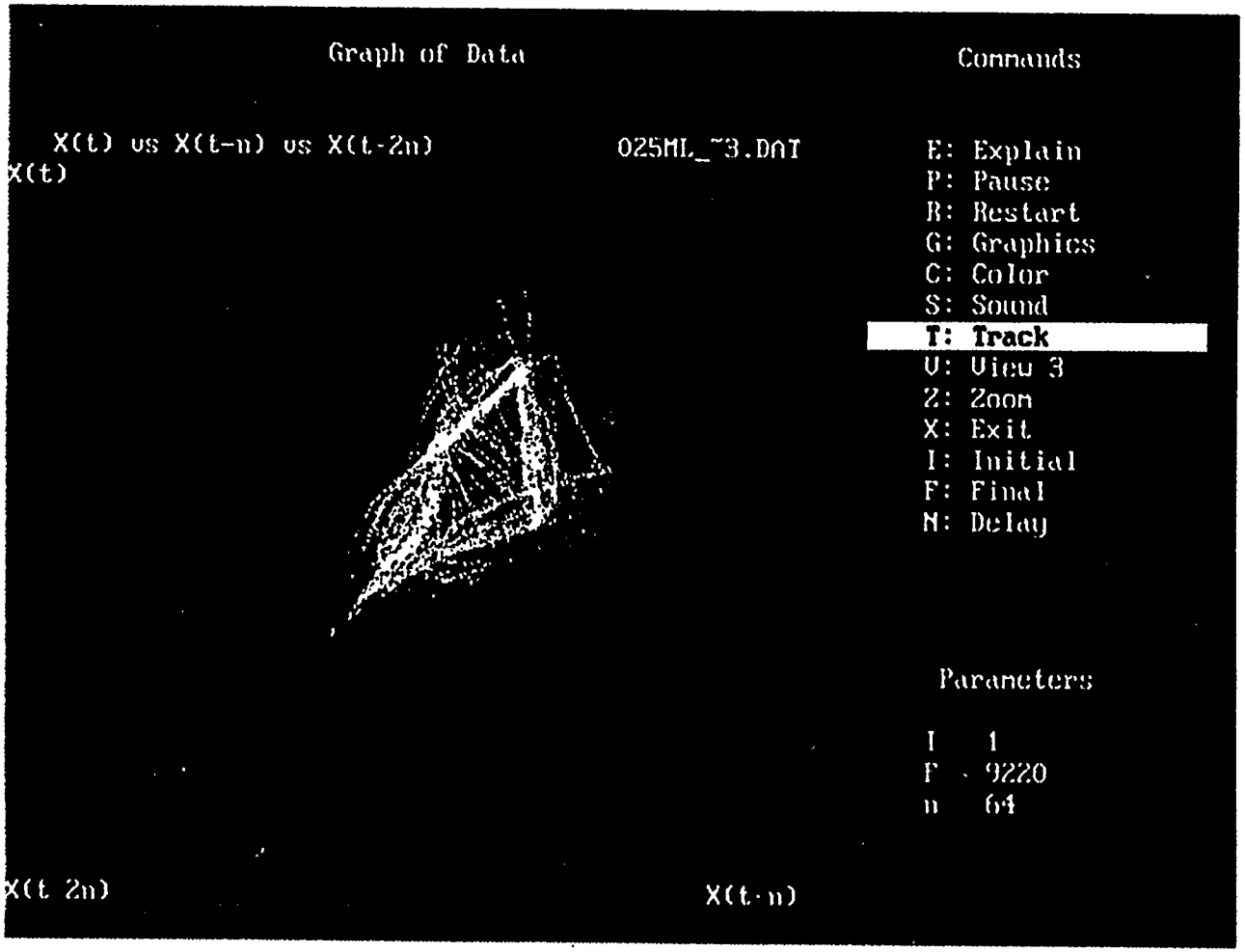
Graph of Data
Commands
X(t) vs X(t-n) vs X(t-2n)
025ML_~3.DAT
X(t)
E: Explain
P: Pause
R: Restart
G: Graphics
C: Color
S: Sound
T: Track
V: View 3
Z: Zoom
X: Exit
I: Initial
F: Final
N: Delay
Parameters
I 1
F 9220
n 64
X(t-2n)
X(t-n)

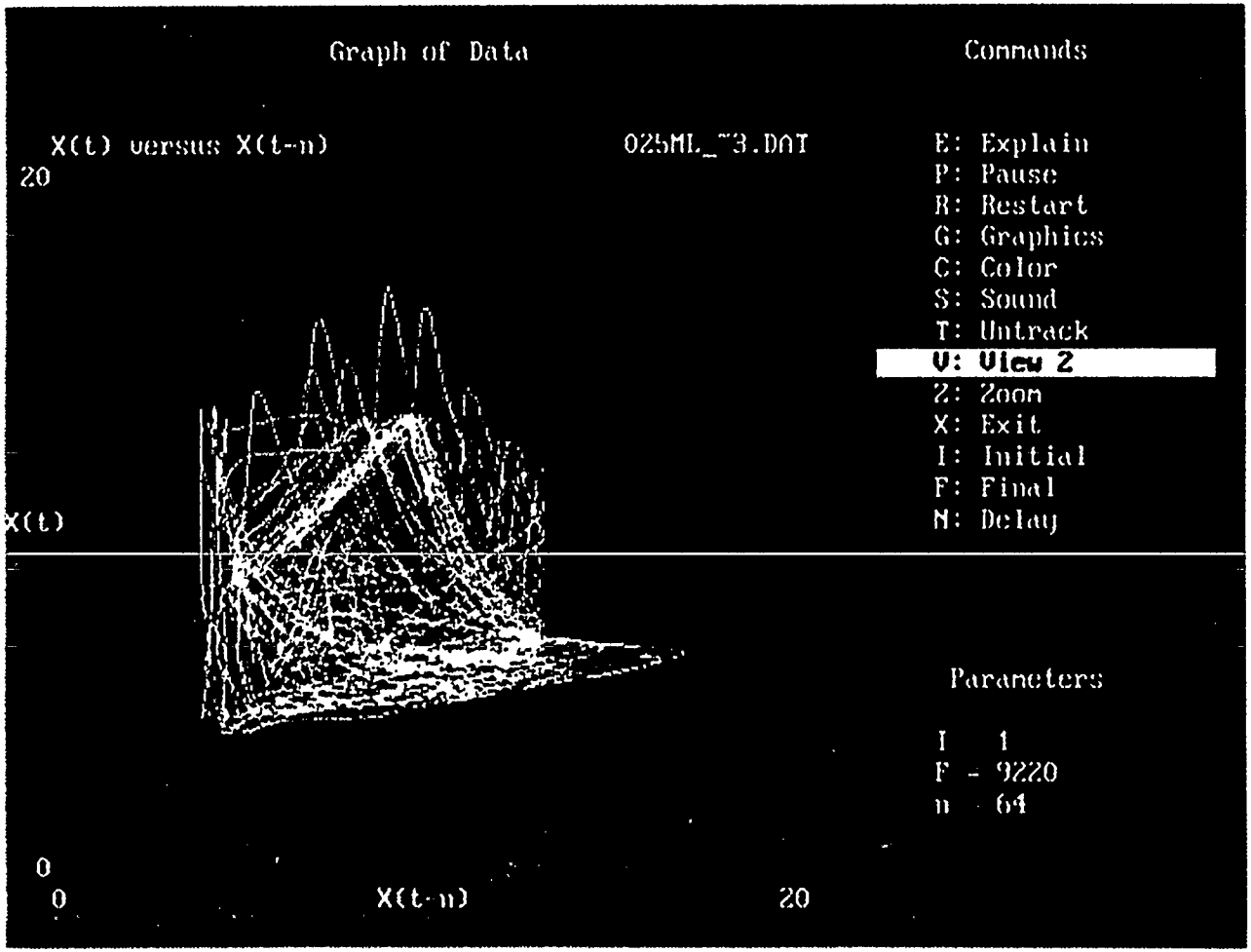
Graph of Data
Commands
X(t) versus X(t-n)
025ML_~3.DAT
E: Explain
P: Pause
R: Restart
G: Graphics
C: Color
S: Sound
T: Untrack
V: View 2
Z: Zoom
X: Exit
I: Initial
F: Final
N: Delay
20
X(t)
Parameters
I 1
F - 9220
n - 64
0
0
X(t-n)
20

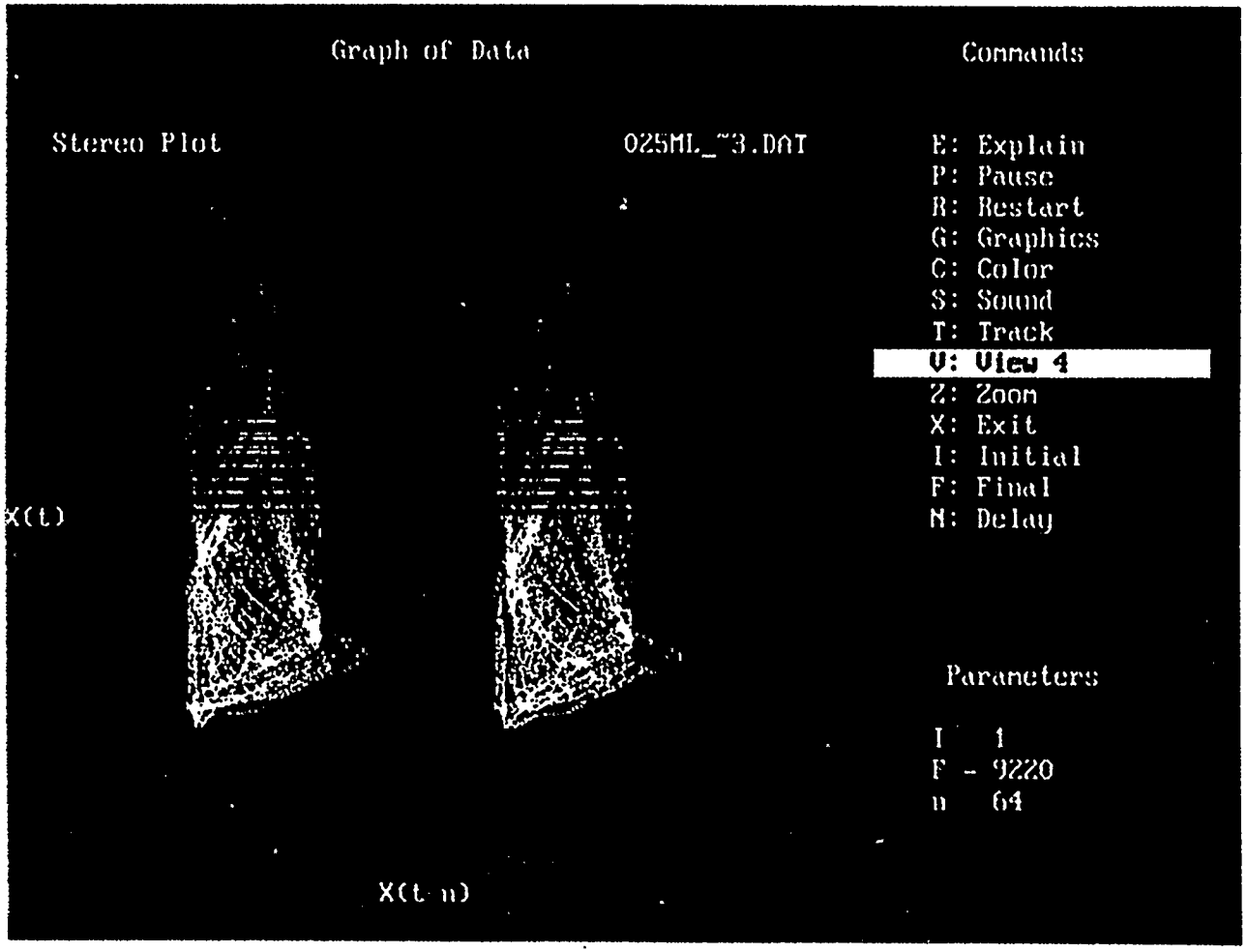
Graph of Data
Commands
Stereo Plot
025ML_~3.DAT
E: Explain
P: Pause
R: Restart
G: Graphics
C: Color
S: Sound
T: Track
V: View 4
Z: Zoom
X: Exit
I: Initial
F: Final
N: Delay
X(t)
Parameters
I 1
F - 9220
n 64
X(t-n)

III.

Life Cycle Planning for Chaotic-Dynamical Research Project

1st Year *(completed)*

INEEL

Hells Half Acre

Focus of the research effort was to collect a data set on a small scale field site of sufficient quality and size in order to perform chaotic-dynamical analysis. This data was supported by tensiometer, temperature, head and flow data and instrument development.

Box Canyon — Supported Box Canyon tests.

LBNL

Lab

Understand the physics of flow in fractures, and collect data of sufficient quality and size in order to determine if flow in fractures is a chaotic-dynamical process.
Investigated impact of tensiometer on measurements in a fracture using core study

Box Canyon

Evaluated possible preferential flow using geophysics
Understand the impact of monitoring approach on data collected
Repeated infiltration tests using tracers and electrical resistivity
Modeled flow using TOUGH2
Data analysis using chaotic-dynamical approach (may lead to a transition from chaotic model at the small scale to a stochastic model at larger field scale)

Reno

Develop a theoretical approach for data analysis based upon the Navier-Stokes equation

2nd Year
INEEL

Hells Half Acre

Repeat small scale test at one or more sites and modify the test approach based upon the analysis of 1997 data, laboratory testing and instrument development. New testing will involve the use of tracers and geophysics. At the end of the field season a tested fracture will be excavated intact and shipped to Berkeley Lab for further testing

Lab — Verification of monitoring equipment and testing of new instruments

LBNL

Lab
- Data analysis
- Testing will be performed on a variety of plate textures
- Testing on fractured core
- Tracer testing
- Testing on etched glass (etching patterned after Box Canyon Outcrop)

Box Canyon
- Pulsed infiltration
- Ponding concurrent with drainage
- Geophysics (use slanted wells and ER probes)
- Development and testing of flow meter for fractured rock (saturated)

Modeling
- HHA modeling?
- Lab scale modeling?
- Coordinate modeling with geophysics (use moisture content from TOUGH2 for inverse modeling?)
- Develop approach and software for chaotic-dynamical modeling
- Use CPN moisture content for modeling?

LSIT — Revisit data set using chaotic-dynamical approach?

Instrument Development
- Impact of monitoring device on the data collected
- Fractured core tensiometer experiment
- Passive/active monitoring approach
- Flow meter for saturated fractured rock and for vadose zone
- Piezo-strips in slanted wells - dripping or flowing along the borehole

Reno — To be included

3rd Year

INEEL

Hells Half Acre

Focus on building ties from lab-scale to small-scale to intermediate-scale to full scale
Continued data analysis
Instrument development
Additional Hells Half Acre Testing based on data needs

General

Work with problem holders to develop strategies for implementation of technical proposals

Lab — Verification of monitoring equipment and testing of new instruments

LBNL

Lab — Continued data analysis
Testing of Hells Half Acre fracture using test approaches developed in year 2
Analysis of fracture sediment infilling
Evaluate geometry of field added dye
Cross-comparison of lab results to INEEL Hells Half Acre field measurements

Box Canyon — Possibility of limited field testing at Box Canyon site
Basic monitoring of drain-out from year 2 tests and natural wetting and drying events

Modeling — Modeling at different scales - this may involve a chaotic-dynamical model at small scale and a deterministic model at a larger scale. Probably multi-component. May require some code development.
With problem holder involvement do a preliminary comparison using new chaotic-dynamical approach to evaluate flow and transport from CERCLA site and contrast to the results from a RI/FS fate and transport model using conventional equivalent porous media approach

Instrument Development

Produce demo quality prototype instruments and a conceptual approach for potential application at "live" site
Develop an "Instrumentation Strategy" including:
Instruments, passive/active components, hydrogeological and geophysical components

Reno

To be included

IV.

Name		Company	E-mail	Phone
Becker	Alex	LBNL	alexb@socrates	
Borglin	Sharon	LBNL	seborglin@lbl.gov	x7515
Cox	Lea	LBNL	lea@ux8.lbl.gov	x4717
Doughty	Chris	LBNL	cadoughty@lbl.gov	x6453
Faybishenko	Boris	LBNL	bfayb@lbl.gov	x4852
Finsterle	Stefan	LBNL	safinsterle@lbl.gov	x5205
Geller	Jil	LBNL	jtgeller@lbl.gov	x7313
Jacobsen	Janet	LBNL	jsjacobsen@lbl.gov	x4450
LaBrecque	Doug	SteamTech	labrecque@steamtech.com	(520) 744-9332
Persoff	Peter	LBNL	persoff@lbl.gov	x5931
Peterson	John	LBNL	jepeterson@lbl.gov	x4267
Podgorney	Rob	INEEL	podgrk@inel.gov	(208) 526-1224
Pruess	Karsten	LBNL	K_Pruess@lbl.gov	x6732
Seol	Soon Jee	LBNL	ssj@hfem.lbl.gov	x5502
Simmons	Ardyth	LBNL	asimmons@lbl.gov	x7106
Song	Yoonho	LBNL	song@hfem.lbl.gov	x5502
Steiger	Michael	LBNL	mtsteiger@lbl.gov	x7083
Stoops	Tom	INEEL	thms@inel.gov	(208) 526-4262
Wood	Tom	INEEL/Parsons	TQW@INEL.gov	(208) 526-1293
Yang	Jeong-Seok	LBNL	jsyang@ce.berkeley.edu	x7083